DESIGN AND DEVELOPMENT OF NANOEMULSIONS AND HYDROGEL BASED SYSTEMS FOR ENHANCED INTESTINAL PERMEABILITY AND CONTROLLED RELEASE OF PHYTOCHEMICALS

Thesis submitted in fulfillment of the requirements for the degree of

DOCTOR OF PHILOSOPHY

By

ARUN KUMAR

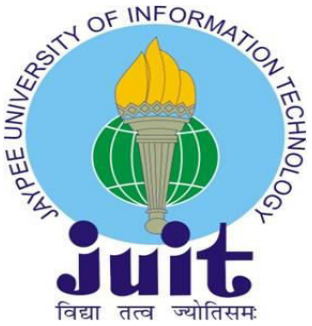

Department of Pharmacy

JAYPEE UNIVERSITY OF INFORMATION TECHNOLOGY

WAKNAGHAT, DISTRICT SOLAN, H.P., INDIA

February 2018

Dedication

Every challenging work needs self effort as well as guidance of elders especially those who were very close to our heart.

My humble effort I dedicate to my sweet and loving

Father& Mother,

Whose affection, love, encouragement and prays of day and night make me able to get such success and honor,

Along with all hard working and respected

Teachers

TABLE OF CONTENTS

DECLARATION

I hereby declare that the work reported in the Ph.D. thesis entitled **"Design and development of nanoemulsions and hydrogel based systems for enhanced intestinal permeability and controlled release of phytochemicals"** submitted at **Jaypee University of Information Technology, Waknaghat, India,** is an authentic record of my work carried out under the supervision of **Dr. Udayabanu Malairaman**. I have not submitted this work elsewhere for any other degree or diploma. I am fully responsible for the contents of my Ph.D. Thesis.

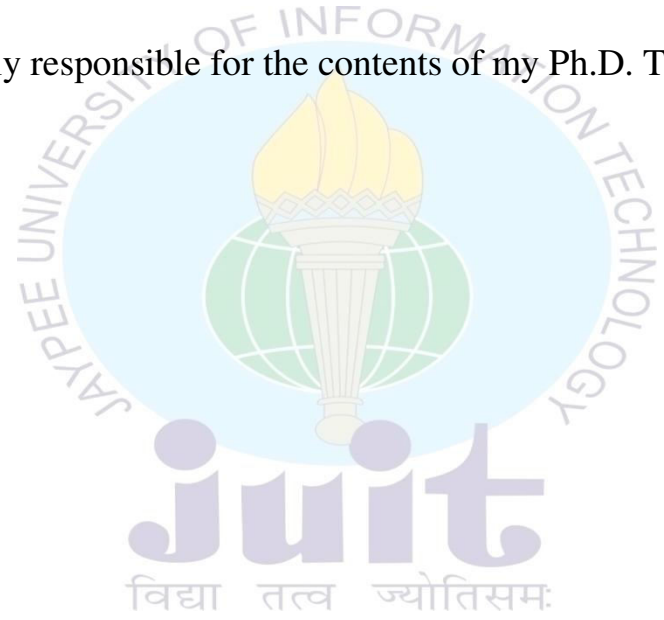

Arun Kumar **Date:**

Enrollment No. 126752

Department of Pharmacy

Jaypee University of Information Technology

Waknaghat, Solan, H.P., India

CERTIFICATE

This is to certify that the work reported in the Ph.D. thesis entitled **"Design and development of nanoemulsions and hydrogel based systems for enhanced intestinal permeability and controlled release of phytochemicals"** submitted by **Mr. Arun Kumar** at **Jaypee University of Information Technology, Waknaghat**, **India,** is a bonafide record of his original work carried out under my supervision. This work has not been submitted elsewhere for any other degree or diploma.

Supervisor:

Dr. Udayabanu Malairaman **Date:**
Assistant Professor
Department of Pharmacy
Jaypee University of Information Technology
Waknaghat, Solan, H.P., India

ACKNOWLEDGEMENT

This thesis represents not only my work at the keyboard; it is a milestone in more than one decade of work at JUIT and specifically within the Nanobiotechnology lab. My experience at JUIT has been nothing short of amazing. I have been given unique opportunities and taken advantage of them. This includes working at the JUIT for over four years, starting as PhD research scholar in the summer of 2012. Throughout these years I have learned that there are those who build tools and those who use them; my passion is in creating the tools used in cutting edge research. This thesis presents the lessons learned in creating one of those special tools: SPHERES. A SPHERE is the result of work by dozens of people, who I wish to thank. But this thesis is also the result of many experiences I have encountered at JUIT from dozens of remarkable individuals who I also wish to acknowledge.

First and foremost I wish to thank my supervisor ***Dr. Udayabanu Malairaman, Assistant professor, JUIT, Solan, India****. He has been supportive since the days I began working on the origins testbed as research scholar; I remember he always used to say something like "you're always the first one in and the last one out working on that project!" to encourage me to stay in the lab. Ever since, he has supported me not only by providing a research assistantship over almost four years, but also academically and emotionally through the rough road to finish this thesis. He helped me come up with the thesis topic and guided me over almost a year of development. And during the most difficult times when writing this thesis, he gave me the moral support and the freedom I needed to move on.*

A special group from the JUIT is not mentioned yet, because they deserve their own part: the SPHERES team. I praise the enormous amount of help, teaching, moral support by ***Prof (Dr) R.S. Chauhan, Dean and HOD, Department of Biotechnology, JUIT*** *throughout these years. Thank you to those who helped the project as graduate students and staff:* ***Preeti Fista, Esha, Abhishek Thakur, Sanjay Chauhan, Abhishek Gupta, Nitesh Kashyap, Tsering Nyima*** *and* ***Shivani Sharma.*** *Also thank you to everyone at JUIT who has helped with the project and supported me in many ways:* ***Mrs. Sonika Gupta, Mrs. Somlata Sharma, Mrs. Mamta Mishra, Mr. Ravikant, Mr. Baleshwar*** *and* ***Mr. Kamlesh****.*

*I am also indebted to Prof. (**Dr) Veena Koul, Professor, Indian Institute of Technology, Delhi***(IIT) for allowing me to work in her lab and providing instrumental facilities.

*I am deeply obliged to **Dr. Dharmendra Jain, Assistant professor, Department of pharmacy, Dr. H.S. Gour Vishwavidyalaya, Sagar, M.P, India** for his incessant guidance, whenever I needed.*

*I emphatically extend my sincere thanks to the worthy administration of JUIT, **Prof (Dr) S.C. Saxena (Acting vice chancellor), Prof (Dr) S.D. Gupta (Director, Academics), Brig. (Retd.) Balbir Singh (Director, Administration), Prof (Dr) T. S. Lamba (Dean, Academics and Research)** and **Prof (Dr) S.K. Kak (Former vice chancellor)** for providing opportunity to pursue a Doctorate Degree, fellowship and lab infrastructure.*

Special Acknowledgement

*No expression of thanks will be sufficient without recognition of help and support rendered by my senior, my friend and my roommate **Mr. Archit Sood** whose constant help during writing made this a successful venture.*

*A special thanks to my family. Words cannot express how grateful I am to my parents **Sh. Balak Ram** and **Smt. Uma Dhiman** and my elder brother **Gulshan Dhiman** for all of the sacrifices that you've made on my behalf. Your prayer for me was what sustained me thus far. I would also like to thank to my maternal uncle **Sh. Satpal Dhiman** and my maternal aunt **Smt. Sampatti Dhiman**. Thank you for supporting me for everything, and especially I can't thank you enough for encouraging me throughout this experience. To my beloved sister **Banita Dhiman**, I would like to express my thanks for being such a good sister always cheering me up. Finally I thank my God for letting me through all the difficulties. I have experienced your guidance day by day. You are the one who let me finish my degree. I will keep on trusting you for my future. Thank you, Lord.*

Arun Kumar

ABSTRACT

The present investigation involves the use of different herbal extracts and "green chemistry" for the development of lipid based nanoemulsions and silver nanoparticles loaded nanocomposite hydrogels for controlled drug delivery. To fulfill this objective in the first process, nanoemulsion (NEs) and self nanoemulsifying drug delivery system (SNEDDS) were prepared using *Tinospora cordifolia* (TC) and *Berberis aristata* (BA). Nanodroplet size and zeta potential of these nanoemulsions and SNEDDS were found to be in the range of 33.7 nm to 147.1 nm and -23.30 mV to -31.2 mV, respectively. Sustained release profile of the extract from nanoemulsion and SNEDDS was found up to 20 (~81) and 34 h (~96 %), respectively. While in the second process, *Ocimum sanctum* (OS) and *Ficus benghalensis* (FB) extracts were utilized for the green synthesis of silver nanoparticles (AgNPs) with further utilization in the development of PVA/CH (Polyvinyl alcohol/Chitosan) and PVA/SA (Polyvinyl alcohol/Sodium alginate) nanocomposite hydrogels. The formation of silver nanoparticles was confirmed by UV-visible spectroscopy (λ_{max} 430 nm), optical microscopy, and particle size analysis (20-35 nm).

Silver nanoparticles loaded PVA/SA sprayed hydrogel dressing (SHD) film was designed and executed using polyvinyl alcohol and sodium alginate as polymeric components while, boric acid and calcium chloride were used as respective cross-linkers to form spontaneous sprayed dressing. On the other hand, silver nanoparticles loaded with PVA/CH hydrogel was prepared by using freeze thaw process so as to bypass the toxic effects associated with chemical cross-linking. FTIR spectra of nanocomposite hydrogels showed polymeric interaction due to formation of coordination among the function group present in the nanocomposite hydrogels with the AgNPs, while SEM images showed highly cross-linked, porous and uniformity in surface morphology. The results of thermo-gravimetric analysis showed that the introduction of silver nanoparticles in the PVA/CH and PVA/SA hydrogels network increases the thermal stability. It was noticed from the release profile study that ~87±1.78 % and ~82±1.67 % of FB extract and silver ions were released from the PVA/SA SHD films, respectively. The results of microbe penetration (no penetration across the film) and antimicrobial activity tested against *S. aureus* and *E. coli* bacteria showed a concentration dependent zone of inhibition for up to 24 h respectively. The obtained results strongly encourage the use of these nanoemulsions and polymeric nanocomposite hydrogels for the controlled delivery of these phytochemicals.

LIST OF ABBREVIATIONS

(D)	Drug
µl	Micro liter
AAS	Atomic absorption spectroscopy
ADP	adenosine diphosphate
$AgNO_3$	Silver nanoparticles
$AlCl_3$	Aluminium chloride
ANOVA	Analysis of variance
ATP	Adenosine triphosphate
BA	*Berberis aristata*
BA	Boric acid
BCG	Bromocresol green
BCS	Biopharmaceutical classification system
BS	Bile salt
BSA	Bovine serum albumin
$CaCl_2$	Calcium chloride
CH	Chitosan
Chito-TBA	Chitosan-thiobutylamidine
C_{max}	Maximum plasma concentration
CMC	Carboxymethyl cellulose
CM-chitosan	Carboxymethylated chitosan
CNS	Central nervous system
D_{eb}	Deborah number
DEN	Diethyl nitrosamine
DG	Di-glycerides
DMSO	Dimethyl sulfoxide
DPPH	2, 2-diphenyl-1-picrylhydrzyl

DTA	Differential thermal Analysis
DTG	Differential thermal gravimetery
DW	Distilled water
EDTA	Ethylene diamine tetra acetic acid
EE	Encapsulation efficiency
ER	Endoplasmic reticulum
ERK	Extracellular signal –regulated kinase
ESR	Equilibrium swelling ratio
FA	Fatty acid
FB	*Ficus benghalensis*
FDA	Food and drug administration
FDC	Franz diffusion cell
FITC	Fluorescein isothiocyanate
FTIR	Fourier transforms infrared spectroscopy
GIT	Gastro intestinal tract
GRAS	Generally recognized as Safe
HCC	Hepatocellular carcinoma
HLB	Hydrophilic lipophilic balance
HPMC	Hydroxypropylmethylcellulose
IPN	Interpenetrating polymeric network
J_{ss}	Flux
KRB	Krebs ringer solution
LBDD	Lipid based drug delivery
LP	Lipoproteins
M	Mucosal
MCT	Medium chain triglycerides
mg	Milligram

MG	Monoglycerides
MIC	Minimum inhibitory concentration
ml	Milliliter
mM	Millimolar
mV	Millivolts
NaCl	Sodium chloride
$NaNO_2$	Sodium nitrite
NaOH	Sodium hydroxide
NE	Nanoemulsion
Nm	Nano meter
NPs	Nanoparticles
O	Oral
Oc	Ocular
OS	*Ocimum sanctum*
P	Parenteral
PAA	Polyacrylic acid
PBS	Phosphate buffer saline
PCL	Polycaprolactone
PEG	Polyethylene glycol
PEO	Polyethylene oxide
PG	Propylene glycol
PGD	Propylene glycol Dilaurate
P-gp	P-glycoprotein's
PHEMA	Poly (2-hydroxyethl methacrylate)
PLA	Polylactic acid
PLSNE	Pluronic F68 self nanoemulsions
POE	Polyoxyethylene

PVA	Polyvinyl alcohol
PVP	Polyvinyl pyrollidone
RBC	Red blood cells
rpm	Revolutions per minute
SA	Sodium alginate
SD	Standard deviation
SDS	Sodium dodecyl sulfate
SEM	Scanning electron microscopy
SGOT	Serum glutamic oxaloacetic transaminase
SGPT	Serum Glutamic pyruvate transaminase
SHD	Sprayed hydrogel dressing
SMEDDS	Self micro-emulsifying drug delivery system
SNEDDS	Self nanoemulsifying drug delivery system
S_w	Swelling interface number
T	Topical
TC	*Tinospora cordifolia*
T_f	Final temperature
TG	Triglycerides
TGA	Thermo gravimetric analysis
T_i	Initial temperature
T_{max}	Maximum temperature
TPGS	Tocopheryl polyethylene glycol succinate
TRITC	Tetramethylrhodamine
TWSNE	Tween 80 self nanoemulsions
VLDL	Very low density lipoproteins
ZOI	Zone of inhibition
ZP	Zeta potential

LIST OF FIGURES

LIST OF TABLES

CHAPTER-1

INTRODUCTION

1.1 INTRODUCTION

A perfect formulation system achieves the goals of enhanced therapeutic response with least toxicity. By way of the progress and advancement in time, knowledge and tools, drug formulations have been enlarge from simple blend and tablets, to extremely complicated structure, which are famous as novel drug formulation systems. Drawbacks in intravenous administration such as extravasations of drug or blood, thrombosis and catheter infections can be prevented by administering the drug orally and thus making the oral drug delivery system the most accepted way of administration [1]. Though, oral drug deliverance is restricted by issues related to physico-chemical properties of the drug i.e. poor solubility, low intestinal permeability, instability in the harsh acidic environment followed by rapid metabolism, all of which decreases oral bioavailability [2].

With the advancement in the drug design, various molecules have been created to facilitate a potential medicinal effect. But the majority of the recently discovered molecules or chemical molecules is of high molecular weight (Phytochemicals) and belongs to biopharmaceutical classification system (BCS) –IV, with low water solubility and low intestinal permeation property. Hence these properties limit the bioavailability of orally administered drugs [3]. This poor aqueous solubility not simply gives the low oral bioavailability of drug but also leads to elevated inter and intra matter inconsistency and lack in amount proportionality [4]. Various techniques like micronization, complexation, solid dispersion and permeation improver with surfactant have been cited to overcome low solubility and intestinal permeation issues [5].

In the last few decades, lipids based drug delivery systems have gained a huge interest as a delivery service for the targeting of drugs with poor water solubility [6]. The availability of novel lipid based excipients with tolerable regulatory and security profiles has helped in the improvement of lipid based nanoformulations as a drug delivery vehicle. Lipid based drug delivery (LBDD) system have attained a good deal in the current time owing to their capability to enhance the dissolution and bioavailability of drugs with least aqueous solubility [7]. The absorption of various drugs from the lipid based nanoformulations depends on several factors including their particle diameter, extent of emulsification, pace of distribution, surface charge and solidification of drug ahead distribution [8]. LBDD system consist of release of a drug dissolved in a blend of individual or additional oily substances which can be a mono, di and tri-glycerides (i.e.

oil phase), lipophilic and hydrophilic surfactant and a co-surfactant. Oil based systems may comprise of oil solution or emulsions, suspensions and self micro or self nanoemulsifying drug delivery systems (SMEDDS/SNEDDS) [8, 9]. The successful formation of lipid delivery system depends on an appropriate selection of lipid vehicle, formulation strategies and rational delivery system design [10]. An aqueous in-soluble drug can be synthesized as a lipid like systems when the drug shows oil like properties (e.g., ethyl icospentate, tocopherol nicotinate, teprenone, indomethacine farnesil and dronabinol) or once usual delivery techniques like granulation or dissolved liquids in capsule do not improve the oral bioavailability [11].

1.2 Lipid based drug delivery systems

Lipids are basically a collection of physical molecules e.g. fats, sterols, waxes, fat soluble vitamins, mono, di, triglycerides and phospholipids. Lipids have many applications in food industry and in nanoformulations world. Lipids can be largely defined as lipophilic or amphiphilic molecules that let them to make small structures such as vesicles, uni and multilameller Liposomes. LBDD system consists of targeting the drug in a mixture of mono, di and tri-glycerides, oil soluble and water soluble surfactant and co-surfactant. As soon as a drug is targeted through the oil based nanoformulations, it remains in the soluble form all the way through its transportation in the GIT. The transportation of the drug through oil based system is improved because the dissolution step is to some extent evaded. A list of various lipid and oil based system is mentioned in table 1.1.

1.3 NANOEMULSIONS

Nanoemulsions are oil in water (o/w) emulsion with globule size between 50 to 500 nm. Typically, the normal globule size is stuck between 100 to 500 nm. Globules can exists as oil in water and water in oil, in which the center of the drop is either oil or water phase, respectively. These emulsions are generally made from emulsifiers accepted for human use and common food materials that are “Generally Recognized as Safe” (GRAS) by the Food and drug Administration (FDA). The surfactants are the compounds that lower the interfacial tension (or surface tension) linking the two immiscible liquids or a liquid and a solid part. Emulsifiers are generally crude substances with the property of both hydrophobic as well as hydrophilic groups in their structure (Figure 1.1). Therefore, an emulsifier contains both aqueous insoluble (oil soluble) and aqueous soluble components.

These nanoemulsions can be simply formulated in huge amounts by incorporating a oil phase with water soluble phase under elevated force or motorized extrusion method [13].

Table 1.1 List of various types of lipid based drug delivery systems [12]

Emulsions	Vesicular system	Lipid particulate system
Microemulsion	Liposomes	Lipospheres
Self nanoemulsifying drug delivery system (SNEDDS)	Niosomes	Solid lipid nano-particles
Nanoemulsion	Phytosomes	Solid lipid micro-particles
	Ethosomes	Nano-structured lipid carriers
	Micelles	Lipid drug conjugates
	Vesosomes	
	Transferosomes	
	Herbosomes	

Nanoemulsions are too known as miniemulsion, very-fine emulsions and sub-micron emulsions. Phase behavior studies of these nanoemulsions have revealed that the dimension of the globule is regulated by the structure of emulsifier part (bi-continuous microemulsion) at the turning point actuate by either high temperature or excipients mixture. The capability of these nanoemulsions to solubilize huge amount of lipophilic drugs along with their joint compatibility and capability to save the medicines from hydrolysis and enzymatic conditions build them perfect vehicles for oral drug delivery. Further, the regularity and dose regimen of injection can be condensed all through the drug treatment as these emulsions promises the discharge of drugs in controlled and sustained manner. Moreover, deficiency of the flocculation, creaming and sedimentation, in combination with a huge surface area offers advantages over emulsions of larger droplet size. Decreasing globule size to nano-scale results in extremely attractive physical properties such as optical transparency and un-usual elastic behavior. The major advantages of nanoemulsion as drug targeting carriers include improved drug encapsulation, enhanced drug solubility and bioavailability, decreased patient inconsistency, protection from enzymatic degradation and controlled drug release [14].

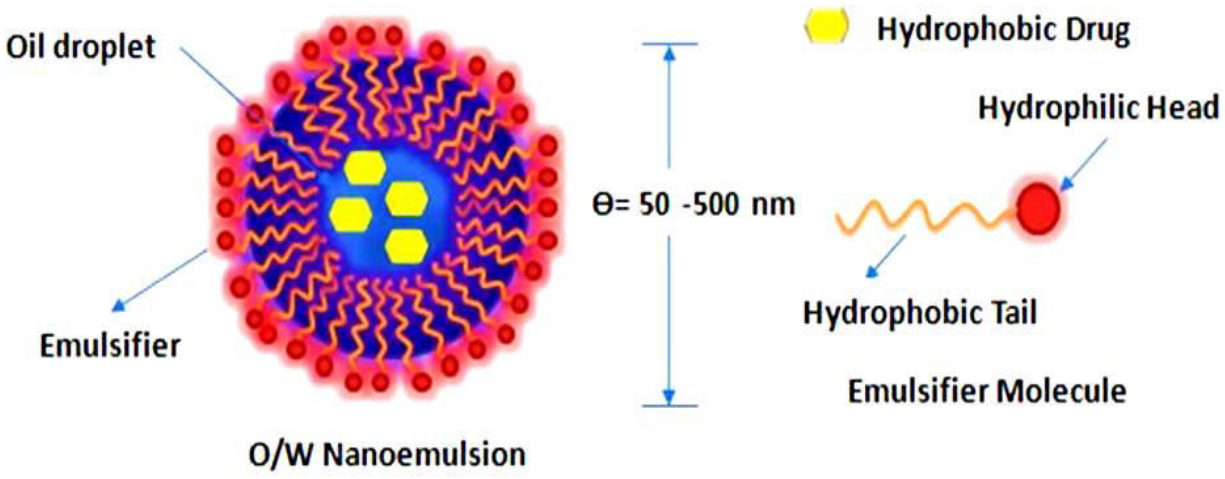

Figure 1.1 Oil in water (o/w) nanoemulsion showing structure of a surfactant, droplet diameter and incorporation of lipophilic drug

A bunch of methods are presented for improving the absorption of low aqueous-soluble drugs with the help of lipid-based systems. Thus, improvement in aqueous solubility in such case is an important aim to fruitfully prepare them into bioavailable dosage forms. A variety of new strategies are presently being formulated for efficient targeting of low aqueous soluble drugs, such as the synthesis of amorphous solid, nanoparticles, micro-emulsion, solid dispersions, melt extrusion, salt formation and synthesis of water-soluble complexes . Amongst all, the most accepted approach is the lipid-based formulation [15, 16]. Lipid-based formulations enhance the absorption by enhancing solubilization increasing gastric residence time, stimulating intestinal lymphatic transport, altering intestinal permeability, reduced action of efflux transporters and reduced metabolism .

1.3.1 Formation of Nanoemulsions

In comparison to micro-emulsion, relatively small is known about creating and controlling nanoemulsions. This is mainly because of intense shear has to be applied to overcome the effects of surface tension to break the oil droplets in to a nano-scale regime, which is beyond the capability of normal mixing devices [17]. Luckily, the development of high pressure homogenizers in the past 10 years makes it possible to explore nanoemulsions. Nanoemulsion shows exciting delivery properties ranging from lipophilic materials to flavors and visual properties ranging from opaque to nearly transparent, which drives growing research activity in nanoemulsion [18, 19, 20, 21].

Nanoemulsions are non-equilibrium systems and cannot form instinctively [22, 23]. Consequently, energy input from a mechanical device is required for the formation of nanoemulsions. As with the conventional emulsions, nanoemulsions are generally formulated by mixing an oil phase and aqueous phase together in the presence of water soluble emulsifier (i.e. surfactant). Under mechanical energy, the interface between the two phases is deformed to such extent that droplets forms and they are subsequently broken up or disrupted into smaller ones. The formation of conventional emulsions and the role of surfactant have been well documented [24]. On the other hand, a number of factors are responsible for the formation of stable nanoemulsions.

1.4 Self nanoemulsifying drug delivery system (SNEDDS)

Self nanoemulsifying drug delivery systems are nanoemulsions pre-concentrates or anhydrous form of nanoemulsion. These emulsions are isotropic mixture of oil, surfactant and co-surfactant and drug, which when mixed with aqueous phase under gentle agitation, spontaneously form oil in water (o/w) nanoemulsions (with particle size of less than 200 nm) [25]. In the human body the agitation required by the SNEDDS to form nanoemulsions is provided by the digestive motility of the GI tract and peristaltic movement of muscles. SNEDDS can also contain co-surfactant or co-solubilizer in order to facilitate nano-emulsification to improve the drug incorporation in the SNEDDS .

Compared to nanoemulsions with ready to use, SNEDDS can offers advantages such as:

- Better physical and chemical strength for longer period of time.
- Possibility of filling them in unit dosage form i.e. hard and soft gelatin capsules or hydroxypropylmethylcellulose (HPMC) capsule, which further improves their commercial utilizations and patient conformity.
- No palatability-related issues as SNEDDS can be filled into capsules .

1.4.1 Formulation considerations and potential components of SNEDDS and nanoemulsion

Successful formulation of SNEDDS depends on the systematic perceptive of spontaneous nanoemulsification process and also on physiological and biological properties of component used for the synthesis of SNEDDS. The various factors influencing the formation of self nanoemulsification are:

- The concentration of oil, surfactant and co-surfactant and physicochemical nature.
- The ratio of the component especially oil to surfactant ratio.
- The temperature and pH of aqueous phase where self emulsification occur.
- Physicochemical properties of drugs i.e. hydrophilicity, lipophilicity, polarity and pKa (Partition coefficient).

Apart from the above mentioned factors, Pouton et al. [26] also describes few factors that should be considered while selecting a lipid excipients; (a) regulatory issues-toxicity (b) solvent capacity (c) miscibility (d) morphology at room temperature (e) self dis-persibility (f) digestibility and fate of digested products (g) capsule compatibility (h) purity, chemical stability and cost. Various formulation aspects with respect to SNEDDS and nanoemulsions are discussed below.

1.4.1.1 Oil phase

The oil phase plays a critical role in the formation of nanoemulsion especially in SNEDDS as it is responsible for the solubilization of the drug and physiological properties of oils (e. g., molecular volume, structure, polarity and viscosity) governs the spontaneity of the self emulsification process, droplet size and biological fate of drug and nanoemulsion as well [27, 28, 29]. Usually the oil phase which has highest solubilizing capacity for drug is selected as an oil phase for the formation of nanoemulsion as well as SNEDDS. This further helps to achieve the maximum drug loading for the nanoemulsion and SNEDDS. At the same time, the chosen oil phase should be capable to yield nanoemulsions with small droplet diameter. Hence, the choice of oil phase is often a compromise between its capability to dissolve the drug and its capability to facilitate the formation of nanoemulsion with desired characteristics. It is known that oil with long hydrocarbon chains such as fixed oils (e.g. soybean oil) or long chain triglycerides are hard to nanoemulsifying, where as oils with moderate triglycerides chain and oils with short chain (or low molecular volume) are easy to nanoemulsifying in comparison to long chain triglycerides [30, 29]. The lipophilicity and concentration of oil phase are directly proportional to the nanoemulsion size .

Interestingly, long chain triglycerides have shown great ability to improve intestinal transport of drugs (by bypassing first pass metabolism) in comparison to medium chain tri, di and mono-glycerides [9, 31, 32]. On the other hand, medium chain mono and di

glycerides have higher solubilization potential for hydrophobic drugs [33]. Hence, it may be hard for an oil phase to have optimum properties with respect to nanoemulsification process and drug delivery. In certain cases, mixture of oil can also be used to meet optimum properties of the oil phase. For example, a mixture of fixed oil and medium chain triglycerides is used in certain cases to maintain a good balance between drug loading and emulsification process. Various oily component used for the preparation of SNEDDS and nanoemulsion are listed in Table 1.2

Table 1.2 Commonly used oil phases in SNEDDS and nanoemulsions [34]

General class	**Examples**	**Commercial name**	**Acceptability**
Fixed oils	Castor oil, soybean oil	_	P/O/T/Oc/M
MCTs	Triglycerides of capric/caprylic acid	Miglyol 810, 812, Labrafac CC, Captex 300, 355, 500	P/O/T/Oc/M
Medium chain mono and di-glycerides	mono and di-glycerides capric/caprylic acid	Capmul MCM, Imwitor 742, Akoline MCM	OT
Long chain mono-glycerides	Glyceryl monooleate/monolinoleate	Peceol, Capmul-GMO	OT
PG fatty acid esters	PG monocaprylate, monolaurate, dicaprylate	Capryol 90, Capmul PG-8, Miglyol 840, Captex 200	OT
Fatty acid esters	Ethyl oleate, isopropyl myristate and palmitate	Crodamol EO	P/O/T/Oc/M

Fatty acids	Oleic acid, caprylic acid	Crossential O94	O/T/M

MCT: Medium chain triglycerides; Oc: Ocular; P: Parenteral; M: Mucosal; PG: Propylene glycol; T: Topical; O: Oral.

1.4.1.2 Surfactant

Surfactants are surface active agent that reduces the surface tension at oil/water interface and stabilize the internal phase in an emulsion. The selection of surfactant is significant for the formulation of SNEDDS and nanoemulsions. The properties of the surfactant such as Hydrophilic Lipophilic Balance (HLB) (in oil), cloud point, viscosity and affinity towards the oil phase have great significance on the nanoemulsification process, self nanoemulsification region, droplet size and zeta potential of the nanoemulsion [15, 25, 35]. The concentration of surfactant in the nanoemulsions and SNEDDS has great influence on the droplet size and zeta potential of the nanoemulsion [15]. The acceptability of the selected surfactant for the preferred route of administration and its regulatory status (e.g., generally regarded as safe [GRAS] status) must be considered during the selection of a surfactant. It should be noted that surfactant have favorable or unfavorable biological effects depending upon the chemical nature and concentration .

Many non-ionic surfactants, such as Cremophor EL, polyethylene glycol (PEG) have the ability to enhance the intestinal permeability of the drugs that are susceptible to P-glycoprotein mediated efflux mechanism [36, 37, 38]. However, these surfactants have concentration, route of administration and structure dependent side effects; for example Cremophor EL can be responsible for anaphylactic shock on parenteral administration [38], whereas, on oral administration it is well tolerated [31]. Non-ionic surfactants are with high hydrophilicity are commonly used in the formulation of SNEDDS. Proper selection of surfactant is based on its HLB value and its safe consideration. A surfactant with HLB value of more than 12 is necessary for the formulation of SNEDDS to form a fine o/w nanoemulsion when diluted with distilled water or when dispersed in the GI fluid. Polyethoxylated lipid derivatives are usually used surfactants in the lipid based drug delivery. These lipids can be fatty acids, alcohols or glycerides which are linked to a number of repeating polyethylene oxide units through ester linkage (fatty acid and glycerides) and either linkage (alcohol). The polyethylene provide hydrophilic characteristics to the surfactant for example Polyethoxylated fatty acid ester (Myri and

Solutol HS 15), Polyethoxylated alkyl ethers (Brij), Polyethoxylated sorbitan esters (Tweens) and Polyethoxylated glycerides (Cremophor and Labrasol) [39]. Tweens, Cremophor and Labrasol are the most commonly used surfactant in the SNEDDS. Surfactants of natural origin are mostly preferred due to safety considerations but are not widely used to their poor self emulsification properties [40]. Non-ionic surfactant are less toxic and possess good emulsion stability over wider range of ionic strength and pH than that of ionic surfactant [41], but may also cause changes in intestinal permeability. To prevent the gastric irritation least possible surfactant concentration should be used. The necessary concentration to form stable SNEDDS ranges from 30% w/w to 60% w/w [42]. The surfactant used being amphiphilic and can dissolve large quantity of hydrophobic drug. They can contribute in the total solubility of drugs and thus prevent drug precipitation upon aqueous dilution and keeps the drug in solubilized state in the GI tract for further absorption and permeation [43]. Table 1.3 lists different classes of surfactants with commercial names and their acceptability for oral, parenteral and dermal routes [44, 45].

Table 1.3 Commonly used surfactants in SNEDDS and nanoemulsions [34]

General class	**Examples**	**Commercial name**	**Acceptability**
Polysorbates	POE-20-sorbitan monooleate POE-20-sorbitan monolaurate	Tween® 80,Crillet 4 Tween® 20, Crillet 1	P/O/T/Oc/M
Sorbitan esters	Sorbitan monooleate Sorbitan monolaurate	Span ® 80, Crill 4 Span 20, Crill 1 Span 60, Crill 3	P/O/T/Oc/M P/O/T/Oc/M O/T/M
PEO-PPO-block copolymers	Poloxamer 188, Poloxamer 407	Pluronic F 68, Pluronic F 127	P/O/T/Oc/M O/T/Oc/M
POE castor oil	POE-35-castor oil	Cremophor ® EL,	P/O/T/Oc/M

Polyglycolyzed glycerides	Linoleoyl macrogol glycerides, Oleoyl macrogol glycerides	Labrafil ® 2125CS, Labrafil 1944CS	O/T O/T
Phospholipids	Soybean lecithin		All routes
Sucrose esters	Sucrose laurate Sucrose palmitate		O/T O/T

Oc: Ocular; P: Parenteral; M: Mucosal; PG: Propylene glycol; T: Topical; O: Oral; PEG: Polyethylene glycol; POE: Polyoxyethylene.

1.4.1.2.1 Classification of surfactants

Most commonly surfactants are classified according to their hydrophilic head groups.

(a) Anionic surfactants carry a negative charge at their head such as sulfate, sulfonate, carboxylate and phosphate. e.g. Docusate (dioctyl sodium silfosuccnate), perfluorooctanessulfonate (PFOS), alkyl ether phosphate and alkyl-aryl ether phosphates.

(b) Cationic surfactants carry a positive charge at their head e.g. Cetrimonium bromide (CTAB), Cetylpyridinium chloride (CPC) and Benzalkonium chloride (BAC).

(c) Nonionic surfactants are uncharged. Prominent among these are fatty alcohol, stearyl alcohol, cetyl alcohol and cetostearyl alcohol. e.g. Polyoxyethylene glycol, sorbitan alkyl esters: spans

(d) Zwitterionic surfactants have both cationic and anionic centers linked to the same molecule. The cationic part contains primary, secondary and tertiary amines or quaternary ammonium cations . e.g. phospholipids phosphatidylserine, phopshatidylethanolamine and sphingomyelins

1.4.1.2.2 Hydrophilic lipophilic balance (HLB)

HLB value of a surfactant is an empirical expression of its hydrophilic and lipophilic groups. The HLB system is typically useful to identify the surfactants for oil and water emulsifications . Basically there are two type of emulsions

- Water in oil (w/o): in which water is dispersed in oil phase and requires low HLB value.

- Oil in water (o/w): in which oil is dispersed in water phase and requires high HLB value .

Surfactant selection for an o/w emulsion can be easy if HLB system is applied. Oils have HLB numbers that identify the HLB value necessary to give good o/w emulsification. Table 1.4 below gives the list of HLB values along with their typical properties .

Table 1.4 List of various HLB values and their properties

HLB value	Properties
<10	Lipid soluble (water insoluble)
>10	Water soluble (lipid insoluble)
1.5 to 3	Anti-foaming agents
3 to 6	w/o (water in oil) emulsifier
7 to 9	Wetting and spreading agents
13 to 15	Detergents
12 to 16	o/w (oil in water) emulsifier
15 to 18	Solubiliser or hydrotrope

1.4.1.3 Co-surfactant or co-solubilizer

Water soluble co-surfactants are generally used for the preparation of SNEDDS, nanoemulsions or lipid based drug delivery systems. Ethanol, polyethylene glycol (PEG), glycerol and propylene glycol are examples of co-surfactant used. The main role of the co-surfactant is to increase the solvent capacity of the drugs which are freely soluble in them. Table 1.5 illustrates commonly used co-surfactants. They can be incorporated in the SNEDDS or nanoemulsions for the following purposes :

- To increase the drug loading in the SNEDDS and nanoemulsions
- To amend the self nanoemulsification time of the SNEDDS
- To amend the droplet size of nanoemulsion

Therefore, surfactant (hydrophilic or lipophilic) or amphiphilic solubilizer with pharmaceutical tolerability are used for this purpose. The incorporation of co-surfactant in the SNEDDS may result in expanding self-nanoemulsification region in the phase diagram. Nepal et al. [46] evaluated the potential of Lauroglycol^{TM} FCC (propylene

glycol dilaurate; HLB 4) as a co-surfactant in the SNEDDS. In certain cases short chain alcohols, such as ethanol have also been used [47]. However, these co-solubilizer increase drug loading in the SNEDDS and nanoemulsion, they might compromise with droplet diameter of the nanoemulsion in certain cases, as reported by Anton and Vandamme [29].

Table 1.5 Commonly used co-surfactants in SNEDDS and nanoemulsions [34]

General class	Examples	Acceptability
Short-chain alcohols	Ethanol, benzyl alcohol	P/O/T/Oc/M
Alkane diols and triols	Propylene glycol Glycerol	P/O/T/Oc/M P/O/T/Oc/M
Polyethylene glycols	PEG 400	P/O/T/Oc/M
Glycol ethers	Diethylene glycol monoethyl ether (Transcutol®)	O/T

1.4.1.4 Aqueous phase

The droplet size and stability of nanoemulsions are influenced by the nature of aqueous phase. Hence, pH and ionic strength of aqueous phase should be given much importance while designing the SNEDDS and nanoemulsions. The physiological environment has diverse pH ranges varying from pH 1.2 (stomach pH) to 7.4 and greater (pH of blood and intestine). In addition, the presence of various ions in the physiological environment can also have significant effect on the properties of nanoemulsions synthesized from SNEDDS. It is well-known that electrolytes can modulate the characteristics of nanoemulsion such as droplet size, zeta potential and physical stability [48]. Hence, it is necessary to evaluate the self-nanoemulsification of the SNEDDS and the properties of the resultant nanoemulsion in the aqueous phase with varying pH and/or electrolyte concentration. In addition to distilled water, phosphate buffer saline, Ringers solution, simulated gastric fluid (pH 1.2), intestinal fluid (pH 6.8) can also be used as aqueous phase to evaluate spontaneous nanoemulsification region of SNEDDS .

1.4.2 Mechanism of Self-emulsification

According to Reiss et al. [49] self emulsification occurs when the entropy change that favors dispersion is more than the energy required to increase the surface area of the dispersion. The free energy is the direct function of the energy required to create a new surface tension between the two phases and can be described by the equation

$$\Delta G = \sum Ni\pi r2\sigma$$

Where ΔG, the free energy associated with the process, N is the number of droplets having radius r and σ represents the interfacial energy. Emulsification process occurs spontaneously with SNEDDS because the energy required to from emulsion is either low or positive or negative. It is essential for the interfacial to show no conflict against surface shearing in order for emulsification to take place [40, 50]. The interface between the oil and aqueous phases is formed upon addition of binary mixture (i.e. oil/non-ionic surfactant) to the water. Thus, subsequent mild agitation of the self-emulsifying system, water will rapidly penetrate into the aqueous cores and leads to droplet formation .

1.4.3 Physiochemical characterization of nanoemulsions and SNEDDS

Nanoemulsions have several interesting physical properties that differentiate them from the usual micro-scale emulsions. Micro-scale emulsions typically exhibits strong and multiple scattering in the visible light and as a result has white appearance. The multiple scattering occur due to refraction of light from the droplets, films and thus provide a significant refractive index between the dispersed and continuous phase. Nanoemulsions may lose their transparency with respect to time as a result of increase in the droplet diameter. Nanoemulsions have a much larger surface area to volume ratio than that of ordinary emulsions, so the concentration of surfactant required to stabilize them is larger than for micro-scale emulsions. Different physiochemical parameters for nanoemulsion are discussed below .

1.4.3.1 Morphology of nanoemulsion

The morphology of nanoemulsion as well as SNEDDS can be determined by transmission electron microscopy (TEM) and scanning electron microscopy (SEM) [51]. SEM gives a three dimensional image of droplet. The nanoemulsion samples are examined at suitable accelerating voltage, normally at 20 kV and at different

magnifications. In TEM, high resolution images of disperse phase can be obtained. Firstly, the samples of dispersed phase is negatively stained with 1% aqueous solution of phosphotungstic acid or by 2 % uranyl acetate solution on to a 200 μm mesh size Pioloform coated grid and examined under TEM .

1.4.3.2 Nanoemulsion droplet size, zeta potential and polydispersity index

Dynamic light scattering (DLS) or Photon Correlation Spectroscopy (PCS) is used to record the fluctuations in the intensity of scattering by droplets/particles due to Brownian motions. The above parameters i.e. droplet size, zeta potential and polydispersity index can be analyzed using particle size analyzer [52]. The polydispersity index indicates the quality and homogeneity of the dispersion. Laser diffraction is another technique for measuring the particle size. The fundamental particle size distribution derived by this technique is volume based and is expressed in terms of volume of equivalent spheres .

1.4.3.3 Viscosity determination

Viscosity of nanoemulsion is calculated using a viscometer. The viscosity of a nanoemulsion is a function of the surfactant, water, oil and their concentration. Increase in the water content results in decrease in the viscosity, while if we decrease the concentration of surfactant and co-surfactant, interfacial tension increases between oil and water phase which further increases viscosity. Measurement of viscosity is an important parameter for the stability and efficient drug release profile. Various instruments and methods are available for the measurement of rheological properties of nanoemulsion carriers .

1.4.3.4 Thermodynamic stability and surface properties

Although the physical appearance of a nanoemulsion is same as that of microemulsion, in both the cases the formulation may be transparent with low viscosity [53]. A nanoemulsion is kinetically stable (possess higher stability against sedimentation and creaming than microemulsion due to smaller particle size) while microemulsion are thermodynamically stable.

1.4.4 Plants as a source for the delivery of phytochemicals constituents

For the past 10 to 20 years, natural phytochemicals are bagging great attention from clinician due to their huge number of actions. Natural phytochemicals have demonstrated potential role in the prevention and management of various diseases such as cancer, diabetes, hepatitis and arthritis. Recently, many research based pharmaceutical companies and even WHO encourages use of medicinal herbs of natural origin because chronic disease requires long term therapy, and using synthetic drugs in that case may cause dubious adverse effects. Herbal extracts are now a days one of the most widely used medicines due to their ease of availability and low production cost. During 2001-2010, 34 herbal based drugs were approved by Food and Drug Administration (FDA) and around 100 new products are under clinical trials, showing the importance of herbal products in drug development [54]. The majority of phytochemicals suffer from problems such as poor water solubility, low bioavailability, gastric instability and hepatic metabolism which further limit their use in the clinic. As mentioned previously, oil base nanoemulsions can significantly improve the oral bioavailability as well as therapeutic efficacy of several natural phytochemicals such as natural antioxidants, tri-terpenoids, essential oils, alkaloids, carotenoids and hepatoprotective agents . Based on the clinical importance, therapeutic efficacy and solubility in the oil phase *Berberis aristata* and *Tinospora cordifolia* were selected as a plant source for the delivery of berberine and other phenolic components.

1.4.4.1 *Berberis aristata*

Berberis aristata (BA) Linn. is an important medicinal plant belonging to family Berberidaceae.BA is also known as “Daruhaldi and Rasaut” and widely distributed from Himalaya to Sri-lanka, Bhutan and hilly areas of Nepal. The word “Rasaut” used is an ayurvedic preparation prepared using the yellow roots of this plant. The plant is a valuable medicine used for the treatment of many diseases such as diabetes, remittent fevers, oxidative stress and also as a tonic remedy for liver and heart. Berberis is a genus of spiny deciduous evergreen shrubs ranging from 2 to 3 meters in height; the bark of the plant is yellow to brown from outside and dark yellow from inside. The plant contains berberine (Figure 1.2), oxycanthine, taximaline, oxyberberine, pseudo-berberine chloride, pseudo-palmitine, berbamine and palmatine as major chemical components among which berberine exhibit multiple pharmacological activities. It has antifungal, hypotensive, wound healing, skin diseases, jaundice, immune-stimulating, anti-inflammatory, antimicrobial, anti-protozoal, anti-cholinergic and anti-arrhythmic [55].

Taxonomical classification

Kingdom: Plantae
Division: Magnoliophyta
Class: Magnoliopsida
Order: Ranunculales
Family: Berberidaceae
Genus: Berberis
Species: *aristata*

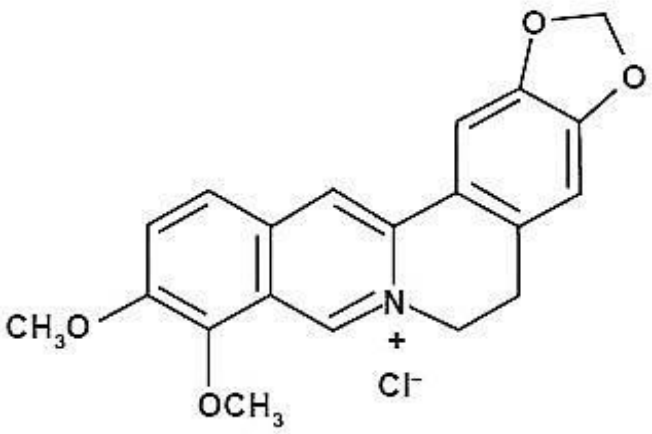

Figure 1.2 Chemical structure of Berberine

1.4.4.2 *Tinospora cordifolia*

Tinospora cordifolia (TC) is an important drug or phytochemical of Ayurvedic System of Medicine (ASM) belonging to family Menispermaceae and found many classical importance in the treatment of diseases such as jaundice, fever, diabetes and skin diseases etc. TC is also known as "Amrita" or "Guduchi" and beneficial for numerous chemicals, pharmacological, preclinical and clinical investigations. The term "Amrita" is used for TC extract of its capability to convey youthfulness, vitality and longevity to its patron.

The plant contains tinosporine, choline, berberine (Figure 1.2), palmatine and β-sitosterol as major chemical components among which berberine and tinosporine exhibit multiple pharmacological activities. It has anticancer/anti-tumor, anti-diabetic/hypoglycemic, anti-oxidant, anti-inflammatory, anti-stress, anti-ulcer, digestive, hypolipidaemic, wound healing, skin diseases, jaundice, liver disorders and urinary infections.

Taxonomical classification

Kingdom	Plantae
Order:	Ranunculales
Family:	Menispermaceae
Genus:	Tinospora
Species:	*cordifolia*

1.4.5 Factor affecting oral bioavailability of phytochemicals

- **Dissolution rate-limiting absorption:** It has been known that approximately 40% of the existing therapeutic agents have poor solubility in the physiological environment. These therapeutics agents belong to BCS class II and IV. The poor dissolution property of these compounds is responsible for poor absorption from the GI tract. The compound used for the synthesis of SNEDDS has a very high dissolution property as compared to the pure drug or phytochemicals. Furthermore, SNEDDS spontaneously present the drug in very fine nano-droplets offering very high surface area for absorption. This helps in the quick absorption and improves the oral bioavailability of the drugs .
- **Poor permeability:** Poor permeability is also one of the major factors that is responsible for the low oral bioavailability of the several drugs including phytochemicals. Owing to poor permeability such drugs and phytochemicals have to be administered at significantly higher doses. Interestingly, several SNEDDS components have the capability to enhance the membrane permeation of the therapeutic agents. For example oily phases (e.g., oleic acid, propylene glycol, monoglycerides of caprylic acid and), surfactants (e.g., Labrasol® and Polysorbate 80) and co-surfactant (e.g., PEG 400, Transcutol and alcohol) are known to have permeation enhancement property [33, 56, 57]. Bruesewitz et al. [58] in his study evaluated the role of Poloxamer based nanoemulsions on Caco-2 cell permeability of various drugs such as Metoprolol (BCS class I), Atenolol (BCS class III) and Danazol (BCS class II). Interestingly, they observed a significant increase in Caco-2 cell permeability by nanoemulsion without causing any damage of toxicity to the Caco-2 cells .

- **High degree of hepatic first pass metabolism:** Oral bioavailability of a huge number of molecules, such as antihypertensive and cardiovascular agents [β-blocker, calcium channel blockers and angiotensin-converting enzyme (AGE's)], anti-hyperlipidimic agents (3-hydroxy-3-methylglutaryl-CoA reductase inhibitors), antidiabetic agents (repaglinide) and antibiotics (e.g. Cephalosporin's) is restricted by presystemic hepatic metabolism. Several SNEDDS components including Gelucire® 44/14 and Labrasol have the capability to change/inhibit activity of cytochrome P450 and gut metabolizing enzymes [59, 60]. Both of the mechanism are responsible for reducing or preventing the first pass hepatic metabolism and thus improve oral bioavailability .
- **P-glycoprotein efflux mechanism:** The P-glycoprotein is an efflux pump present at the several sites and tissue of the body, including the GI tract. P-glycoprotein prevents the entry of the drugs to the systemic circulation, thus decrease the oral bioavailability of the drugs. Many surfactants (e.g., vitamin E TPGS, Solutol® HS 15, Labrasol, Cremophor EL, Polysorbate 80) and oily phases (e.g., Imwitor® 742, Akoline MCM® i.e. mono and di-glycerides of caprylic acid and Peceol®) have the potential to inhibit the P-gp efflux process and thus improves the oral bioavailability of drugs [15, 61]. Table 1.6 lists various natural, pharmaceutical formulation approaches and pharmaceutical excipients as P-gp inhibitions .

Table 1.6 List of various natural, pharmaceutical formulation approaches and pharmaceutical excipients as P-gp inhibitions [62]

Inhibitory strategy	Examples
Natural products as P-gp inhibitors	
Glycosides	Picroside II, Acetoside
Curcumin	*Curcuma longa*
Ginsenosides	Ginseng
Piperine	*Piper nigrum*
Flavanoids	Diosmin, Quercetin, Gingko, Naringin, Biochannin, Silymarin
Terpenoids	Citronellal, β-citronellol
Pharmaceutical formulation approaches	Nanogels, Nanoparticles,

Polymer formulation Lipid formulations	Microparticles and Microspheres Micelles, Liposomes, Niosomes, SNEDDS, Nanoemulsions and Phytosomes
Pharmaceutical excipients as P-gp inhibitors Surfactant and solvents Polymer Lipid excipients Thiomers	 Tween 20, Tween 80, Cremophores, Pluronic F68 Poly-(ethylene-oxide), poly-(propylene-oxide) Peceol and Gelucire Chitosan-thiobutylamidine (Chito-TBA)

1.4.6 Strategies for improving the therapeutic property and oral bioavailability of berberine

In order to improve the oral bioavailability of berberine , researchers have made numerous efforts. To reach a significant plasma level of berberine, certain strategies have been applied.

1. Designing of novel lipid based drug delivery system that will bypass efflux mechanism and hepatic metabolism.
2. Administration of P-gp inhibitors in the formulations

The first and second technology is easily feasible due to advances in novel lipid and polymer based technology. Fortunately, certain lipids and surfactants used in lipid based formulation have the ability to inhibit P-gp mediated efflux mechanism and P-gp inhibitors [63]. Therefore co-administration of drugs as well as herbal extracts with suitable pharmaceutical excipients (P-gp inhibitors) in optimized concentration can be used to improve the intestinal permeability and the targeting of drug to a particular site .

1.4.7 Role of nanoemulsion and SNEDDS in improving oral delivery and absorption of phytochemicals through lymphatic system

In this era, natural phytochemicals are being given attention by clinicians due to their huge number of actions. The majority of phytochemicals suffer from problems such as

poor water solubility and metabolic stability which further limits their use. As mentioned previously, NEs and SNEDDS can be an attractive approach for the drugs with poor aqueous solubility and metabolic stability .

1.4.7.1 Outline of intestinal lymphatic drug transport

The lymphatic system exists in all the parts of human body except the central nervous system (CNS). The major parts of the system are the spleen, bone marrow, lymph nodes, thymus gland. Other organs, including the heart, lungs, intestines, liver and skin also contains the lymphatic tissue. This system is ultimately responsible for the transport of the lymph (i.e. clear watery fluid). Throughout the whole body, lymph distributes lymphocyte cells and various others immune related factors. Functionally lymphocyte immune cells are important as they protect the body against antigens that attack the body such as viruses and bacteria. While lymphatic system is thought to be the drainage system that actually collects the drainage fluid from the cells and tissue to later return the fluid back to the circulatory system. The role of lymphatic system in the fat absorption and transportation is also a main functional component of the lymphatic system. With respect to the intestinal absorption and transportation of lipids, the ducts of the lymphatic system that interconnected lymph organs are also important in providing transportation for the proteins, fats and other substances in the lymph. Transport typically started with blind-ended vessels found in tissue (i.e. lymph capillaries) creates a capillary system in which lymph is drained. The lymph capillaries are extremely permeable and are not pressurized allowing the lymph fluid to exhaust easily from the tissue into the lymph capillaries. The lymph vessel forms a network throughout the body and overall this lymphatic system functions in unidirectional manner in which lymph is drained from the tissue and is returned to the systemic blood .

1.4.7.2 Lipid digestion and drug absorption via intestinal lymphatic system

The intestinal lymphatic system is a pathway through which food-derived lipids; fat soluble vitamins and lipophilic peptide like molecules are transported into the systemic circulation. Drug transported via the lymphatic system bypass the liver and thus avoid first pass hepatic metabolism. The mechanism by which various lipophilic drugs are transported via lymphatic system following oral administration are complex, but are simplified as follow. Firstly, the typical intestinal tract is richly supplied with both lymph

and blood because the lamina propia that covers the enterocytes is in close proximity with blood and lymph vessels .

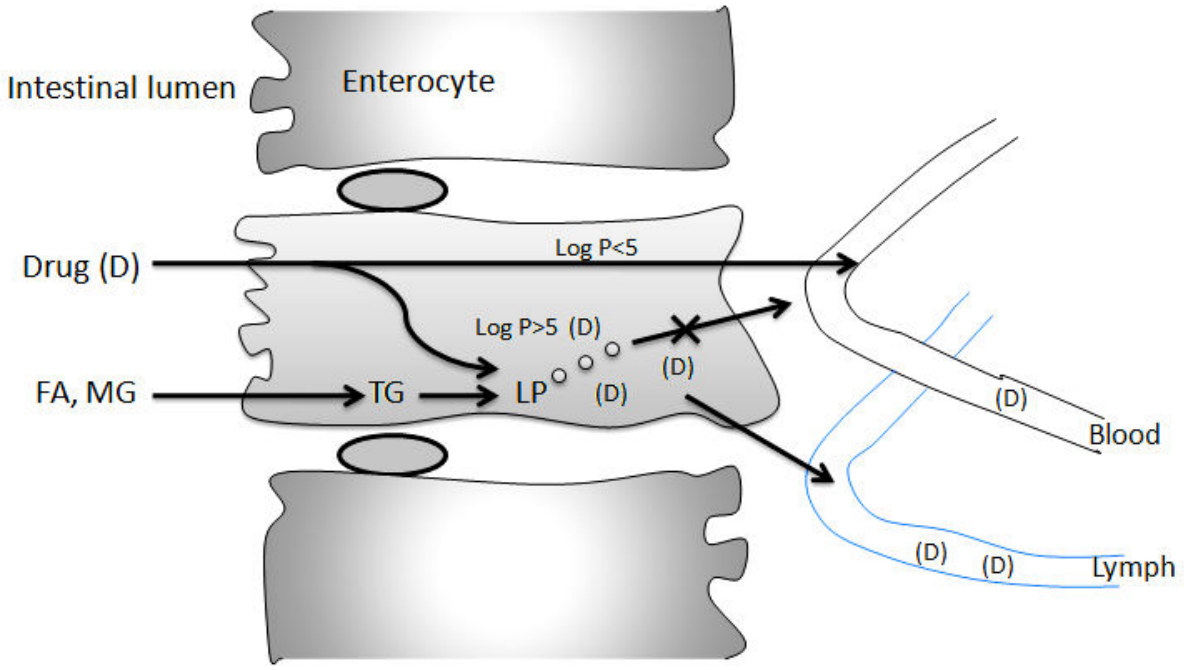

Figure 1.3 Drug absorption via intestinal lymphatic system and portal vein; FA = Fatty acid, MG = Monoglycerides, TG = Triglycerides, LP = Lipoproteins, D= Drug [64]

After being absorbed across the enterocytes, two potential pathways can occur. The first situation is where drugs prefer entry into the blood capillaries and second situation where drugs enter the lymph capillaries is favored. The first condition includes the absorption of the drugs into portal blood, is more common mechanism because of higher rate of fluid flow in the portal blood as compared to that of intestinal fluid (500-fold higher for the portal blood) [65]. High molecular weight drugs have limited or unable to diffuse across the blood capillaries; thus utilize the permeable lymphatic capillaries for absorption. Furthermore, the lipoprotein size limits that diffusion and the remaining unhindered diffusion across the lymphatic capillaries results in preferential access of lipoproteins along with the drug to the lymphatic's (Figure 1.3).

Once the lipid has been absorbed into the enterocytes, its chain length calculates its subsequent intracellular processing. Short and medium chain lipids ($C_{<12}$) generally diffuse across the enterocytes, while long chain triglycerides (TG) ($C_{>12}$) generally migrate to the endoplasmic reticulum (ER), where they are re-acylated and assembled into lipoproteins before secretion into the mesenteric lymph [66, 67]. It has been reported

that short/medium chain fatty acid (FA) and monoglycerides (MG) are directly transported to the systemic circulations. Long chain FA and MG are converted into phospholipids and apo-proteins to form lipoproteins [i.e. chylomicron and very low density lipoproteins (VLDL)] through glycerol-3-phosphate pathway [68, 69]. Furthermore, the chylomirons are released into the intercellular space by exocytosis in the form of lymph. Finally, the lymph enters the systemic circulation at the junction of left jugular and left subclavian veins thus avoiding first pass hepatic metabolism .

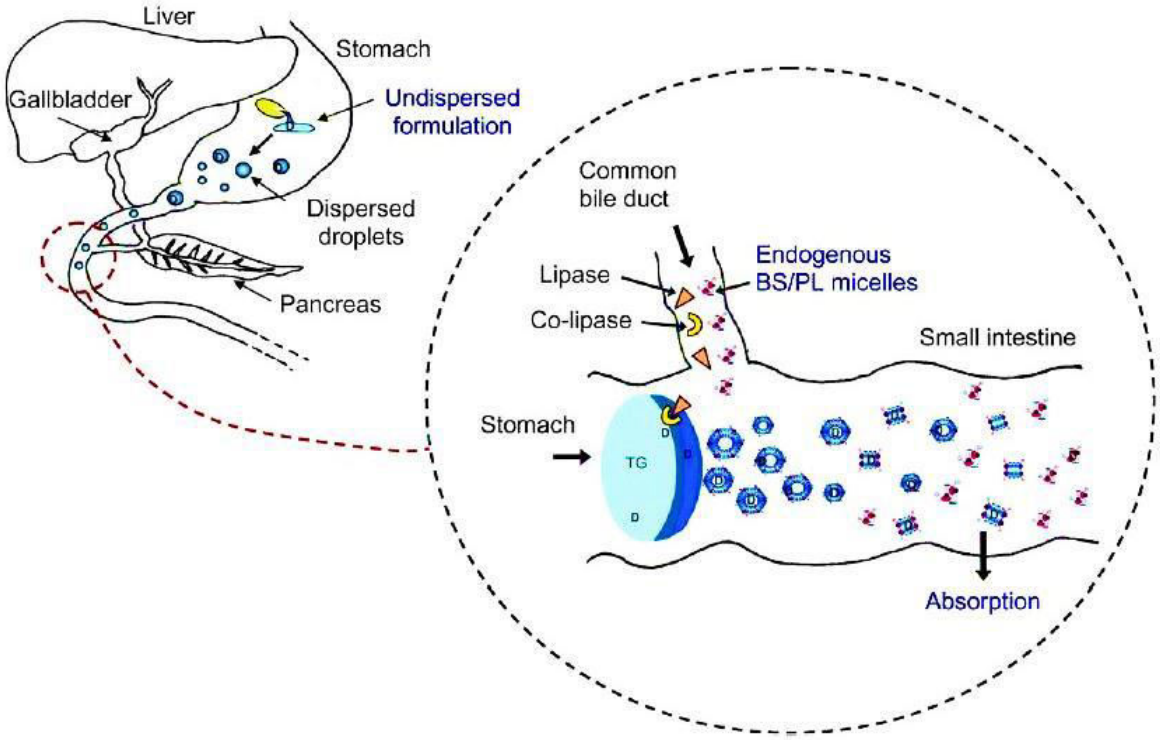

Figure 1.4 Lipid digestion and drug solubilization in the small intestine from lipid based dosage form [70]

Figure 1.4 showed that during the ingestion of NEs and SNEDDS, the formulation initially dispersed in the stomach where the digestion of exogenous lipid is initiated by gastric lipase. Shear in the stomach helps in emulsification of the formulation before emptying into the duodenum. Inside the small intestine, pancreatic lipase together with its co-factor i.e. co-lipase completes the breakdown of its dietary glycerides to di-glycerides (DG), MG and FA (represented by different degree of shading on the surface of lipid droplet). In the presence of raised concentration of bile salts (BS), the products of lipid breakdown are then included into a series of colloidal structures including multilameller

and unilammelar vesicles and micelles. Together all these molecules expand the solubilization capacity of the small intestine for both lipid digestion and drugs [70].

1.4.8 Current status of nanoemulsions and SNEDDS in herbal drug delivery systems

Mahdi and coworkers conducted studies on the formation of palm kernel oil esters (PKOEs) based nanoemulsion loaded with *Phyllanthus urinaria* extract using spontaneous emulsification method [71]. The particle diameter, drug release profile study and antioxidant activity of extract released from nanoemulsion were of the interest. The prepared *P. urinaria* extract loaded nanoemulsions was further evaluated for particle size, zeta potential, release profile, antioxidant activity and rheological behavior. Results showed that the nanoemulsions were obtained with a smallest size of 30.74 nm. From the drug release profile study it was found that around 51.30 % and 51.02 % of the loaded extract was released from two different formulations using an artificial cellulose membrane, which further scavenge 29.89 % and 30.05 % of DPPPH radicals, respectively.

Quintao et al. [72] reported on *Vellozia squamata* nanoemulsion by using phase inversion method. The prepared nanoemulsions loaded with hydro-alcoholic extract of *V. squamata* were evaluated for the accelerated stability test, followed by its release profile and antioxidant activity of the extract using DPPH assay. Results of prepared extract loaded nanoemulsions showed a potential application of hydro-alcoholic extract from *V. squamata* in the development of products with antioxidant properties and demonstrate a promising pharmaceutical product.

Jafari et al. [73] conducted study on the synthesis of d-limonene nanoemulsions using Ultrasonication and micro-fluidization method. Whey protein concentrate (WPI) and modified starch (HI-Cap®) were selected as emulsifiers . The results of prepared nanoemulsions showed that both Micro-fluidization and Ultrasonication were capable of producing nanoemulsion with mean droplet diameter (MDD) within the range of 150 to 700 nm. The MDD decreased initially with increasing pressure and number of passes through micro-fluidizer; however, the emulsions become over processed when pressure was above a critical point .

Butnariu and Giuchici [74] reported use of lycopene extract loaded nanoemulsions in the skin protective mechanism against UVA radiation. The prepared nanoemulsions were than evaluated for particle size distribution, zeta potential, FTIR studies, drug release studies and *in-vitro* anti-inflammatory activity. The experimental system offered a sustained release of the extract for eight hours. It was also found that extract loaded nanoemulsion proved a better therapeutic efficiency as compared to that of standard solution, they also provide a better therapeutic efficiency coupled with extended time interval of tested parameters (24 hrs). Based on preliminary examination of tissues and local application of extract loaded nanoemulsion, it was found that NEs did not irritate and has a high potential both regarding its efficiency (i.e. analgesic effect) and therapeutic safety .

Recently, Chaiittianan and Sripanidkulchai [75] formulated a nanoemulsion loaded with *Phyllanthus emblica* branch extract using high pressure homogenization technique. The HPLC analysis of *P. emblica* extract indicated several phenolic compounds including gallic acid, vanillic acid, epigallocatechin (EGC), epigallocatechin gallate (EGCG) and ellagic acid. The results of optimized nanoemulsion showed that the NEs has a median particle size of 191.63±4.07 nm, a zeta potential of 10.19±0.54 mV, high entrapment efficiency of 67.99±0.87 % and good stability at 4 ºC after 90 days . The extract loaded NE showed a slower release of active constituents than that of *P. emblica* solution.

In the last two years, extensive work on curcumin NEs was conducted with a focus to improve the oral bioavailability of curcumin [76, 77, 78, 79]. NEs with medium chain triglyceride (MCT) as oil and Tween 20 as surfactant were successfully prepared with MDD ranging from 618 nm to 795 nm. MCT, Tween 20, and water were mixed at a ratio 10/10/80 and homogenized under a pressure ranging from 500 bar to 1500 bar. The results showed that multiple passes and higher pressures generated smaller droplets of nanoemulsions and thus results in higher bioavailability of curcumin .

Recently, the formation of β-carotene nanoemulsions by using high pressure homogenization has been investigated [80, 81, 82, 83]. Modified starches, whey protein isolate (WPI), Tween 20 and mixture of Tween 20 and WPI were experienced to stabilize NEs. The results showed that NEs stabilized with Tween 20 had the smallest droplet size of 132 nm, while NEs stabilized with a mixture of WPI and Tween 20 were nearly all stable. In addition, response surface methodology was used to optimize the formation of

NEs. In the trial, 10% w/w MCT was used as a vehicle and Tween 20 as surfactant. The optimum preparation conditions were suggested to be: pressure 129 MPa, homogenization temperature 47 °C, load of β-carotene 0.82%, and Tween 20 8.2% .

Li and co-workers [84] in his study developed SNEDDS of *Diospyros kaki* leaf extract and characterize to compare its *in-vitro* dissolution and bioavailability profile with marketed tablets (Naoxinqing tablets). The formulation of extract loaded SNEDDS was optimized by an extreme vertices design. The optimized NEs were found to be stable for six month after storing at 40°C, 25°C, 4°C with a drug loading of 44.48 mg/g of total flavanoids. On dilution with water, the SNEDDS droplet size and zeta potential was found to be 34.85 nm and -6.18 mV. In comparison to commercial tablets, the area under curve (AUC) of both quercetin and kaempferol, which are active flavanoids of extract, was increased by 1.5-fold and 1.6-fold respectively .

Overall, the above references gives clear information that Ultrasonication and small molecule surfactants, such as tweens, span and PEG, is a relatively simple and effective method of producing extract loaded nanoemulsions under the proper conditions. The primary focus of previous studies has been the formation of nanoemulsions, while research on the long term stability of nanoemulsions is rare due to the difficulty of preventing Ostwald ripening. The primary application of NEs has been to improve the bioavailability of encapsulated lipophilic actives in nanoemulsions. There has been little work on the enhanced intestinal permeability and physical properties of nanoemulsions (e.g., improved stability and optical transparency). Table 1.7 showed some of the phytochemicals based nanoemulsions with their primary application of formulations .

Table 1.7 Phytochemicals based nanoemulsions and SNEDDS with their primary application of formulations [85]

Formulations	Active ingredients	Application of NE formulation	Method of preparation	Droplet size	Drug loading	Route of administration
SNEDDS Zedoary essential oil	Zedoary turmeric oil	Improved stability, aqueous dis-persibility	Drawing ternary phase diagram	68.3 ± 1.6 nm	30 %	Oral
Triptolide microemulsion	Triptolide	Enhanced penetration through stratum corneum	High pressure homogenization method	<100 nm	_	Topical
Docetaxel submicron emulsion	Docetaxel	Improved residence time	High pressure homogenization method	166 nm	90 %	Intravenous
Berberine NEs	Berberine	Improved residence time	Drawing ternary phase diagram	56.80 nm	0.50 %	Oral
Quercetin microemulsion	Quercetin	Enhanced penetration through corneum	High speed homogenization method	10 - 100nm	_	Topical
Silybin NEs	Silybin	Sustained release	Emulsification method	21.20 nm	0.3% solution	Intramuscular

1.5 Hydrogels

Hydrogels are three dimensional networks composed of hydrophilic polymers, held together via physical intermolecular attractions or cross-linked through covalent bonds. The existence of hydrogels dates back to 1960, when Wichterle and Lim [86] first proposed the use of hydrophilic network of poly (2-hydroxyethl methacrylate) (PHEMA) in contact lenses. Since then, the use of hydrogels has been extended in the biomedical and drug delivery applications [87, 88]. In comparison to other synthetic biomaterials hydrogels look like living tissues due to their close physical properties (because of high water, soft, rubbery and biocompatible nature). Several terms have been coined for the hydrogels, such as 'intelligent gels' or 'smart hydrogels' [89]. The smartness of any material is the ability to receive, transmit or process stimuli and respond by producing useful effects [90].

Hydrogels can absorb large amount of water or biological fluids, from 20% up to several thousand % and also swell readily without dissolving. The high hydrophilicity of the hydrogels is mainly due to the presence of a number of hydrophilic moieties such as amino acid, carboxyl, amide and hydroxyl groups distributed along the backbone of the polymeric strands. Hydrogels usually attains equilibrium swelling when a balance occurs between the osmotic and cohesive forces exerted by the polymeric strands. This cohesive force tends to resist the hydrogel expansion and the magnitude of these forces depends mainly on the cross-linking density [91, 92]. In general, the more hydrophilic the polymer forming hydrogel, the higher the total water absorbed by the hydrogel, the lower the extent of the gel hydration. In the dried form hydrogels are usually referred as ***'Xerogels'***. When some drying techniques, such as freeze drying or drying using solvent extraction are applied, the resulting hydrogels are extremely porous. The porous dried hydrogels are known as '***Aerogels***'. The relatively high water content of hydrogels also makes them permeable to oxygen, nutrients and metabolites. This high solute permeability makes them ideal materials of choice as devices for the controlled drug release. Research on the hydrogels has been focused on the application in the controlled drug delivery. Different techniques have been applied for the characterization of hydrogels and to investigate their parameters. Table 1.8 lists some examples of these techniques .

Table 1.8 Examples of techniques used for the characterization of hydrogels

Parameters	Measurement techniques	References
Extend of cross-linking	Change in the polymer solubility with time Ultimate compressive strength	[93]
Network pore size	Scanning electron microscopy Mercury porosimetry Rubber elasticity measurement	[94]
Degree of swelling	Equilibrium swelling ratio Dimensional changes with time Equilibrium water content	[95]
Mechanical strength	Ultimate compressive strength	[96]

1.5.1 Hydrogels and Controlled drug release technology

The design of a drug delivery device is typically based on the drugs physiochemical and pharmacokinetics property. Conventional delivery system suffers from the limitation of immediate release and minimal synchronization between the time required to achieve therapeutically effective drug plasma concentrations and the actual drug release profile exhibited by the dosage form. From the last few years, the way of administering the drugs have gained much attention due to the advancements in the novel drug delivery systems. Development of administration methods that allow the patient to safely treat themselves is as important as any other health care system, particularly in poor countries where doctors, clean syringes, sterile needles and sophisticated instruments are rare [97]. Conventional dosage forms such as pills, capsules, tablets, suppositories, injections, creams, ointments and aerosols provide and instantaneous release of drugs in bolus form. For drugs which get cleared rapidly from the body, achieving and maintaining the drug concentration within the therapeutically effective range requires a multiple dosing

treatment often more than once a day. Such an inconvenient dosing treatment results in the deficiency in the patient compliance with dosing instruments. With such conventional formulations, the concentration of the drug released is initially high, peaks and then declines sharply below the minimum therapeutic level [97, 98]. Consequently, for drugs whose actions correlate with their concentration in the serum, such type of fluctuation in the drug level frequently cause intolerable side effects at the peak followed by deficient therapy in the troughs. Moreover, the conventional dosage forms, which are still prominent for the pharmaceutical products, are not able to control either the rate of drug delivery or the target area of administration. In contrast, regulating the rates of drug release with the help of controlled drug release formulations offers several advantages over conventional dosage forms. The main advantages of controlled release formulations are described below [99].

- Controlled release of drugs result in the reduction in the frequency of the drug administration .
- The controlled release of the drug is the most appropriate for the application point of view. The control could be in terms of the onset of release (i.e. delayed vs. immediate), the duration of release and release profile itself .
- The drug can be released in the target region. This can be carried out either by timed released or tailoring the carrier matrix to release the drug in that particular site. The targeting of the drug could maximize the drug efficacy .
- Systemic exposure of drug could be reduced upon its targeting to the desired environment and decreasing the systemic side effects (i.e. for toxic drugs).
- The controlled release formulations protect the drugs from the physiological environment for longer period of time.

Controlled release formulations are differentiate under different technologies which differ slightly from each other's, specifically, (1) delayed release, (2) prolonged release, (3) sustained release and (4) repeated action dosage forms. In delayed release products; release of drug is delayed for finite "lag time", after which release is unrestricted [e.g. enteric coated or "gastro retentive" tablets or capsules which remain intact in the stomach and only disintegrates in the higher pH of the intestine]. In prolonged release products or formulations; the rate of release of active substances from the formulation has been reduced, in order to maintain therapeutic level and to reduce toxic effects. Sustained

release products are designed to release loading dose to produce an immediate response, followed by constant dose (maintenance dose) which is required to maintain the therapeutically effective level. A repeated dosage form is designed to release initially the corresponding of a usual single dose of drug and then after certain period of time another single dose of the drug is released [100].

1.5.2 Conventional drug formulations versus controlled release formulations

Providing control over the drug delivery is the most important factor at times when traditional oral, tablets, injectable drug formulations cannot be used. These includes the situations requiring the slow release of water soluble drugs, the fast release of low soluble drugs, drug delivery to specific sites etc. the ideal drug delivery system could be inert, biocompatible, mechanically strong, comfortable for patients capable of achieving high drug loading, simple to apply or administer and remove as well as easy to sterilize and fabricate .

Controlled release formulation aimed to achieve a delivery profile that would yield a high blood level of the drug over a longer period of time. With traditional formulations, the drug level in the blood follows the profile as shown in Figure 1.5 a, in which the concentration of drug in the blood rises after each administration and then decreases until the next administration. With traditional drug administration, blood level of the drug exceeds toxic level immediately after drug administration and falls down below effective level after some time. Controlled drug delivery formulations are designed for long term administration where the drug level in the blood follows the profile as shown in Figure 1.5 b and remains constant [101].

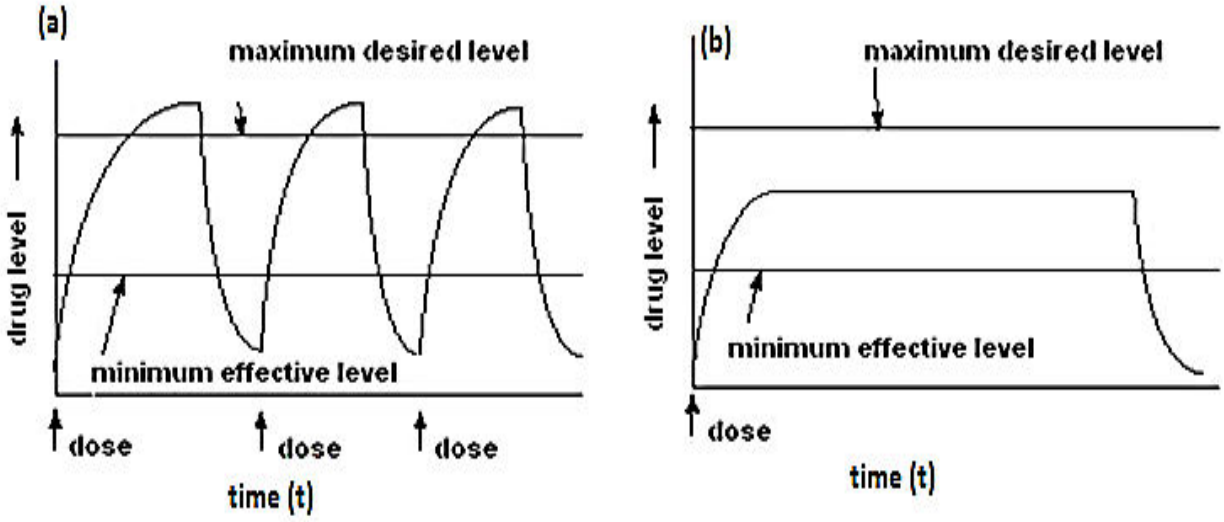

Figure 1.5 Levels of the drugs in the blood plasma (a) conventional dosage form, (b) controlled delivery dosing [101]

1.5.3 Mechanism of drug release

Most of the hydrogels are glassy in their dry form and drug release generally involves immediate incorporation of water and release of drug via a swelling controlled mechanism [102]. The rate controlling factor mediating drug delivery is the resistance of the polymer to an increase in the volume and change in the shape of the polymer [103]. A polymeric hydrogel on coming in contact with water or any other thermodynamically friendly medium, allows the diffusion of solvent into free spaces between the macromolecular chains and shell. When sufficient water has entered the matrix of the polymeric structure, the glass transition temperature of the polymer drops to the investigational temperature. The presence of the solvent in the glassy polymer causes the enlargement of stresses that are accommodated by an increase in the radius of gyration and distance of the polymer molecules which seen macroscopically on swelling. The movement of solvent molecules into the dry hydrogel takes place with a well known velocity front and simultaneous increase in the thickness of the polymer matrix. Such swelling and diffusion do not generally follow a Fickian diffusion mechanism. The existence of a slow macromolecular relaxation process in the swollen region is believed to be responsible for the observed non-Fickian behavior [104].

Various approaches used for predicting these mechanisms are

- Fitting of release data with a power function of time [105].

- Determination of various dimensionless parameters, such as swelling interface number (S_w) and Deborah number (D_{eb}) [106].
- Analysis of moving boundary in drug release from swellable polymers with concentration dependent diffusions, using microscopic imaging under polarized light [107].

Diffusion controlled or swelling controlled system may be either reservoir type devices in which drug formulation is presented as a core surrounded by a polymeric membrane, or monolithic devices where a dispersed or dissolved drug is uniformly distributed through a polymeric matrix (Figure 1.6 a and 1.6 b)

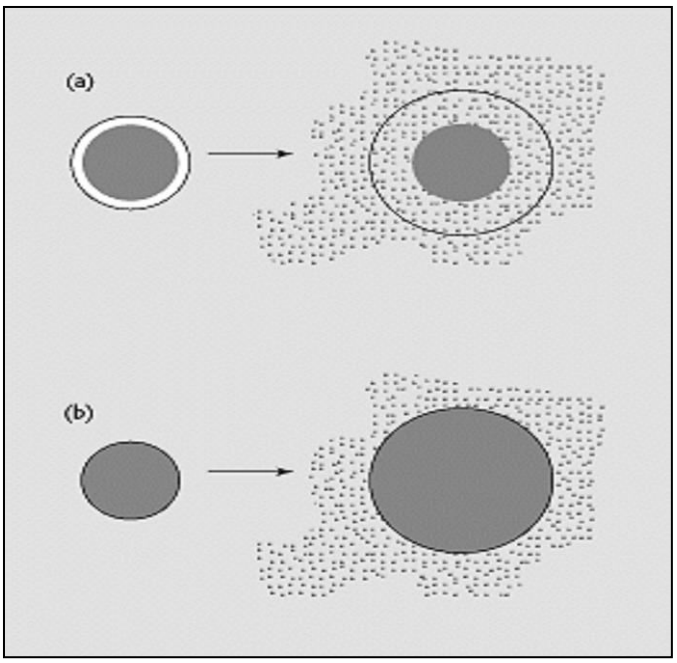

Figure 1.6 Drug release from (a) reservoir type (b) monolithic swelling-controlled release system [108]

1.5.4 Gels versus hydrogels

A common misunderstanding in the polymer science is the use of term "gels" and "hydrogel" synonymously. As a polymeric network, both gels and hydrogels might be similar chemically but they are physically different . Gel is a colloidal condition in which one is easier to recognize than to define [109]. Technically, gels are semi-solid system comprise small amounts of solid, dispersed in relatively large amount of liquid and possess more solid like than liquid like character [110]. Sometimes hydrogels are also known as aqueous gels because of prefix 'hydro'. Although the term 'hydrogel' implies

a material already swollen in water, in a right manner hydrogels are cross-linked network of hydrophilic polymers. They possess the capability to absorb large amount of water and swells in acidic as well as basic medium and maintains their three-dimensional structure [95]. This definition differentiate hydrogels from gels, which are polymeric network already swollen to equilibrium and further addition of fluid results only in dilution of polymeric network (Figure 1.7). Although some of the gels are rigid and maintain their structure under stress conditions, after exceeding the yield value, gel flexibility is seen with loss of polymer structure. A hydrogel exhibit swelling in aqueous media for the same reason that an equivalent linear polymer dissolves in water to form usual polymer solution . Usual gels can also build up small levels of cross-links as a result of expand in energy under the control of shear forces.

Because of the basic support of both the gels and hydrogel in the polymer network, these polymers produce systems that cover a range of rigidities, starting with a sol and increasing to mucilage, jelly, gel and hydrogels [110]. Hydrogels are frequently prepared to a measurable configuration. Occasionally, polymers such as carbopol® are also referred to as hydrogel because of their cross-linked configuration. Although, these polymers reveal swelling in the aqueous atmosphere, at equilibrium their swelling contributes to a gain in viscosity, leading to aqueous gel formation. Because polymeric systems are similar to each other, several misrepresentations exists in their classification, which can be disallowed by a detailed understanding of their physical, mechanical, chemical and behavioral characteristics.

1.5.5 Classification of hydrogel products

Hydrogels products can be classified in different classes based on their polymeric composition, cross-linking, chemical, appearance, physical and electrical charge as described below [111].

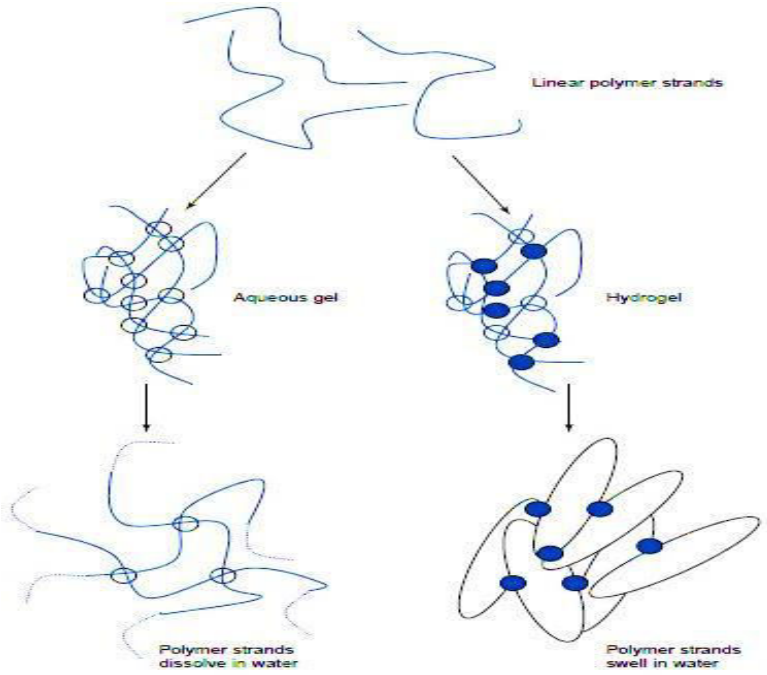

Figure 1.7 Polymer strands forming a gel and a hydrogel, showing different behavior in an aqueous environment. A solid circle represents covalent cross-links and hollow-circles shows virtual cross-links formed by entanglements [111]

1.5.5.1 Classification based on their polymeric composition

The method of preparation polymeric composition leads to the formation of some important classes of hydrogels . These can be explained as given below.

(a) Homo-polymeric hydrogels are the type of hydrogels which are derived from a single species of monomer unit, which is basic structural unit of any polymeric network [112]. Homopolymers may have the cross-linked structure depending on the nature of the monomer and the polymerization techniques used for the preparation of hydrogel network.

(b) Co-polymeric hydrogels consist of two or more different types of monomer species with at least one hydrophilic component, arranged in a random, block or alternating configuration along the chain of polymeric network [113].

(c) Multi-polymer Interpenetrating Polymeric Hydrogels (Full-IPN), an important class of hydrogels and is made up of two independent cross-linked synthetic or natural polymer component, with in a network. While in semi-IPN hydrogels, one component is cross-linked polymer and other is a non-cross-linked polymer [114].

1.5.5.2 Classification based on the configuration

The classification based on the configuration (physical and chemical structure) is described below:

(a) Amorphous (non-crystalline)
(b) Semi-crystalline: A composite mixture of amorphous and crystalline phases
(c) Crystalline

1.5.5.3 Classification based on the type of cross-linking

Hydrogels can be divided into two classes based on their physical and chemical nature of cross-linked junctions. Chemically, cross-linked network have permanent junctions, while physically cross-linked networks have transient junctions that occur either from polymer chain entanglements or physical interactions such as ionic interaction, hydrogen bonds or hydrophobic interactions [114].

1.5.5.4 Classification based on their physical appearance

Based on physical appearance hydrogels can be matrix, film or microsphere forms depend on the method of polymerization concerned in the preparation process .

1.5.5.5 Classification based on the network electrical charge

Hydrogels can be categorized into four different classes based on the presence or absence of net electrical charge located on the cross-linked network or chain:

(a) Nonionic (neutral).
(b) Ionic (anionic or cationic).
(c) Amphoteric electrolyte (Ampholytic) contains both acidic and basic groups .
(d) Zwitterions (polybetains) contain both anionic and cationic groups in each structural unit .

Hydrogels from natural polymers includes proteins such as collagen, gelatin and polysaccharides such as starch, agarose and alginate. Synthetic polymers that form hydrogels are conventionally prepared using chemical polymerization methods .

1.5.6 Method of preparation of hydrogels

Cross-linked networks of various synthetic polymers such as polyethylene oxide (PEO) [115], polyvinyl pyrollidone (PVP) [116], polylactic acid (PLA) [117], polyacrylic acid (PAA) [118], polyethylene glycol (PEG) [119] or natural polymer such as carrageenan, hyaluronan, aliginate, chitosan, and carboxymethyl cellulose (CMC) have been reported. The various preparation methods adopted are physical cross-linking [120], chemical cross-linking [121], grafting polymerization [122] and radiation cross-linking [123]. Such modification improves the mechanical behavior and visco-elasticity necessary for the application in the biomedical and pharmaceutical drug delivery applications [121]. The general methods used to produce physical and chemical gels are described below :

1.5.6.1 Physical cross-linking

Now a day, there has been an interest in the physical and reversible gels due to relative ease of the production and advantages of not using cross-linking agent. Careful selection of hydrocolloid type, concentration and pH can lead to the formation of a broad spectrum of gel consistency and is currently with an area receiving significant attention, mainly in the food industry. The various methods reported in the literature to obtain physically cross-linked hydrogels are as follow :

1.5.6.1.1 Heating/cooling a polymer solution

Physically cross-linked hydrogels are formed when a hot solution of gelatin or carrageenan is cooled. The result gel is a result of helix formation, association of the helices and formation of junction zones [124]. Carrageenan in hot solution above the melting transition temperature is present as a random coil transformation. Upon cooling it transforms to rigid helical rods. In some cases hydrogels can be formed directly by warming the polymer solution that causes the block copolymerization. Some of the examples are polypropylene oxide, polyethylene glycol-Polylactic, polyethylene oxide-[125] and acid hydrogels [120].

1.5.6.1.2 Ionic interaction

This method of preparation involves the cross-linking of the ionic polymers with di or tri-valent counter-ions. This method underlies the principle of gels a polyelectrolyte solution (e.g. Sodium alginate) with a multivalent ion of opposite charges (e.g. Ca^{2+} + $2Cl^{-}$) (Figure 1.8). Some of the other examples of the ionic interaction involves chitosan-

polylysine [126], chitosan glycerol phosphate salt [127], chitosan-dextran hydrogels [120].

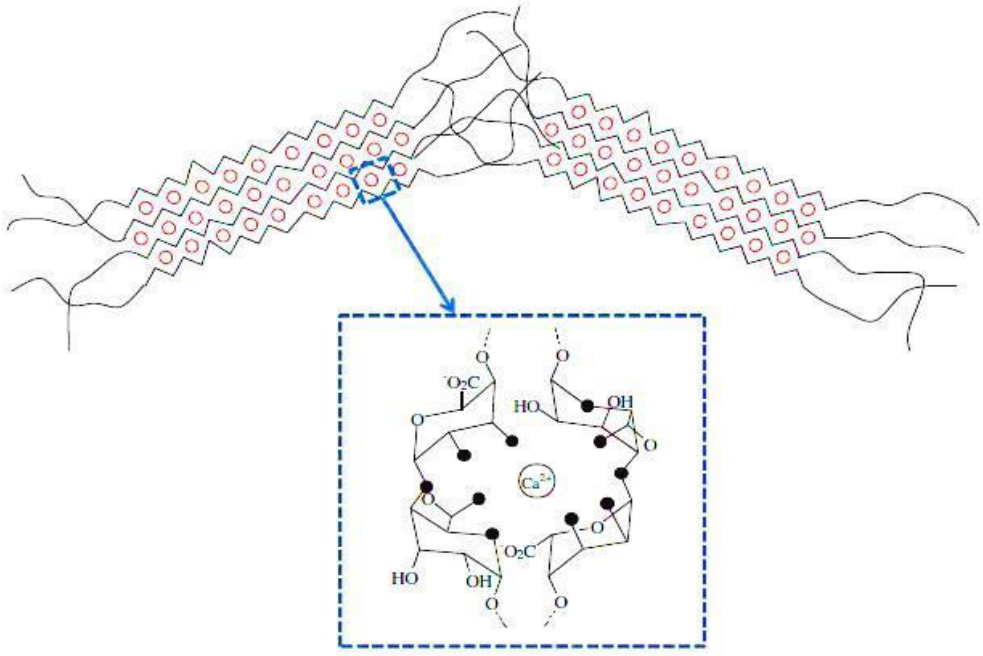

Figure 1.8 Ionic interactions between the anionic groups on the alginate (COO^-) with divalent metal ions of calcium (Ca^{2+})

1.5.6.1.3 Complex co-acervation

This type of method involves the mixing of poly-anion with that of poly-cation. The fundamental principle behind this method is that polymers with opposite charges sticks together and forms soluble and insoluble complexes based on the concentration and the pH of the resulting mixture (Figure 1.9). Proteins below its isoelectric point are positively charged and are likely associated with anionic hydrocolloids and form poly-ion complex hydrogel [128].

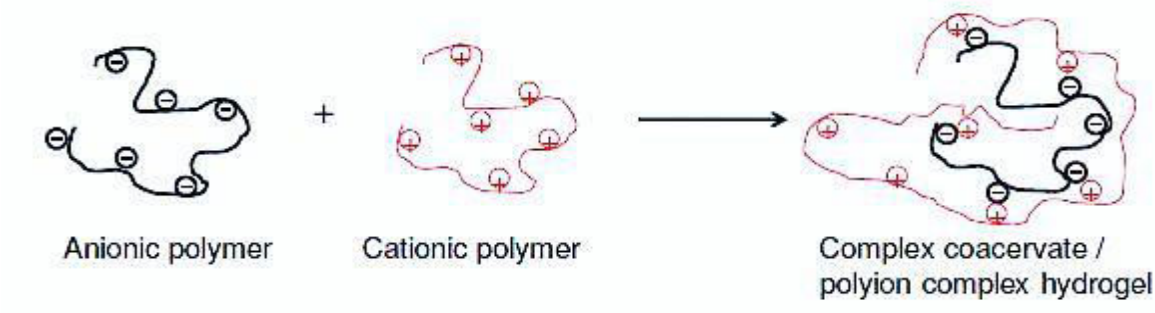

Figure 1.9 Complex co-acervation formations between a poly-anion and poly-cation

1.5.6.1.4 Hydrogen bonding

Hydrogen bonded hydrogel can be obtained by decreasing the pH of polymer aqueous solution carrying carboxyl groups. The examples of such hydrogels are a hydrogen bonded CMC (Carboxymethyl cellulose) network formed by dispersing CMC into 0.1 M HCl [129]. The mechanism behind the formation is replacement of sodium in the CMC with hydrogen in the acid solution to promote hydrogen bonding. The hydrogen bond results in the decrease in the solubility of CMC in water which further results in the formation of elastic and rubbery hydrogel. Carboxymethylated chitosan (CM-chitosan) hydrogels can also be synthesized by means of cross-linking .

1.5.6.1.5 Freeze thawing of polymer solution

This method involves the physical cross-linking of a polymer solution or combination of polymer solution to form its hydrogels using freeze thaw technique. The mechanism involves the synthesis of micro-crystals in the structure due to freeze thawing. Examples of this type of gelation are hydrogels based on xanthan and polyvinyl alcohol [130].

1.5.6.2 Chemical cross-linking

Chemical cross-linking involves the grafting of a monomer on to the backbone of a polymer or the use of cross-linkers involves linking of two polymer chains. The cross-linking of natural as well synthetic polymers involves the reaction of their functional group (e.g. OH, COOH, and NH_2) with that of cross-linkers such as aldehyde (e.g. gluteraldehyde, adipic and dihydrazide). There are number of methods reported in the literature to obtain chemically cross-linked hydrogels . The below section reviews the major methods used to produce hydrogels:

1.5.6.2.1 Chemical cross-linkers

Cross-linkers such as gluteraldehyde and epichlorohydrin have been widely used to obtain the cross-linked hydrogel network. The technique involves the introduction of new groups between the polymeric chains to produce cross-linked chains (Figure 1.10). One of such example is synthesis of starch and polyvinyl alcohol hydrogels using gluteraldehyde as cross-linking agents. The formulated membrane of hydrogel could be used as artificial skin and used to deliver various nutrients/ healing factors medicaments, drugs at the wound site.

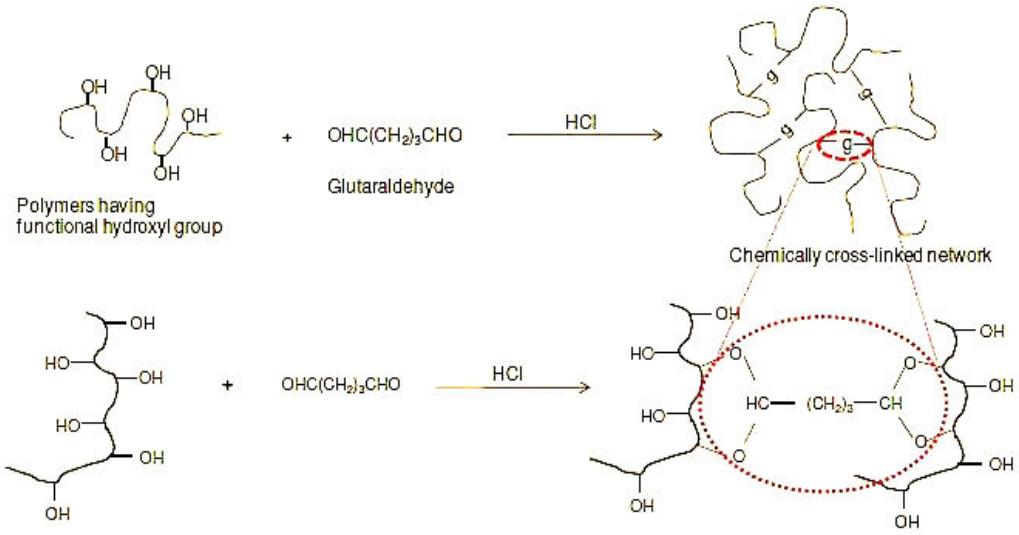

Figure 1.10 Schematic representation of using a cross-linker to obtain a chemically cross-linked hydrogel network

1.5.6.2.2 Grafting technique

Grafting technique involves the polymerization of a monomer on the backbone of a preformed polymer. The resulting polymer chain was activated by the action of a chemical reagents, or treatment with a high energy radiation. The growth on the functional monomers on activated macro radicals loads to branching and further cross-linking .

1.5.6.2.2.1 Chemical grafting

In this technique, macromolecular backbones are activated by the action of chemical reagent e.g. starch grafted with acrylic acid by using N-vinyl-2-pyrrolidone [131]. Such kind of hydrogels showed an excellent swelling depending on pH with an ideal characteristic to be used in the pH dependent drug delivery application especially in the small intestine .

1.5.6.2.2.2 Radiation grafting

This type of method involves the use of high energy of radiation such as gamma and electron beam to initiate grafting. For e.g. electron beam irradiation were used for the preparation of CMC hydrogels by grafting with acrylic acid. Electron beam was used as a source to initiate the free radical polymerization of the acrylic acid on the backbone of

CMC. Irradiation of both CMC and monomer produces free radicals that combine to produce hydrogels .

1.5.6.3 Radiation cross-linking

Radiation cross-linking is extensively used method since it does not involve the use of chemical agents and therefore retains the biocompatibility of the polymer. Also, the alteration and sterilization can be achieved in single step hence it is a cost effective method to modify biopolymers having their important use in biomedical applications [132]. The technique is mainly based on producing free radicals in the polymers on exposure to high energy source such as gamma ray, x-ray or electron beam .

1.5.7 Nanocomposites hydrogels from metal and metal oxide nanoparticles

In the recent year's nanotechnology have made the nanoscience one of the most research area of science in the last two decades. Nanocomposites are new classes of materials in which the diameters of dispersed particles occur in nanometer range i.e. in polymer-metal nanocomposites the diameter of the dispersed particles occur in nanometer range. Polymeric nanocomposites research has become an attraction and also much important due to their enhanced property in comparison to the bulk material [133]. Due to their wide functionality, process ability, easy synthesis, potential for large scale manufacturing and lighter than metals made them an important material for number of applications. The properties of nanocomposite hydrogels are greatly influenced by high surface energy that is due to high surface area to volume ratio and relatively small pores. It is also possible to control the physical and chemical properties of the by designing 3D gel structure .

The advanced applications of metallic nanoparticles require new techniques that are capable to synthesize the nanoparticles in cost effective and eco-friendly manner. Many techniques for the synthesis of metallic nanoparticles have been developed however, the nanoparticles with control over size, shape and stability remains a challenge [134]. Various types of metallic nanoparticles used for the synthesis of nanocomposite hydrogels include gold (Au), silver (Ag) and other noble metal nanoparticles. Whereas, metal oxide nanoparticles include iron oxide, alumina, zirconia and titania .

Polymeric nanocomposites can be prepared by physical, chemical as well as green approach. The physical method involves the division of bulk precursor to nanoparticles. Chemical approach involves the reduction of metal ions to metal atoms followed by

controlled aggregation of the particles. Whereas, green approach involves the use of herbal extract for the reduction of metal ions to metal atoms. The most common synthesis of polymer nanocomposite hydrogels has focused on utilizing poly (ethylene oxide), poly (vinyl alcohol) or poly (acryl amide) as polymers. Therefore, nanocomposite hydrogels containing these polymers have received greater part of our interest in recent publications . Metal nanocomposites hydrogels can be defined as cross-linked network swollen in water containing metallic nanoparticles or nanostructures

1.5.8 Current status of silver nano-composites hydrogels as controlled drug delivery systems

Nguyen and co-workers synthesized polyvinyl alcohol/chitosan hydrogel using ultraviolet (UV) irradiation and acrylic acid (AA) monomer as the cross-linker, without using any additional photo-initiator [135]. The synthesized hydrogels with a high cross-linking property, a dense inter-porous structure were utilized both as nano-reactors and the immobilizing the polymer matrix for the formation of silver nanoparticles (AgNPs). The NPs were formed through *in-situ* reduction of silver nitrate by glucose and the accelerator sodium hydroxide. The composite hydrogels were characterized using UV spectroscopy, X-ray diffraction (XRD), Fourier-transform infrared spectroscopy (FTIR), transmission electron microscopy (TEM), scanning electron microscopy (SEM) and mechanical testing. The overall results confirmed that extremely stable and consistently distributed AgNPs were obtained over the whole hydrogel networks. The tensile test showed that the effective incorporation of AgNPs within the hydrogel networks rendered the nanocomposite hydrogels more elastic. Because of its distribution patterns, inter-porous structure, good mechanical properties as well as the green synthesis method, the AgNPs-loaded PVA/CTS hydrogel thin film can be utilized as a drug delivery device in medical applications .

Ravindra and co-workers reported antimicrobial competence of cotton fibres loaded with silver nanoparticles (AgNPs) by using herbal extracts, of *Eucalyptus citriodora* and *Ficus benghalensis* [136]. The formation, structure and morphology of AgNPs on the cotton fibres were observed by UV spectrophotometer and electron microscopy with a size of ~20 nm. The antibacterial activity of cotton fibres loaded with AgNps was evaluated against gram negative *Escherichia coli* bacteria. The results synthesized AgNPs suggest excellent antibacterial activity in response to 2 % leaf extracts on cotton fibres. These

fibres have also revealed greater antibacterial activity even after numerous washings indicating their usage in medical and infection prevention applications .

Gulsonbi et al. [137] reported green synthesis of silver nanocomposite hydrogels with N, N' – Methylene-bisacryl-amide (MBA) and Carboxy methylcellulose (CMC). The silver nanoparticles have been obtained with hydrogels network as nano-reactors via in-situ reduction of silver nanoparticles using (*Azadirachta indica*). The formulated nano-composites hydrogel was characterized using UV–vis spectroscopy, FTIR, SEM and Thermo gravimetric analysis (TGA). The antibacterial activity of silver nanoparticles loaded hydrogel was investigated for the synthesized hydrogel-silver nanocomposite.

Very recently, Shaik and co-workers reported a novel green approach for the synthesis of silver nanoparticles using *Tridax procumbens* (TD) in the starch-co-PAAm hydrogel network [138]. The formation of AgNPs was confirmed by UV-visible spectroscopy, thermo-gravimetric analysis, SEM, TEM and X-ray diffraction studies. ~22% of loss in weight between hydrogel and silver nanocomposite hydrogel (SNCH) indicates the formation of silver nanoparticles by TGA. TEM images indicate that the AgNPs are in the range of 5 to 10 nm in size with spherical shape. The developed SNCHs were than further used to study the antibacterial potential by zone of inhibition method against gram-negative and gram-positive bacteria .

Garg et al. [139] in his study reported wound healing potential of silver nanoparticles using *Arnebia nobolis* hydrogels. The synthesized nanocomposite hydrogels were further characterized using UV-visible spectrophotometer; TEM, X-ray diffraction, SEM, and Fourier transform infra-red spectrometry. The results of TEM and XRD showed that the prepared AgNPs were found to be spherical and crystalline in nature. Furthermore the synthesized AgNPs were found to be active against both Gram positive and Gram negative bacteria . The authors also investigated the wound healing potential of silver nano-composites hydrogels on excision animal model. The results of wound healing activity provided a novel therapeutic direction for wound healing in the clinical practice.

1.5.9 Plants as a source for the synthesis of silver nanoparticles

The synthesis technique, instability, immediate release and local toxicity of silver are major concern for its biological application as reduction of silver salt using synthetic chemicals such as sodium borohydride is hazardous to environment while high concentration of silver in wound tissue adversely affects nascent tissues and thus hamper the healing progression . To improve stability, controlled release, toxicity issue, silver

nanoparticles were synthesized using green chemistry (phytochemicals as reducing agent) to tackle the issues related with the toxicity and immediate release of silver. AgNPs exert its effect by lowering the bacterial burden in the ulcers, while phytochemicals does it by reducing the oxidative stress. The combination of AgNPs and hydrogel dressing further overcome the problems related with mechanical property of hydrogels and silver toxicity as it releases in a controlled manner from the polymer matrix system. Hydrogels offer large free spaces between the cross-linked networks in the swollen stage that can act as a nano-reactor for the nucleation and growth of the nano-Ag. This approach offers short reaction times, the use of phytochemicals as reducing agent, high efficiency in converting the silver cations (Ag+) to nano-Ag and control over the size of nano-Ag has been welcomed for the delivery of silver ions as an antimicrobial agent.

1.5.9.1 *Ficus benghalensis* (FB)

Ficus benghalensis Linn, is a well-known ayurvedic medicine and universally known as *"banyan tree"* in the ayurvedic system of medicines. Milky juice from stem, seed and fruits of the plant is applied topically in rheumatism and to the ulcers of feet when inflamed [140]. Whole parts of the plant have diarrhea, dysentery, astringent, anti-inflammatory , anti-arthritis, anti-oxidant, analgesics, anti-cancer, anti-diabetic, wound healing and anti-diarrheal activities. Phytochemicals investigation of FB extract showed the presence of amino acids, flavonoids, carbohydrates, saponins and tannins. The main chemical constituents of FB extract are Rutin, Friedlin, Taraxosterol, Lupeol, β-sisterol and Quercetin-3-galactoside.

Taxonomical classification

Kingdom	Plantae
Phylum	Traceophyta
Class	Magnoliopsida
Order	Urticales
Family	Moraceae
Genus	Ficus
Species	*benghalensis*

1.5.9.2 *Ocimum sanctum* (OS)

Ocimum sanctum is an aromatic plant commonly known as "Tulsi", belonging to the family lamiaceae, which is native to the Indian subcontinent and cultivated all over the Southeast Asian tropics [141]. The plant is an erect, branched and 30 – 60 cm tall with hairy stem. The plant is cultivated for religious and medicinal purposes. The medicinal plant is commonly used as herbal tea in Ayurveda, and has an important role in the Vaishnava tradition of Hinduism, in which devotee's present worship involving holy basil plants or leaves. The main chemical constituents of OS are Oleanolic acid, Eugenol, Rosmarinic acid, Carvacrol, linalool, Ursolic acid, β-caryophyllene (8 %), β-elemene (11 %) and Germacrene D (~2%). The leaves of tulsi have anti-microbial, anti-oxidants, anti-diabetic, anti-cancer, analgesics, anti-ulcers and anti-arthritic activities.

Taxonomical classification

Kingdom	Plantae
Order	Lamiales
Family	Lamiaceae
Genus	Ocimum
Species	*sanctum*

CHAPTER-2

Design and development of *Tinospora cordifolia* extract loaded nanoemulsions for improved intestinal permeability and controlled release

ABSTRACT

Clinical efficacy of phytotherapeutics has been limited due to their poor stability, solubility and oral bioavailability. The present study focused on design and development of lipid based nano-formulation for improved efficacy and oral bioavailability of phytotherapeutics of *Tinospora cordifolia* (TC) stem extract. Nanoemulsions were prepared by sonication solvent evaporation method and optimized for encapsulation efficiency, release kinetics as well as stability parameters by pseudo-ternary phase diagrams. Clove oil was used as lipid phase while Span 80 and Tween 20 were used as lipophilic surfactant and hydrophilic surfactant in order to enhance drug loading and permeation across the intestinal membrane. Increasing concentration of span 80 resulted in increased droplet size, while the reverse effect was observed by increasing the co-surfactant concentration . Based on the droplet size and zeta potential an optimized formulation was developed consisting of clove oil, Span 80, Tween 20 and ethanol (7.7:4:0.5:21 w/w) and loaded with 83.8% of TC stem extract. The mean particle size of formulated nanoemulsion was found within the range of 33.7 nm to 377 nm. The active components remained stable in the optimized nanoemulsion during study for 3 months. 79.4±1.5% and 80.5±0.9% of extract were released from solution and nanoemulsion after 12 h and 20 h, respectively. Approximately 3.95 fold enhancement in permeability coefficient of TC extract was noticed upon formulating it as nanoemulsion in comparison to control by everted gut model. These results revealed the successful application of SNEDDS for improved permeation of potential phytotherapeutics across GIT towards enhancement of therapeutic efficacy.

2.1 INTRODUCTION

In this era, Nanoformulations has brought a revolution in creating devices with novel concepts and in drug delivery systems [142]. Recently, many lipid based formulations (solid lipid nanoparticles, nanostructured lipid carriers , nanoemulsion and liposome's) have been investigated to overcome the bioavailability issues associated with the oral administration of drugs [143, 43]. Avoidance of first pass metabolism of drug, improve mucosal adhesion, improved permeation across the intestinal membrane barrier, protection against harsh GI environment and controlled release are major mechanisms which further enhance the bioavailability, effectiveness of phyto-medicines as well as their tunable release profile in blood circulation. Besides that, lymphatic system plays an essential role in absorption of long chain fatty acids, triglyceride, cholesterol, esters, lipid soluble vitamins and xenobiotic [144, 145]. Nanoemulsions (NE) are lipidic nanoformulations with droplet diameter in nanometer range have established tremendous attention as drug delivery formulations for lipophilic drugs due to their capability to increase solubility, permeation across biological membranes as well as their therapeutic efficiency of lipid soluble drugs due to predictable size-distribution, high drug loading and stability under biological environment [146, 147]. O/W NE possesses a core–shell assembly wherein core shell acts as a pool for the assimilation of poorly water soluble drugs and hydrophilic shell provides a protective interface between the core and the external medium [148, 149].

Phytotherapeutics contain numerous active constituents that work simultaneously against the factors that are responsible for diseases. Due to their outstanding anti-oxidative, anti-inflammatory, immune-modulatory properties, these phytochemicals have proven their potential for health maintenance and for improved functional efficiency of overall biological system [150, 151]. Besides that, secondary metabolites are increasingly accepted globally as potential therapeutics not only for avoidance of a particular disease but also for treatment of diseases such as cancer, arthritis, diabetes vascular and aging complication caused by oxidative damage [152, 153], but most of the phytochemicals has limited clinical competency due to their low bio-stability, poor permeation across mucosal barrier and liver first pass metabolism [154, 155]. It has been the main reason for emergence of novel formulation based approach to deliver the natural phytochemicals, which further not only increase the bioavailability of phytochemicals so that they can be used up to their full potential against tumor [156].

The plant *Tinospora cordifolia* (guduchi) is a prominent, wide leafed, deciduous hiking shrub and has been reported to possess medicinal properties such as anti-arthritic, anti-diabetic, anti-stress, anti-cancer, anti-leprotic, hepatoprotective, anti-inflammatory and immune-modulatory activities [157, 147]. Newly isolated compounds (di-terpenoid) have been reported to have promising chemo-preventive potential in rats against diethyl-nitrosamine (DEN) induced hepatocellular carcinoma (HCC) [147, 148] by diminishing the anti-oxidant activities via suppressing the activity of CAT, SOD, and of detoxification enzymes like GSH, GPx. Moreover, it has showed increased activities of the hepatic markers i.e. Serum Glutamic Pyruvate Transaminase (SGPT), Serum glutamic oxaloacetic transaminase (SGOT), LDH, and decreased serum transaminase level [148].

At present, none of the research work has been published towards utilization of these nanocarriers for delivery of anti-cancer phyto-therapeutic extract. This article comprises the designing of nanoemulsion with encapsulation of methylene chloride extract of *T. Cordifolia* stems and *in-vitro* investigation for their content estimation, drug release profile, stability and permeation through intestinal membrane. Furthermore, the formulated nanocarriers were evaluated for their particle size, shape and distribution of drug using fluorescent microscopy.

2.2 MATERIALS AND METHODS

2.2.1 Materials

Fresh stems of TC were collected from local region of Shimla (near Chaura Maidan, 6,117 ft.) of Himachal Pradesh, India. Various non-ionic surfactants, i.e. Span 80 and Tween 20 were purchased from Loba Chem. Pvt. ltd, India. All the oils used in this study were purchased from Konarks herbals and health care Products, Mumbai, India . Calcein and Rhodamine B were purchased from FINAR® Chem. Pvt. ltd and Oxford laboratory, Mumbai, India, respectively. All hydrophilic dyes used in during study were of analytical grade. Dialysis membrane was purchased from (Himedia, LA 401-5MT; Mol wt. 12000-14000). Quercetin dehydrates and Atropine was purchased from Himedia laboratories, Mumbai, India. Tannic acid was purchased from sigma Aldrich, India. Ethanol and methanol, 99.9% absolute was purchased from Merck, Germany.

2.2.2 Methods

2.2.2.1 Collection and authentication of plant materials

The fresh stems of TC were collected from the local region local region of Shimla (near Chaura Maidan, 6,117 ft.) of Himachal Pradesh, India. The collected stem along with the leaves were than subjected for the preparation of herbarium sheet for the authentication of plant. The plant specimens pressed and dried inside the herbarium sheet using plant press followed by submission of the same to Dr. Yashwant Singh Parmar University of Horticulture and Forestry, Solan (Nauni), H.P with voucher specimen number 13525 for future reference. After authentication, the collected stem of *TC* was washed 2-3 times with distilled water and air dried for further use.

2.2.2.2 Extraction of stem extract of *Tinospora cordifolia*

Stems of plant *Tinospora cordifolia* (TC; Family: Menispermaceae) were collected in the month of November from north western Himalayan region. Stem (100 g) of plant TC were chopped into very tiny pieces, dried under dark and roughly powdered using a ball mill. According to polarity of solvents the TC stems were firstly extracted with petroleum ether (60-80 ºC) for removal of fatty material followed with methylene chloride using a laboratory soxhlet apparatus". The whole extraction process takes one week for the extraction of active constituents from the TC stem. One week extraction time is necessary for the complete removal of complex lipids (complex lipids may hamper with the solubility of the phytochemicals) as well as for the low consumption of solvents. After complete extraction, the mixture was filtered and filtrate was evaporated using Rota-evaporator (Heidolph, Germany). The final yield of extract obtained around 1.2 % w/w of raw material.

2.2.2.3 UV- characterization of *T. cordifolia* extracts (λ_{max})

The various concentration of the TC extracts (i.e. 2, 4, 6 and 8 mg/ml) were recorded from a region of 200 to 700 nm in the UV spectrophotometer for the obtaining the specific absorption maxima (for getting specific wavelength, TC extract solution was further scanned between 280-350 nm). The absorbance of all the concentration was recorded in order to get λ_{max} (wavelength) at which maximum absorbance (peak) is observed for the preparation of standard curve of TC extract.

2.2.2.4 Standard curve of TC extract

For the preparation of standard curve , a mixed stock solution of 1 mg/ml was prepared by weighing accurately 25 mg of TC extract into 25 ml of volumetric flask and making the volume up to the mark with ethanol. Different running solutions were prepared from the stock solution by appropriate dilution in ethanol for the preparation of calibration curve. All the solutions were kept in dark place until used under UV spectrophotometer (230 nm).

2.2.2.5 Phytochemicals screening of stem extract of TC

To determine the flavonoids content 1.5 ml of distilled water was mixed with 0.25 ml of extract (1 mg/ml; pre-solubilized in ethanol), followed by addition of 90 µl of 5% sodium nitrite ($NaNO_2$). After six minute later 180 µl of 10% $AlCl_3$ was added and mixture was allowed to set for 5 min before addition of 0.6 ml of 1M NaOH. At the end, final volume was made up to 3 ml by adding distilled water. Absorbance of the above solution was measured at λ_{max} 510 nm using UV-visible spectrophotometer [158].

For the determination amount of total alkaloid, the method of Manjunath et al. [159] was used with slight modification. Atropine standard curve was used for determination of total alkaloid (Figure 2A; Appendix).

For determination of total alkaloid 1 mg/ml of plant extract solution (1 ml) was mixed with 5 ml of acetate buffer (pH 4.7), followed by addition of 5 ml BCG solution and 4 ml of chloroform in separating funnel. After forceful shaking, the chloroform layer having plant extract was collected in volumetric flask and absorbance was measured at 470 nm using UV spectrophotometer (Elico SL-210, India).

For the determination of total glycosides a standard curve of syrigin (Standard glycoside) was made. For preparation of the standard curve, 10 mL of different concentrations (12.5-100 mg/L) of Syrigin were prepared (Solich et al., 1992). For determination of total glycosides, a 10% w/v solution of TC extract (ethanol as co-solvent) was mixed with 10 mL freshly prepared Baljet's reagent (95 mL of 1% picric acid + 5 mL of 10% NaOH). After an hour, the mixture was diluted with 20 mL distilled water and the absorbance was measured at 266 nm by Shimadzu UV/VIS spectrophotometer (Elico SL-210, India).

2.2.2.6 Solubility study

The solubility of TC extract in a mixture of oil (calendula, clove, neem, turmeric and mentha oil), surfactant (Pluronic-F68, Tween 20 and Span 80,), co-surfactant (methanol

and ethanol) and various pH medium i.e. pH 2, 6.8 and Krebs ringer solution was calculated by mixing excess amount of extract in 1 ml of the mixture using vortex mixer. The mixture vials were then incubated at 25±1.0 °C in an isothermal shaker (Labnet 311DS, USA) for 72 h to reach equilibrium. The equilibrated samples were then finally centrifuged at 3,000 rpm for 15 min and the concentration of extract in mixture was determined using calibration curve of TC extract at λ_{max} 230 nm [160-162].

2.2.2.7 Screening of surfactant

Four non-ionic surfactants i.e. Span 80, Tween 20, Tween 80, and Poloxamers-F68 were selected for the screening purpose. Initially 15 % surfactant solution was prepared and mixed with 4 µl of oil . If a single phase clear solution formed then addition of oil is repeated until the whole mixture become turbid. At the end of screening of oil, surfactant and co-surfactant pseudo ternary phase diagram was drawn in order to get the best nanoemulsifying region [160].

2.2.2.8 Screening of co-surfactant

Methanol, ethanol and isopropyl alcohol were chosen as co-surfactant and mixed with Tween 20. At a fixed ratio of various surfactants mixture (S_{mix}) of 1:1, pseudo ternary phase diagrams was drawn. Twelve different combinations at different weight ratios of oil and S_{mix} (1:9, 1:8, 1:7, 1:6, 1:5, 1:4, 1:3, 1:2, 1:1, 6:4, 7:3 and 9:1) were taken so that maximum ratios were covered in order to describe the boundaries of nanoemulsion formation region Table 2.1 [160].

2.2.2.9 Preparation of *T. cordifolia* loaded nanoemulsion

2.2.2.9.1 Preparation and construction of Pseudo-ternary phase diagram

Nanoemulsion was prepared using various non-ionic surfactants. TC extract was dissolved in a mixture of oil, emulsifier (span 80) and co-emulsifier (ethanol). The resultant mixture was then added drop wise to the aqueous phase containing Tween® 20 (HLB value ~16.7; hydrophilic surfactant) under continuous stirring. The pre-mixture containing oil, S_{mix} (surfactant and co-surfactant) and water was heated up to 50 ºC for 1 min followed by sonication for 10 min at 45 % amplitude (Sonics and materials, USA) [164]. Sonication step was carried out in ice bath in order to alleviate the thermal effect associated with the ultrasound and to maintain a constant temperature throughout the sonication process. To form nanoemulsion with attractive quality (i.e. encapsulation efficiency, size, stability and drug release profile), a pseudo-ternary phase diagrams was

constructed among various oils, water, surfactants and co-surfactant mixtures using aqueous titration method.

2.2.2.10 Effect of surfactant and co-surfactant concentration on particle size and zeta potential

Droplet diameter and zeta potential for formulated nanoemulsions i.e. blank nanoemulsion and extract-loaded nanoemulsion were measured by using Nanotrac Zetasizer (Microtrac, USA). To investigate the effect of surfactant concentration on to the droplet diameter and zeta potential , nanoemulsions were formulated with increased surfactant concentration and decreasing co-surfactant amount (10% of each) while keeping the oil amount constant. On the other side, the effect of co-surfactant on nano-droplet size was investigated by 10% increment (from 10% to 50%) of its concentration while the concentration of surfactant was decreased (from 50% to 10%) by the same percentage.

2.2.2.11 Thermodynamic stability study

The thermal or physical stability of nanoemulsion depends on the ratio of two phases i.e. oil and water phase. Phase separation reflects the thermodynamic instability and inconsistency of nanoemulsion which can be seen visually. Physical stability of formulated NEs was investigated by centrifuge at 3500 rpm for 30 min. The thermodynamic stability was observed by slow heating of the NEs on a water bath to visually observe the cloud point as the presence of cloudiness [164, 165]. The formulations which did not show any sign of phase separation on previous testing were then subjected to freeze-thaw cycle (i.e. -20 °C overnight followed by thawing for one hour at room temperature).

The stability of the optimized nanoemulsion was then recorded in different pH medium by mixing the prepared nanoemulsion in pH 2, 6.8 and Krebs ringer solution and confirmed by checking any sign of phase separation, flocculation, cloudiness, particle size, zeta potential and precipitation caused by the chemical reaction in these medium.

2.2.2.12 Physicochemical characterization of nanoemulsions

2.2.2.12.1 Fluorescent microscopy

The morphological behavior of the formulated nanoemulsion was performed using fluorescent microscope (Olympus BX53, USA). Nanoemulsions were synthesized by

loading calculated amount of Rhodamine B and Calcein dye into nanoemulsion and then analyzed at emission and excitation wavelength of 625 nm and 540 nm using FITC and TRITC filters detector, respectively. Oil containing core-shell morphology of the NEs was visualized by using Niel Red dye.

2.2.2.13 Encapsulation efficiency

Encapsulation efficiency was calculated by a method earlier mentioned by Jiang et al, with slight modification [166]. Approximately 5 ml of prepared nanoemulsion was centrifuged (Eppendrof, 5810R, Germany) at 12000 rpm for 30 min. The quantity of TC extract in the aqueous phase was calculated by reading the absorbance using UV-visible spectrophotometer at wavelength of 230 nm. The amount of extract in the aqueous phase was calculated using equation

$$\%EE = \frac{Wa - Ws}{Wa} \times 100$$

Where Wa is initial amount of extract and Ws is amount of extract in the oil phase.

Table 2.1 Formulation design for screening of drug loaded nanoemulsion [For preparation of blank nanoemulsion the formulation code is same (without drug)]

Formulation code	Clove oil (ml)	Tween 20 (ml)	Ethanol (ml)	Span 80 (ml)	Water (ml)	TC extract (mg)
F1	0.3	0.1	0.1	0.1	25	40
F2	0.3	0.1	0.2	0.1	25	40
F3	0.3	0.1	0.3	0.1	25	40
F4	0.3	0.1	0.4	0.1	25	40
F5	0.3	0.1	0.5	0.1	25	40
F6	0.3	0.1	0.6	0.1	25	40
F7	0.3	0.1	0.7	0.1	25	40
F8	0.3	0.1	0.1	0.2	25	40
F9	0.3	0.1	0.1	0.3	25	40
F10	0.3	0.1	0.1	0.4	25	40
F11	0.3	0.1	0.1	0.5	25	40
F12	0.3	0.1	0.1	0.6	25	40

2.2.2.14 *In-vitro* drug release profile

In-vitro drug release study from nanoemulsions incorporating TC extract was performed using dialysis bag method [167, 168]. An appropriate amount of nanoemulsions was suspended in the dialysis bag (Himedia, LA 401-5MT; Mol wt. 12000-14000) and immersed into the release medium (buffer medium; pH 6.8) at 37±0.5 °C. The drug release study was carried out under proper sink condition by maintaining constant stirring (75 rpm) under magnetic stirrer as well as by replacing 3 ml of aliquot with same volume of fresh medium at predetermined time intervals. For the determination of amount of extract released from nanoemulsions, a standard curve of the TC extract was prepared at 230 nm. A control experiment was also performed to determine the release behavior of the free extract. The above procedure of drug release was performed for the nanoemulsions system too. Each experiment was performed in triplicate (n=3).

2.2.2.15 *Ex-vivo* permission study

2.2.2.15.1 Non-everted gut-sac method

Ex-vivo intestinal permission study was studied using non-everted gut sac method using chicken ileum [169, 170]. The separated jejunum segment was washed six times with Krebs ringer solution along with permanent aeration at room temperature . Following washing, two intestinal segments were filled with nanoemulsion as well as TC aqueous solution. These tissue segments were tightened with both ends and placed into a beaker filled with 50 ml of Krebs's solution, under continuous aeration with the atmospheric air at a range of ~10-15 bubbles per minute. The gut sack bath is surrounded by an outer water jacket for maintaining the temperature at 37 ± 0.5 ºC. After a particular time interval, samples of drug solution was withdrawn and replaced with fresh medium. The amount of TC extract released was determined using UV spectrophotometer at 230 nm and compared the absorbance with raw extract permeated through intestinal membrane. The slope of linear portion gives the flux J_{ss} (The slope of linear portion was calculated as flux J_{ss} (µg/cm^2.h) and from the given equation permeability coefficient was calculated as

$$Ks_p = Jss / C_V$$

Where Ks_p is the permeability coefficient and C_V is the total amount of drug.

2.3 RESULTS AND DISCUSSION

The objectives of present study focused on utilizing nanoformulations based approach towards enhancement in the oral bioavailability and intestinal permeability by inhibition of p-glycoprotein efflux mechanism along with improvement in stability of phytochemicals in GIT (i.e. degradation of phytochemicals in the acidic pH of the stomach) by directing their absorption through lymphatic system. The objectives has been achieved by developing nanoemulsions based system for TC extract using oil, surfactant and co-surfactant which offered improved encapsulation(~83.8 %), smaller size (~ 33.7 nm-377 nm) and controlled release (~80.7 %) for up to 24 h, stability and enhanced permeation across the intestinal membrane.

2.3.1 UV characterization, phytochemicals screening and quantitative estimation of extract

The quantitative estimation of TC extract was done with the help of calibration curve of TC in phosphate buffer (pH 7.4). The absorbance of the TC extract at different concentrations was shown in Figure 2.1. TC is a rich source for many phytochemicals particularly for glycosides and has been reported as a major phytochemicals for many formulations [171]. The chemical composition of methylene chloride extract of TC (figure 2.2) showed the maximum content of glycosides (29.3 µg/mg) followed by flavonoids (17.5 µg/mg) and alkaloids (16 µg/mg).

2.3.2 Screening of oil, surfactant and co-surfactant

The solubility study of TC extract in various oil phases including (Clove, Turmeric, Mentha, Neem, and Calendula oil) and in a mixture of oil and surfactant (S_{mix}) were investigated and shown in (Table 2.2). Among these above oil phases, the maximum solubilization ability was observed in a mixture of clove oil and S_{mix} (20.9 ± 0.0036 mg/ml), followed by clove oil (18.25 ± 0.0009 mg/ml) and neem oil (15.6 ± 0.0007 mg/ml). The maximum solubility in the release medium i.e. pH 6.8 and Krebs ringer solution was found to be 5.23 mg/ml and 6.53 mg/ml respectively.

Table 2.2 Solubility profile of *T. cordifolia* extract in various oils and surfactant combinations

S. No	System (Oil)	Solubility (mg/ ml)
1	Mentha	7.24
2	Turmeric	12.48
3	Clove	18.25
4	Calendula	11.89
5	Neem	15.6
6	Clove oil + Surfactant + co-surfactant	20.9
7	pH 6.8	5.23
8	pH 2	3.5
9	Krebs ringer solution	6.5

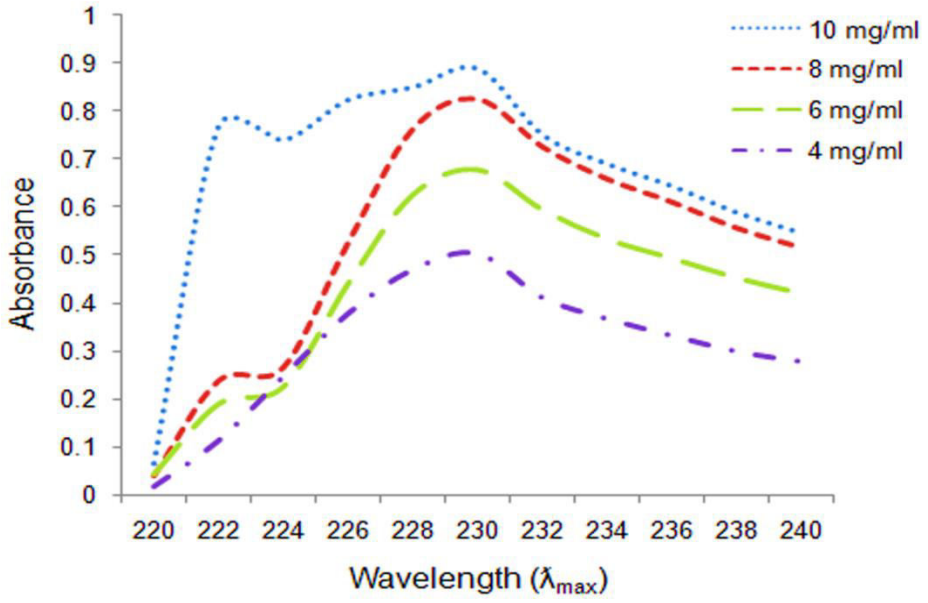

Figure 2.1 Scanning of *Tinospora Cordifolia* extract at various concentrations for UV absorbance in the range of 220-240 nm for determination of maximum absorbance (λ_{max})

For the preparation of pseudo-ternary phase diagram, the NE region in the phase diagram was compared at fixed S_{mix} (1:1), by keeping the surfactant concentration steady and

rising the co-surfactant concentration (Figure 2.3). On the reverse, the co-surfactant concentration was kept constant and increasing the surfactant content. For high surfactant concentration the droplet diameter increased up to 377 nm, which was found to reduce with low surfactant concentration.

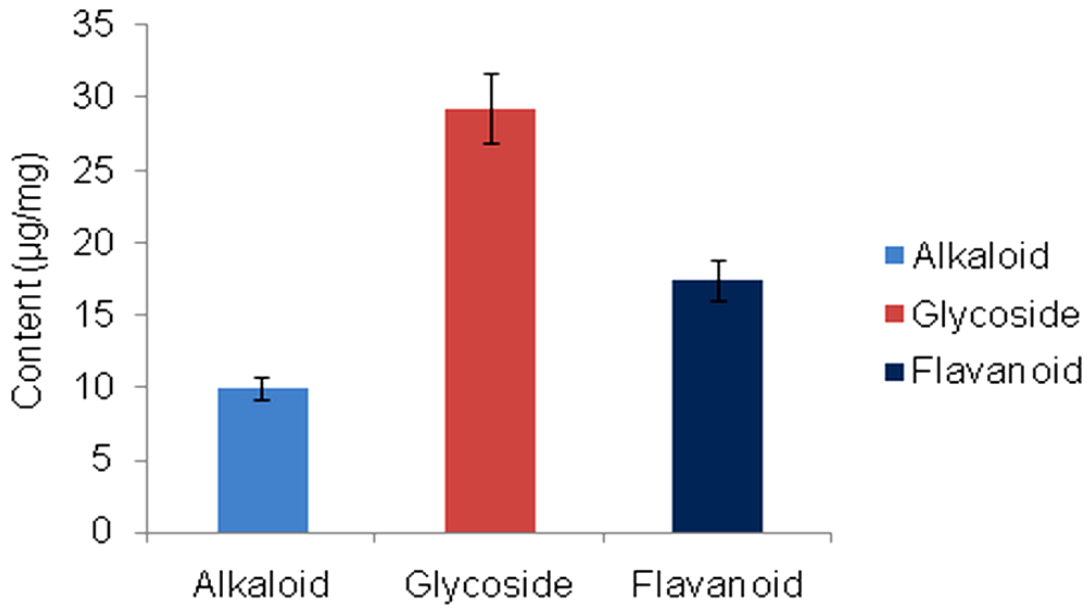

Figure 2.2 Quantitative compositions of phytochemicals from stem extract of *Tinospora cordifolia*

2.3.3 Effect of surfactant and co-surfactant on droplet size and zeta potential

The outcome of surfactant and co-surfactant concentration on droplet diameter was evaluated to optimize the formulations . Figure 2.3 depicted pseudo ternary phase diagrams as the effect of surfactant and co-surfactant on formulation aspects of nano-droplet while, figure 4 showed the histogram of particle size distribution of TC loaded nanoemulsion. From figure 2.3, a low nanoemulsion zone was observed when span 80 was used alone i.e. ethanol (S_{mix} 1:0). On the other side, when the amount of co-surfactant is low, the span 80 is not able to reduce the surface tension. An o/w emulsion was formed towards the water rich side of the phase diagram. It was also found that increasing the concentration of span 80 from 10 to 50% average droplet diameter was increased significantly from (33.7 nm – 377 nm).

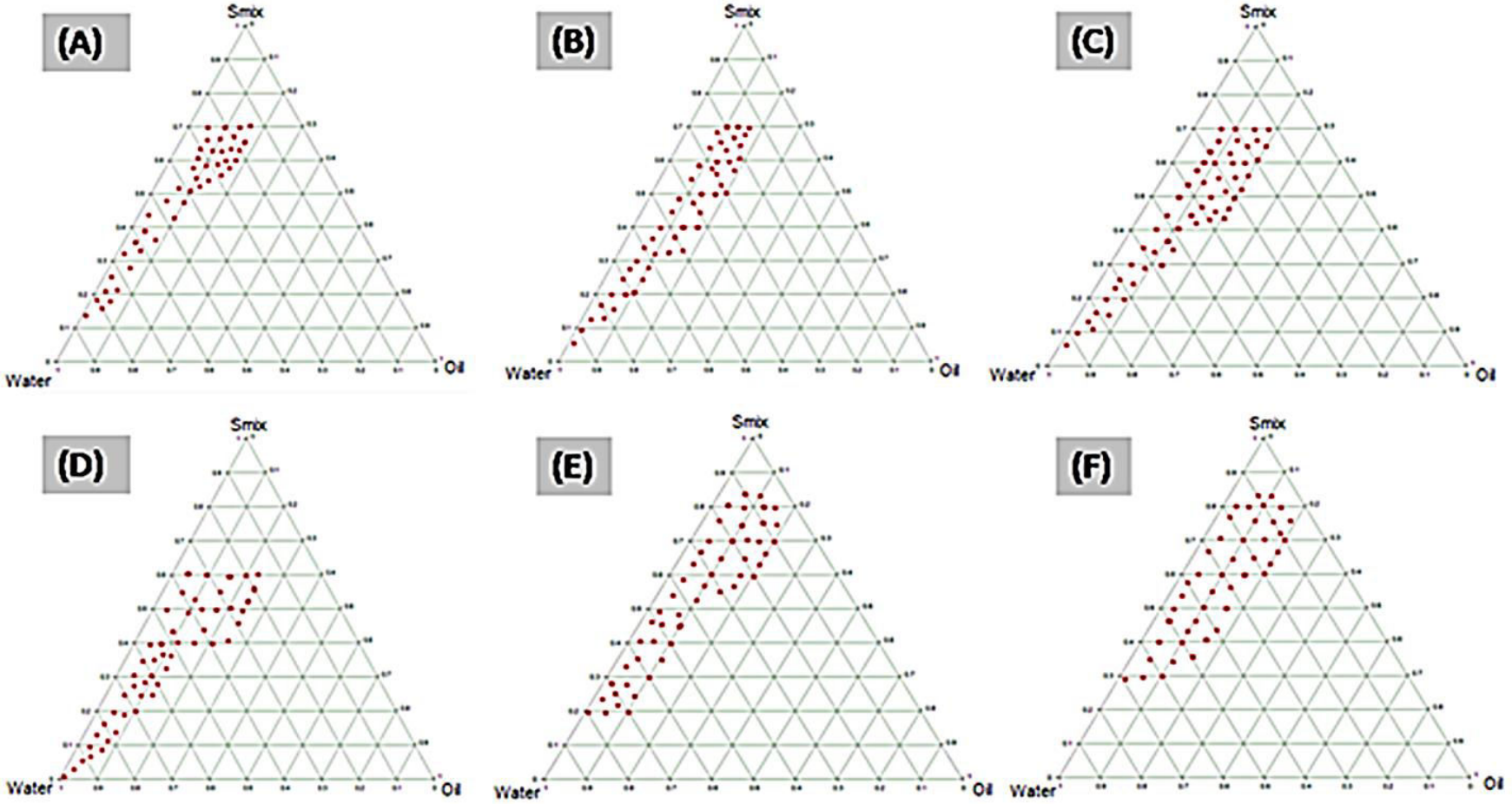

Figure 2.3 Pseudo-ternary phase diagrams indicating o/w nanoemulsion region with water and clove oil as two apices of the triangle and third apex comprising of span 80 and ethanol as different S_{mix} ratio 1:0, 1:1, 2:1, 3:1, 1:2, and 1:3 (Mentioned as A, B, C, D, E and F, respectively)

Furthermore, the reverse order was obtained on increasing the amount of co-surfactant (i.e. decrease in the average diameter). With varying surfactant concentration from 0-40 % at constant oil and co-surfactant concentration, a significant ($p < 0.01$) increase in zeta potential from – 23.3 mV to 42.1 mV was found while opposite results were obtained on increasing the co-surfactant concentration. These results showed good stability sketch of nanoformulations as it has been suggested that high zeta potential values (± 30 mV) gives high energy hurdle for coalescence of the dispersed droplets [172]. Figure 2.4A showed the Particle size distributions of blank nanoemulsion and figure 2.4B showed the Particle size distributions of nanoemulsion containing *Tinospora cordifolia* extract (F5)

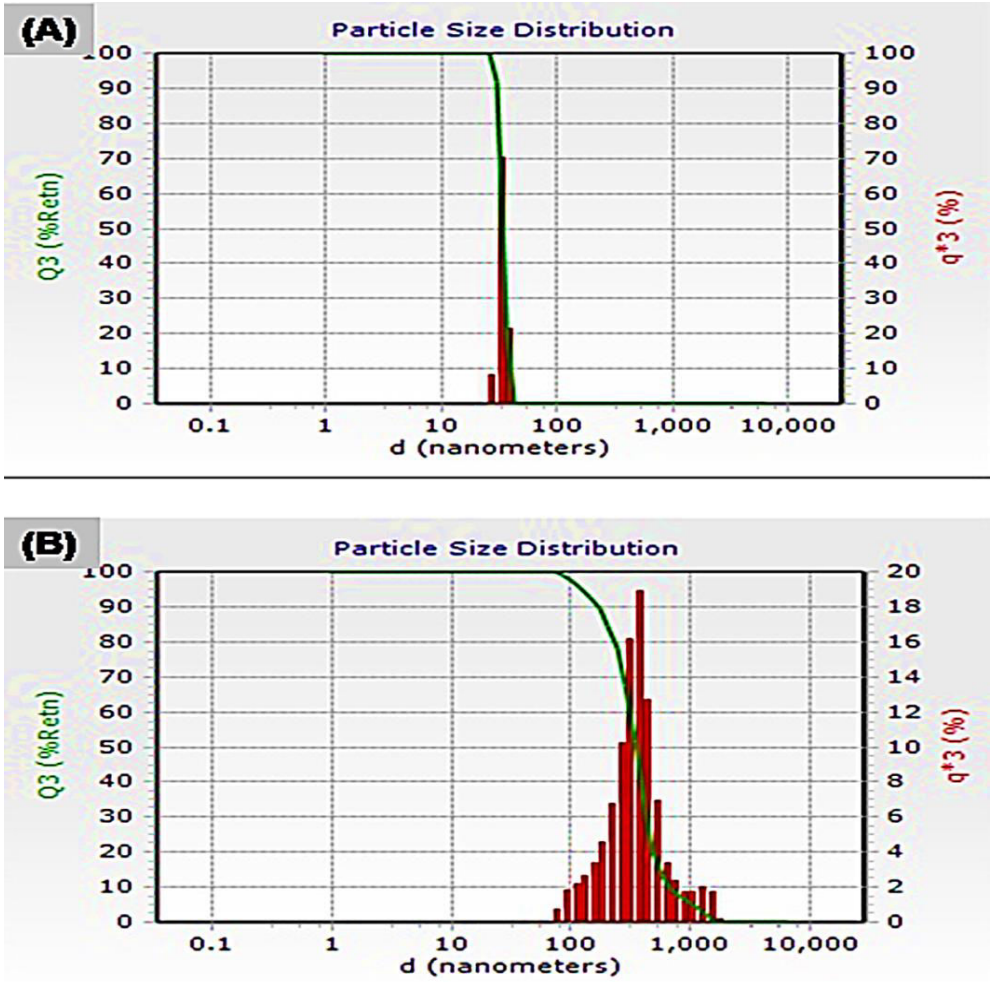

Figure 2.4 Particle size distributions of (A) blank nanoemulsion and (B) nanoemulsion containing *Tinospora cordifolia* extract (F5)

Zeta potential value (ZP) is a marker of stability profile of nanoformulations. High ZP values of (– 23.3 mV to 42.1 mV) these NE shows its kinetic stability in the nanoformulations. This could be due to depletion of surface area for adsorption of hydroxyl ions in the existence of increased amount of surfactant at the interface [65, 173]**.** While particle size is increased on increasing the concentration of surfactant , so the optimized formulation consist of optimal amount of surfactant (i.e. 0 to 40%) to get high zeta potential value with minimum particle size in a tunable manner. From the above finding it has been concluded that magnitude of zeta potential and adsorption of hydroxyl ions from the poly-oxy-ethylene available at border totally depends upon the increased surfactant concentration. The kinetic stability of these nanoformulations droplets could be due to steric stabilizing effect of non-ionic emulsifier (Span 80) in which it forms a broad steric barrier in opposition to droplet collision and thus prevents the flocculation and coalescence.

The most important formulation part was choice of optimum concentration of surfactant as it may cause toxicity as well as irritation when given orally or topically [161]. According to Kommuru et al. [174] to form O/W nanoemulsion the HLB value of surfactant should be greater than 10. Span 80 was selected on two basis, 1) solubility of TC in the mixture of oil and surfactant and, 2) highest nanoemulsion formation zone. Co-surfactants were added in order to improve the formulation efficiency of surfactant [175]. Mainly short to medium chain alcohols (C3-C8) were used as co-surfactant which further reduces the interfacial tension and also increase the fluidity of the interface [176, 41]. The presence of co-surfactant/surfactant ratio affects the phase performance of the nanoemulsion. Based on results, ethanol was used as an optimum co-surfactant to achieve its maximum nanoemulsion region.

2.3.4 Thermodynamic stability studies

It was found that optimized NEs did not show any sign of instability i.e. precipitation, phase separation, creaming and cracking, under exposure to centrifugation, heating and cooling and freeze thaw cycles. It was also observed that the formulated nanoemulsions were found to be stable in different acidic pH as there is no sign of turbidity, flocculation, and coalescence of particles, precipitation and phase separation (separation of oil from aqueous phase) .

The excellent stability of nanoemulsion droplets could be due to steric stabilizing effect of non-ionic emulsifier (i.e. Span 80) in which it is responsible for the formation of a thick steric barrier against droplet collision and thus prevents the flocculation and coalescence. At temperature above than the cloud point, an irreversible phase separation occurs due to dehydration of ingredients, which may affect the drug absorption [177, 178].

2.3.5 Physical characterization of the nanoemulsion

2.3.5.1 Morphology of optimized nanoemulsion

Flourescent microscope was used to see the shape, size and stability of the nanoemulsions. Figure 2.5 (A &B) depicted the shape and size of optimized formulation in phase contrast images while fluorescent microscopic images figure 2.5 (C, D, E and F) were indicated the core-shell structure as well as drug distribution in nanoformulations. Calcein and Rhodamine B dyes are used to confirm the distribution and leakage of drug from the lipid core. Figure 2.5 clearly indicated the physical stability of the formulated nanoemulsion with 100-200 nm particle size with no sign of aggregation of the particles. Rhodamine B and Calcein dyes were used as fluorescent dyes to see the drug distribution inside and outside the lipid part. Figure 2.5 (A, B, C and F) showed the core-shell images of nano-droplets while figure 2.5 (D, E) showed distribution of dyes within the nanoemulsion.

2.3.6 Encapsulation efficiency and *In-vitro* release study

The encapsulation efficiency of formulated nanoemulsion system (i.e. uniformity in particle diameter, thermal stability and elevated zeta potential value) was found in the range of 83.8±1.5 %. Drug encapsulation efficiency greatly dependent upon the solubility of the TC extract in oil and mixture of surfactants (S_{mix}). The lower drug encapsulation with increasing S_{mix} can be attributed to reduced amount of clove oil, which eventually led to decreased amount of TC extract loading into the nanoemulsions. One more mechanism behind the elevated encapsulation efficiency also depends upon higher partition coefficient value of TC extract (1.24) in the oil phase. The enhanced lipophilicity of TC extract contributed to its increased solubility in the oil phase and therefore, improved the entrapment efficacy in the nanoemulsion system.

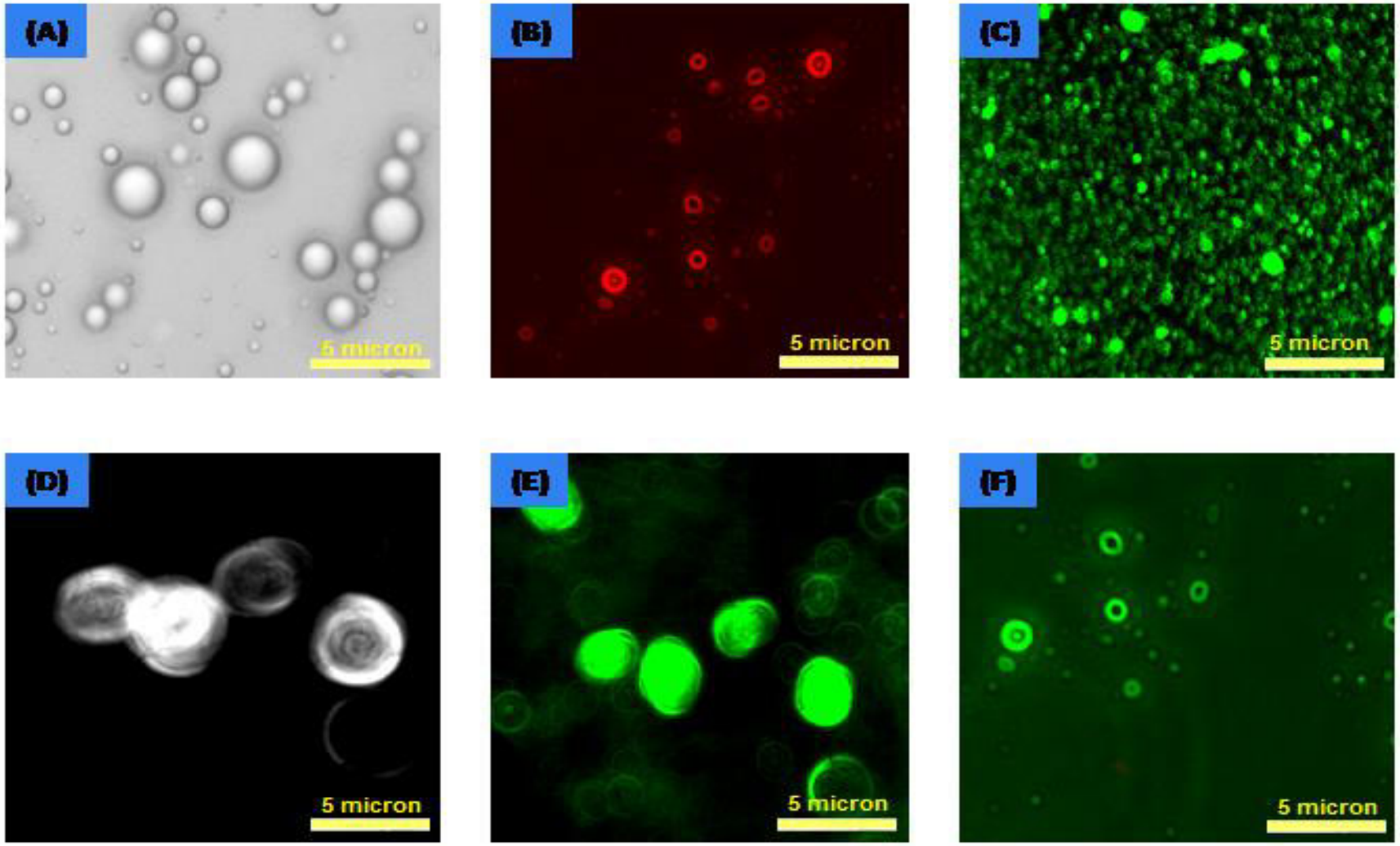

Figure 2.5 Phase contrast image of (A) nanoemulsion showing particle shape (Magnification 40 x); (B, C and F) showed localization and distribution of extract within the nanoemulsion and (D, E) showed inner morphology of nanoemulsion (Rhodamine B-red and Calcein-green)

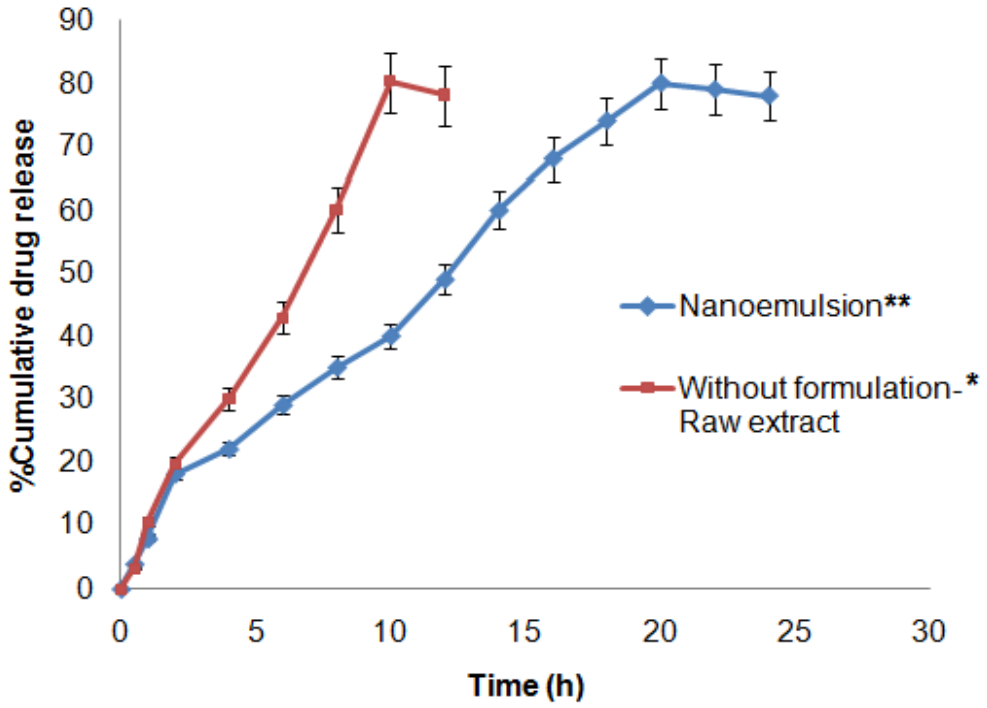

Figure 2.6 Release studies of TC extract from nanoemulsion showing percentage cumulative release from nanoemulsion and raw extract across dialysis membrane (n=3; ±SD). The p values were obtained by one way ANOVA ($p \leq 0.05$). *Significant at $p<0.05$, ** significant at $p<0.01$, ***significant at $p<0.001$

Drug release profile study of the TC extract through dialysis membrane is a useful marker for quantitative measurement of its active constituents available for absorption as well as its transfer through the lipid membrane. Approximately 26.70 ± 2.2 % and 19.51 ± 0.5% of extract was released from TC solution and nanoemulsion system respectively, within 4 h (Figure 2.6). More than 75% and 80 % of the drug was released out from the TC solution and nanoemulsion system within 12 h and 20 h respectively, indicating a slow diffusion of TC from the lipid matrix. This phenomenon can be attributed to increased hydrophobicity of TC extract in nanoemulsion (i.e. increased solubility in the oil) and secondly, a hydrophobic interaction between TC extract and oil system may help to retain the drug in the matrix of the lipid [167].

Sustained and long term release from the lipid membrane has an advantageous in terms of patient convenience as well as better absorption of the drug. Encapsulation of the drug is the main cause behind its sustained release as the drug was diffused out gradually from the oil matrix which raw extract exposed at once to dissolve and prone to diffuse to according to its solubility in the medium. According to Zhao et al [167], this phenomenon can also be attributed due to increased hydrophobicity of the TC extract (i.e.

due to its solubility in the oil phase) which leads to hydrophobic-hydrophobic interaction between the drug and the oil phase and helped in retaining the drug in the lipid matrix for a longer period of time [167].

2.3.7 *Ex-vivo* gut permeation study

Ex-vivo everted gut sac method provides a tangible link between the absorption and permeation of the drug with that of bioavailability of the drug. It has been found from the Figure 2.7A and 2.7B that the percentage drug permeated per unit surface area increases with respect to time, this is due to the incorporation of the extract inside the lipid matrix (i.e. solubility of the TC extract in the oil phase) and as well as nanosized of the droplets; while in case of raw extract (without nanoemulsion) the permeation across the membrane is very less and was due to the P-gp associated efflux mechanism that directly target the raw extract as unavailability of p-gp inhibitor (Tween 20 & Span 80) [179-181]. Nearly 3.95 fold improvement in the permeability coefficient of TC extract was noticed upon formulating it as nanoemulsion while flux (Jss), gives a quantitative estimation of the extract permeated per unit of surface area. As depicted in the Table 2.3 there is a noticeable increase in the extent of the flux in case of nanoemulsion as compared to that of raw extract. *Ex-vivo* membrane gut permeation studies showed that the nanoformulations composed of lipids and surfactants has better permeation.

The effect of formulation excipients i.e. Span® 80 and Tween® 20 on the permeation of phytochemical extract across the intestinal membrane was studied to exhibit its practical utility. Drug efflux by P-gp transporter in the gut wall has been known to supply in majority for low oral bioavailability and permeation of herbal extracts [182]. Tween 20 and Span 80 as pharmaceutical excipients are excellent inhibitor of the P-gp by interfering with ATP hydrolysis which further altering the integrity of cell membrane [183, 184].

The non-ionic surfactant i.e. span 80 used in our study does not report any charge to the formulated nanoemulsion, to a certain extent act as permeation enhancer by performing some of important tasks (i) Fluidizing agent of intestinal membrane [184], (ii) They also act as p-glycoprotein inhibitors (Specific permeation proteins that directly interfere with the drug permeability across the intestinal membrane through efflux mechanism) and acts by interacting with that of bilayers polar head and modify the hydrogen

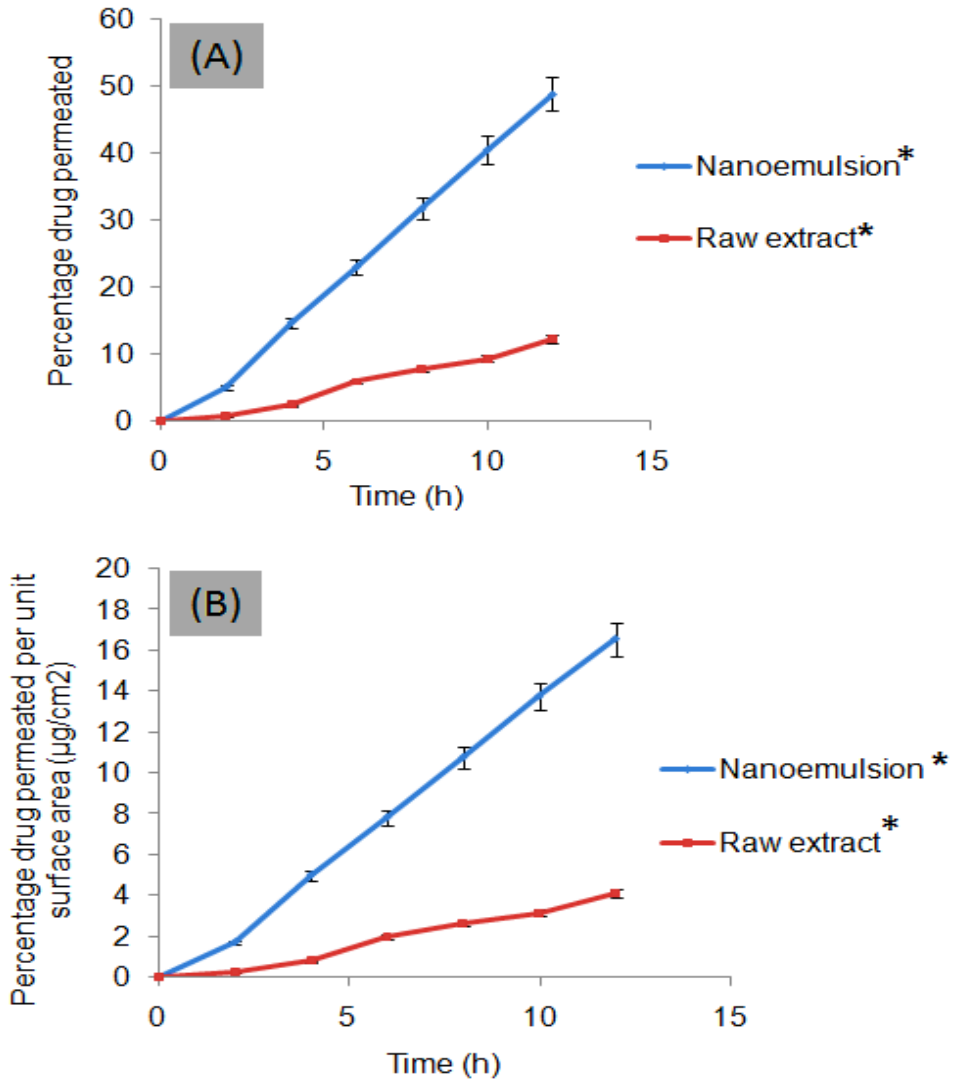

Figure 2.7 (A) Drug permeation studies though intestinal membrane using non-everted gut-sac model (n=3; ±SD). (B) Amount of drug permeated per unit surface area through intestinal membrane (n=3; ±SD). The p values were obtained by one way ANOVA ($p \leq 0.05$). *Significant at $p<0.05$, ** significant at $p<0.01$, ***significant at $p<0.001$

or ionic bond forces [184]. Nearly 3.95 fold enhancement in the permeability coefficient of TC was noticed upon formulating it as nanoemulsion. Another permeability parameter i.e. flux (Jss) provides a marked increase in the magnitude of the flux in case of nanoemulsion as compared to that of TC solution (raw extract). Although higher absorption/permeation rates were observed when incorporated inside the nanoemulsion to deliver extract as anticancer agent in comparison to raw extract. *Ex-vivo* gut permeation

studies showed that the formulation composed of lipids and surfactants has better permeation.

Table 2.3 Flux and permeability coefficient of nanoemulsion and raw extract

S. No.	SNEDDS formulation	Flux ($\mu g/cm^2hr$)	Permeability coefficient ($Kp\times10^{-3}$) cm^2/hr
1	Nanoemulsion	4.19*	0.838×10^{-3}*
2	Raw extract	1.06*	0.211×10^{-3} *

The p values were obtained by one way ANOVA ($p\leq0.05$). *Significant at $p<0.05$, ** significant at $p<0.01$, ***significant at $p<0.001$.

2.4 CONCLUSION

Nanomedicinal approach has been successfully explored for controlled delivery and improved permeation of TC extract across the biological membranes and evaluated for their *in-vitro* and *ex-vivo* parameters. The droplet size below 100 nm (~33.7 nm) and high loading efficiency (83.8 %), increased thermal as well as acidic stability were unique features of these nanoemulsions. The *in-vitro* release study demonstrates that nearly 80.5 ± 0.9 of extract was released in a sustained manner from nanoemulsion up to 24 h which is a critical step towards its improved bioavailability and permeation parameters. The permeation studies indicated that TC nanoemulsion can be easily penetrates through the intestinal membrane in comparison with raw extract (3.95 fold enhancement in the permeability coefficient). The nanomedicinal approach will certainly improve the therapeutic activity of TC extract as an anticancer, immune-modulator, anti-spasmodic, anti-osteoporotic, anti-inflammatory, anti-arthritic, and anti-diabetic agents as well as facilitate the reduction in toxic effect associated with synthetic drugs by means of increased permeability across the intestinal membrane, protection of extract from acidic degradation and by absorption through lymphatic system.

CHAPTER-3

Design and development of self nanoemulsifying drug delivery system (SNEDDS) of *Berberis aristata* for improved intestinal permeability and controlled release

ABSTRACT

In the present study, we design and develop self nanoemulsifying drug delivery system (SNEDDS) containing *Berberis aristata* (BA) extract with an objective of improving its oral intestinal bioavailability as well as its anti-diabetic efficacy. These nanoformulations were evaluated for their physico-chemical parameters such as particle size, zeta potential, drug release studies, anti-oxidant (free radical scavenging) and *in-vitro* antidiabetic efficacy. Further, *ex-vivo* drug permeation studies were performed using non-everted gut-sac model. Nanodroplet size and zeta potential of nanoformulations were optimized using two surfactants, i.e. Tween 80 and Pluronic F 68, noted as 145.7 nM, 147.1 nM and -23.30 mV, -31.2 mV, respectively. Sustained release profile of the extract from SNEDDS was examined using UV-visible spectrophotometer (λ_{max} 350 nm), was found up to 34 h. The effect of extract and SNEDDS formulation on retardation of *in-vitro* glucose diffusion was comparatively investigated. The SNEDDS showed greater reduction of glucose diffusion i.e. ~126% of raw extract and ~138% of control for 120 mins while, Inhibition of hemoglobin glycosylation by SNEDDS was observed to be ~41% higher in comparison to raw extract. Moreover, approximately 5.77 and 5.86 fold enhancement of *ex-vivo* permeability coefficient of *BA* was noticed upon formulating it as SNEDDS using two surfactants i.e. Tween 80, Pluronic F68, respectively. Improved permeability across intestinal membrane, sustained release for 34 h, greater inhibition of glucose diffusion and hemoglobin glycosylation indicates that these nanoformulations are promising carriers for oral delivery phytotherapeutics with improved stability and intestinal permeability which otherwise appeared as challenging issues upon oral administration.

3.1 INTRODUCTION

Herbal medicines elicit their pharmacological activities owing to one or more active molecule within extract. However, each component having distinct biological activity but they all work together in a synergistic manner [185]. Poor aqueous solubility, biological instability in harsh gastric environment, poor permeation across gastric mucosa and first-pass metabolism are few major issues concern with most of the phytotherapeutics and synthetic drugs (> 40%) [79]. These issues led to diminished oral bioavailability of these drugs. In general, plant based medicines have given in very high dose regimen to counter bioavailability issue but this strategy make the medicine a deficient drug candidate and offers related complications as well [186].

Lipid based formulation, especially nanoemulsion, liposome's, nanostructured lipid carriers and self nanoemulsifying drug delivery system (SNEDDS) [31] offers many advantages over other nanocarriers to tackle bioavailability issue such as minimum application of toxic organic solvents, utilization of compatible lipid bases, bypass liver metabolism by absorption via lymphatic routes, better absorption due to higher penetration through gastro-intestinal wall as well as improve stability in gastric pH. SNEDDS is an isotropic mixture of drug, oil, surfactant and co-surfactant, which forms oil in water nanoemulsion with particle size less than 100 nm when it comes in contact with aqueous medium under gentle agitation [187].

The major active constituent present in the roots of *Berberis aristata* (BA) mainly contains berberine which is isoquinoline alkaloids and contains quaternary ammonium salt with a molecular mass of 336.36 g/mol [188]. It has been reported to possess anti-hyperglycemic, anti-lipidemic, antioxidant and antimicrobial activity. *In-vivo* anti-diabetic activity of the ethanolic extract of this plant has been reported to regulate glucose homeostasis by way of lessening gluconeogenesis and oxidative stress [189]. *In-vitro* cell based studies reported that it amplify insulin receptor mRNA expression through kinase C dependent protein as promoter [190], while other studies suggest that the lipid lowering effect of berberine is due to stabilization of hepatic LDL-C receptor, extracellular signal –regulated kinase (ERK) Like most of the herbal phytotherapeutics , extremely low bioavailability (Maximum plasma concentration (C_{max}) of 0.4 ng/ml per 400 mg oral administration) is the most challenging task for formulation scientists [191]. After intragastric dosing nearly half of the berberine ran intact throughout the gastro-

intestinal tract and half of the berberine inclined of by the small intestine leading to an extremely low oral bioavailability in rats (0.36 %) [192].

In this research work, emulsion based nanoformulations (SNEDDS) were developed with the objective of enhancing the anti-diabetic efficacy of BA by means of their sustained release, improved permeability across biological membrane and improved bioavailability utilizing nanomedicine approach. In addition, the effects of surfactants (Tween 80 and Pluronic F68) on solubility of extract, its metabolism and on inhibition of intestinal P-glycoprotein (P-gp), were investigated. Furthermore, the formulated formulations were evaluated for their particle size, zeta potential, and distribution of drug using fluorescent microscopy, drug release profile, and antioxidant activity.

3.2 MATERIALS AND METHODS

3.2.1 Materials

Fresh roots of BA were collected from local region of Shimla (6,117 ft.) of Himachal Pradesh, India. Nonionic surfactant, i.e., PEG 400 and Tween 20 were purchased from Loba chemical private limited, India. Calendula oil was purchased from Konarks herbal and health care Products Mumbai, India. Rhodamine B was purchased from Oxford laboratory, Mumbai, India. Calcein was purchased from FINAR® Chem. Pvt. Ltd. Mumbai, India. All dyes used in this study were of AR grade. 2, 2-diphenyl-1-picrylhydrzyl (DPPH), dialysis membrane (LA 401-5MT; Mol wt. 12000–14000), Atropine and Quercetin dehydrate were purchased from Himedia laboratories, Mumbai, India. Ethylene diamine tetra acetic acid was purchased from Fisher scientific, Mumbai, India. Tannic acid was purchased from Sigma-Aldrich, India. Ethanol and methanol, 99.9% absolute was purchased from Merck, Germany. Double distilled water was used throughout the investigation and preparation of solutions .

3.2.2 Methods

3.2.2.1 Collection, authentication and extraction of plant

Berberis aristata roots were collected from Shimla, Himachal Pradesh, India and were shade dried, powdered and chopped in small pieces before proceeding for extraction process. The collected plant stem along with the leaves were also collected for the preparation and authentication of plant. The plant specimens pressed and dried inside the herbarium sheet using plant press. Fatty material was extracted out using hexane (8 h)

followed by soxhlation for 24 h with 200 ml of 70% ethanol at 60 °C. 70% ethanol was used for the extraction of solid extract in our study because of polar nature of active phytochemicals. As most of alkaloids e.g. berberine has more solubility in 70% ethanol. In addition, 70 % ethanol has strong penetration ability as well as low consumptions of solvents throughout the plant material used. After complete extraction, the mixture was filtered and filtrate was evaporated using Rota-evaporator (Heidolph, Germany) and freeze dried using lyophilizer to get powdered extract. The yellow colored powder extract (Yield 4.5%) was stored at -20 °C until use.

3.2.2.2 UV- characterization of *BA* extracts (λ_{max})

The various concentration of the BA extracts (i.e. 2, 4, 6 and 8 mg/ml) were recorded from a region of 200 to 700 nm in the UV spectrophotometer for the obtaining the specific absorption maxima for polyphenols present (280-350 nm). The absorbance of all the concentration was recorded in order to get λ_{max} (wavelength) at which maximum absorbance (peak) is observed for the preparation of standard curve of BA extract.

3.2.2.3 Standard curve of BA extract

For the preparation of standard curve, a mixed stock solution of 1 mg/ml was prepared by weighing accurately 25 mg of BA extract into 25 ml of volumetric flask and making the volume up to the mark with distilled water . Different running solutions were prepared from the stock solution by appropriate dilution in distilled water for the preparation of calibration curve. All the solutions were kept in dark place until used under UV spectrophotometer.

3.2.2.4 Screening of potential phytochemicals from BA root extract

Total phenolic content was quantified by using Gallic acid standard curve (Figure 2B; Appendix) [193]. 0.2 ml of plant extract (1 mg/ml) and 0.4 ml of Folin-Ciocalteu reagent was mixed and was allowed to stand at 25 °C for 5-8 min before adding 0.2 ml of 7% sodium carbonate solution. Volume was made up to 10 ml and kept at room temperature for 2 h. Absorbance was measured at 765 nm.

Total tannins content was determined by method reported by Tyler et al. [194] by using tannic acid as standard curve (Figure 2C; Appendix). 5 ml of plant extract (1 mg/ml) was

added with 0.2 ml of 0.1M ferric chloride solution. The absorbance was measured at 395 nm using UV (Elico SL-210, India) spectrophotometer.

Total flavanoids were assessed by the method as mentioned by Dewanto et al. [158] 1.5 ml of distilled water was added to 0.25 ml sample extract (1 mg/ml), followed by addition of 90µl of 5% sodium nitrite ($NaNO_2$). After addition of 180µl of 10% $AlCl_3$, the mixture was allowed to stand for 5 min before adding 0.6 ml of 1M NaOH. Final volume was made with water up to 3 ml and absorbance was measured at λ_{max} 510 nm using UV spectrophotometer. Quercetin standard curve was used for the calculation of total flavanoids (Figure 2D; Appendix).

Total alkaloids were determined by the method as mentioned by [159]. Atropine standard curve (Figure 2A; Appendix) was used for the determination of total alkaloids. For determination of total alkaloids 1 ml of plant extract (1mg/ml) was mixed with 5 ml of acetate buffer pH 4.7, followed by mixing of 5 ml BCG solution and 4 ml of chloroform in separating funnel. Bromocresol green (BCG) solution was prepared by heating 8.7 mg BCG with 3 ml of 2N NaOH and 5 ml of distilled water and volume was made up to 125 ml with distilled water. Finally, the chloroform layer containing plant extract was collected in the volumetric flask and absorbance was measured at λ_{max} 470 nm using UV spectrophotometer.

3.2.2.5 Solubility study

The solubility of BA extract was determined by mixing excess amount of extract in 0.5 ml mixture of calendula oil, surfactant and co-surfactant, separately in 2 ml of eppendrof and mixed using vortex mixer . Calendula oil was used as oil phase as it is less viscous and has the ability to inhibit the free radicals and advanced glycation end products, which are directly associated with aging and diabetes mellitus [195]. The above mixture was kept at 25±1.0 °C in an isothermal shaker (Labnet 311DS, USA) for 72 h to reach equilibrium followed by centrifugation at 3,000 rpm for 15 min. The supernatant was filtered through 0.22 µm membrane filter and the concentration of extract in mixture was determined using UV spectrophotometer at λ_{max} 350 nm using linear equation of BA extract [161].

3.2.2.6 Screening of Surfactant

Tween 20, Tween 80, Span 80 and Pluronic F68 were used for screening of nanoemulsion formulation. In water 2.5 ml of 15 % surfactant solution was prepared , and mixed with 4 µl of oil with vigorous vortexing. In order to optimize the oil content required for nanoemulsion (NE) formation, oil was continuously added until a cloudy tint appeared. The oil contents were drawn on ternary phase diagram [161].

3.2.2.7 Screening of co-surfactant

Tween 80 (TWSNE) and Pluronic F68 (PLSNE) were combined with PEG 400 as co-surfactant. At fixed S_{mix} ratio of 1:1, pseudo ternary phase diagrams were constructed . Twelve different combinations of oil and S_{mix}, 1:9, 1:8, 1:7, 1:6, 1:5, 1:4, 1:3, 1:2, 1:1, 6:4, 7:3 and 9:1 (weight ratio) were taken so that maximum ratios were covered to describe the boundaries of nanoemulsion formed in the phase diagram [161].

3.2.2.8 Design and development of self nanoemulsifying drug delivery system

3.2.2.8.1 Miscibility study

BA was blended with a minimum mixture of oil, surfactant and co-surfactant (1 ml) and vortex for 10 min equilibrated at room temperature for 24 h followed by centrifugation at 3500 rpm for 10 min . Miscibility criteria was evaluated on the basis of presence of any immiscible particle at the bottom.

3.2.2.8.2 Pseudo-ternary phase diagrams

A series of self emulsifying systems were prepared with varying weight percentage of oil, surfactant, co-surfactant and drug at room temperature. The prepared SNEDDS formulation (0.1 ml) was mixed with 100 ml of distilled water in a glass beaker at room temperature . The tendency to emulsify spontaneously within the distilled water was assessed visually using the grading criteria according to Shafiq et al. [16]. Rapidly forming formulations with a clear and slightly bluish or a slightly less clear microemulsion (with in 1 min), were labeled as “A” as the best emulsification region. If bright white emulsion is formed (with in 2 min) the region will be labeled as “B” and was still considered to have meet the self emulsification criteria. A dull, grayish white emulsion with either poor or less emulsification region with large oil drops floating on the surface was labeled as “C” in the phase diagram.

3.2.2.8.3 Effect of surfactant and co-surfactant concentration on droplet size and zeta potential

To investigate the effect of surfactant concentration on the droplet size [Nanotrac wave Zetasizer (Microtrac, USA)] and zeta potential, blank SNEDDS and extract-loaded SNEDDS were prepared with increasing surfactant concentration and decreasing co-surfactant by 10% and keep the oil percentage constant to maintain the concentration of total component as 100%. The samples were diluted to 1:100 with Milli-Q water. On the other set of experiment, the effect of co-surfactant was investigated with increasing concentration of co-surfactant by 10% while decreasing the same percentage of surfactant.

3.2.2.9 Thermodynamic stability study

Selected formulations were subjected to different thermodynamic stability test to assess their physical stability. Six cycles of temperature were conducted (4 °C and 40 °C) at each temperature for not less than 48 h and formulations were examined for stability (phase separation, creaming, and cloudiness) at these temperatures. Selected formulations were centrifuged at 3,500 rpm for 30 min and formulations were assessed for their physical stability like phase separation and emulsion creaming. The optimized SNEDDS formulations were diluted in a ratio of 1:250 with distilled water. The diluted samples were heated gradually on a water bath and the cloud point was observed visually at which there is sudden appearance of cloudiness [165].

3.2.2.10 Physicochemical characterization

The physicochemical characterization of blank and extract loaded SNEDDS were evaluated for droplet size analysis, zeta potential determination and fluorescent microscopic analysis .

3.2.2.10.1 Fluorescent microscopy

The fluorescent microscopy of the prepared SNEDDS was analyzed using fluorescent microscope (Olympus BX53, USA) for its shape and drug distribution. The Rhodamine B and Calcein dye were used as fluorescent model drug to check out the drug distribution inside the liquid lipid (oil phase). Rhodamine B and Calcein dye loaded SNEDDS were prepared by dissolving Rhodamine B and Calcein (equivalent to that of BA amount) in a

mixture of oil, surfactant and co-surfactant. The prepared mixture (0.1 ml) was diluted with 100 ml of distilled water in a glass beaker to get SNEDDS and analyzed at excitation and emission wavelength of 540 nm and 625 nm using FITC and TRITC filters detector, respectively

3.2.2.11 Drug loading and encapsulation efficiency

Encapsulation efficiency (EE) of drug loaded SNEDDS was estimated by the method proposed by [196]. Briefly 10 ml of diluted SNEDDS formulation was centrifuged at 3,000 rpm for 10 min. Elutes containing drug loaded SNEDDS were collected and dilute up to 10 ml with ethanol followed by vortexing for 3 min to dissolve the BA. Then the resulting mixture was centrifuged at 12,000 rpm for 15 min and the amount of drug in the supernatant liquid was calculated using UV spectrophotometer at a λ_{max} of 350 nm using equation .

$$EE = \frac{W_{entrapped\ drug}}{W_{initial\ drug}} \times 100$$

Where $W_{initial\ drug}$ represents the initial amount of drug added and $W_{entrapped\ drug}$ represents the amount of drug entrapped in the nanoemulsion.

3.2.2.12 *In-vitro* drug release profile

In-vitro release of BA from the SNEDDS was evaluated using a dialysis bag-diffusion method [167]. An appropriate amount of BA SNEDDS was filled in dialysis bag and immersed in distilled water (100 ml) at 37 ± 0.5 °C, under sink conditions at constant stirring on magnetic stirrer. After certain time intervals, 3 ml aliquot was withdrawn from the vessel and replaced by the same volume of fresh medium. The amount of BA released in the medium was calculated using UV spectrophotometer at 350 nm. To determine the release behavior of the free drug (BA) from dialysis bags, a control experiment was also performed. Then procedure, described above for the SNEDDS formulation was followed. Each experiment was performed in triplicate (n=3).

3.2.2.13 *In-vitro* free-radical scavenging activity of the extract released

The free radical scavenging activity of the extract (released into the medium) was evaluated using DPPH (2, 2-diphenyl-1-picrylhydrazyl) scavenging assay [197]. A 500 µl

sample of the released medium containing drug (BA) was added to 1 ml of 0.1 mM w/v solution of DPPH in ethanol at room temperature and stored in dark at room temperature for 30 min. The radical scavenging activity was measured using UV spectrophotometer at 517 nm and expressed as the percentage of DPPH reduced by the BA released from the formulation using equation, where A_0 is the absorbance of the control i.e. DPPH alone and A_1 is the absorbance of the test i.e. BA released from the formulation. The experiment was carried out in triplicate and results were showed as mean ± standard deviation . The antioxidant activity of the extract released from SNEDDS was compared with the radical scavenging activity of the raw extract and standard ascorbic acid using DPPH assay.

$$\% \text{ inhibition} = \frac{A_0 - A_1}{A_0} \times 100$$

3.2.2.14 *In-vitro* anti-diabetic activity

3.2.2.14.1 *In-vitro* inhibition of hemoglobin glycosylation

3.2.2.14.1.1 Collection of blood sample and preparation of hemoglobin

Blood sample were collected from freshly slotter goat (local slotter house, Solan, HP, India) into a blood bottle containing ethylene diamine tetra-acetic acid as anticoagulant (EDTA) [198]. From the procedure, the collected blood was washed thrice with 0.14 ml of NaCl solution and 1 volume of red blood cells suspension was lysed with 2 volume of 0.01 M phosphate buffer, pH 7.4 and 0.5 ml of carbon tetrachloride. The Haemolysate was centrifuged at 3000 rpm for 15 min at room temperature for the separation of hemoglobin rich plasma .

3.2.2.14.1.2 Estimation and effect of extract on hemoglobin glycosylation

Non-enzymatic glycosylation of hemoglobin was estimated by the method as reported by Adisa et al. [199]. In to three different tests tubes, each containing 1 ml of different concentration of glucose (2, 10 and 20 mg/ml) in PBS (pH 7.4) was mixed with 1 ml of hemoglobin fraction followed by 72 h incubation. A blank solution without glucose solution was used as control. Formation of nano-molar concentration of hydroxymethyl-furfural was estimated at different time intervals of 0, 24, 48 and 72 h which was an indicator of degree of glycosylation. For determine the antidiabetic activity of

phytochemicals and the effect of nanoformulations, 5.0 µl of Gentamycin, 25 µl of Gallic acid (standard) and extract released from SNEDDS was added to 1 ml of glycosylated hemoglobin solution and incubated in dark at room temperature for different period of 0, 6, 12, 24, 48 and 72 h and was estimated calorimetrically at 443 nm. The tests were conducted in triplicate . Percentage inhibition was calculated as method [199].

$$\% \text{ inhibition} = \frac{A_{control} - A_{extract}}{Acontrol} \times 100$$

3.2.2.14.2 *In-vitro* inhibition of glucose diffusion

In-vitro glucose diffusion assay was performed as per the method proposed by Srichamroen & Chavasit, with slight modification [200]. 1 ml of plant extract and SNEDDS were placed in different dialysis membrane along with glucose solution i.e. 0.22 mM in 0.15 M sodium chloride. The dialysis membrane was then tied from both the end immersed in beaker containing 40 ml of 0.15 N sodium chloride and 10 ml of distilled water. A control sample is also run without plant extract (blank). The beaker was then placed on orbital shaker at room temperature. The movement of glucose into external solution was monitored after 15, 30, 60, 90 and 120 min. All the test were performed in triplicate (n=3).

3.2.2.14.3 Inhibitory effect of the extract and SNEDDS on conversion of starch to glucose in starch/α-amylase system

The inhibitory effect of the BA extract and SNEDDS was studied as per the protocol published [201]. 4% starch solution was dissolved in 200 ml of 0.05 M phosphate buffer (pH 6.5) at 65 °C for 30 min. A starch solution containing known amount of plant extract (1 mg/ml) and SNEDDS was mixed with gentle stirring on the water bath at 65 °C for 5 mins. Starch solution containing α-amylase at 0.4% (w/v) was added into the dialysis bag against 200 ml of distilled water at 37 °C as dialyzing medium. A control sample is also run without using the plant extract to compare glucose diffusion in the receptor medium. Sample were collected after 0, 15, 30, 60, 90 and 120 min and replaced by the same volume of fresh medium. All the experiments were conducted in the triplicate (n=3).

3.2.2.15 *In-vitro* permeation Studies

3.2.2.15.1 Non-everted gut-sac method

Oral absorption of plant extract from SNEDDS was studied using non-everted gut sac method using chicken ileum [169]. Jejunum segment was washed six times with Krebs ringer solution (KRB) with continuous aeration. After washing, it was filled with SNEDDS (extract loaded) as well as with raw extract (dissolved in distilled water), separately and ligated into beakers containing 50 ml of KRB with continuous air bubbling maintained at 37 ± 0.5 °C. After particular time intervals, aliquots of drug solution were withdrawn and replaced by the same fresh medium. The amount of BA was determined by it absorbance at 350 nm through UV-visible spectrophotometer and compared with that of raw extract permeated through intestinal membrane The slope of the linear portion was calculated as flux Jss (µg/cm^{2}hr) and from the given equation permeability coefficient was calculated as

$$K_p = J_{ss}/C_v$$

Where K_p is the permeability coefficient and C_v is the total amount of drug. Results were expressed as mean ±standard deviation (n=3).

3.3 RESULTS AND DISCUSSION

The present research work focused on utility of SNEDDS towards enhancement in the oral bioavailability, intestinal permeability and *in-vitro* antidiabetic activity with minimization of stability issue related with phytochemicals like degradation of extract in the acidic pH of the stomach by absorption through lymphatic system. The objective was achieved by development of SNEDDS based nanoemulsion system of BA extract using calendula oil, PEG 400, tween 80 and Pluronic F68. With improved stability, enhanced permeation across the intestinal membrane and *in-vitro* antidiabetic activity through these oil based system can be used as a promising technology to improve the bioavailability and stability issues related with phytochemicals.

3.3.1 Phytochemicals screening of extract

Flavonoids and phenolic compounds are primarily responsible for antioxidant activity of BA [202]. 70 % ethanolic extract have showed 114.8 µg/mg of alkaloids followed by tannins (23.1 µg/mg), phenols (8.82 µg/mg), and flavonoids (15.62 µg/mg) (Table 3.1) (Figure 2E, supplementary data)

Table 3.1 Phytochemicals composition of *B. aristata*

Phytochemicals	Quantity (µg/mg)
Tannins	23.1
Flavanoids	15.62
Phenols	8.82
Alkaloids	114.85

3.3.2 Screening of oil, surfactant and co-surfactant

The selection of surfactant is also a key factor for stabilized droplet size while designing a formulation . Non-ionic surfactants have recognized as safe and biocompatible, as they remain unaffected by change in pH or ionic strength. The maximum solubility of drug in a mixture of oil, surfactant and co-surfactant was found out to be 14.2 ± 0.8 mg/ 500 µl. Tween 80 and Pluronic F68 having HLB value of 15 and 24 were used as surfactant because of its larger capacity to form O/W SNEDDS. (Figure 3.1) showed the formulated (A) blank SNEDDS, (B) BA loaded SNEDDS and (C) Diluted SNEDDS with distilled water.

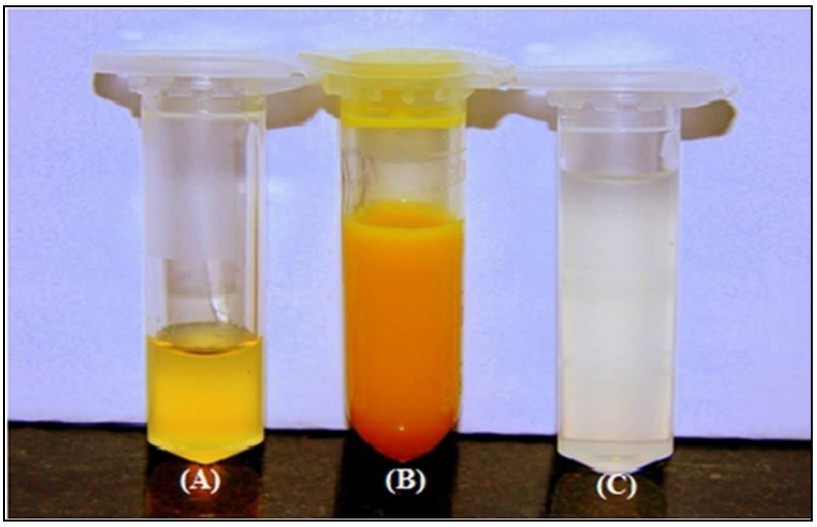

Figure 3.1 Optical images of SNEDDS formulations. (A) Blank SNEDDS (light yellow color is due to Tween 80 and calendula oil), (B) *B. aristata* loaded SNEDDS (The dark and slight pink color is due to extract and excipients), (C) Diluted SNEDDS with distilled water (1:50)

Co-surfactants are used to enhance the mobility of hydrocarbon chain and also increase the miscibility of the aqueous and oily phase by being partitioned between two phases [160]. PEG 400 was used as it improves permeation across GI lumen when incorporated in the formulation [160].

3.3.3 Pseudo-ternary phase diagram

Drawing of ternary diagram gives an idea about the composition of the selected formulation and the nature of the resultant dispersion i.e. self nano-emulsifying region, micro-emulsion, phase separation, micro gels and coarse emulsion and hence gives an idea of selecting optimum formulation. As indicated in (Figure 3.2) Pluronic F68 formed higher emulsifying region than that of Tween 80 (Figure 3.3) with calendula oil.

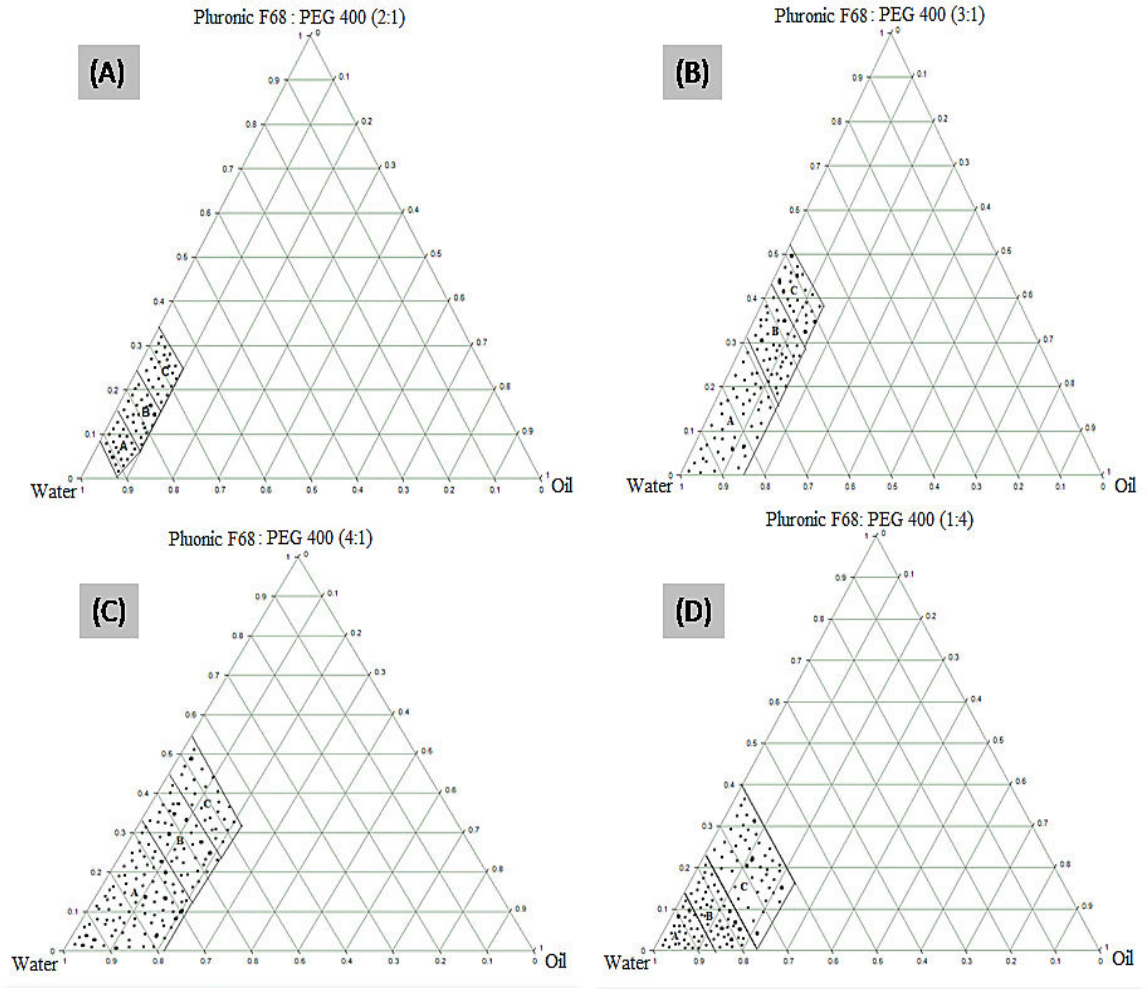

Figure 3.2 Ternary phase diagram drawn with water and calendula oil as two apices of a triangle and third apex consist of mixture of Pluronic F68: PEG 400 in a ratio of 2:1, 3:1, 4:1, and 1:4 (mentioned as A, B, C, & D respectively)

Better emulsification of Pluronic F68 may be due to its HLB value in higher hydrophilic region as required to form o/w emulsion [175]. It has been observed from [Figure 3.2 & 3.3 (A-D)], that increasing concentration of Pluronic F68 and Tween 80 i.e. 2:1, 3:1, 4:1 resulted in increase in the self nano-emulsifying region, but owing to decreasing concentration of Tween 80 and Pluronic F68 it resulted in small SNEDDS region.

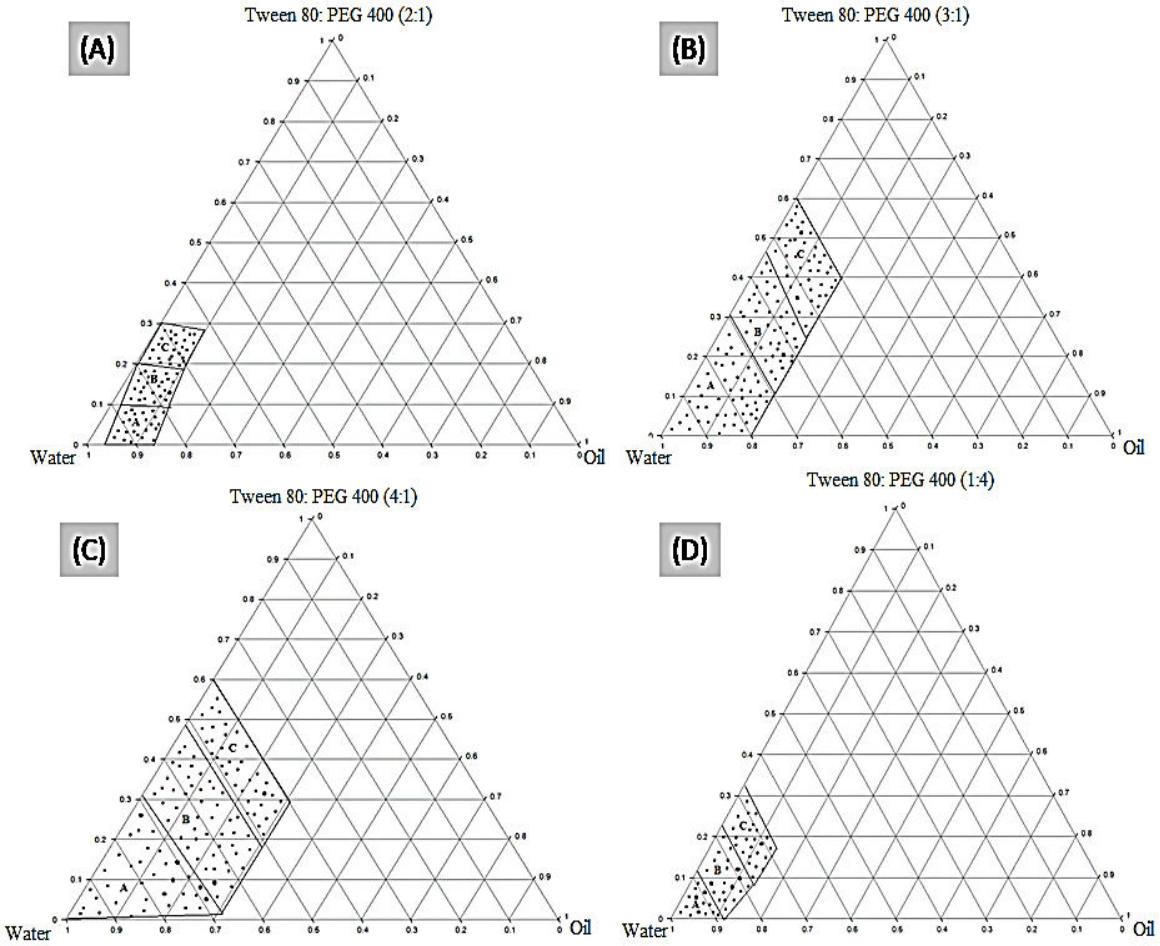

Figure 3.3 Ternary phase diagram drawn with water and calendula oil as two apices of a triangle and third apex consist of mixture of Tween 80: PEG 400 in a ratio of 2:1, 3:1, 4:1, and 1:4 (mentioned as A, B, C, &D respectively)

3.3.4 Development of SNEDDS formulation

3.3.4.1 Effect of excipients concentration on the droplet size and emulsion time

The effect of surfactant concentration on droplet size of the formulated nanoemulsion was shown in [Figure 3.4 (A)]. It was found that increasing concentration of Tween 80 from 10% to 50% the average droplet size was decreased from 307 nm to 144 nm while in case of Pluronic f68, increasing the concentration from 0% to 45% decreased the average droplet size from 307 nm to 139.3 nm. Such a decrease in the droplet size may be due to the formation of firm interface between the oil and water, which provides stable surface by reducing the interfacial tension [203].

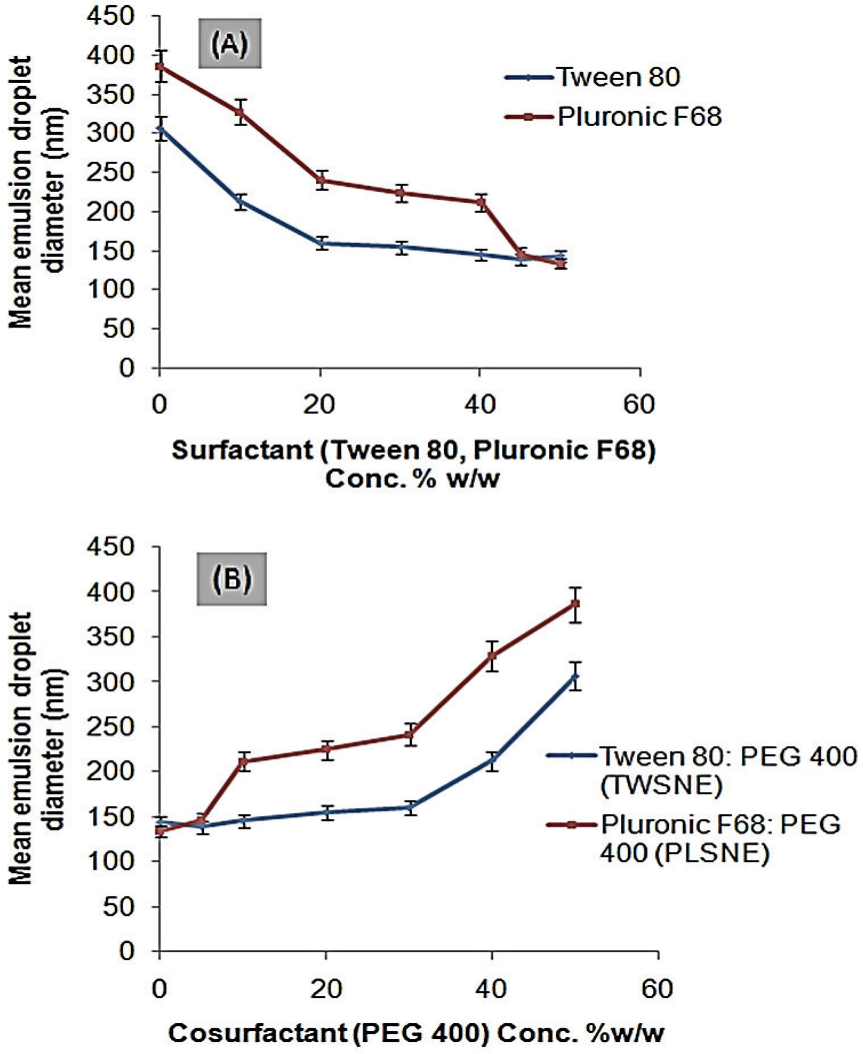

Figure 3.4 (A) Effect of Tween 80 and Pluronic F68 on the mean droplet size of SNEDDS formulations, (B) Effect of co-surfactant (PEG 400) concentration on droplet size of SNEDDS formulations

The effect of co-surfactant concentration on the nanoemulsion droplet size is shown in [Figure 3.4 (B)]. In case of TWSNE composition, it was observed that with an increase in

the concentration of co-surfactant from 0 to 50%, the average diameter was increased from 144 nm to 307 nm. The increase of the droplet size was relatively flattened with co-surfactant concentration from 0 to 30% and increased steeply with 30 to 50%. It was mentioned that mean droplet size was decreased with increasing surfactant content from 30-50% which can be attributed reduction in the surface tension between oil and water phase and thus provide stable formulation .

On increasing the concentration of tween 80 from 10 to 50%, increase in average droplet size was observed [Figure 3.4 (A, B)], such a decrease in the droplet size may be due to the formation of rigid interface between the oil and water, which provides stable surface by reducing the interfacial tension [203]. Zeta potential is one of the indicators for the physical stability of the emulsion formed. However, high zeta potential value (± 30 mv) should preferably be achieved for all the emulsion to ensure high energy barrier for coalescence of the dispersed droplets [172] but in our formulations, zeta potential decreases (from +43.7 to -23.3 mv) on increasing the surfactant concentration. The negative charge on the emulsion is generally imparted by the free fatty acid and hydroxyl ions present in the surfactant (PEG 400) .

3.3.4.2 Effect of excipients concentration on the zeta potential

Zeta potential is one of the indicators of physical stability of the emulsion system. With increasing surfactant concentration from 0-40% (v/v) (at constant oil and co-surfactant level), zeta potential decrease significantly from 43.7 to -23.3 mv [Table 3.2 (A) and 3.2 (B)]. The negative charge on the emulsion is generally imparted by the free fatty acid and hydroxyl ions present in the surfactant (PEG 400). The zeta potential was found to be within the range of 43.7 to -14.68 mv and 45.2 to -27.8 mv for TWSNE and PLSNE, respectively [Table 3.2 (A) and 3.2 (B)] and drug loading is 40% for the optimized formulation. In addition, the droplet size also remains less than 100 nm when these SNEDDS were diluted 200-2000 times with distilled water.

3.3.5 Morphology of SNEDDS

Phase contrast images of optimized SNEDDS formulation depicted the morphology and distribution (Figure 2F; supplementary data) while fluorescent microscopic images were indicated the core-shell structure as well as drug distribution in nanoformulations. Rhodamine B and Calcein dyes are used to check out the distribution and leakage of drug

from the lipid core. Spherical shaped globules were observed within the range of 100-200 nm [Figure 3.5 (A&B) supplementary data] without any sign of aggregation, an indicator of physical stability of the optimized formulation. Fluorescence images showed consistent distribution with smaller particle size and drug distribution. Calcein and Rhodamine B, both are hydrophilic fluorescent dyes which stain the hydrophilic structure and encapsulated inside the lipid membrane indicates the core structure of the o/w nanoemulsion respectively.

Table 3.2A Effect of Tween 80 (TWSNE) and PEG 400 ratio on the nanoemulsion droplet size and zeta potential

Formulation code	Calendula oil (%w/w)	Tween 80 (%w/w)	PEG 400 (%w/w)	Droplet size (nm)	Zeta potential (mV)
F1	50	0	50	307	43.7
F2	50	10	40	213.1	-4.30
F3	50	20	30	160.3	-11.34
F4	50	30	20	155	29.6
F5	50	40	20	145.7	-23.30
F6	50	45	5	139.3	-14.68
F7	50	50	0	144	31.45
F8	50	25	25	129	-5.67

Table 3.2 B Effect of Pluronic F68 (PLSNE) and PEG 400 ratio on the nanoemulsion droplet size and zeta potential

Formulation code	Calendula oil (%w/w)	P F68 (%w/w)	PEG 400 (%w/w)	Droplet size (nm)	Zeta potential (mV)
F1	50	0	50	387	23.1
F2	50	10	40	329	-23.4
F3	50	20	30	242.1	-11.9
F4	50	30	20	224.7	-4.56
F5	50	40	20	212	-27.8
F6	50	45	5	147.1	-31.2
F7	50	50	0	164	45.2
F8	50	25	25	847	-9.6

3.3.6 Thermodynamic stability studies of SNEDDS

Thermodynamic stability studies predict the kinetic stability of the formulations as well as the chemical reaction among the drug and excipients of the formulation. Ideally, SNEDDS system should not exhibit stability issues in GI fluid, i.e. precipitation, phase separation, creaming and cracking [169]. Some optimized formulations were selected and it was observed that both the optimized formulations, i.e. TWSNE and PLSNE did not show any such signs under exposure for centrifugation, heating and cooling cycle and freeze thaw cycles, were indicators of stability of nanoemulsion that could be due to steric stabilizing effect of surfactants against droplet collision. (Table 3.3) showed the long term stability study for up to six months.

Determination of cloud point is an important factor for the optimized formulation containing non-ionic surfactant. The cloud point for optimized formulation TWSNE and PLSNE was found to be 65-69 °C and 82-85 °C respectively. At temperature higher than the cloud point, an irreversible phase separation occurs due to dehydration of ingredients, which may affect the drug absorption [177]. Hence to avoid phase separation the SNEDDS formulation cloud point should be above body temperature (i.e. 37 °C)**.**

Table 3.3 Long term stability study of SNEDDS at 25 °C

S. No.	Time (month)	Particle size (nm)	Zeta potential (mV)
1	0	147.1	-31.2
2	1	146.4	-31.7
3	2	147.9	-30.2
4	4	146.4	-30.9
5	6	149.1	-31.8

The optimized formulation didn't show any signs of instability (change in particle size, zeta potential, phase separation and flocculation) under exposure for centrifugation, heating and dilution under various acidic pHs, and this could be due to steric stabilizing effect of surfactants against droplet collision. At temperature higher than the cloud point, an irreversible phase separation occurs due to dehydration of ingredients, which may affect the drug absorption [177]. Hence to avoid phase separation the SNEDDS formulation cloud point should be above body temperature (i.e. 37 °C)**.**

3.3.7 *In-vitro* antidiabetic activity

The hemoglobin present in the RBC has a tendency to bind non-enzymatically with glucose in a proportional manner which is known as glycosylated hemoglobin [204]. The percentage inhibition of glycosylation by SNEDDS was found to be ~41% higher (47.37% versus 33.56%) in comparison to raw extract while standard Gallic acid (positive control) showed 61.19% inhibition [Figure 2G, (A); Appendix]. Moreover, results showed that raw extract was able to inhibit the hemoglobin glycosylation only for 24 h whereas, SNEDDS showed inhibitory activity for more than 72 h.

Furthermore, glucose diffusion assay gives an idea about the ability of drug to prevent glucose transport across the intestinal membrane. **[**Figure 2G, (B); Appendix] shows glucose concentration in the dialysate containing glucose/raw extract and glucose/SNEDDS system. Raw extract and SNEDDS system retard the glucose diffusion across the membrane by 13.6 % and 35.5 % respectively after 120 min [Figure 2G, (B); Appendix] showed that sustained release of extract from SNEDDS prevent the glucose to diffuse from the membrane for longer period of time (200 mins) in comparison to raw extract (i.e. 120 mins) (Table 2A; supplementary data). Inhibition of glucose permeability due to BA was due to the fact that BA found to be completely dissolved in water and creates a strong network which traps the glucose [200]. In order to examine the concentration dependent effect of BA on inhibition of glucose permeability, two different glucose concentrations i.e. 32 & 100 mM was used (Table 2B; supplementary data). 32 mM was selected as it is the approx. concentration of glucose in the rat intestine, post meal [205]. For testing at elevated glucose concentration, 100 mM glucose concentration was selected. In the later case, the raw extract and SNEDDS formulation showed its inhibitory effect for 12 and 24 h respectively. At 32 mM glucose concentration, the raw

extract and SNEDDS inhibited glucose diffusion by 45.42% in 12 h and 38.13% in 24 h due to the sustained release of the extract from SNEDDS respectively.

We examined the effect of extract as well as nano-formulation on α-amylase inhibition activity via α-amylase-starch system. In biological system, starch is digested by α-amylase and produces maltose, maltotrioses (get completely hydrolyzed by maltase and isomaltase) and free glucose before it gets absorbed [206]. The results showed that raw extract and SNEDDS retard the glucose diffusion by 33.30% and 41.18% respectively (Table 2C; supplementary data). Noticeable that raw extract retard the glucose diffusion only for 120 min as it diffused out along with glucose while SNEDDS maintain its inhibitory action up to 180 mins as showed in [Figure 2G, (C); supplementary data].

The hemoglobin present in the RBC has a tendency to bind non-enzymatically with glucose in a proportional manner which is known as glycosylated hemoglobin [204]. As the amount of extract released from SNEDDS increases, formation of glucose-hemoglobin complex decreases (as observed through absorbance in visible range (at λ_{max} 443 nm). Such hemoglobin-glucose linkage is either constant or remain stable throughout the life span of RBC (60-120 days) if not treated (in case of diabetic patient). Long term and increased antidiabetic activity of formulation could be due to the sustained release of BA extract from the SNEDDS.

Furthermore, glucose diffusion assay gives an idea about the ability of drug to prevent glucose transport across the intestinal membrane **[**Figure 2G, (B); Appendix]. A Concentration dependent effect of BA was examined on two different concentration i.e. 32 and 100 mM and it was found that in both the cases raw extract was able to delay the glucose diffusion only for 12 h while SNEDDS showed its inhibitory effect for more than 24 h and this could be due to the sustained release pattern of the extract from the lipid matrix. We also examined the effect of extract as well as nano-formulation on α-amylase inhibition activity via α-amylase-starch system. Starch is hydrolyzed by α-amylase into free glucose, which was measured in the dialysate.

In biological system, starch is digested by α-amylase and produces maltose, maltotrioses (get completely hydrolyzed by maltase and isomaltase) and free glucose before it gets absorbed. Extremely low bioavailability (Maximum plasma concentration (C_{max}) of 0.4 ng/ml per 400 mg oral administration) is the most challenging task for formulation scientists [190]. Sustained release of BA extract from the SNEDDS results in

improvement in the concentration of BA extract in the blood which further shows concentration dependent inhibition of alpha amylase. *In-vivo* anti-diabetic activity of the ethanolic extract of this plant has been reported to regulate glucose homeostasis by way of lessening gluconeogenesis and oxidative stress [188]. The SNEDDS showed inhibitory effect on glucose diffusion in a sustained manner for up to 180 min in comparison to120 min by raw extract.

3.3.8 *In-vitro* release studies and radical scavenging activity

Release and transport of extract through dialysis membrane is a useful indicator of quantitative estimation of the phytochemicals available for absorption as well as its absorption through the lipid membrane. BA solution released 22 ± 0.75% of extract within 4 h while more than 80% of the drug was released from the BA solution within 12 h. In contrast, the percentage cumulative release of extract from SNEDDS was only 13.16 ± 1.17% after 4 h whereas, less than 50% of extract was released within 12 h and ~ 96.83% extract was released up to 34 h as shown in figure 3.5 (A). These results showed that there was no burst release from SNEDDS and significant ($p<0.05$) sustained diffusion of BA extract from the lipid matrix.

The prolong inhibition of DPPH radicals were observed in case of SNEDDS formulation loaded with BA extract for 22 h in comparison with the raw extract (only for 16 h). The scavenging activity of released extract was compared with that of scavenging activity of standard ascorbic acid which scavenges almost same percentage of free radical in comparison to SNEDDS for up to 22 h [Figure 3.5 (B)]. The *in-vitro* scavenging activity of formulations confirmed that sufficient polyphenolic compounds which were released and maintain oxidative free zone over a period of 22 h.

Controlled and sustained release from the lipid membrane has an advantageous in perspective of patient convenience as well as better absorption of the drug for longer period of time. It indicated a slow diffusion of BA extract from the lipid matrix. This phenomenon can be attributed to increased hydrophobicity of BA extract in SNEDDS formulation and may also be due to hydrophobic-hydrophobic interaction between drug and matrix lipids. Furthermore, controlled release of BA extract results in the inhibition of free radicals which further confirms that sufficient polyphenolic compounds were released over a period of 22 h.

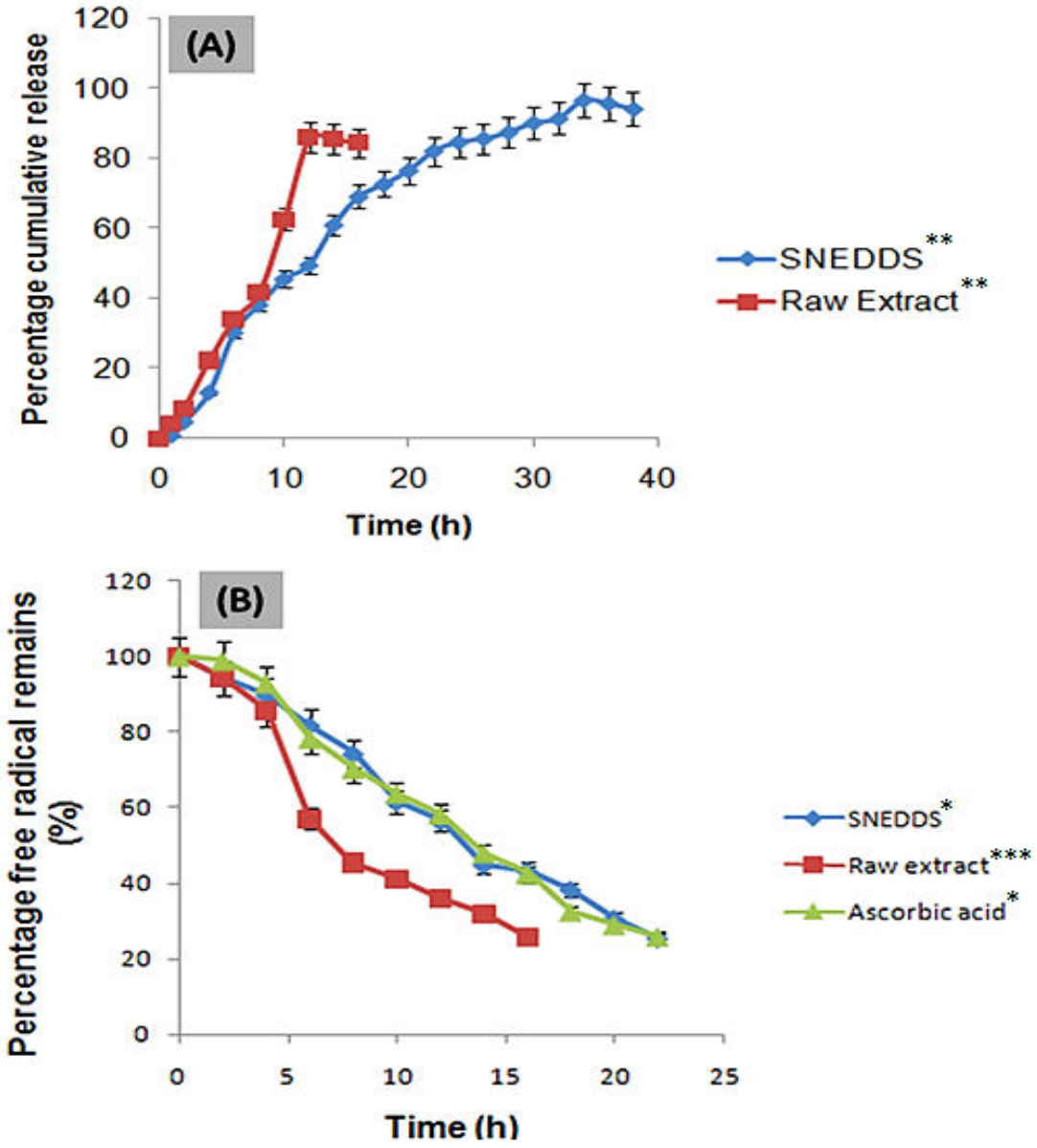

Figure 3.5 (A) Release studies of *B. aristata* extract from SNEDDS across dialysis membrane (n=3; ±SD); (B) Free radical scavenging activity of *B. aristata* loaded SNEDDS in comparison with ascorbic acid (n=3; ±SD). The p values were obtained by one way ANOVA ($p \leq 0.05$). *Significant at $p<0.05$, ** significant at $p<0.01$, ***significant at $p<0.001$

3.3.9 *In-vitro* permeation study

To evaluate the effect of two surfactant type (i.e. Tween 80 and Pluronic F68) on flux and permeability coefficient, *in-vitro* everted gut sac method was used as it is an established method to provide a tangible link between the absorption and permeation of the drug with its bioavailability. The permeability coefficient of raw extracts and two formulations i.e.

TWSNE and PLSNE were shown in (Table 3.4). Permeability coefficient of BA was nearly same [i.e. 5.81(TWSNE) and 5.86 (PLSNE)] (Figure 3.6). Another permeability parameter is flux (J_{ss}) that provides an estimate of the drug permeated per unit surface area. A marked increase in the magnitude of the flux in case of TWSNE (5.77 fold) and PLSNE F68 (5.86 fold) was observed in comparison to raw extract (Table 3.4).

Efflux by P-gp transporter in the gut wall has been known to contribute in majority for diminished oral bioavailability and permeation of herbal extracts across the intestinal membrane [182]. Tween 80 and Pluronic F68 as pharmaceutical excipients are known to inhibit the P-gp by mechanism of interfering with ATP hydrolysis, altering the integrity of cell membrane [183]. The possible causes for enhanced intestinal permeability of BA extract through nanoemulsion are 1) solubilization of BA extract in the oil phase and embedding into the nanoemulsion system, 2) protection from enzymatic degradation, 3) inhibition of glycoprotein (P-gp) efflux pump (P-gp mediated efflux of BA) by nanoemulsion system containing P-gp inhibitors i.e. Tween 20 and oil phase, 5) surfactant induced membrane fluidity that improved permeability and, 6) the intestinal lymphatic transport for BA nanoemulsion system (bypass the hepatic portal system of usual drug absorption thus reduce metabolic degradation of phytotherapeutics).

Permeability parameters i.e. flux (J_{ss}) that provides an estimate of the drug permeated per unit surface area. A marked increase in the magnitude of the flux in case of TWSNE (5.77 fold) and PLSNE F68 (5.86 fold) was observed as compared to the raw extract (Table 3.4). The result clearly demonstrated that the optimized SNEDDS formulation was significantly increase the drug permeation across the intestinal membrane, primarily by inhibiting the P-gp efflux.

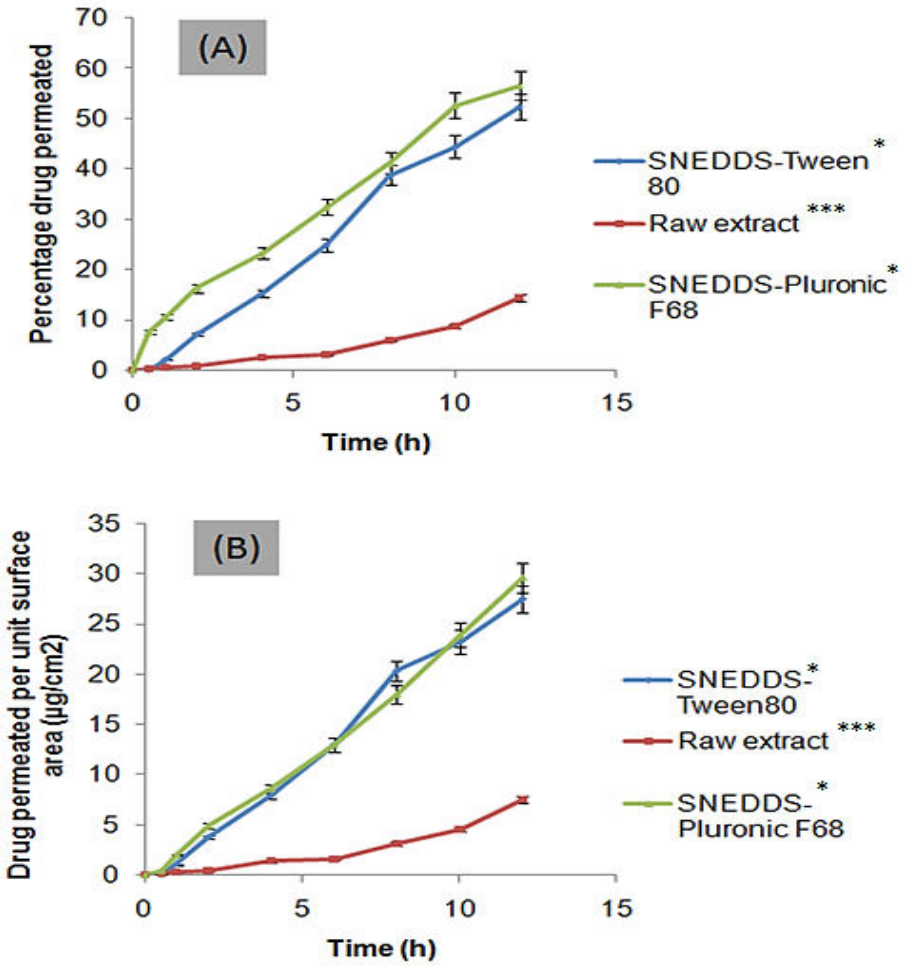

Figure 3.6 (A) Drug permeation studies though intestinal membrane using non-everted gut-sac model (n=3; ±SD). (B) Amount of drug permeated per unit surface area through intestinal membrane (n=3; ±SD). The p values were obtained by one way ANOVA ($p \leq 0.05$). *Significant at $p<0.05$, ** significant at $p<0.01$, ***significant at $p<0.001$

Table 3.4 Flux and permeability coefficient using Tween 80 and Pluronic F68

S. No.	SNEDDS Formulation	Flux (µg/cm^{2}hr)	Permeability coefficient (Kp×10^{-3}) cm^2/hr
1	SNEDDS-Tween80(TWSNE)	4.68	0.93×10^{-3}
2	Raw extract	0.81	0.162×10^{-3}
3	SNEDDS-PluronicF68 (PLSNE	4.75	0.95×10^{-3}

The p values were obtained by one way ANOVA ($p \leq 0.05$). *Significant at $p<0.05$, ** significant at $p<0.01$, ***significant at $p<0.001$.

3.4 CONCLUSION

Oral delivery of numerous drugs as well as phytochemicals hindered due to their high lipophilicity, stability issues in the harsh acidic environment as well as low permeability issues due to P-gp efflux mechanisms. The present study involves the successful synthesis of BA extract loaded SNEDDS using two different surfactants i.e. Tween 80 and Pluronic F 68. SNEDDS loaded BA is a promising strategy for improved stability, permeation across the intestinal membrane and in turn, will enhance the therapeutic efficacy and bioavailability of BA with varying surfactant and oil types to achieve maximum drug loading, sustained drug release profile and size range, in tunable manner. Small droplet size, stability in the acidic environment as well as Controlled and sustained release (22 h) from the lipid membrane has an advantageous in perspective of patient convenience as well as better absorption of the drug for longer period of time. The developed novel formulation results in 5.86 fold enhancement in the permeability parameters. Overall, our studies demonstrated that SNEDDS formulation can be used as a possible alternative to traditional oral formulation to improve its stability, permeability and dissolution rate leading to enhanced bioavailability and oral delivery.

CHAPTER-4

Design and development of PVA/SA nanocomposite sprayed hydrogel dressing for controlled release of *Ficus benghalensis* extract and synthesis of silver nanoparticles using green chemistry

ABSTRACT

In-situ forming dressing offers excellent patient compliance and contamination free self-shaped protective covering without wrinkling or fluting in the wound bed. Such a novel concept was designed and executed using polyvinyl alcohol (PVA) and sodium alginate (SA) as polymeric components while boric acid and calcium chloride were used as respective cross-linkers to form spontaneous sprayed dressing. The sprayed hydrogel and silver nanoparticles were characterized for size, surface morphology, degradation profile and thermal analysis and biological parameters i.e. hemocompatibility, protein adsorption release profile of silver nanoparticles and phytotherapeutics as well as sustained anti-microbial and anti-oxidant properties. The highly stable and uniformly distributed Ag nanoparticles were obtained. FTIR spectra show polymeric interaction with AgNPs while SEM images showed surface morphology of the SHD film. Equilibrium swelling ratio and degradation profile in aqueous media (distilled water and buffers) are found to dependent upon PVA/SA ratio. Polymeric combination exhibit pseudoplastic behavior with Farrow's constant >1. Uniformly distributed AgNPs (particle size~27.55±2.01 nm), high water retention (~13 fold) and biodegradable (~5 days) nature of dressing along with sustained release profile of both AgNPs for 24 h with concentration-dependent antimicrobial activity have been observed. The results of microbe penetration (no penetration across the film) and antimicrobial activity tested against *S. aureus* and *E. coli* bacteria showed a concentration dependent zone of inhibition for up to 24 h respectively. Self shaped, biodegradable, aseptic, prolong anti-oxidative, non-hemolytic, blood compatible and hemostatic properties of SHD film appears as promising dressing for superficial wounds.

4.1 INTRODUCTION

The design of drug delivery is usually drug physico-chemical and kinetic properties. Conventional drug delivery system suffers from the limitation of minimal synchronization between the required time for therapeutically effective drug plasma concentration and actual drug release exhibited by the dosage form. In order to meet demand for emerging innovative products, higher cosmetic expectations of patients as well as rising incidence of chronic wounds such as diabetic wounds, pressure ulcers and surgical injury, researchers have to explore novel concepts of skin wounds management [207]. The selection of biomaterials, texture of dressing and its biochemical properties need to be controlled very precisely as chronic wound healing is a very complex biological process, involves cascade of overlapping events [208]. The complexities of chronic wounds can be resolved through designing of modern dressing which provide moist and aseptic microenvironment with regular availability of anti-inflammatory and wound healing promoting agents in a controlled manner with excellent patient convenience for chronic wounds management [209].

In this era, nanotechnology is one of the most interesting fields which are used to describe the creation and utilization of polymeric materials as antimicrobial agent. In recent years, the fabrication of silver nanocomposite hydrogel has attracted much attention due to the stabilizing capacity of the nanoparticles [210]. The use of silver nanoparticles has exhibited good antibacterial activity than bulk silver due to high surface area, leading to the incorporation of more nanoparticles in the bacteria, and therefore improves its efficacy in a sustained manner [210, 211]. Polyvinyl alcohol (PVA) is a biocompatible and chemically neutral polymer which has been explored for drug delivery and maintains a continuous moist environment around the wound surface. While sodium alginate (SA) has been chosen for this study due to its high hydrophilicity, high protein adsorption ability, high gelling property and also possess good biological properties without any unexpected behavior. Meanwhile PVA/SA film blend combines advantages of both; PVA film alone possesses high mechanical properties while SA has good physical, biological and adhesive properties.

Several terms have been coined for hydrogels, such as “intelligent gels” or “smart hydrogels”. Hydrogels are three dimensional network composed of hydrophilic polymers and proven dressings in this context with immense water retention properties and tissue

mimetic consistency. There are some commercialized hydrogels available in market in various branded products in forms of gels, foam, sheets such as Tegaderm® CHG (3M Healthcare), Vigilon gel, Ivalon, Aqua gel, Kik gel, Lyofoam (Seton Health care), Normlgel (Molnlycke), Ameda Comfort Gel and SPAND-Gel™. Various synthetic polymers such as PVA, poly (caprolactone), polyurethanes and their combinations with natural counterpart i.e. gelatin, collagen, chitosan, alginates and cellulose derivatives have been investigated by various research groups for the development of hydrogel based dressings. Majority of formulations offered patient inconvenience due to their low mechanical property, low swelling, high thickness, sticking to the wound surface and instability under high stresses. Furthermore, application of secondary dressings causes further trauma at the site [212]. To overcome such complications, researchers have been investigating polymeric nanocomposite hydrogels dressings towards designing of novel dressing with high mechanical property, high swelling capability with higher degradation. Natural world has encouraged investigator to build nanocomposite hydrogels loaded with clays [213], cross-linked structure of new materials as a result of their soft, wet and non-swellable hydrogel with high mechanical property [214, 215]. Sun et al. [216] prepared a new class of viscoelastic hydrogels from polyampholytes with enhanced mechanical properties. Gong et al. [217] formulated double network hydrogels as a replacement for articular cartilage and connective tissue using blend of hydrophilic polymers with extremely high mechanical property, swelling (60-90%) and also showed high wear resistance due to their extremely low coefficients of friction. Balakrishnan et al. [218] synthesized *in-situ* forming hydrogel using gelatin, oxidized alginate and borax which have further showed enhanced migration of epithelial cell in full thickness rat model. Dong et al. [219] prepared bioactive injectable hydrogel dressing using polyethylene glycol (PEG)-based thermo responsive hyperbranched copolymer and thiol-modified hyaluronic acid for wound healing applications. Long-term viability of adipose derived stem cells and prevention of unwanted wound contraction was achieved which may otherwise cause scars, painful contractures and mobility dysfunction in the cases of large, deep wounds such as extensive burns.

Silver nanoparticles are basically broad spectrum antimicrobial agents and used against resistant species and are commercially available as various brand names such as Contreet (Coloplast), Actisorb Silver (Smith & nephew), Allevyn Ag, Polymem (Ferris Mfg. Corp.), and many more brands. The synthesis technique and local toxicity of silver are major problems for its biological application as reduction of silver salt using synthetic

chemicals such as sodium borohydride is hazardous to environment as well as human body, while high concentration of silver in wound tissue adversely affects nascent tissues and thus delayed the healing progression [220].

To overcome these issues, present research used green chemistry of *FB* extract (a natural reducing agent) for synthesis of AgNPs, while instability problems and concentration dependent toxicity issue was controlled by sustaining its release using a cross-linked network of PVA and SA. Furthermore, *in-situ* sprayed hydrogel film was developed in association with AgNPs to provide mechanical strength to the film. The *FB* extract was utilized as an antioxidant as well as haemostatic agent which immediately coagulate the blood and acts against oxidative stress on its application in a cost effective and sustained manner. PVA is a biocompatible and chemically neutral polymer which has widely explored for drug delivery and biomedical applications. It is a good film forming agent and able to maintain a continuous moist environment around the wound surface while, SA is a natural polysaccharide possessing high gel forming ability, biocompatible, high protein adsorption ability [221].

In this chapter, PVA/SA sprayed films loaded with AgNPs (synthesized using *FB* extract) were synthesized by spraying mixture of PVA/SA as polymers, BA and $CaCl_2$ as physical cross-linkers. Boric acid is a weak acid of boron and often used as antiseptic and insecticides. The solution of PVA, SA is prepared in such a way that it can easily come out of the aerosolized system as fine droplets and immediately cross-linked (BA and $Cacl_2$) to form a thin film over the wound surface. PVA/SA sprayed films results in formation of matrix of chemically cross-linked polymer for controlled drug delivery. The main emphasis in this investigation is to utilize the *FB* extract as antioxidant and hemostatic agent which immediately coagulate the blood on the wound surface and also acts against oxidative stress in a cost effective manner. Properties of sprayed films such as swelling behavior, degradation study, morphology and in addition release of AgNPs and *FB* extract from sprayed films was also investigated. Finally *in-vitro* bio-evaluation of sprayed films as wound dressing characters like protein absorption, Hemocompatibility, *in-vitro* antimicrobial and hemostatic activity of extract loaded sprayed films studies were also investigated.

4.2 MATERIALS AND METHODS

4.2.1 Materials

Sodium alginate (SA), PVA (Mol. Weight ~77,000 g/mol), sodium dodecyl sulfate (SDS) were purchased from (Loba Chemie. Pvt. Ltd. Mumbai, India), 2, 2-diphenyl-1-picrylhydrzyl (DPPH), Calcium chloride (Merck specialties Pvt. Ltd. India) and bovine serum albumin were purchased from (Himedia, Mumbai), Boric acid, methanol, nitric acid, hydrochloric acid and were purchased from (Merck, Mumbai, India), Silver nitrate ($AgNO_3$), ethylenediamine tetra acetic acid (EDTA), sodium chloride (Fisher Scientific, Mumbai, India) and all other chemicals and reagents used in this study were of analytical grade. Double distilled water was used throughout the investigation, solubility study and preparation of solutions.

4.2.2 Methods

4.2.2.1 Collection and authentication of plant materials

The stem bark of *Ficus benghalensis* were collected from the local region of Ghumarwin, district Bilaspur (Himachal Pradesh). The collected stem along with the leaves were than subjected for the preparation of herbarium sheet for the authentication of plant. The plant specimens were than pressed and dried inside the herbarium sheet using plant press. The collected stem bark of *F. benghalensis* was washed 2-3 times with distilled water and air dried for the synthesis of silver nanoparticles.

4.2.2.2 Preparation of plant extract

The stem bark of *F. benghalensis* was dried under shade, crushed into small pieces and powdered using mechanical grinder. The powder was loaded into the soxhlet extractor and subjected to successive extraction starting from non-polar solvent i.e. petroleum ether to a more polar solvent i.e. 70 % ethanol. The obtained ethanolic extract was than collected in a beaker followed by its filtration and drying using rotary evaporator (Heidolph, Germany)". The obtained dry product is than preserved in refrigerator under well closed container (4 ℃; because of its hygroscopic nature) until further use. The obtained extract has a brownish color with a final yield of 2.1 % w/w.

4.2.2.3 UV- characterization of *F. benghalensis* extracts (λ_{max})

The various concentration of the FB extracts (i.e. 2, 4, 6 and 8 mg/ml) were recorded from a region of 200 to 700 nm in the UV spectrophotometer for the specific absorption maxima of phenolic compounds (280-350 nm). The absorbance of all the concentration

was recorded in order to get λ_{max} (wavelength) at which maximum absorbance (peak) is observed for the preparation of standard curve of FB extract.

4.2.2.4 Standard curve of FB extract (Phenolic compounds)

For the preparation of standard curve, a mixed stock solution of 1 mg/ml was prepared by weighing accurately 25 mg of FB extract into 25 ml of volumetric flask and making the volume up to the mark with distilled water. Different working solutions were obtained from the stock solution by appropriate dilution in distilled water for the preparation of calibration curve (λmax 275 nm; Figure 2H; Appendix). All the solutions were kept in dark place until used under UV spectrophotometer.

4.2.2.5 Synthesis of silver nanoparticles

Green synthesis method was used for the synthesis of silver nanoparticles [222]. Briefly, different concentration of aqueous solution of *FB* extract (i.e. 2% to 6 % w/v) was mixed with equal volume of 1 mM aqueous silver nitrate solution (5 mL) and allowed to react at 45 ºC under continuous agitation (200 rpm) under magnetic stirrer. The formation of silver nanoparticles was achieved by periodic sampling after 0, 10, 20 and 25 min in order to monitor the change in color and UV absorbance (Elico SL-210, India) of the solution.

4.2.2.6 Characterization of silver nanoparticles (AgNPs)

4.2.2.6.1 Particle size, zeta potential and UV spectroscopy analysis

The droplet diameter and zeta potential of AgNPs were observed using Nanotrac Wave Zetasizer (Microtrac, USA) at room temperature at an angle of 180 degree. To determine the time point of maximum production of silver nanoparticles, the absorption spectra of the sample were taken 300-500 nm using UV-vis spectrophotometer. The de-ionized water was used as blank.

4.2.2.7 *In-vitro* antimicrobial activity

4.2.2.7.1 Test microorganisms and growth media

The two gram positive and gram negative bacteria *i.e. E. coli* (ATCC-723) and *S. aureus* (MTCC-3160) were chosen as test micro-organism based on their pharmacological and clinical importance. Nutrient broth (NB) was used as a growth medium for growing these

cultures at 37 ℃ for 24 h and stored at 4 ℃ until further use. The growth in the culture medium was confirmed based on turbidity appearance.

4.2.2.7.2 Minimum inhibitory concentration (MIC) of silver nanoparticles

Broth dilution method was used for the calculation of minimum inhibitory concentration of silver nanoparticles [223]. Serial dilutions were made by mixing bacterial culture grown in nutrient broth (100 µl and PBS (900 µl) from the stock solution). From this solution 100 µl of the mixture was again mixed with 900 µl of PBS (10^{-1}) and which was further diluted to get a maximum diluted concentration of 10^{-9}. The control plates (without AgNPs) were prepared by spreading 100 µl of culture (micro-organism) in different dilutions (i.e. 10^{-2}, 10^{-4}, 10^{-5}, 10^{-6} and 10^{-8}) to get 150 to 200 countable colonies. The test agar plates were prepared by mixing and pouring different concentration of AgNPs (test) with that of nutrient agar followed by spreading of culture (10^{-5}). The concentration of AgNPs at which no colony remains on the culture plate, was chosen as MIC of AgNPs and that amount was loaded in the PVA/SA sprayed hydrogel dressing (SHD).

4.2.2.8 Preparation of PVA/SA sprayed hydrogel films

Physically cross-linked hydrogels of sodium alginate (SA) and PVA solution were prepared using boric acid and $CaCl_2$ as cross-linkers respectively. Briefly, aqueous solution of PVA (6% w/v), sodium alginate (3% w/v), $CaCl_2$ (3% w/v) and Boric acid (8% w/v) solutions were prepared by dissolving them in distilled water. Different ratios of PVA/SA (1:1, 1:2, 1:3, 2:1, 3:1 and 4:1) containing known quantity of *FB* extract and AgNPs were mixed uniformly. The prepared mixtures of the polymers were than sprayed on a glass-slide and immediately cross-linked with the help of mixture of $CaCl_2$ & boric acid as cross-linkers, simultaneously. The film was than peeled out carefully and kept in freezer until further studies.

4.2.2.9 Physicochemical Characterization of Spray Hydrogel Dressing (SHD)

4.2.2.9.1 Fourier-transform infrared spectroscopy (FTIR)

The prepared hydrogel samples were dried by lyophilization technique (Alpha 1-2 LD plus, Germany) and compressed to get fine powder for further analysis. The FTIR

spectrums were obtained by recording bands between 4000 and 400 cm^{-1} with a resolution of 2 cm^{-1}.

4.2.2.9.2 Scanning electron microscopy (SEM)

The surface morphology and internal morphology of the SHD films were investigated by using SEM with 15 kV voltages for secondary electron imaging. The different ratio of PVA/SA (1:0, 0:1, 1:1, 1:2, 2:1 and 3:1) hydrogel films were prepared by snap freezing technique using liquid nitrogen and coated with gold using an ion sputter coater (Hitachi S3400N, US).

4.2.2.9.3 Thermal gravimetric analysis (TGA)

The TGA analysis of the PVA, SA alone, blank SHD films and PVA/SA/AgNPs loaded SHD film was performed using a TGA-Pyres-6TGA (EXSTAR TG/DTA 6300, Woodland, CA) by heating the SHD films from 50 ºC to 750 ºC at a heating rate of 20 ºC/min under a nitrogen flow. A derivative plot was used to calculate the initial (T_i), maximum (T_{max}) and final decomposition (T_f) temperatures of the sprayed films.

4.2.2.10 Determination of swelling behavior

The swelling behavior of SHD hydrogels were carried out by using gravimetric method [239]. For calculation of swelling behavior, the SHD hydrogels were kept in glass petri plates and dried at 40 ºC for 4 h in an oven. Briefly, the dried samples *(W_e;* ~10 mg*)* of SHD films were kept in distilled water and different acidic and basic buffers (pH 1.2, 6.5 and 7.4) further supplemented with 0.04 % w/v of sodium azide as antifungal agent and stored at 37 ± 0.2 ºC in an incubator. After predetermined intervals of time i.e. 1, 3, 6, 12 and 24 h, swollen SHD films were weighed (W_s) on analytical balance (n=3, after blotting on filter paper), till constant weight achieved. Water uptake capacities of SHD film specimens were determined using given equation [224].

$$\text{Equilibrium swelling ratio (\% ESR)} = \frac{W_s - W_e}{W_e} \text{ x } 100$$

4.2.2.11 *In-vitro* weight loss profile

The *in-vitro* weight loss profile of SHD films was calculated by means of measuring the change in weight as a function of time [225]. Dry SHD hydrogel specimens (~10 mg)

were placed in glass petri plates containing phosphate buffer (pH 6.5). The SHD hydrogel samples were than incubated at 37 ± 0.2 ℃ (sodium azide 0.04% w/v as antifungal agent) at 50 rpm in an incubator shaker (Labnet 311DS, USA). After a predetermined time interval, fresh medium i.e. phosphate buffer pH 6.5 was added (replaced) and films were weighed. The percentage loss in weight was calculated using the following formula given below

$$\text{Percentage Degradation (\%)} = \frac{\text{Wt}_{(i)} - \text{Wt}_{(t)}}{\text{Wt}_{(t)}} \text{ x } 100$$

Where $\text{Wt}_{(t)}$ is the weight of the films at time t and $\text{Wt}_{(i)}$ is the initial weight of the films at time zero.

4.2.2.12 Effect of PVA concentration on to the rheological property of SHD films

The flow property of the PVA alone and PVA/AgNPs solutions at different concentrations (2, 4 and 6 % w/v) was studied using Brookfield viscometer (RVT, Brookfield Engineering Laboratories, Inc., USA) at a rotation speed of 20 rpm using spindle no 64. The corresponding reading was noted in order to get viscosity value. The viscosity values obtained was used to calculate the Farrow's constant (indicator of pseudo-plasticity).

4.2.2.13 Atomic absorption spectroscopy (AAS)

The content uniformity and distribution pattern of silver nanoparticles was calculated using Atomic absorption spectroscopy using three randomly selected sites of the film. SHD hydrogel film specimens were than prepared by boiling the dried weighted SHD hydrogel samples in aqua regia (i.e. mixture of nitric acid and hydrochloric acid; 1:3). A flame atomic absorption spectrophotometer (AAS) (Perkin Elmer 3100, MA, USA) was used with a silver hollow cathode-lamp, at an operating current of 2 mA, a wavelength and a spectral bandwidth of 328.1 and 0.2 nm, respectively. For standard specimens, AgNPs prepared by chemical reduction method using sodium borohydride (0.1 mg/mL) were used to compare the concentration of silver nanoparticles.

4.2.2.14 Drug loading

To determine the distribution and amount of *FB* extract in sprayed hydrogel film, dried samples of hydrogels (~ 20 mg) were kept in 50 ml buffer solution (pH 7.4) to swell. The

above solution is than centrifuged for 15 mins at 13000 rpm in order to leach out the FB extract from the SHD films. The above solution was filtered and analyzed using UV spectrophotometer (λ_{max}, 275 nm). The percentage drug loading was calculated using the equation [226].

$$\% \text{ Drug loading } = \frac{\text{Wt}_{(\text{drug in film})}}{\text{Wt}_{(\text{film})}} \text{ x } 100$$

4.2.2.15 *In-vitro* drug release and release kinetics studies

The *in-vitro* drug release profile of *FB* extract as well as AgNPs from the SHD films was carried out using dialysis membrane (cellulose nitrate membrane; pore size 0.22 µm) and Franz diffusion cell (FDC) [227]. The FDC cell consist of two chambers, 1) the donor compartment was open from the top and exposed to atmosphere while, 2) the receptor compartment consists of sampling port and release medium (pH 6.5; 37 ± 0.5 ºC). The SHD film specimens loaded with silver nanoparticles and FB extract were placed on the donor compartment containing cellulose acetate membrane and, at a predetermined time interval, i.e. 0.5, 1, 2, 4, 6, 8, 10, 12, 14 and 24 h, 1 mL of samples were withdrawn from the sampling port and replaced by the same amount or volume of the fresh medium in order to maintain the sink conditions. Samples were analyzed for content release (*i.e.* FB extract and AgNPs) under UV spectrophotometer at λ_{max}, 275 nm and 430 nm, respectively. The percentage cumulative release of FB extract and silver was calculated using the standard curve of FB extract and standard silver, respectively (Figure 2I; Appendix).

The release behavior of FB extract and silver nanoparticles from the SHD hydrogels network was studied using zero-order equation:

$$f = k_1 t$$

Where f is the fractional of solute release (M_t/M_∞), M_t is the cumulative release of the FB extract and AgNPs at time t, M_∞ is the initial concentration of the in the SHD film, M_t/M_∞ is the fraction of FB extract and AgNPs released with respect to the value of infinite time and k_1 is zero order release rate constant.

The Korsmeyer-Peppas model was used to analyze the drug release mechanism from various polymeric hydrogel matrices [224]. The model equation is

$$f_t = k_2 t^n$$

Where f_t (M_t/M_∞), is the fraction of FB extract and AgNPs released at time t, K_2 is the Korsmeyer release constant dependent on the polymer characteristics and n is a release exponent which defines the mechanism of drug release i.e. whether it is diffusion controlled or both diffusion and erosion controlled. The value (n) was determined from the slope of the plot of the logarithm of release rate and logarithm of time (t).

4.2.2.16 Biological Evaluation of Hydrogel Film

4.2.2.16.1 Hemocompatibility study

The blood compatibility experiment was carried out for the prepared PVA/SA (loaded with AgNPs and FB extract) using the method reported by Chhatri et al. and Singh et al. [228, 229]. Accordingly, sprayed films were first equilibrated with saline solution (NaCl 0.9 w/v at 37 ºC for 24 h). For conducting the experiment anti-coagulated blood was used for this test. The equilibrated PVA/SA sprayed films were transferred in to polypropylene test tubes and 7 ml of phosphate buffer saline (pH 7.4) was followed by incubation for 72 h. The PBS was removed from the last test tubes and 1 ml of anti-coagulated blood (ACD) sample was added to the same test tube (incubated at 37 ºC for 3 h). Positive and negative controls were prepared by adding the same amount to 1 ml of Triton X and PBS, respectively. Each incubated tubes were inverted gently each 30 min to ensure the continuous contacting of membrane and ACD blood. The fluids were transferred to eppendrof and centrifuged at 3000 rpm for 20 min. The supernatant containing hemoglobin released by hemolysis was calculated by measuring the absorbance at 540 nm using UV spectrophotometer. The percentage hemolysis was calculated by using the equation

$$\text{Hemolysis (\%)} = \frac{A_{(\text{Sample of film})} - A_{(\text{negetive control})}}{A_{(\text{Positive control})} - A_{(\text{negetive control})}} \times 100$$

Where, $A_{(\text{sample of film})}$ is the absorbance of tested material sample while $A_{(-)\text{ control}}$ and $A_{(+)\text{ control}}$ are the absorbance of –ve and +ve control, respectively. According to the hemolytic activity of polymeric materials, the results of hemolysis test were classified into three types as follows: (a) hemolytic materials have hemolysis >5%, (b) slightly hemolytic material having hemolysis between 2% and 5% and (c) non-hemolytic materials have hemolysis < 2% [230].

4.2.2.16.2 *In-vitro* hemostatic activity

4.2.2.16.2.1 Coagulation time determination

For the determination of coagulation time the Blood samples were collected from local slaughter house (Solan, H.P, India) in blood bottles containing ethylene diamine tetra acetic acid (EDTA) as an anticoagulant. Coagulation time was determined according to the method reported by Behrens et al. [231]. Briefly, 0.5 mL, 1 mL and 2 mL of anti-coagulated blood was added into 3 different vials containing FB extract (20 mg), sprayed films (blank) and film loaded *FB* extract (~100 mg of dry weight equivalent to 20 mg extract). Samples in the vials were than recalcified with 10 mM $CaCl_2$ solution. All the vials were than inverted after every minute in order to check the clotting of the blood. The time taken by the blood to coagulate was recorded. All the experimental as well as control groups were run in triplicate (n=3).

4.2.2.16.3 Study of protein absorption on to the surface of sprayed films

The amount of protein (bovine serum albumin) adsorbed was determined by using UV spectrophotometer according to the method reported by Lin et al. [232] with little modifications. SHD hydrogel film samples were cut into square shape (1 × 1 cm) and immersed in 5 mL of phosphate buffer saline (PBS, pH 7.4) containing 30 mg/mL of bovine serum albumin (BSA) and kept under shaking at 50 rpm for 4 h at 37 ℃. Afterwards, samples were taken out gently and washed three times with PBS to detach loosely attached protein. The extraction of surface adhere protein was done by stirring with 1% (w/v) aqueous solution of sodium dodecyl sulfate (SDS) for 1 h at room temperature. The amount of protein adsorbed onto the surface of film was calculated by plotting calibration curve of BSA (Figure 2J; Appendix) in SDS solution using UV absorbance at λ_{max} 630 nm [247].

4.2.2.16.4 *In-vitro* free radical scavenging activity

The free radical scavenging activity of FB extract released from the SHD films was calculated with respect to time using DPPH (2, 2-diphenyl-1-picrylhydrazyl) scavenging assay as reported by Mahdi et al. [71]. Sustained release of FB extract and prolong oxidation stress free environment in the wound milieu are desirable for long term utility of the dressing. A 500 µl sample of *FB* extract samples (collected from the release medium) was mixed with 1 mL of 0.1 mM w/v alcoholic solution of DPPH. The above

mixture was incubated for 30 min in dark at room temperature and then measured UV absorbance at 517 nm λ_{max}. The results were expressed as 'percentage of DPPH reduced or percentage inhibition of free radicals' using the following equation given below. Where, A_0 is the absorbance of the control i.e. DPPH alone and A_1 is the absorbance of the test i.e. *FB* extracts released from the SHD hydrogel films. Each experiment was conducted in triplicate (n=3) and results were shown as ± standard deviation [71].

$$\text{Percentage inhibition} = \frac{\text{A0} - \text{A1}}{\text{A0}} \times 100$$

4.2.2.17 *In-vitro* antimicrobial activity

4.2.2.17.1 Microbe penetration

The microbe penetration test was performed by the method as reported by Kokabi et al. [233] to evaluate the physical resistance or the property of formulated PVA/SA hydrogel films against microbe's penetration from the environment to the wound surface. Circular samples of SHD film (diameter ~5 cm and thickness ~3 mm) were washed three with de-ionized water and sterilized under UV light for 1 h. The sterilized SHD film samples were placed on the nutrient agar plate followed by addition of a drop of bacterial suspension (*S. aureus*; concentration of 10^9 mL^{-1}) on the top of the film and incubated it at 37 ºC (temperature for the growth of bacteria) in an incubator. The SHD film samples were visually monitored for a weak on a regular basis for the presence of bacterial growth or colonies of bacteria on the nutrient agar medium beneath the film.

4.2.2.17.2 Determination of zone of inhibition

The zone of inhibition (ZOI) due to the presence of AgNPs in the SHD films was determined using agar-well diffusion assay [234]. 20 µl of microbial culture was spread on the surface of pre-sterilized glass petri plates containing solidified media i.e. nutrient agar. A 6 mm holes were made using metallic punches and filled them with (i) *FB* extract (E) solution made in dimethyl sulfoxide (DMSO) (1 mg/mL), (ii) AgNPs (10.8 µg/mL) and (iii) DMSO; negative control; C) while, (iv) SHD film samples containing AgNPs were placed on the inoculated agar plates without creating holes. All test specimens were kept for incubation for 24 h at 37 ºC and zone of inhibition was observed. The antimicrobial efficiency of the AgNPs, SHD specimens containing samples was measured as the diameter of the zone of inhibition in comparison to negative control. The same

procedure was followed for the determination of zone of inhibition of Ag ions released from the SHD samples.

4.3 RESULTS AND DISCUSSION

In-situ sprayed hydrogel dressing was a novel and new approach in treatment of wound as it offers tunable, contamination free and a self forming films having protective covering without wrinkling or fluting in the wound exudates with tremendous patient observance. In addition, SHD hydrogel films were biocompatible, moist and biodegradable in nature which maintains anti-oxidative and sterile environment in the wound area.

4.3.1 Synthesis of AgNPs, particle size and *in-vitro* antimicrobial activity

The formation of silver AgNPs was basically achieved by reducing aqueous solution of silver nitrate (1 mM) in the presence of *FB* extracts (2, 4 and 6 mg/ml). It was known that silver AgNPs exhibit reddish brown color, having intense absorption spectra in the range of 400-450 due to surface Plasmon excitation vibrations in the metal nanoparticles as shown in Figure 4.1 (A & B). The particle size of the prepared silver nanoparticles were found in the range of 27.55 ± 2.01 nm (Figure 4.1 D) with a pdi of 0.66. The FB extract acted as a natural reducing agent due to the presence of polyphenolic components such as saponins, flavanoids and anthocyanin derivatives [235]. These natural phytochemicals used not only convert $AgNO_3$ into AgNPs but also predictable to decrease the *in-vivo* oxidative stress, critical for wound healing process. Among these, various natural and synthetic hydrophilic polymers containing hydroxyl (-OH), carboxylic (-COOH), amino ($-NH_2$) or thiol groups also offers reduction capabilities. In addition, they also stabilize the AgNPs by providing a protective covering over the silver nanoparticles [236].

To determine whether the prepared AgNPs are bacteriostatic or bactericidal culture of 10^{-5} dilution was used for measurement of MIC of the silver nanoparticles, as countable colonies (i.e. 143) were obtained at that dilution. The MIC of AgNPs against *S. aureus* and *E. coli* was found to be 47 µg/mL and 61µg/mL of AgNPs [Figure 4.2 (A, B, C and D]. it has been reported that silver ions (Ag^+) is antimicrobial in nature while it is unstable to store as such. Therefore, AgNPs (Ag^+) have been stored as reservoir of Ag^+ ions which on release in the medium, act as antimicrobial agent. Ag NPs showed its activity in concentration as well as size dependent approach [237]. The difference in the

MIC of gram positive and gram negative bacteria to silver nanoparticles may be due to the variations in the susceptibility, thickness and constituents of their cell membrane structure.

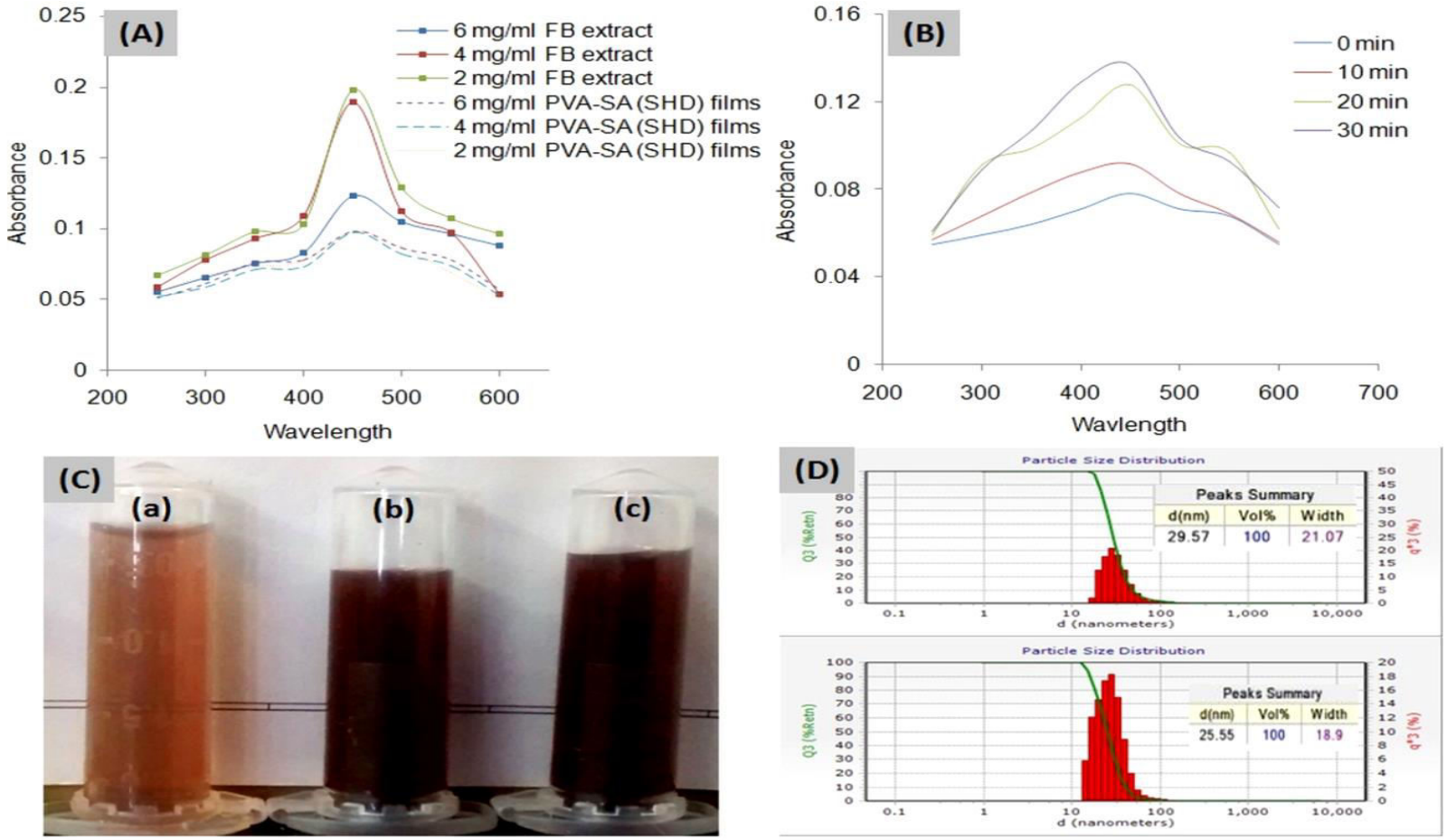

Figure 4.1 Green synthesis of AgNPs using *FB* extract (A) UV-visible spectra of AgNPs from its solution and from PVA/SA SHD films (B) UV-Visible spectra of AgNPs after 0, 5, 10 and 20 min during synthesis (C) Images showed (a) FB extract, (b) and (c) AgNPs synthesized using 4, 6 mg/mL of *FB* extract and, (D) bar graph showed particle size of AgNPs

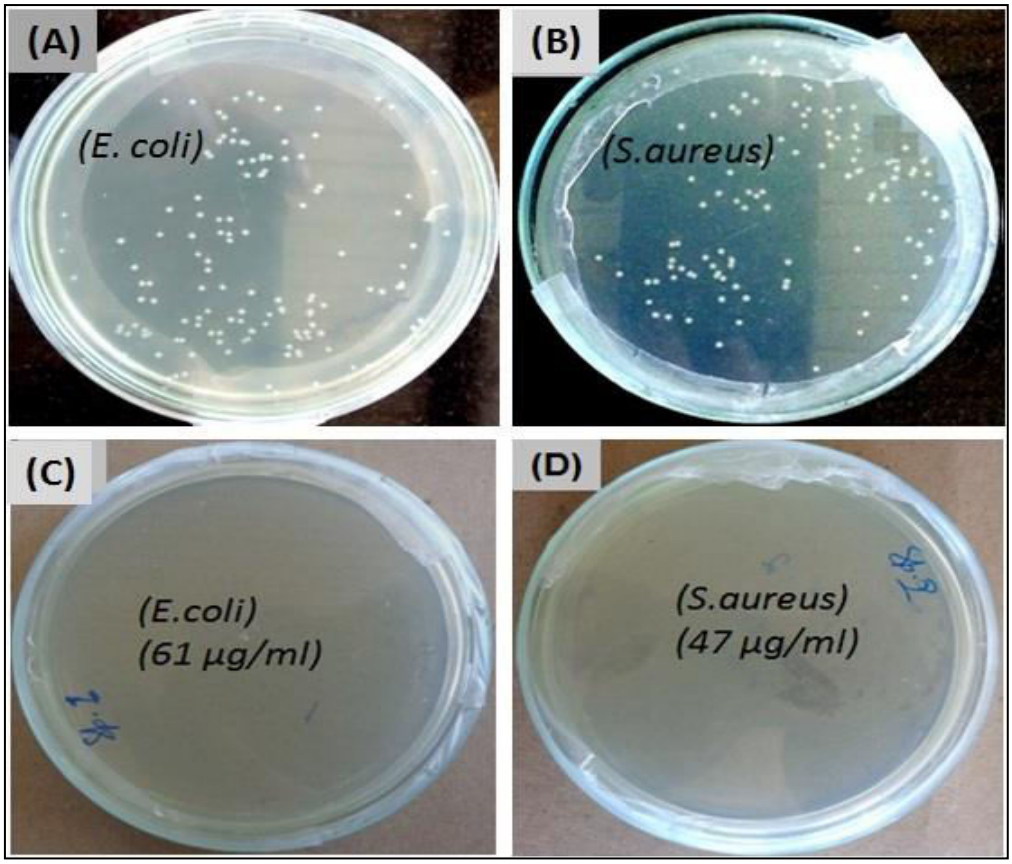

Figure 4.2 Photographs (A & B) showing MIC of control against *E. coli* and *S. aureus* while figure (E & F) showing MIC of AgNPs (i.e. test) against *E. coli* and *S. aureus*

4.3.2 Synthesis of PVA/SA sprayed hydrogel (SHD) film

The combination of PVA/SA *in-situ* sprayed hydrogels films loaded with AgNPs were synthesized using a mixture of boric acid and calcium chloride as cross-linker, respectively. In the synthesis of PVA/SA SHD films two moles of PVA containing hydroxyl groups were cross-linked with acidic groups of boric acid, while SA having carboxylic groups (-COOH) were cross-linked with the help of Ca^{+2} ions of calcium chloride thus formed full interpolymer network (IPN) [238, 239] (Figure 4.3).

On the other hand, the rate of cross-linking was not extensively affected by the concentration of AgNPs used but SHD films loaded with AgNPs retained their form better, in terms of their mechanical property, flexibility and elasticity than films without AgNPs. For the formation of stable film (i.e. maximum cross-linking) required ≥ 8% BA and ~3% $CaCl_2$ concentration that took ~5-10 seconds to form as a film. Figure 4.4(A) showed sprayer used to spray the mixture of (i) SA/PVA, (ii) BA/$CaCl_2$ (B) and (C) showed prepared sprayed hydrogel films; while the inset image showed the flexibility and

elasticity of prepared sprayed SHD films, respectively. Boric acid and calcium chloride are hydrophilic cross-linkers and presented an advantage of initiating cross-linking of PVA and SA within few seconds, at room temperature.

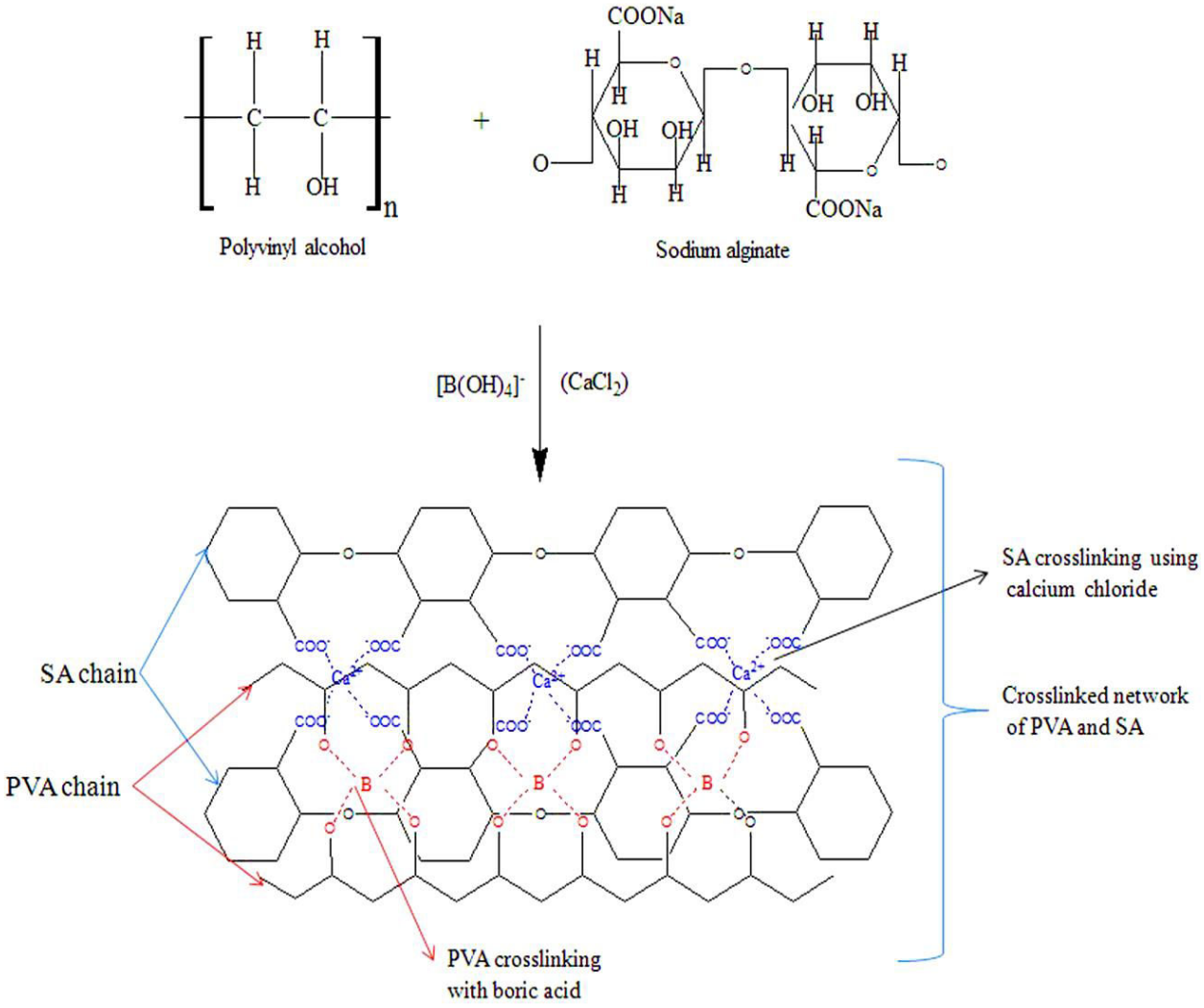

Figure 4.3 Schematic representation of synthesis of cross-linked SHD film of PVA/SA through cross-linking with $CaCl_2$ and boric acid, respectively

With concern of needful biocompatibility, high mechanical property as well as swelling and degradation profile, SA was selected as natural polymer for the synthesis of SHD. The SA is a biocompatible, hydrophilic and pretty financially viable polymer and has been used for the synthesis of wound dressing along with PVA due to its high swelling, flexible nature which impacts the limited wound environment away from moisture management [240].

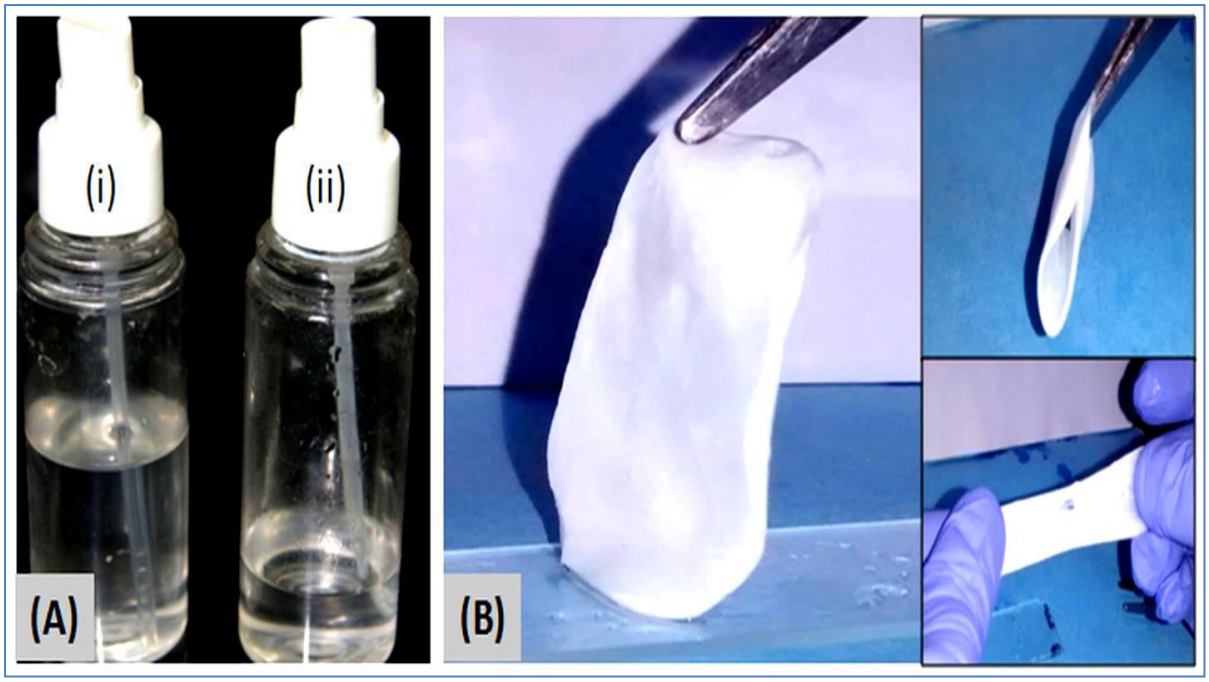

Figure 4.4 Photograph of SHD films of PVA/SA demonstrated (A) sprayers used for spraying mixture of (i) PVA/SA and (ii) BA/$CaCl_2$, (B) strength of SHD film (image showed flexibility and elasticity of SHD films)

4.3.3 Physicochemical characterization of SHD films

4.3.3.1 Fourier Transform Infrared Spectroscopy (FTIR)

FTIR was used to observe peak shift caused due to the interaction between the two or more blended polymeric components such as hydrogen bonding or any other complex or formation of coordination bonds among the blended component. The FTIR spectra show spectral characteristics features same as to that for individual polymers, but some bands shifts from their original positions. The FTIR spectra exhibit characteristic of stretching and bending vibrations of the prepared PVA/SA SHD films. FTIR absorption, bands positions and assignment of all the prepared samples are listed in figure and marked with arrows. Figure 4.5 (a)-(d) depicts the FTIR spectra of PVA/SA Film (without AgNPs), PVA alone, SA alone and PVA/SA loaded with AgNPs films respectively. The FTIR spectrum of PVA alone [Figure 4.5 (b)] showed the typical broad spectrum bands at 1093 cm^{-1} and 1418 cm^{-1} (C–O groups), 2918 cm^{-1} (symmetric –CH_2–) and at 3300 cm^{-1} for –OH stretching. The FTIR spectra of Sodium alginate alone [figure 4.5 (c)] showed its characteristics band at 2931 cm^{-1} and is assigned for – CH_2 group, while 1614 cm^{-1}, 1416

cm^{-1} and 1306 cm^{-1} is assigned for carboxyl anions and is due to the presence of asymmetric and symmetric stretching vibrations.

Figure 4.5 (a) showed the FTIR spectra of PVA/SA SHD film without AgNPs. Typical bands of –OH and $–CH_2–$ were also observed in the FTIR spectrum of PVA/SA SHD films with elevated intensity. In this spectrum, typical or characteristics bands of –OH and –COOH (of PVA and sodium alginate) was observed at 1614 cm^{-1}, 1418 cm^{-1}, 1306 cm^{-1} and 1093 cm^{-1} [241]. Figure 4.5 (d) depicts the FTIR spectra of PVA/SA film loaded with AgNPs. The characteristic features of SA and PVA were related to those of blank SHD films except with lower intensity stretching band of –OH in comparison to blank film. The above theory indicated the probable interaction between the reduced silver ions and the hydroxyl group (–OH) of the PVA and carboxylate group of sodium alginate polymers. It has been found from the figure that the –COO– band of silver loaded SHD film has shifted to higher wave number i.e. from 1614 cm^{-1} to 1670 cm^{-1} (indicated by blue arrow) indicated a strong interaction between SA, PVA and AgNPs. This shifting can be due to the formation of coordination bond between the electron rich groups (such as C=O and OH) present in the SHD hydrogel network.

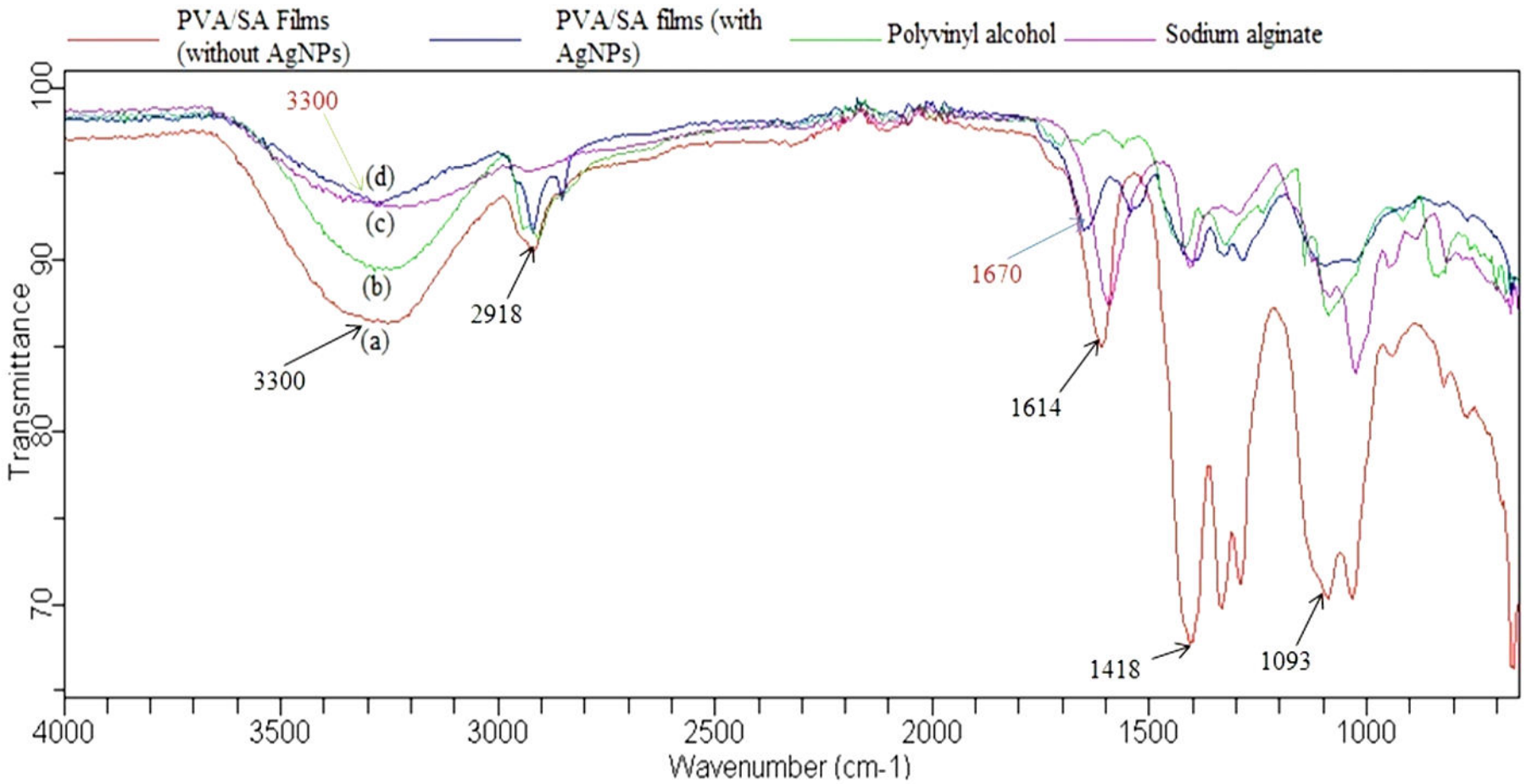

Figure 4.5 Demonstration of comparative ATR-FTIR spectra of (a) PVA/SA SHD films (without AgNPs), (b) PVA, (c) Sodium alginate (SA) and (d) PVA/SA film with AgNPs

4.3.3.2 Scanning electron microscopy (SEM)

Scanning electron microscopy was used to observe the porosity, structure, architecture and cross-linking density of the polymeric blended component. Figures 4.6 (A)-(F) depicts the surface morphology of PVA/SA SHD films with varying PVA/SA ratio in the range of 1:0, 0:1, 1:1, 1:2, 2:1 and 3:1, respectively. It has been found from the figures that the prepared films showed a wrinkled and porous surface or structure with high uniformity which may further participated in sustained release of the silver nanoparticles as well as FB extract. In most of the SHD samples (A), (C), (E) and (F) small pores as well as highly cross-linked network were observed as indicated by the arrows. It was also found that the cross-linked network and the pore size of the SHD films increases as we increase the ratio of the PVA in PVA/SA SHD films from 1:0 to 3:1.

The obtained uniformity and cross-linked network of the prepared SHD films indicated the physical interaction (i.e. hydrogen bonds) among the functional groups present in the PVA/SA blended constituent. The reason for the above difference could be the hydrophilicity of the PVA and highly cross-linking effect of BA. From figure 4.6 (A), (C), (E) and (F), it was clearly seen that cross-linking of PVA resulted in the formation of higher cross-linked ice crystals network (formed during the snap freezing process), while increasing the ratio of SA in PVA/SA from 0:1 to 1:2 resulted in less ice crystals (formation of dense structure), thus accounting less swelling as well as less porous structure. The less porous structure of PVA/SA (0:1 & 1:2) with higher SA content could be due to the higher cross-linking of SA films which further results in shrinking of SHD films at higher cross-linking density.

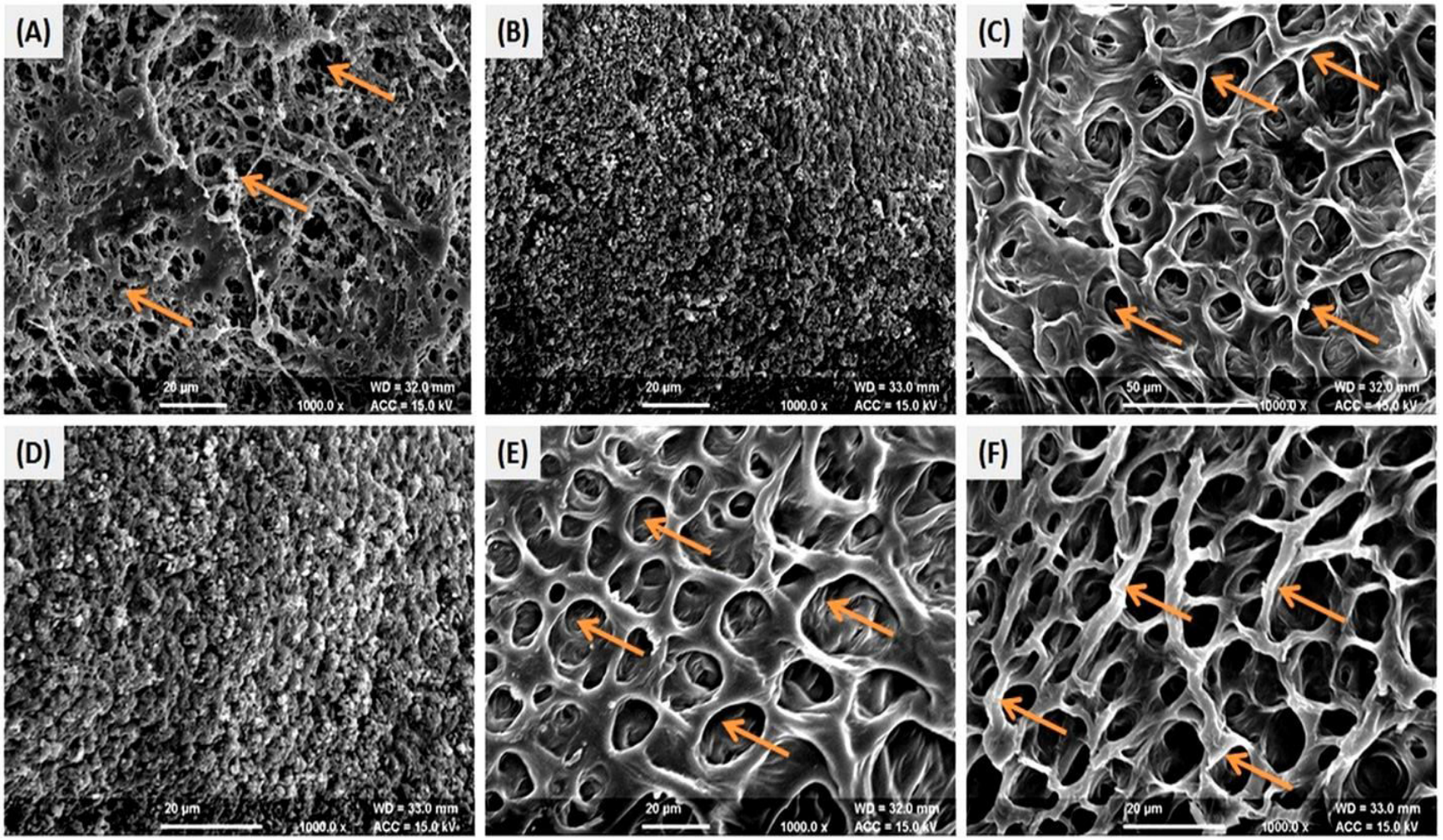

Figure 4.6 SEM images (A)-(F) depicts the surface morphology, porosity and cross-linking of PVA/SA SHD films with PVA/SA ratio varying in the range of 1:0, 0:1, 1:1, 1:2, 2:1 and 3:1 (at magnification of 1000x)

4.3.3.3 Thermo gravimetric analysis (TGA)

To explore the polymeric interactions among the PVA, SA and the effect of Ag nanoparticles on polymeric thermal stability, TG analyses were performed with PVA, SA alone, blank PVA/SA SHD films and SHD film loaded with AgNPs at a heating rate of 10 ºC/min (Figure 4.7 A, B, C and D). The TG curve of PVA and SA alone (Figure 4.7 A&B) indicated the first breakdown at a range of 30 to 250 ºC and 27 ºC to 100 ºC and was accompanied by 5.34 % and 9.47 % weight loss. This stage corresponds to loss of physical water present in the PVA and SA. The second breakdown or decomposition of PVA and SA alone started at 250 ºC and 200 ºC and ending at 700 ºC, corresponds to around ~97 % and ~72 % loss in weight and was indicated by vaporization and burning of volatile oil part produced by the thermal decomposition of the polymeric chain [242]. The second decomposition of PVA and SA was mainly due to the chain scission, subsequent side reactions like cyclization, cross-linking and partial carbonization [242].

Differential thermal gravimetery (DTG) is used to identify the temperature at which maximum weight loss was observed. The T_{DTG} (i.e. the temperature at which maximum weight loss was observed by PVA and SA alone) was found to be 293 ºC (1.45 mg/min) and 247 ºC (0.64 mg/min) respectively, which may be due to the loss of lattice water present in the polymeric network. Whereas, Differential thermal analysis (DTA) is used to measure the temperature difference between the samples and reference for the detection of the exothermic and endothermic weight loss. Two peaks were observed for PVA alone i.e. at 223 ºC (5.99 uV) and 296 ºC (1.43 uV) which gain up to ~ 49 mJ/mg and 324 mJ/mg of heat through endothermic reaction while SA loses up to –258 mJ/mg of heat through exothermic reaction respectively [242].

Similarly, blank SHD films and SHD films loaded with AgNPs degrade in two steps and accomplished by ~86 % and ~ 65% weight loss (Figure 4.7 C & D). The difference in the decomposition between blank SHD and SHD film loaded with AgNPs was found ~ 21%. The presence of nano-silver in the hydrogel network can catalyze CO_2 elimination from polymer chain and thus delayed degradation process. However, the initial thermal degradation temperature of blank SHD and SHD/AgNPs film was greater than that of homopolymers which indicates that there was a specific intermolecular interaction between PVA, SA in the blank SHD and SHD/AgNPs film [243].

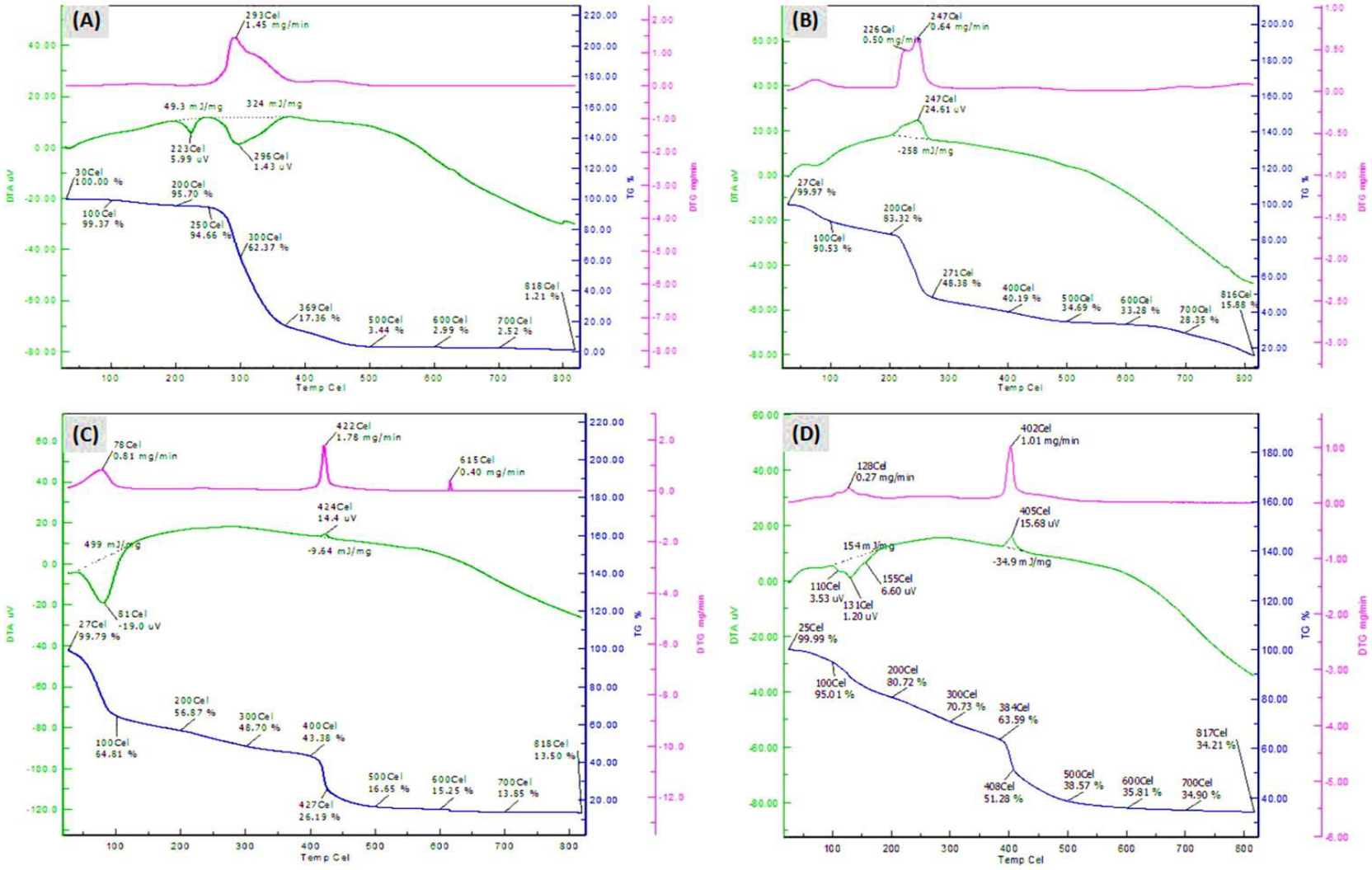

Figure 4.7 TGA studies showed polymeric interaction through thermal degradation behavior of PVA alone, SA alone, PVA/SA SHD and PVA/SA/Ag SHD hydrogels at a heating rate of 10 ºC/min

The DTA curves for blank SHD films and SHD films loaded with AgNPs showed that the thermal behavior are in consistent with the TGA analysis as reflected by the DTA peaks. It was also observed from the DTA curves that the first two peaks are endothermic for blank SHD films (81 ºC) as well as SHD films loaded with AgNPs (131 ºC) which further gain up to 499 mJ/mg and 154 mJ/mg of heat and other two stages were exothermic which loses up to -9.64 mJ/mg and -34.9 mJ/mg of heat respectively (Figure 4.7 C&D). The endothermicity in the first peak (for blank SHD as well as AgNPs loaded SHD) indicated that energy required for vaporizing the absorbed water molecules while exothermicity means that energy released during burning of new chemical bonds [243].

4.3.4 Equilibrium swelling ratio (ESR)

Figure 4.8 (I) & (II) illustrates the effect of PVA ratio on the ESR with respect to different pH media. It has been seen from the results that ESR decreased from 6.89 to 4.27 (1.61-fold; at pH 1.2) on decreasing the content of SA (100% to 66%) while ESR increased from 0.33 to 3.39 (10.27-folds; pH 1.2) on increasing PVA content (33% to 100%) in the PVA/SA SHD films. In distilled water (DW), ESR increased from 0.71 to 4.94 (6.95-folds) with increasing PVA content from 0 to 100% while opposite results were observed at pH 7.4. ESR decreased from 4.22 to 0.93 (4.53-fold) on increasing the PVA content as above. While at pH 6.5 net ESR increased from 2.09 to 8.72 (4.17-fold) on increasing the PVA content (from 0% to 66%), whereas opposite results were obtained on increasing the content of PVA (66% to 100%) i.e. net ESR decreased from 7.99 to 2.51 (3.18-fold).

The swelling behavior of PVA/SA sprayed hydrogel is greatly dependent on to the concentration and extent of cross-linker used (BA and $CaCl_2$). Excess cross-linking of PVA/SA SHD films results in formation of tighter interface and it could be difficult to the surrounding liquid to diffuse into the tightly packed structure thus decreases the swelling capacity. In addition, the extent of ionization of the carboxylic group present in the SA produces larger number of carboxylate ions along the SA polymer chain as the pH increases from 1 to 5. Because pKa of sodium alginate is ~3.2 and most of the carboxylic group present in the sodium alginate exist in unionized form (i.e. -COOH). In the shell, hydrogen bond were formed by –COOH of sodium alginate results in the formation of stronger interaction between the polymers chain and thus reduces the chances of surrounding liquid to diffuse into the tightly packed structure thus [244].

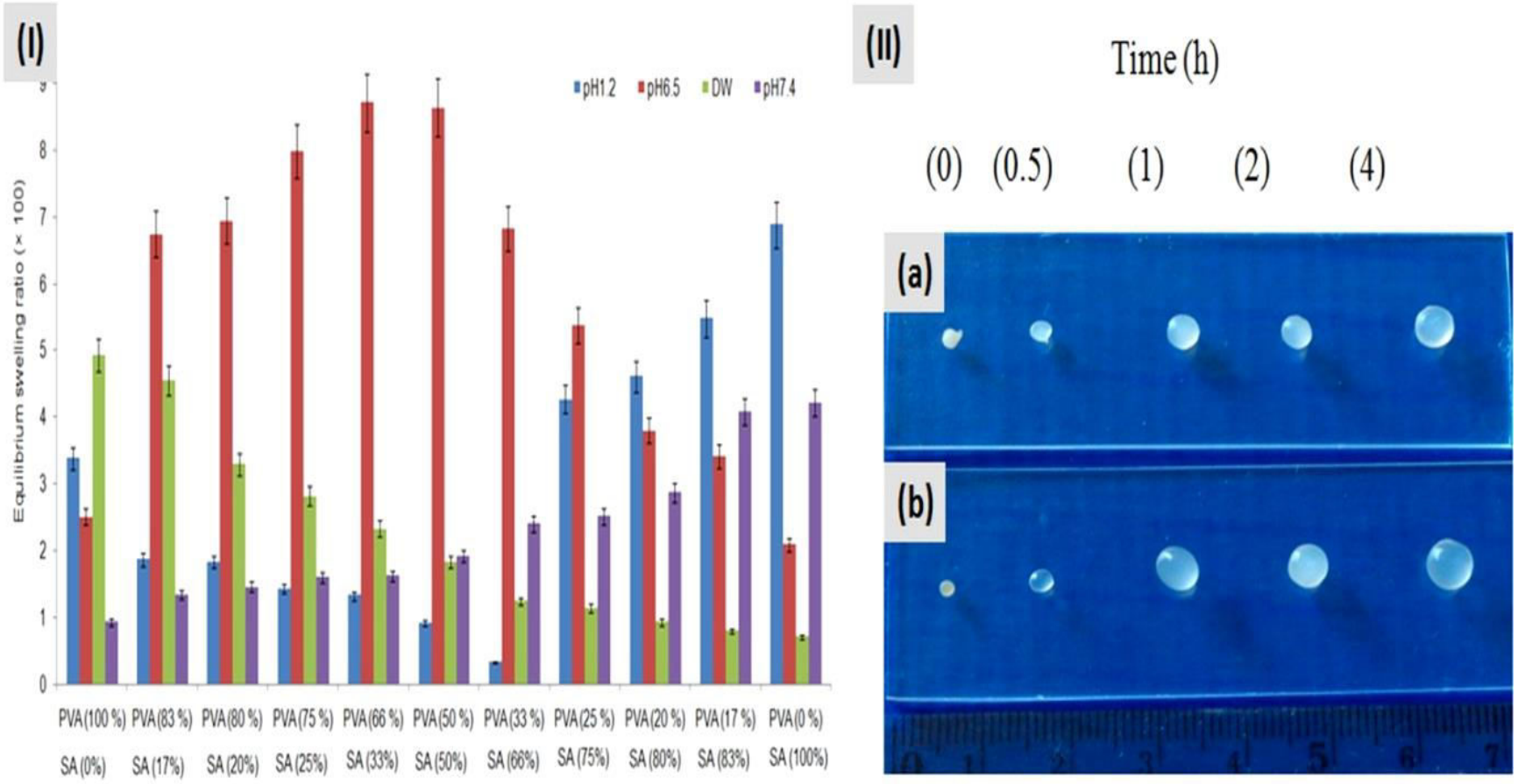

Figure 4.8 (I) Demonstration of the effect of PVA/SA ratio on the water uptake behavior (equilibrium swelling ratio; ESR) of PVA/SA sprayed hydrogel dressing (SHD) in distilled water, pH 1.2, 6.5, and 7.4 (n= 5; mean ± SD), (II) Photographs of (a) SA and (b) PVA beads showed degree of swelling after 30 min, 1, 2 and 4 h, respectively

These carboxylate ions centers repels each other and produce a rapid relaxation in the hydrogel network chain which further resulting in a rise in the degree of fluid uptake. At the basic pH (DW & pH 7.4), all the –COOH groups of SA are converted to $–COO^-$, resulting in higher anion-anion (electrostatic) repulsion and high swelling capacity [244]. A similar behavior with low sodium alginate content in acidic medium has also been reported by Deng and coworkers [245]. While, high swelling with higher PVA content could be due to the hydrophilic nature and presence of hydroxyl group (-OH) in the PVA molecule, which could have participated in the hydrogen bonding and further lead to swelling of the hydrogel in the acidic as well as basic medium [246].

4.3.5 Weight loss profile

Figure 4.9 A & B depicts the weight loss profile of PVA/SA SHD films under *in-vitro* conditions (37 ± 0.2 ºC, pH 6.5). It has been found from the results that with increasing PVA content from 0% to 33% (and decreasing SA content from 100 to 66%) in SHD film, percentage loss in weight decreased from 89.19 % to 78.98 % of its total weight. Further, increase in PVA content from 50% to 100%, the percentage loss in weight decreased from 73.4% to 69.81 % within 72 h. it has been seen that increased PVA content from 50% to 100% provide strength to the films and but reduces the degradation rate.

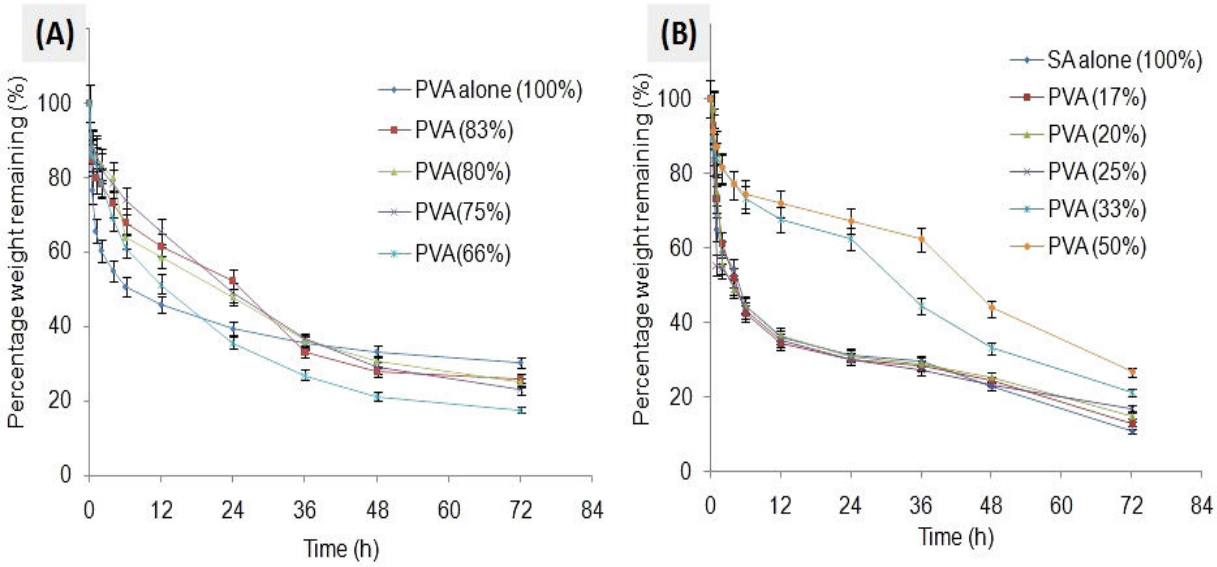

Figure 4.9 (A & B) Weight loss profile of PVA/SA SHD films in pH 6.5 (mean ± SD; n=5)

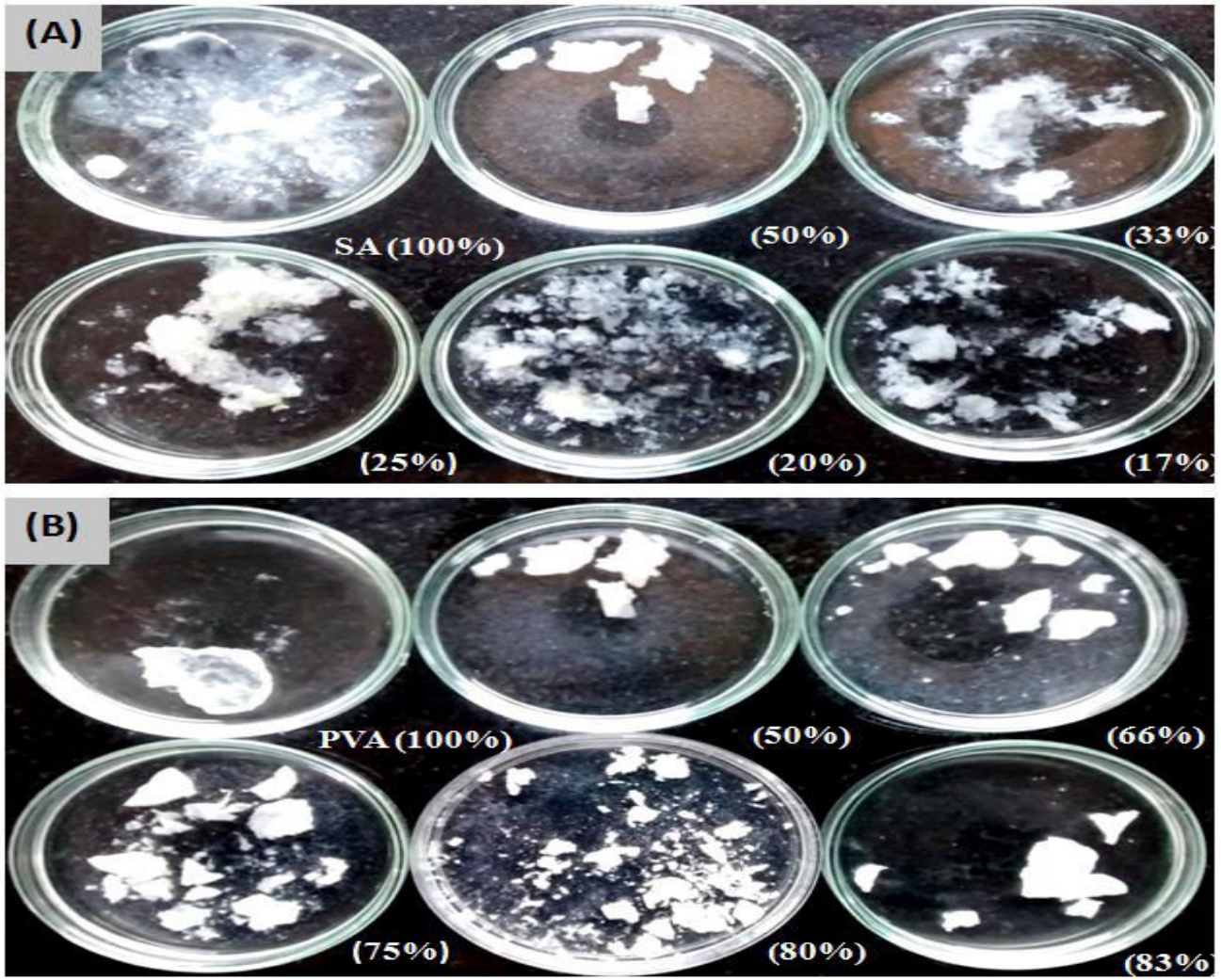

Figure 4.10 Photographs Showing degree of hydrogel degradation (PVA/SA SHD films in pH 6.5), (A) with increasing SA concentration (from 17 to 100%) and (B) with increasing PVA concentration (up to 100%), respectively

The higher rate of degradation with increased content of sodium alginate content can be explained on the basis of their cross-linking and water solubility (gelling ability) ability (Figure 4.10). During cross-linking of SA with calcium chloride, Na^+ ions were replaced by Ca^{2+} ions, resulted in the formation of calcium alginate thus, exhibited higher swelling and degradation. This can further explained on the basis that calcium alginate contained lower ionic cross-linking which further caused dissolution of ionic cross-linked hydrogel [247]. The lower degradation of PVA with increased ratio of PVA in the SHD i.e. (PVA/SA; 5:1) could be due to the formation of firm H-bonding among –OH groups of PVA chain (Figure 4.10) [246].

4.3.6 Rheological behavior

Rheological behavior of polymers are important feature of SHD films as the information of micro-structural surroundings or mobility (fluidity) not only responsible for drug diffusion and compatibility but also useful for handling of the product [248]. The viscosity of the polymers were evaluated to find out the change in the properties of the formulated gels with respect to concentration of its components (i.e. PVA alone and PVA/AgNPs). Figure 4.11 (A, B and C) depicts the rheograms of PVA solutions. It has been found that PVA solution showed Pseudo-plastic flow as evidenced by Farrow's constant (>1) [249]. The Farrow's constant values for 2%, 4% and 8% w/v PVA and PVA-AgNPs solution were found to be 5.26±1.23, 5.71±1.45, 6.25±2.1 and 6±0.89, 4±1.45 and 4.72±0.98, respectively. Moreover, viscosity of PVA solution decreased from 915 to 468.9 cp with increase in shear stress from 200 to 1145 dyne/cm^2 and shear rate 20 to 100 sec^{-1}. It has been also found that upon addition of 8 % v/v AgNPs into PVA solution, viscosity of PVA solution increased from 515 cp to 1002 cp. This could be due to the electrostatic interactions between the PVA and the silver nanoparticles [250].

It has been found that, when PVA alone (without incorporating AgNPs) was used for the measurement rheological properties, viscosity of PVA solution is less than that of PVA/Ag solution; this could be due to the presence of free hydroxyl group and lack of the interaction among the OH groups and Ag nanoparticles. The gels showed a pseudo-plasticity or shear thinning effect as advantageous possessions during topical applications since the gel would become more fluid. In addition, the viscosity would most likely increased when the stress ceased, avoiding the gel to flow from the site of application [250].

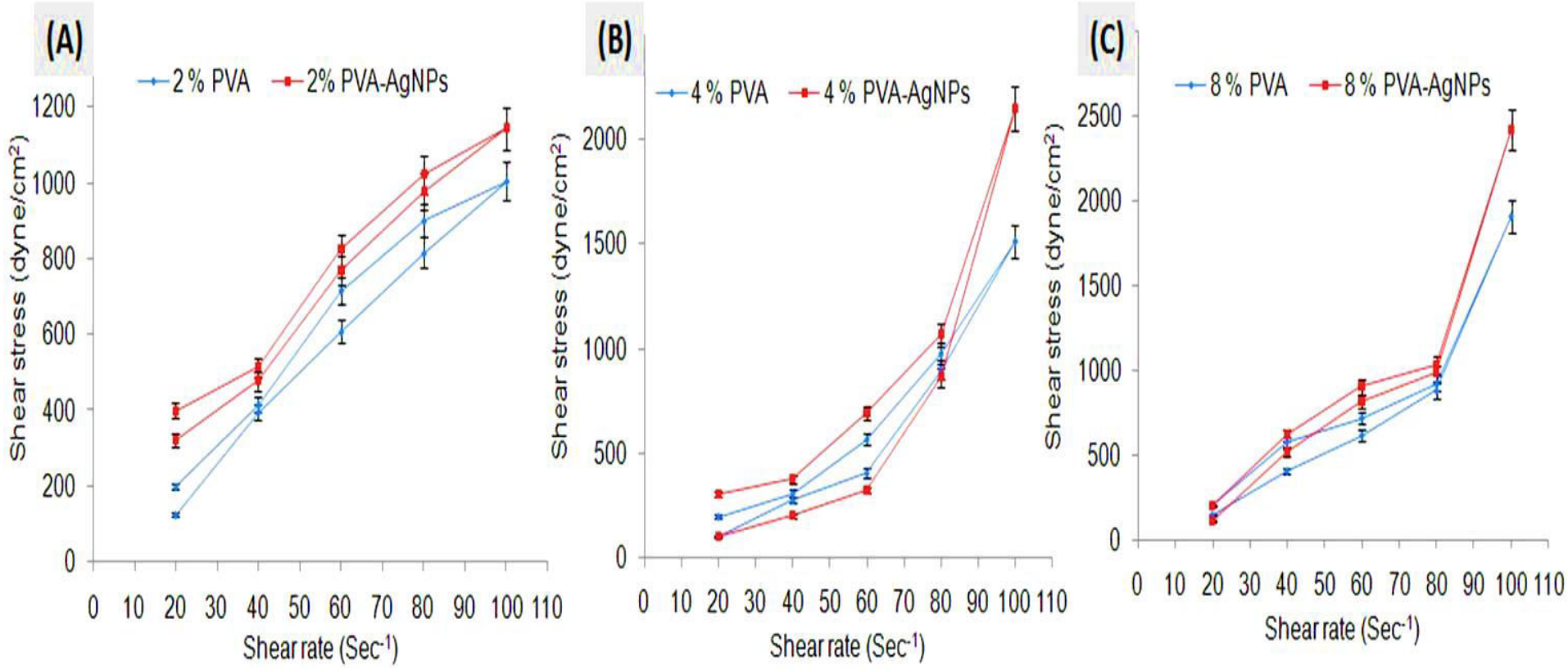

Figure 4.11 Rheograms of prepared PVA gel solution containing (A) 2% PVA solution and 2% PVA-AgNPs, (B) 4% PVA solution and 4% PVA-AgNPs and (C) 8% PVA solution and 8% PVA-AgNPs (mean ± SD; n=3)

Rheological behavior of hydrogels depends on the concentration of the polymer and cross-linking agent which is required to be optimum for better flow properties.

4.3.7 Atomic absorption spectroscopy (AAS)

Atomic absorption spectroscopy technique was used to find out the amount of silver present in the polymeric blend as well as the amount of silver present in the AgNPs solution. To find out the amount of silver nanoparticles present in the PVA/SA SHD films three randomly selected specimens from sprayed hydrogel for content uniformity (Ag) were taken in order to determine the amount of Ag in sprayed hydrogel and AgNPs synthesized using *FB* extract (1 mg/mL) and sodium borohydride (1 mg/mL; for comparison study). From the AAS studies, it has been found that 76.13 ± 0.17 mg/l, 87.05±0.047 mg/l of silver was measured in samples (i.e. $AgNO_3$) synthesized by *FB* extract and sodium borohydride. On the other hand, randomly selected sites of SHD samples contained average of 0.177±0.008 mg/g of silver. The AAS study confirmed content uniformity and considerable immobilization of silver in the PVA/SA SHD films. The results of AAS studies suggested that content uniformity of silver ion present in the SHD films could be due to strong and uniformly interaction of silver ions with PVA and SA chain leading to higher loading and uniformity of the AgNPs in the SHD having equal PVA and SA fraction.

4.3.8 Drug loading and *In-vitro* drug release studies

The percentage loading of FB extract in SHD films was found to be 89.8±1.21%. Higher loading of the FB extract could be due to increased solubilization of extract in the polymeric system. Figure 4.12 (A) depicts the percentage cumulative drug release profile of *FB* extract as well as $AgNO_3$ from the SHD films with respect to time. It was noticed from the release profile study that ~87±1.78 % and ~82±1.67 % of *FB* extract and silver ions were released from the SHD films respectively, in a sustained manner up to 24 h in comparison to their solution forms.

The drug release kinetics was analyzed by plotting the log of cumulative release data versus log of time. According to Korsmeyer-Peppas model, the values of SHD/AgNPs and SHD/*FB* films exponent 'n' is found to be >1 (Figure 4.12 B) which indicated a super case-II transport [251] i.e. AgNPs as well as FB extract was released due to degradation of film as well as through diffusion mechanism. The initial burst release behavior may be due to fast diffusion of the AgNPs as well as FB extract from the surface of SHD films.

Furthermore, higher release rate may be related to the higher swelling ratio of the SHD film under saline and the weak H-bonding interaction between silver ions and polymeric network in the PBS. Sustained release pattern (24 h) indicated that the presence of nano-silver in the SHD hydrogel network cause less swelling with respect to time. It could probably be due to the chelation of some hydroxyl group with nano-silver of the network which further neutralized the repulsions of the network causing sustained release of the silver as well as FB extract.

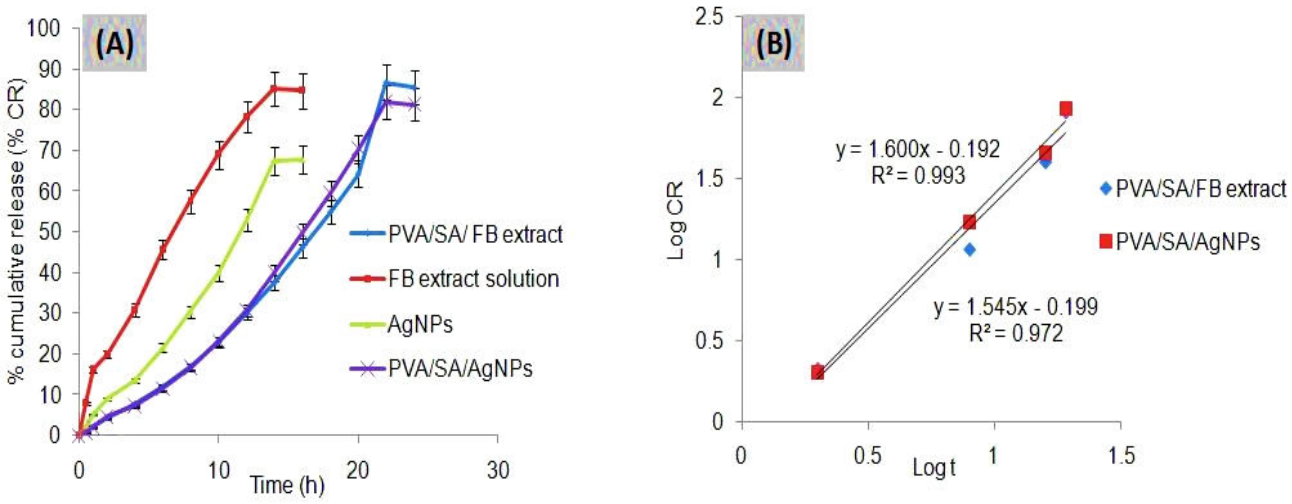

Figure 4.12 (A) Release profile study of FB extract and AgNPs from PVA/SA SHD and (B) release kinetics study of PVA/SA/FB extract and PVA/SA/AgNPs (mean ± SD; n=3)

4.3.9 Biological evaluation of hydrogel film

4.3.9.1 Hemocompatibility and *in-vitro* protein adsorption study

Figure 4.13 (A) depicts the percent hemolysis of the PVA/SA films. According to the classification of the hemolytic tendency of the polymeric material [230], it was indicated from the figure that the percentage hemolysis values decreased from 1.2 to 0.2 % with increasing concentration of sodium alginate in the PVA/SA SHD films, supporting blood compatibility and non-hemolytic property of materials.

The protein adsorption on to the PVA/SA surface was calculated using *in-vitro* experiments. From the figure 4.13 (B), it has been seen that BSA adsorption was increased from 0.2 to 58 µg/cm^2 with increasing concentration of SA from 0-75% in the PVA/SA SHD films. Interestingly, the SHD films loaded with AgNPs showed a possible adsorption of BSA in comparison to blank SHD films. These results are also in agreement

with the results of Kamoun et al. [252]. They have mentioned positive role of SA in enhancement of protein adsorption in the PVA/SA SHD films. When blood comes in contact with unfamiliar materials, plasma proteins first adsorbed over their surface, which further direct the adhesion of platelets, white blood cells and red blood cells. The aggregated platelets than release some materials like ATP and ADP, which further results in formation of plugs. The iso-electric point (of BSA), pKa (of SA) and pH of blood were found to be 4.6, 4 and 7.4, respectively. In addition to that, the surface of these SHD would carry positive charge that attract negatively charged serum protein(when ionized in water at pH 7.4, as found in the body) thus exhibited higher adsorption of proteins on to the surface of SHD [253].

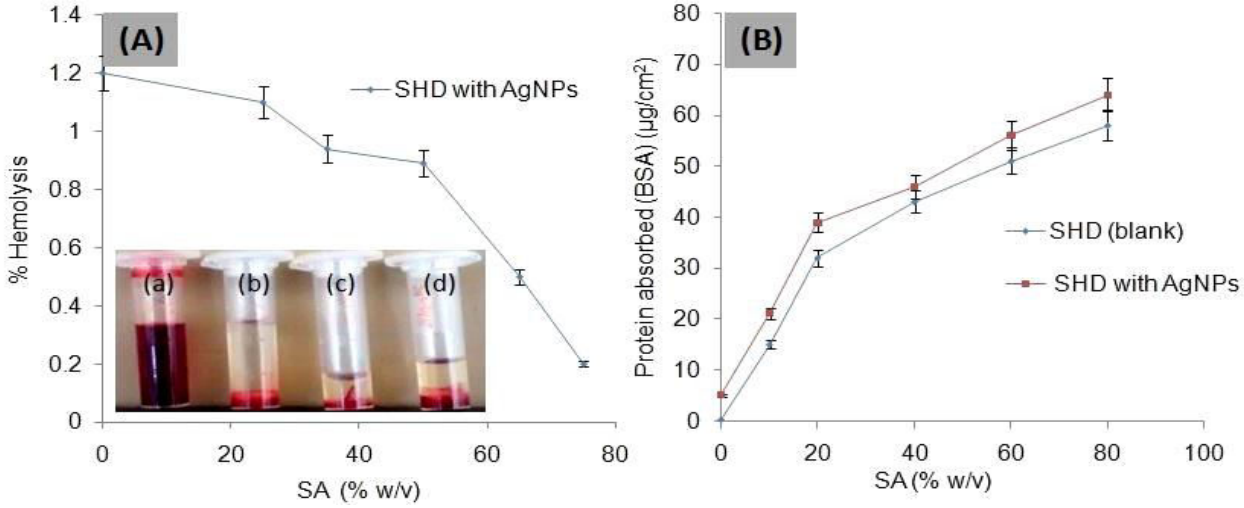

Figure 4.13 (A) Effect of PVA/SA SHD films (SA % w/v) on % hemolysis. Inset, images a, b, c and d showing % hemolysis caused by triton X (+ve control), PBS (-ve control), blank hydrogels and AgNPs loaded hydrogels, respectively, (B) Effect of PVA/SA hydrogels (SA %w/v) on protein adsorption (mean ± SD; n=3)

4.3.9.2 *In-vitro* hemostatic activity

In-vitro blood coagulation time was evaluated in plastic vials to reveal the direct effect on blood coagulation. In both cases, when a recalcified blood mixed with standard chitosan solution (1mg/mL; hemostatic agent) and swollen SHD film, a coagulum occurred faster i.e. 1 min 12 sec and 9 min 36 sec respectively, in comparison with control (no hemostatic activity). On the other hand, standard chitosan solution (Hemostatic agent) showed blood coagulation more than that of test as well as control. However, when the amount of recalcified blood was more than that of SHD film, a delay

in the coagulation of the excess blood was observed, although local aggregate formations were still continued. In both cases, coagulation time was directly depends upon the blood sample volume relative to the amount of SHD films containing *FB* extract. The hemostatic activity of *FB* extract is due to the presence of latex (milky fluid) which is mainly responsible for the formation of hemorrhage [254]. The milky latex is a stable dispersion of polymeric micro particles in an aqueous medium consisting of proteins, alkaloids, starches, sugar, oils, resin and gums that coagulates along with blood on exposure to air. Also *FB* extract contains proteolytic enzyme *benghalensin* [255], which further responsible for its hemostatic or pro-coagulant activity.

4.3.9.3 *In-vitro* free radical scavenging activity

Antioxidants can be explained as reductants, and in-activators of oxidants. The DPPH is a stable radical with a maximum absorption at 517 nm that can readily undergo scavenging by anti-oxidants. It has been widely used to test the anti-oxidant potential of plant extracts and food compounds as free radical scavenger or hydrogen donor. It has been found from the results that the extract released from its solution (i.e. raw solution) and SHD films loaded with FB extract inhibited ~63±1.63 and ~70±1.78 % of free radicals up to 14 and 24 h, respectively (Figure 4.14). The *in-vitro* radical scavenging activity of SHD formulations confirmed that enough poly-phenolic compounds were released over a period of 24 h in a controlled manner. As oxidative stress is major hurdle towards healing of diabetic wounds, these films dressing were able to maintain anti-oxidative environment for 24 h as a crucial advantage towards healing. Phenolic compounds present in *FB* extract were mainly responsible for its antioxidant activity. Phenolic compounds fall into several categories; chief among these are the flavanoids which have potent antioxidant activity [256]. Results of this study revealed that the plant extract contains phytochemicals constituents that are capable of denoting hydrogen atom to the free radicals to scavenge the potential damage.

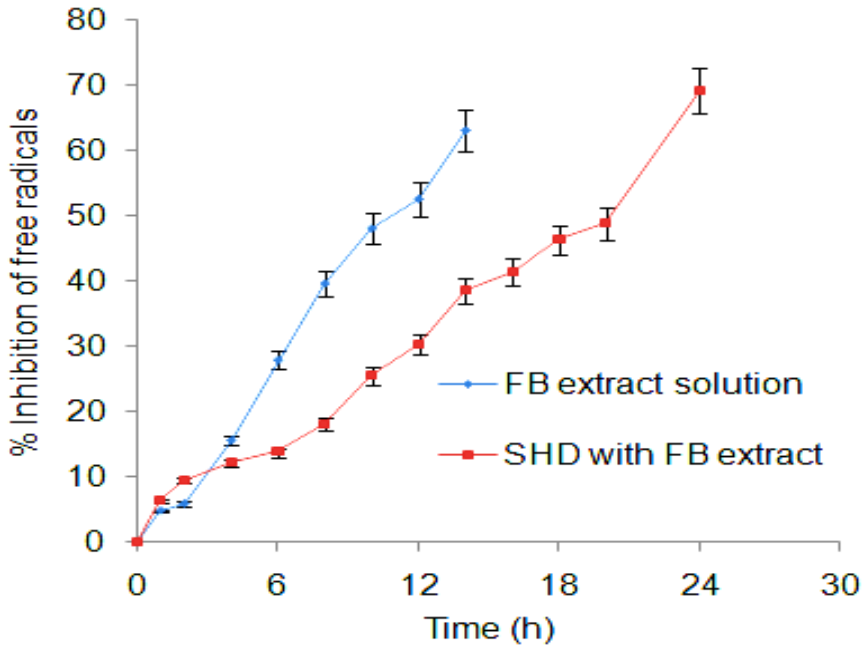

Figure 4.14 *In-vitro* antioxidant profile of FB extract solution and extract released from SHD films (mean ± SD; n=3)

4.3.10 *In-vitro* antimicrobial activity

4.3.10.1 Microbe penetration and zone of inhibition study

The zone of inhibition of *FB* extract, AgNPs and SHD films containing AgNPs were investigated against two bacterial strains i.e. *S. aureus* and *E. coli* (Figure 4.15 A, B,). Table 4.1 exhibited the zone of inhibition of silver nanoparticles and PVA/SA/AgNPs hydrogels against *S. aureus* and *E. coli*. As expected, no zone of inhibition was observed with control while with test specimens, *staphylococcus* has shown higher zone of inhibition (16 mm) as compared to that of *E. coli* (10 mm). The size and shape of nanoparticles plays an important role for their antibacterial as well as many of the clinical applications. The observed difference in the zone of inhibition among both of the bacteria may be due to the susceptibility of the bacteria towards silver nanoparticles. Results were also indicated a concentration and time dependent inhibition of bacterial zone for up to 24 h (Figure 4.15 C & D). Daily investigation of agar plates confirmed that no bacteria were passed through the sprayed hydrogel during a week. This ability of sprayed nanocomposite hydrogel dressing will protect the wound from infection and will accelerate the wound healing process (Figure 4.15 E & F).

Table 4.1 Zone of inhibition of AgNPs and PVA/SA/Ag SHD films against *E. coli* and *S. aureus*

Zone of inhibition (mm) of AgNPs and PVA/SA/Ag SHD films		
Samples	***E. coli***	***S. aureus***
Silver nanoparticles	7.8	12
PVA/SA/Ag SHD films	10	16

The antimicrobial activity of silver loaded SHD films could be attributed to the fact that silver nano-particles can interact with the sulfur containing proteins from cell membrane and phosphorous containing compounds in cell which further attacking the respiratory chain with cell division leading to cell death [257]. It has been claimed that silver ions binds to thiol groups (-SH) in the enzyme and subsequently causes deactivation of the enzyme [258]. The use of AgNPs has exhibited phenomenal antibacterial activity due to high surface area thereby, maintained its efficacy in a sustained manner for 24 h [210, 211]. Uninterrupted antimicrobial environment helps in acceleration of healing progression as sepsis is the major cause of death in chronic wounds.

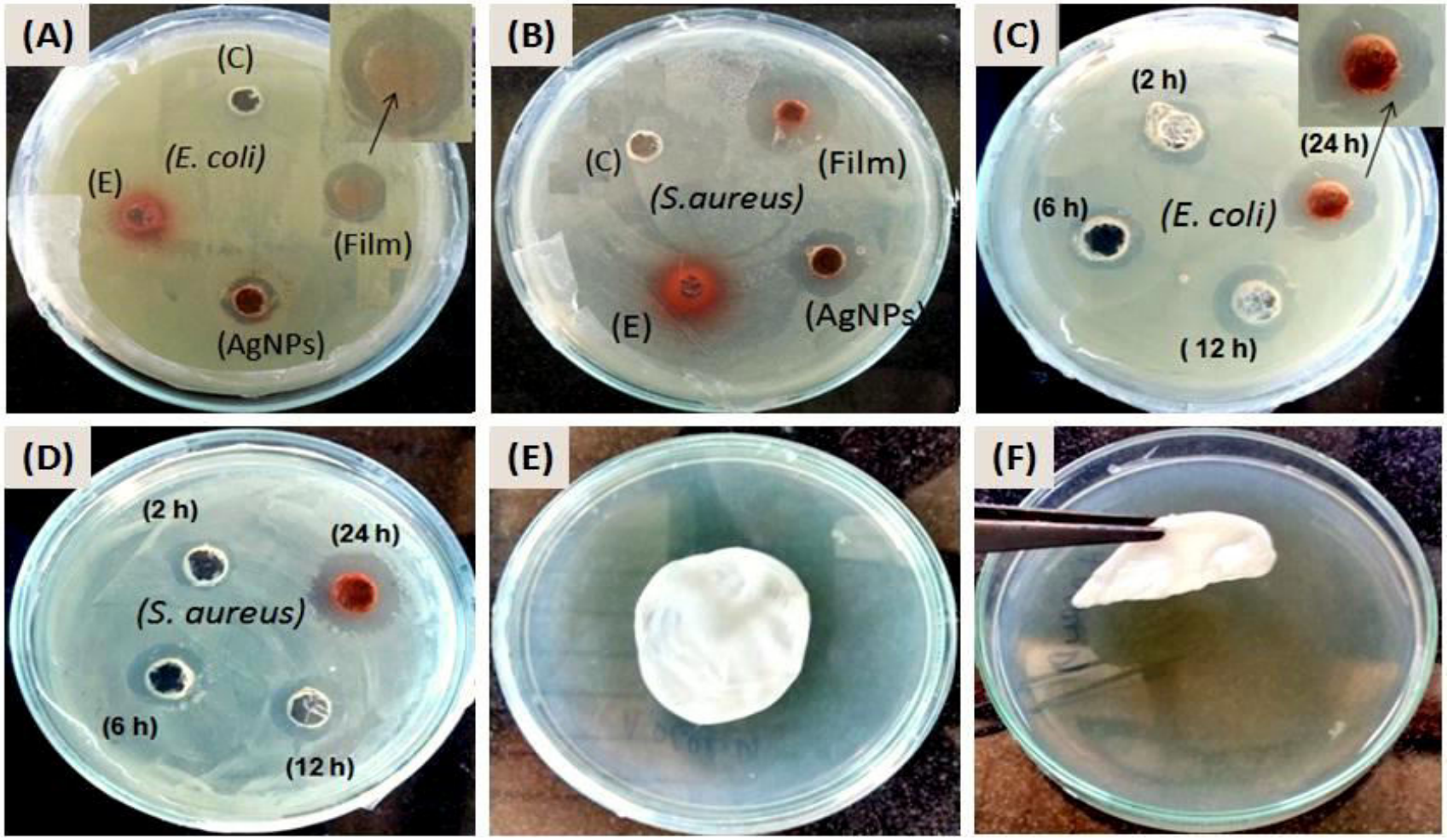

Figure 4.15 (A&B) showing zone of inhibition (ZOI) as control (C), FB extract (E), AgNPs and PVA/SA/Ag SHD films (F) against *E. coli* and *S. aureus,* (C&D) showed the ZOI by Ag ions released from sprayed hydrogel after 2, 6, 12 and 24 h, respectively, while (E&F) showed impermeability of bacteria across the SHD films after one week

4.4 CONCLUSION

Aerosolized nanocomposite hydrogels based on PVA and SA were synthesized in highly practical situation by spraying a mixture of BA and calcium chloride on to a mixture of sodium alginate and PVA under normal atmospheric conditions. The effects of various synthesis parameters like concentration of PVA and SA, cross-linkers concentration, temperature as well as effects of cross-linkers on to the swelling and degradation of nanocomposite hydrogels were investigated. The complexities in management of chronic wounds have been addressed with the delivery of phytochemical, silver nanoparticles and modern dressing which imbibe all the requisite properties and provide an ideal healing environment along with excellent patient convenience. To evaluate the potential of these aerosols based system in wound healing application, some of their important properties such as swelling, degradation, microbe penetration assay and other biological parameters like protein adsorption and hemocompatibility were investigated. It was concluded that quantity of cross-linkers used was a key regulator for the preparation of sprayed films with desirable properties. The results indicate that as we increase the concentration of plant extract for the reduction of silver nitrate solution the size of silver nanoparticles increases. TGA demonstrated that the introduction of silver nanoparticles in the polymeric hydrogel dramatically increases the thermal stability of hydrogels. Because of their unique nature of application, excellent swelling, almost ~100% degradation and biocompatible nature they could be excellent candidates for delivery of phytochemicals as well as silver nanoparticles for the management of topical wounds.

CHAPTER-5

Design and development of PVA/Chitosan based nanocomposite hydrogels for the controlled delivery of *Ocimum sanctum* and synthesis of silver nanoparticles using green chemistry

ABSTRACT

Potential application of phytochemicals for the synthesis of silver nanoparticles is a significant approach towards the field and application of antimicrobial nanomaterials for wound healing applications. Sincere, research efforts have been applied to synthesize PVA/chitosan-silver based hydrogels using freeze thaw process so as to bypass the toxic effects associated with chemical cross-linking, where both phytochemicals and silver nanoparticles could retain their individual effects and characteristics in the system with improved mechanical and stability properties. The formation of silver nanoparticles was confirmed by UV-visible spectroscopy (ƛmax 430 nm), optical microscopy, and particle size analysis which reveal that particle size ranges from 20-35 nm. The mechanism of degradation, surface morphology and compatibility studied of hydrogels were confirmed by TGA, SEM and FTIR studies. The entire *in-vitro* parameters essential for wound healing applications like swelling, degradation profile, protein adsorption and Hemocompatibility were studied and found to be compatible with blood. A controlled release of 84.3 % (28 h) of *Ocimum sanctum* extract was noticed from hydrogel discs which scavenges 69.2 % of free radicals as compared to raw extract 82.5 % (16 h) which scavenges 63.1% of free radicals. Lastly, the *in-vitro* antimicrobial activities of the hydrogel as well as silver nanoparticles were successfully evaluated against gram negative (*E. coli*) and gram positive (*S. aureus*) bacteria. The results showed that silver nanoparticles and hydrogels showed excellent antimicrobial activity though contact angle as well as silver released from hydrogel.

5.1 INTRODUCTION

Nanotechnology is a rapidly growing field with its application in science and technology for the development of new material at nanoscale. The use of monovalent silver such as silver nitrate and silver sulfadiazine are now a day's appeared as antimicrobial agent due to the fact that increasing bacterial resistance to antibiotics caused by their wide spread use [259. An improved bactericidal activity is attributed due to nanosized particles i.e. enhancement of the reactivity of the AgNPs surfaces. AgNPs are generally used to target and destabilize the bacterial plasma membrane that leads to the depletion of intracellular adenosine triphosphate (ATP) [260] and hence resulting in the death of bacterial cell. With an aim to provide economically cost effective product to the public a number of synthetically diverse methods were developed for AgNPs and AgNPs composites by incorporating these Ag^{+} ions in to the thin film of silica, sol-gels, polyelectrolyte multilayer films, porous polymer and viscous resin loaded AgNPs for wound and burn dressings [261].

Several micro-organisms and chemical entities come up with nanofactories, synthesizing metallic NPs of Ag and Au. However, the use of plants and plants extract are now a day's used for the fabrication of nanoparticles because of its eco-friendly, rapid and cost effective protocol with single step synthesis of AgNPs [262]. Biological approaches such as micro-organism and plant materials have been suggested as a valuable alternative for chemical entities to reduce the toxicity issues related to them. Using green tea extract *C. sinesis*as reducing and stabilizing agent silver and gold nanoparticles were produced in aqueous solution at ambient temperature conditions [263].

Polyvinyl alcohol (PVA) is a biocompatible, neutral polymer used in the drug delivery and also maintains a moist environment around the wound surface. While chitosan (CH) in a natural polymer belonging to the class of polysaccharides and is known to possess wound healing activity due to its antimicrobial and hemostatic activity. Furthermore it also possesses other activities like affects macrophage function that helps in faster wound healing [264]. Meanwhile combining PVA and chitosan film blends gives advantages like; PVA provide high mechanical property while chitosan have good biological, physical and adhesive properties. Nanosilver based wound dressing have received approval for their clinical use, but dermal toxicity of these silver results in their limited use [265, 266]. Therefore, combination of gel system with AgNPs would be a better

approach for the treatment of wounds. The main reason of using hydrogel based system for incorporating AgNPs is that it can provide free space between the networks in the swollen state and serve as a nucleation and growth of nanoparticles which further improves the mechanical property of the prepared hydrogel membranes with a controlled release of silver ions for a longer period of time. The approach established by Murali Mohan et al. [266] to obtain ~ 3 nm AgNPs embedded in isopropyl acrylamide hydrogel for antibacterial purpose.

The present work deals with the synthesis and fabrication of polyvinyl alcohol (PVA); chitosan blend incorporating AgNPs (synthesized using *Ocimum sanctum* leave extract) using freeze thaw process for wound healing applications. Sincere research efforts have been applied to synthesize new particulate hydrogel system with AgNPs, where both hydrogels and nanoparticles could retain their individual features and characteristics in the system with improved mechanical and stability properties without any toxic effects. The resultant properties of hydrogel films such as equilibrium swelling behavior, degradation profile, surface morphology, protein adsorption and in addition release of *Ocimum sanctum* extract and silver ions from the hydrogel matrix was also investigated.

5.2 MATERIALS AND METHODS

5.2.1 Materials

PVA (Mol. Weight ~77,000 g/mol), Chitosan (Himedia laboratories, Mumbai), Calcium chloride (Merck specialties Pvt. Ltd. India), 2, 2-diphenyl-1-picrylhydrzyl and bovine serum albumin (Himedia, Mumbai), Methanol, nitric acid, hydrochloric acid and boric acid were purchased from (Merck, Mumbai, India), Silver nitrate, ethylene diamine tetra acetic acid and sodium chloride (Fisher scientific, Mumbai, India), and all other chemicals and reagents were of analytical grade. Double distilled water was used throughout the investigation and preparation of solutions.

5.2.2 Methods

5.2.2.1 Collection and authentication of plant

The fresh leaves of *Ocimum sanctum (OS)* were collected from the local region local region of local region of Bilaspur (Himachal Pradesh). The collected leaves along with their stem were than subjected for the preparation of herbarium sheet for the

authentication of plant. The plant specimens pressed and dried inside the herbarium sheet using plant press. The collected leaves were washed 2-3 times with de-ionized water and shade dried for the synthesis of silver nanoparticles.

5.2.2.2 Preparation of *Ocimum sanctum* leaves extract

Fresh leaves of *Ocimum sanctum* were dried in shade and powdered with mechanical grinder in order to obtain a coarse powder. 100 gm of coarse powder was than subjected to cold maceration with 50% ethanol for 3 days with intermittent, shaking, filtration, evaporation and vacuum drying to get powdered extract. A dark brownish colored extract was obtained and kept in air tight containers until use.

5.2.2.3 UV- characterization of *Ocimum sanctum* extracts (λ_{max})

The various concentration of the OS extracts (i.e. 2, 4, 6 and 8 mg/ml) were recorded from a region of 200 to 700 nm in the UV spectrophotometer for the obtaining the specific absorption maxima (280-350 nm). The absorbance of all the concentration was recorded in order to get λ_{max} (wavelength) at which maximum absorbance (peak) is observed for the preparation of standard curve of OS extract (Figure 2K; Appendix).

5.2.2.4 Standard curve of OS extract

For the preparation of standard curve, a mixed stock solution of 1 mg/ml was prepared by weighing accurately 25 mg of OS extract into 25 ml of volumetric flask and making the volume up to the mark with ethanol. Different running solutions (i.e. 10, 20, 40, 60, 80 and 100 µg/ml) were prepared from the stock solution by appropriate dilution in ethanol for the preparation of calibration curve. All the solutions were kept in dark place at – 40 ºC until used under UV spectrophotometer.

5.2.2.5 Synthesis of silver nanoparticles using OS extract

1 mM solution of silver nitrate (9 ml) was mixed with 1 ml of OS extract so as to make its final concentration 10^{-3} M. The solution was allowed to react at 45 ºC with continuous stirring on magnetic stirrer. Periodic sampling after 0, 10, 20 and 25 min was carried out in order to monitor the color change as well as absorbance for the formation of silver nanoparticles [267].

5.2.2.6 Characterization of silver nanoparticles

5.2.2.6.1 UV-visible spectrophotometer analysis

To determine the time point of maximum production of silver nanoparticles the periodic absorption spectra of samples were taken 300-450 nm using a UV-visible spectrophotometer. The samples from maximum time point were air dried and analyzed for scanning electron microscopy (SEM) for its size, shape, morphology and agglomeration.

5.2.2.6.2 Particle size and zeta potential analysis

Droplet size and zeta potential of AgNPs were observed using Nanotrac Wave Zetasizer (Microtrac, USA) at room temperature at an angle of 180 degree. Samples were diluted 1:10 with Milli-Q water before analysis. The measurements were carried out in fully automatic mode.

5.2.2.7*In-vitro* antimicrobial activity

5.2.2.7.1 Test microorganisms and growth media

E. coli (ATCC-723) and *S. aureus* (MTCC-3160) were chosen based on their pharmacological and clinical importance. Nutrient broth was used as a growth medium for growing these cultures at 37 ºC for 24 h and stored at 4 ºC until further use. The growth in the culture medium was assessed based on turbidity appearance.

5.2.2.7.2 Minimum inhibitory concentration of silver nanoparticles (MIC)

This method is based on the broth dilution assay [223]. Serial dilutions were made by mixing PBS (900 µl) from the stock solution and bacterial culture grown in nutrient broth (100 µl). From this solution 100 µl of the mixture was again mixed with 900 µl of PBS (10^{-1}) and which was further diluted to get a maximum diluted concentration of 10^{-9}. The control plates (without AgNPs) were prepared by spreading 100 µl of culture (micro-organism) made in PBS (i.e. 10^{-2}, 10^{-4}, 10^{-5}, 10^{-6} and 10^{-8}) to get countable colonies (150 to 200). The test agar plates were prepared by mixing and pouring different concentration of AgNPs (test) with that of nutrient agar followed by spreading of culture (10^{-5}). The concentration of AgNPs at which no colony remain on the culture plate, was chosen as MIC of AgNPs and that amount was loaded in the PVA/CH hydrogel.

5.2.2.8 Preparation of PVA/CH hydrogels

PVA/CH hydrogel membranes were prepared by freeze thaw process according to the method reported by [268]**.** An aqueous solution containing 12% w/v of PVA was prepared by heating at 80 ºC and chitosan 1% w/v solution was prepared by dissolving it in 3% v/v solution of acetic acid. Different proportion of silver NPs (1 ml, 2ml, 3ml, 4 ml and 5 ml), chitosan and PVA (0%, 25%, 35%, 50%, 65%, 75% and 100%) were mixed, sonicated and vortexed for one hour to remove air bubble and to ensure thoroughly mixing of polymer solution. Proper amount of this mixer was poured in petri dishes followed by freezing at -20 ºC for 18 h and cooling at room temperature (30 min) for three continuous cycles.

5.2.2.9 Physicochemical Characterization of PVA/CH Hydrogels

5.2.2.9.1 Scanning Electron Microscopy of Hydrogels (SEM)

The surface and internal morphology of the PVA/CH hydrogels were investigated by analytical SEM with 15 kV voltages for secondary electron imaging. The different ratio of PVA/CH (1:0, 0:1, 1:1, 1:2, 2:1 and 3:1) films were made by snap freezing method using liquid nitrogen and coated with gold using an ion sputter coater (Hitachi S3400N, US) lyophilized before lyophilization.

5.2.2.9.2 ATR-FTIR spectral analysis

Selected dried sample of blank as well as drug loaded hydrogel specimens were placed between probe and platform. The transmittance spectra were collected using ATR-FTIR spectroscopy (Agilent technologies, 630 Cary) under constant humidity (42 ±3 % RH) and temperature of 37 ± 0.2ºC.

5.2.2.9.3 Mechanical property measurements

The tensile strength and degree of elongation break of PVA/chitosan blend has been measured using tensile test machine (18). PVA/CH membranes were cut into specific dumb bell shape (6 cm long, 2 cm wide at the ends, and 1 cm at the middle). The analysis was carried out a stretching rate of 20 mm/min with preload of 0.5 N to determine load for each sample. The thickness of the membrane was carried out using digital vernier caliper before examination.

5.2.2.9.4 Thermo gravimetric analysis (TGA)

TGA analysis of the PVA, CH, blank and AgNPs loaded hydrogels was performed using a TGA-Pyres-6TGA (EXSTAR TG/DTA 6300, Woodland, CA) by heating the sprayed films from 50 ºC to 750 ºC at a heating rate of 20 ºC/min under a nitrogen flow. A derivative plot was used to calculate the initial (T_i), maximum (T_{max}) and final decomposition (T_f) temperatures of the sprayed films.

5.2.2.10 Equilibrium swelling ratio

The swelling ratio was carried out using method reported with little modification [269]. Usually a dried hydrogel (~ 10mg) disc of 6 mm in diameter and 2 mm in thickness was immersed in distilled water and buffers (pH 6.8, 1.2 and 7.4) supplemented with 0.04% w/v solution of sodium azide as antifungal and maintained at 37± 0.2 ºC in an incubator (Perfit, India). After predetermined time intervals of 0, 1, 3, 6, 12, 24 h swollen discs were weighed on an analytical digital balance, till equilibrium was achieved (n=3). The ESR was calculated by using the formula.

$$\text{Equilibrium swelling ratio (ESR)} = \frac{\text{Wt(e)} - \text{Wt(i)}}{\text{Wt(i)}}$$

Where $Wt_{(e)}$ is the weight of swollen hydrogels at equilibrium and $Wt_{(i)}$ is the initial weight of the dried hydrogels.

5.2.2.11 *In-vitro* degradation study

In-vitro biodegradation behavior of the prepared hydrogels was studied using the weight loss as a function of time [270]. Dried hydrogels of constant weight were dipped into 5 mL of PBS (pH 6.5; 50 rpm) containing 0.04% w/v solution of sodium azide at 37±0.2ºC in an incubator shaker. The media were changed and replaced by fresh media every day. At predetermined time interval sample discs (n=3) were withdrawn from the PBS washed with distilled water and dried at 50 ºC in an oven till constant weight was obtained. The weight of dried disc was recorded and percentage degradation was calculated using the following formula:

$$\text{Percentage degradation (\%)} = \frac{\text{Wt(i)} - \text{Wt(t)}}{\text{Wt(t)}} \times 100$$

Where $Wt_{(i)}$ is the initial weight of the dried hydrogel disk at time zero and $Wt_{(t)}$ is the final weight of disk at time interval t.

5.2.2.12 Atomic absorption spectroscopy, drug loading, *in-vitro* release and release kinetics studies

Atomic absorption spectroscopy were performed to find out the distribution pattern and content uniformity of AgNPs within PVA/CH hydrogels using three randomly selected sites of the hydrogels. Specimens were prepared by boiling the dried weighted hydrogel discs in aqua regia (mixture of nitric acid and hydrochloric acid; 1:3). A flame atomic absorption spectrophotometer (AAS) (Perkin Elmer 3100, MA, USA) was used with a silver hollow cathode-lamp, at an operating current of 2 mA, a wavelength and a spectral bandwidth of 328.1 and 0.2 nm, respectively. For standard specimens, AgNPs prepared by chemical reduction method using sodium borohydride (0.1 mg/ml) were used.

To determine the distribution and content of *OS* extract in PVA/CH hydrogels, dried specimens were incubate in 50 mL buffer (pH 7.4) to swell followed by centrifugation for 15 mins at 13000 rpm in order to leach out the extract from the hydrogels. The solution was filtered and analyzed using UV spectrophotometer (λ_{max}, 250 nm). The percentage loading was calculated using the equation [260].

$$\text{Percentage drug loading} = \frac{\text{Wt drug in film}}{\text{Wt film}} \times 100$$

The release profile of silver ions and extract from hydrogel disc were studied at phosphate buffer pH 6.8. Approximately 10 mg of extract loaded hydrogel discs containing silver NPs were incubated in 5 ml of buffer pH 6.8 at 37± 0.5ºC at 75 rpm. After predetermined time interval of 0, 1, 2, 4, 6, 10, 12, 14, 16, 20, 24, 28 and 30 h, 3 ml of sample was withdrawn and replaced by 3 ml of fresh media. Optical density of each sample was measured using UV spectrophotometer at 250 nm for OS extract (% CR was calculated using standard curve of OS extract; Figure 2K; Appendix) and 430 nm for silver ions. A control experiment to determine the release behavior of the free extract was also performed. An appropriate amount of extract was dissolved in water and same volume of this solution was placed in dialysis membrane temperature maintained at 37 ± 0.5 ºC. Each experiment was performed in triplicate (n=3). The drug release kinetics of the hydrogel disc was calculated using zero order kinetics**.**

$$f = k_1 t$$

Where f is the fractional solute release (M_t/M_∞), M_t is the cumulative release of the FB extract and AgNPs at time t, M_∞ is the initial concentration of the FB extract and AgNPs in the SHD film, M_t/M_∞ is the fraction of drug release with respect to the value of infinite time and $k_1$is zero order release rate constant.

The Korsmeyer-Peppas model was used to analyze the drug release mechanism from various hydrogel matrices [251]. The model equation is

$$f_t = k_2 t^n$$

where f_t (M_t/M_∞), is the fraction of drug release at time t, K_2 is the Korsmeyer release constant dependent on the polymer characteristics and n is an exponent which defines the mechanism of drug release whether it is diffusion controlled or both diffusion and erosion controlled. The value (n) was determined from the slope of the plot of the logarithm of release rate and logarithm of time (t).

5.2.2.13 Biological Evaluation of Hydrogel Film

5.2.2.13.1 Study of protein adsorption on to the surface of hydrogel

Protein adsorption on to the surface of hydrogel membrane was calculated as reported by with slight modification [232]. A UV-visible spectrophotometer method was used to determine the amount of bovine serum albumin (BSA) adsorbed. In order to find out the concentration of adsorbed protein a standard curve for BSA solution was prepared at 630 nm. Pieces of hydrogel membrane were cut in to 1 cm × 1 cm and immersed in 10 ml of phosphate buffer saline (pH 7.4) and incubated for 24 h at 37 ºC until an equilibrium swelling weight was achieved. The swollen hydrogel discs were transferred into the buffer solution containing BSA (30 mg/ml) and kept in an incubator shaker for 4 h at 37 ºC. After protein adsorption, the hydrogel discs were carefully removed and protein adsorption before and after immersing the hydrogel discs in protein solution was calculated using standard curve of BSA (ƛmax 630 nm).

5.2.2.13.2 Hemocompatibility study of hydrogel membranes

Hemolysis experiments were carried out in order to check out the friendly nature of prepared hydrogel membranes with the blood cells [228]. Typically hydrogel membranes were firstly equilibrated with saline solution (0.9 % w/v solution of NaCl, 37 ºC). Anti-coagulated blood was used for this test. Previously equilibrated hydrogel discs were

transferred to propylene tube containing 7 ml of phosphate buffer saline (pH 7.4) and incubated for 72 h at 37 ºC. The PBS was removed from the tube and 1 ml of anti-coagulated blood was added to hydrogel discs and incubated for 3 h at 37 ºC. Positive and negative controls were prepared by adding 20 % triton X solution and PBS respectively. Each tube was incubated and gently inverted to ensure the thoroughly contacting of the membrane and anti-coagulated blood. The fluids were transferred in to a proper tube and centrifuged at 3000 rpm for 20 min. The hemoglobin released by hemolysis was calculated by determining the optical densities of the supernatant at 540 nm. The percentage hemolysis was calculated using the equation.

$$\text{Percentage Hemolysis (\%)} = \frac{\text{Amemb} - \text{A}(-)\text{control}}{\text{A}(+)\text{control} - \text{A}(-)\text{control}} \times 100$$

Where A is the absorbance of spectrophotometric value, A_{memb} is absorbance of tested hydrogel membrane, $A_{(-)\ control}$ is the absorbance of tube without membrane, $A_{(+)\ control}$ is the absorbance of sample tube containing Triton X without hydrogel discs. According to American society for Testing and Materials, the membrane materials were classified into three types according to their hemolytic index as follow: (1) hemolytic material with hemolysis (> 5%), (2) slightly hemolytic material have hemolysis (between 2 to 5%) and (3) non-hemolytic materials < 2% [230].

5.2.2.13.3 *In-vitro* radical scavenging activity of extract released

The free radical scavenging activity of extract released into the release medium was calculated using DPPH (2, 2-diphenyl -1-picryl hydrazyl) method with slight modification [71]. A 500 µl sample of extract released in to the release medium was mixed with that of 0.1mM w/v solution of DPPH in ethanol in dark conditions at room temperature. The mixture was stored in dark for 30 min for complete reaction of free radical and extract. The radical scavenging activity of the extract released was measured using the UV spectrophotometer at 517 nm calculated using the equation, where A_0 is the absorbance of DPPH alone A_1 is the absorbance of extract (*Ocimum sanctum*) released from the hydrogels. The experiment was carried out in triplicate and results were shown in mean standard deviation. The activity of extract released from the hydrogels was compared with that of standard Ascorbic acid as well as raw extract.

$$\text{Percentage inhibition (\%)} = \frac{(\text{A0} - \text{A1})}{\text{A0}} \times 100$$

5.2.2.14 *In-vitro* antimicrobial activity

5.2.2.14.1 Test microorganisms and growth media

S. aureus (MTCC-3160) and *E. coli* (ATCC-723) were chosen based on their pharmacological and clinical importance. These bacterial cultures were incubated for 24 hours at 37 ºC on nutrient broth medium and stored at 4 ºC until further use. The growth of the culture media was assessed based on the turbidity appearance.

5.2.2.14.2 Determination of zone of inhibition

The zone of inhibition was determined modified agar well diffusion assay [234]. Under aseptic condition inside the bio safety chamber, 20 ml of nutrient agar was dispensed in to the pre-sterilized glass petriplates. Once the media solidifies it was then inoculated with micro-organism suspended in nutrient broth. The media was punched with 6 mm diameter hole and filled with DMSO (Dimethyl sulfoxide) as negative control (C), plant extract (E) prepared in DMSO, silver nanoparticles (AgNPs) and hydrogel disc containing AgNPs. Finally, the petriplates were sealed using paraffin films and kept at 37 ºC for overnight. The diameter of zone of inhibition is indicated by clear area which was devoid of growth of microbes was measured. The same procedure will be followed for the determination of zone of inhibition of Ag ions released from the PVA/Chit hydrogels.

5.3 RESULTS AND DISCUSSION

PVA/CH based hydrogel is a novel approach in wound management as it offers proper adherence, hemostatic activity (chitosan) at the wound site and infection free (AgNPs), transparent covering to the wound bed with excellent patient compliance. In addition, PVA/CH hydrogel is based on physical blending of different proportions of water soluble PVA and chitosan solution without using any chemical cross-linking. Moreover, with "green approach and freeze thaw process" these hydrogels offers biocompatible, biodegradable and provide moist microenvironment as well as maintaining healing promoting anti-oxidative and continuous sterile environment in the wound ambiance.

5.3.1 Synthesis of AgNPS, particle size and *in-vitro* antimicrobial activity

The formation of silver nanoparticles (AgNPs) basically achieved by reducing aqueous solution of silver nitrate in the presence of OS leaves extract. The formations of AgNPs were confirmed by UV-visible spectrophotometer having intense absorption spectra in the

range of 400-450 nm. Figure 5.1 A and B showed the UV-visible spectra of AgNPs containing different proportion of *OS* extract, hydrogels containing AgNPs (2, 4 and 6 mg/ml) and formation of AgNPs at different time intervals (0, 10, 20 and 25 min) respectively. Figure 5.1 C (a, b, c and d) showed the photographs of *OS* extract solution, AgNPs prepared with 2, 4 and 6 mg/ml of *OS* extract. The particle sizes of the prepared AgNPs were found to be in the range of 23.57- 30.1 nm (Figure 5.1 D) with pdi of 0.84. The size of AgNPs increases as we increase the amount of OS extract from 2 to 6 mg/ml while opposite results were obtained in case of zeta potential i.e. zeta potential of AgNPs decreases from -7.7 to 10.6 mv showed less stability of the prepared AgNPs. To improve the stability issues and to improve the mechanical property, AgNPs were further incorporated in the hydrogel matrix system.

To determine whether the prepared AgNPs are bacteriostatic or bactericidal, the countable colony of bacteria was achieved by sequential dilution. Culture of 10^{-5} dilution was used for assessment of MIC of the nanoparticles, as countable colonies (i.e. 173) were observed at that dilution. MIC of AgNPs against *S. aureus* and *E. coli* was observed as 42 µg/ml and 72 µg/ml. Figure 5.2 A, B, C and D showed reduction in the bacterial colonies against *S. aureus* and *E. coli*. The variation in the MIC of gram positive and gram negative bacteria to silver nanoparticles was due to the difference in the thickness, susceptibility and constituents of their membrane structure.

5.3.2 Synthesis of PVA/CH hydrogels containing silver nanoparticles

In the present research work, PVA/CH hydrogel blend containing AgNPs were synthesized using "green approach and freeze thaw process" without using any chemical reducing agents or stabilizers. Till date, different approaches have been employed for the synthesis of AgNPs and AgNPs containing hydrogels such as UV or γ-ray irradiation, ultrasound or chemically cross-linking methods. Frequently, these methods are expensive or chemically toxic that hampers their bio-compatibility with skin tissues as well blood cells. This unique synthesis route was based on physical blending of different proportions of water soluble PVA and chitosan solution. Beside, improving the network density of hydrogel network, PVA at the freezing process turn from isotactic structure to syanotactic

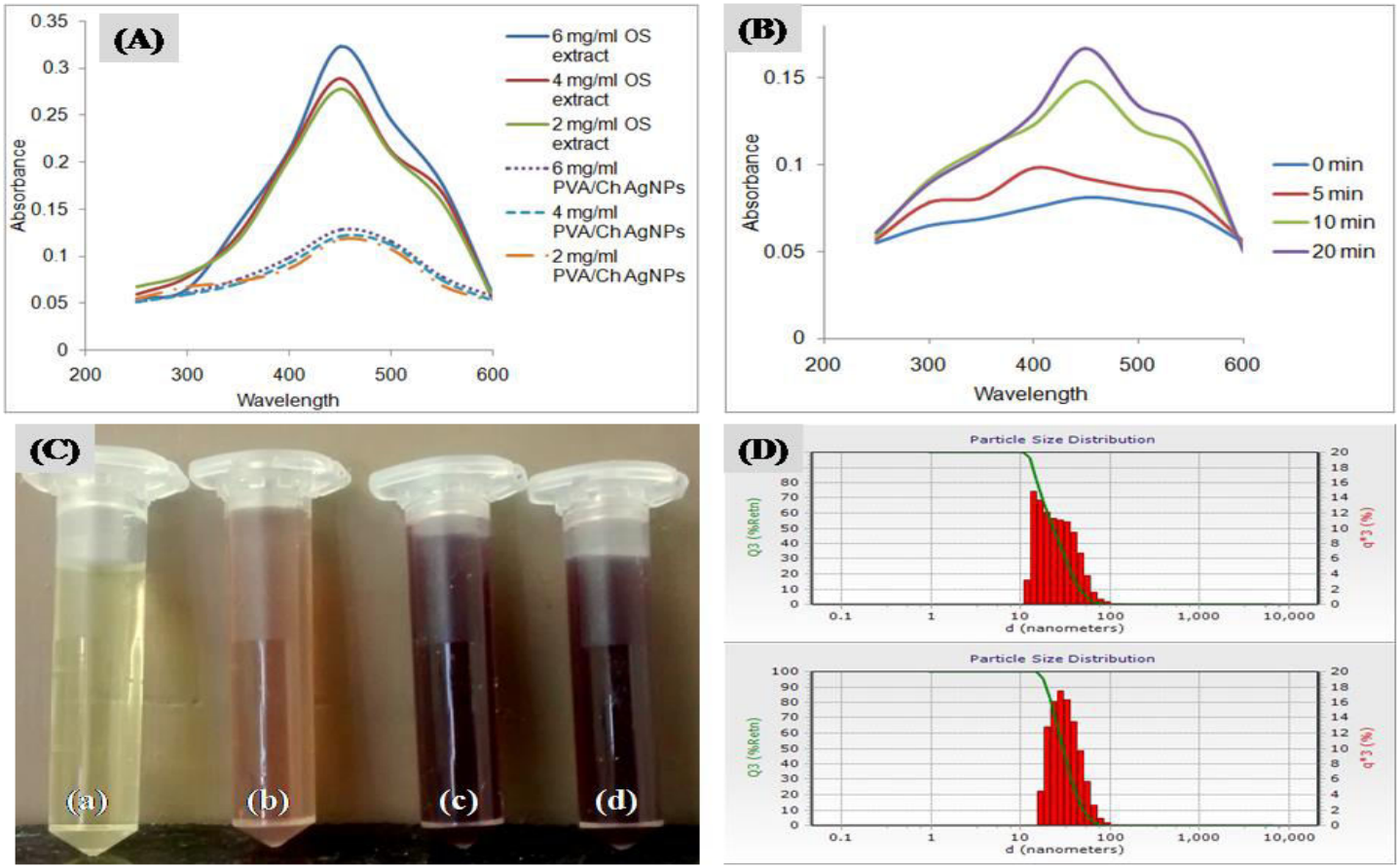

Figure 5.1 Green synthesis of AgNPs using *Ocimum sanctum* leave extract (A) UV-vis spectra of silver nanoparticles and AgNPs loaded PVA/Chit hydrogels formed using 2, 4 and 6 mg/ml of OS extract and (B) UV-vis spectra of AgNPs after 0, 5, 10 and 20 min (C) images showing synthesis of AgNPs as (a) corresponds to blank (without $AgNO_3$ solution) (b), (c) and (d) corresponds to AgNPs synthesized using 2, 4 and 6 mg/ml of OS extract respectively and (D) Particle size of prepared silver nanoparticles showing 100% uniformity in particle size

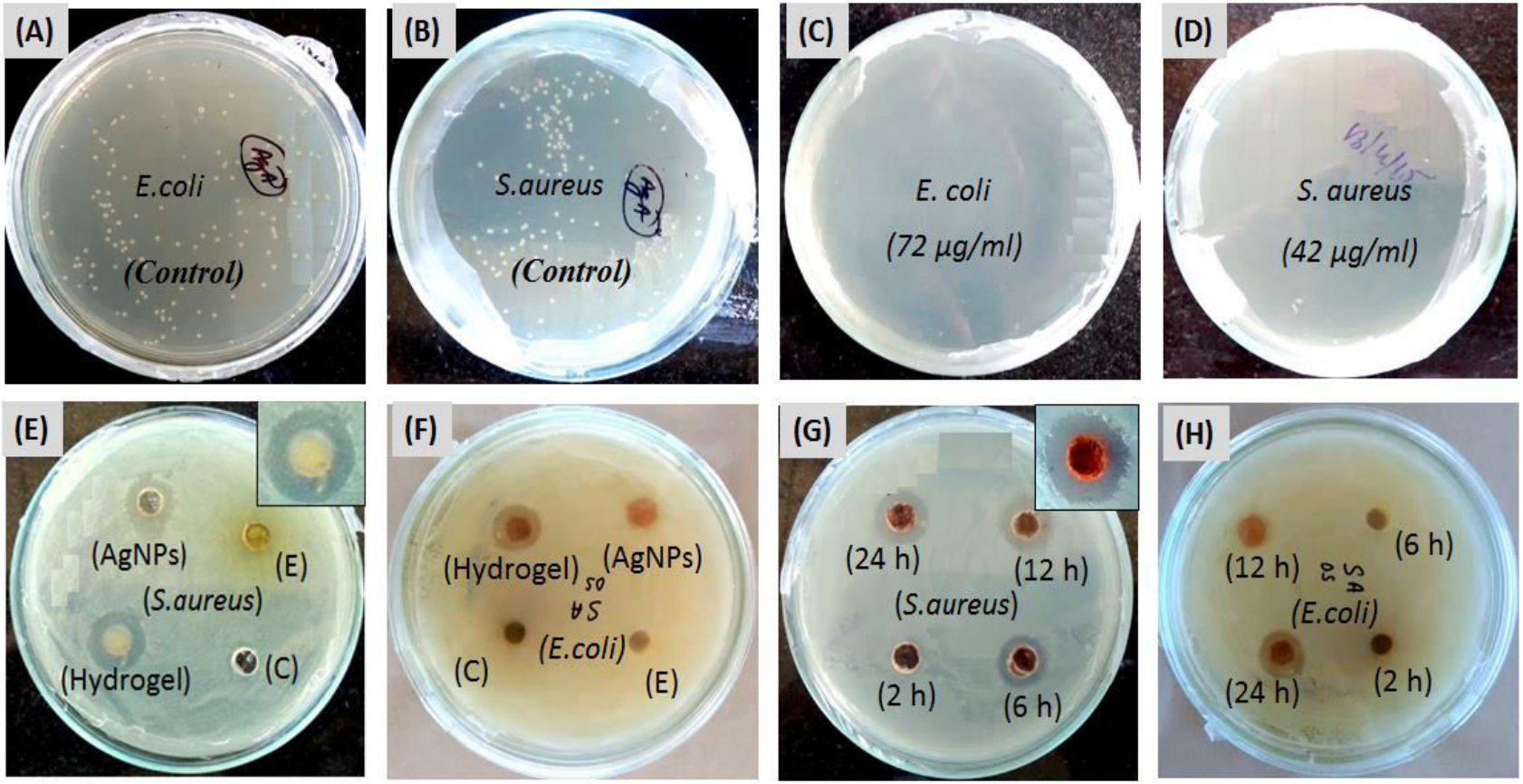

Figure 5.2 Photographs showing antimicrobial activity of AgNPs and PVA: CH/AgNPs hydrogel matrices against *S. aureus* and *E. coli* (A, B, c &D) showing MIC (minimum inhibitory concentration) of AgNPs against *E. coli* and *S. aureus*, (E &F) showing zone of inhibition by AgNPs and PVA: CH hydrogels against *S. aureus* and *E. coli,* (G &H) showing the zone of inhibition by Ag ions released from hydrogel matrices after 2, 6, 12 and 24 h respectively

structure, responsible for formation of hexagonal structure through formation of hydrogen bond with that of water molecules. Moreover, the basic mechanism behind the freeze thaw mechanism involves the crystallization of the polymers (i.e. PVA and CH) that involves the molecular alignment of their molecular chains. These chains folds together and form ordered region called lamelle, which compose larger spheroidal structures named spherulites.

Figure 5.3 (A, B, C and D) showed transparency of blank hydrogel, silver loaded hydrogel disc, elasticity of prepared hydrogels and hydrogel pallets after washing with distilled water. The present approach involves the use of OS leaves for the synthesis of AgNPs. The functional group (-OH, -COOH, NH_2 and thiol) presents in these molecules are known to reduce Ag salt to AgNPs and also provides stabilization due to their high molecular chain.

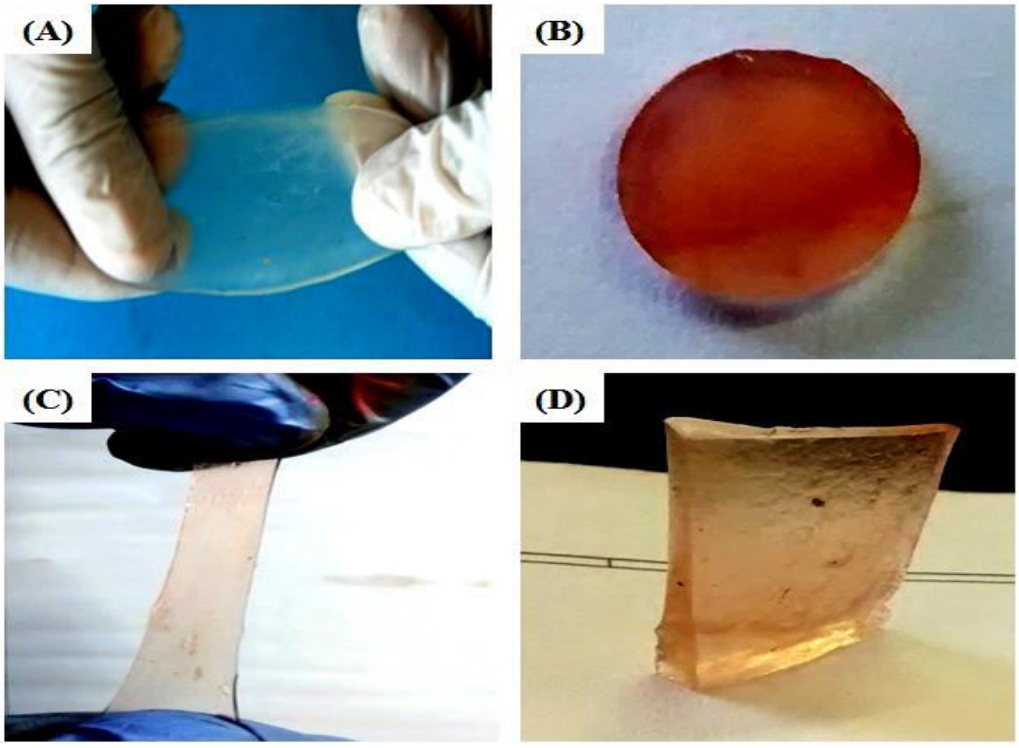

Figure 5.3 Photograph of hydrogels matrices; (A, B, C and D) demonstrates transparency of blank hydrogel, silver loaded hydrogel discs, elasticity of prepared AgNPs loaded hydrogels and hydrogel pellets after washing with distilled water respectively

The synthesis of hydrogels containing AgNPs involves three steps (Scheme-1) Figure 5.4. In details, (step 1) different proportion of AgNPs (1ml, 2ml and 3ml) were mixed with different ratios of optimized hydrogels followed by sonication for 5 minutes in order to

remove the air bubbles present in the mixture to ensure thoroughly mixing or distribution of AgNPs, (step 2) during this step the mixtures is freeze for 18 h at –20 ºC and cooled (thaw) at room temperature (30 min) for three consecutive cycles. This step is important because mechanism of physical cross-linking of hydrogel containing AgNPs was based on the existence of regularly pendent hydroxyl group on PVA chains which further able to form crystallites network structure by strong inter chain hydrogen bonding, (step 3) this step involves the removal of excess or weekly bound AgNPs on the hydrogel by repeated washing with distilled water.

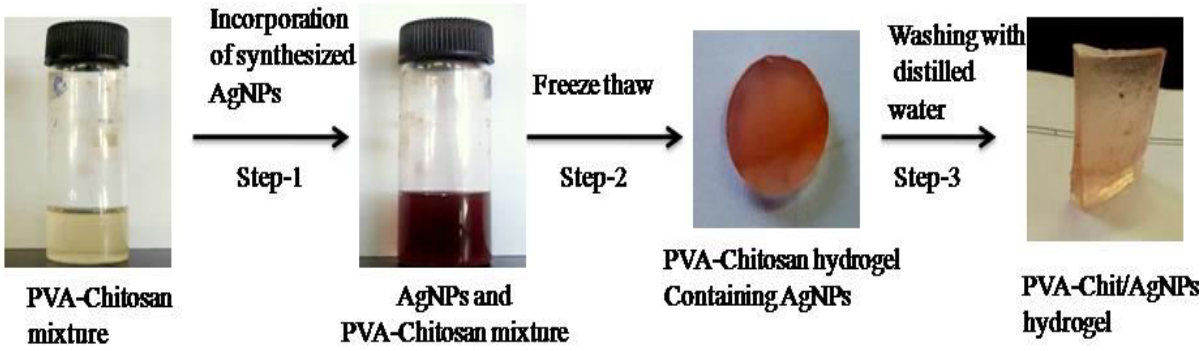

Figure 5.4 Schematic illustration of silver nanoparticles loaded PVA/Chit hydrogels preparative method which consist of three steps (1) mixture of PVA-Chit was mixed with AgNPs synthesized using OS leaves extract, (2) physical cross-linking of the PVA-Chit mixture containing AgNPs using freeze thaw method, (3) washing of the prepared AgNPs loaded PVA-chit hydrogel to leach out surface adhere AgNPs because of poor binding

5.3.3 Physicochemical characterization of PVA/CH hydrogels

5.3.3.1 Scanning electron microscopy (SEM)

Many researchers have extensively studied the structure and morphology of nanocomposite hydrogels prepared by physical method. Figures 5.5 (A, B, C and D) depict the surface morphology of the PVA/chitosan hydrogels with PVA/CH ratio varying in the ratio of 1:0, 0:1, 1:1, 1:2, 2:1 and 3:1, respectively. The SEM images showed the core-shell structure as well as cross-linking of the PVA/SA SHD hydrogels. The dried hydrogels showed a wrinkled, rough and nonporous surface which mats further helps in sustained release of extract as well as silver nanoparticles. The homogeneity of the prepared hydrogels was mostly due to the interaction of hydrogen bonds among the functional group of the blend component. The less porous and rough surface of hydrogel

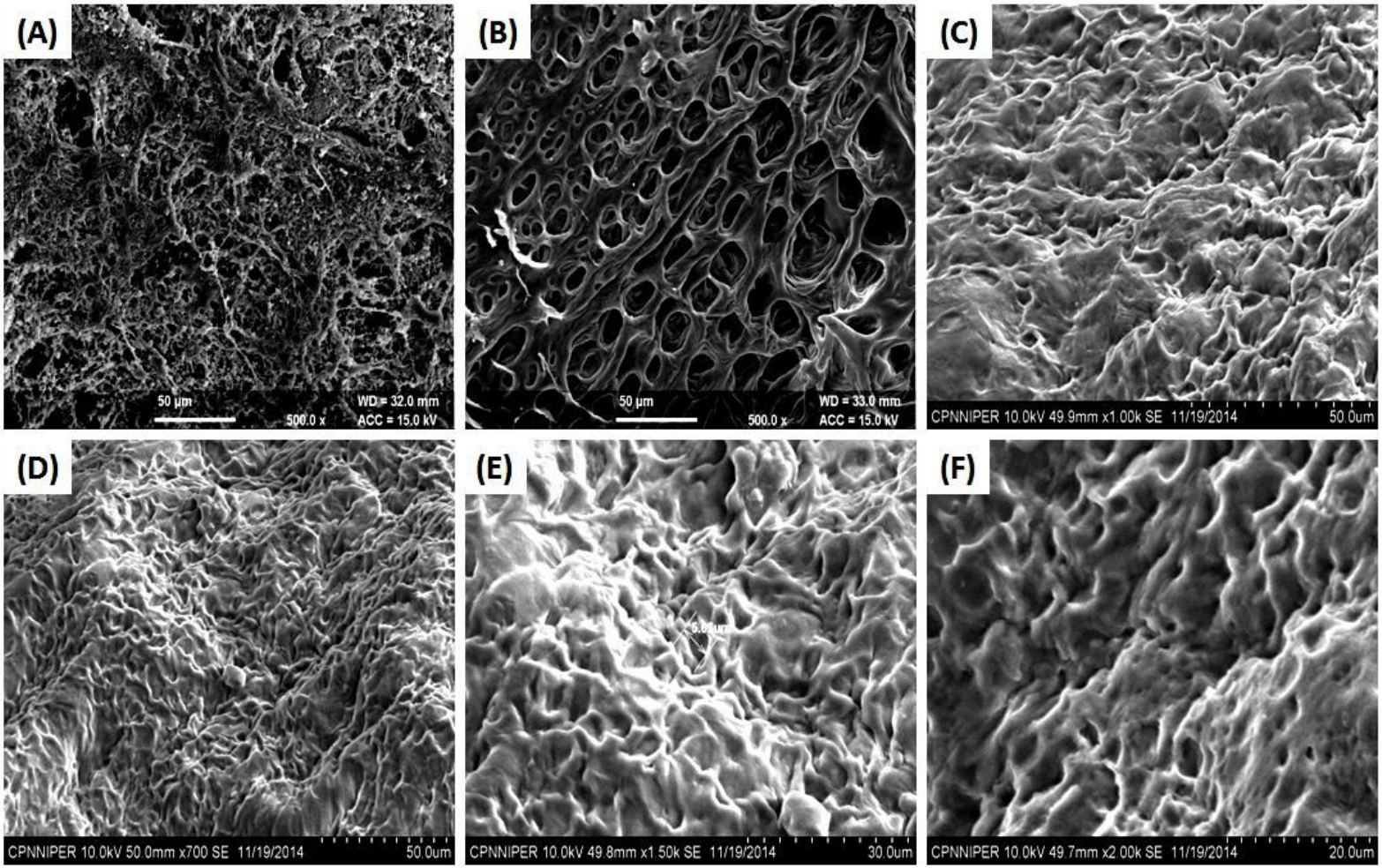

Figure 5.5 SEM images (A–F) depicts the surface morphology, porosity and cross-linking of PVA/CH nanocomposite hydrogel with PVA/CH ratio varying in the range of 1:0, 0:1, 1:2, 1:1, 2:1, and 3:1 (at magnification of 500X and 1000X)

is responsible for the prolonged release of the extract as well as Ag ions. In most of the matrices uniformity of cross-linked network was observed. The uniformity of cross-linked network of PVA/CH hydrogels indicated the physical interaction (i.e. hydrogen bonds) among the functional groups of the blended component. The reason for the above anomaly could be the hydrophilicity of the PVA and ability to crosslink physically.

5.3.3.2 Mechanical testing

To investigate the influence of PVA and silver nanoparticles on the mechanical property of PVA/CH hydrogels, their tensile strength and percentage elongation were evaluated. The tensile strength provides an indication of the strength and elasticity of the film. It is suggested that a film used for biomedical applications such as wound dressings should be strong and flexible [271]. The mechanical strength of prepared PVA alone, PVA/CH and PVA/CH/Ag hydrogels are evaluated by means of tensile strength apparatus and are given in the figure 5.6. The results of tensile strength showed that as we increase the concentration of PVA in PVA/CH hydrogels from 33 % to 100 % (Figure 5.6), the force required to extend the hydrogels increases from 0.36 to 14.56 N and 29 to 89 mm, respectively. Moreover, to check out the effect of AgNPs on the tensile property of hydrogels, PVA/CH/Ag hydrogels were tested for tensile strength. In case of PVA/CH hydrogels containing silver nanoparticles force and extension values were also increased from 0.49 to 11.15 N and 45 to 129 mm (Figure 5.6), respectively. The results of all the samples with respect to increased content of PVA (from 33 to 100%) in PVA/CH hydrogels (Figure 2L, 2M, 2L, 2O, 2P and 2Q; Appendix) as well as AgNPs loaded PVA/CH hydrogels (2R, 2S, 2T and 2U; Appendix) are given in the Appendix files.

The results clearly indicates that as we increase the ratio of PVA in PVA/CH nanocomposite hydrogels, net tensile strength and elongation at break increases due to highly elastic and hydrophilic nature of PVA. However, the difference in the tensile strength between the PVA/CH and PVA/CH/Ag is not great; however it is appreciable when comparing the two PVA/CH and PVA/CH/Ag hydrogels. In addition, the elongation of break was improved considerably for the hydrogels containing AgNPs in comparison with the hydrogels without AgNPs. These observations indicated that the prepared hydrogels are tough, hard, soft and flexible. This might be due formation of hydrogen bonding among the blended component or intermolecular interaction between

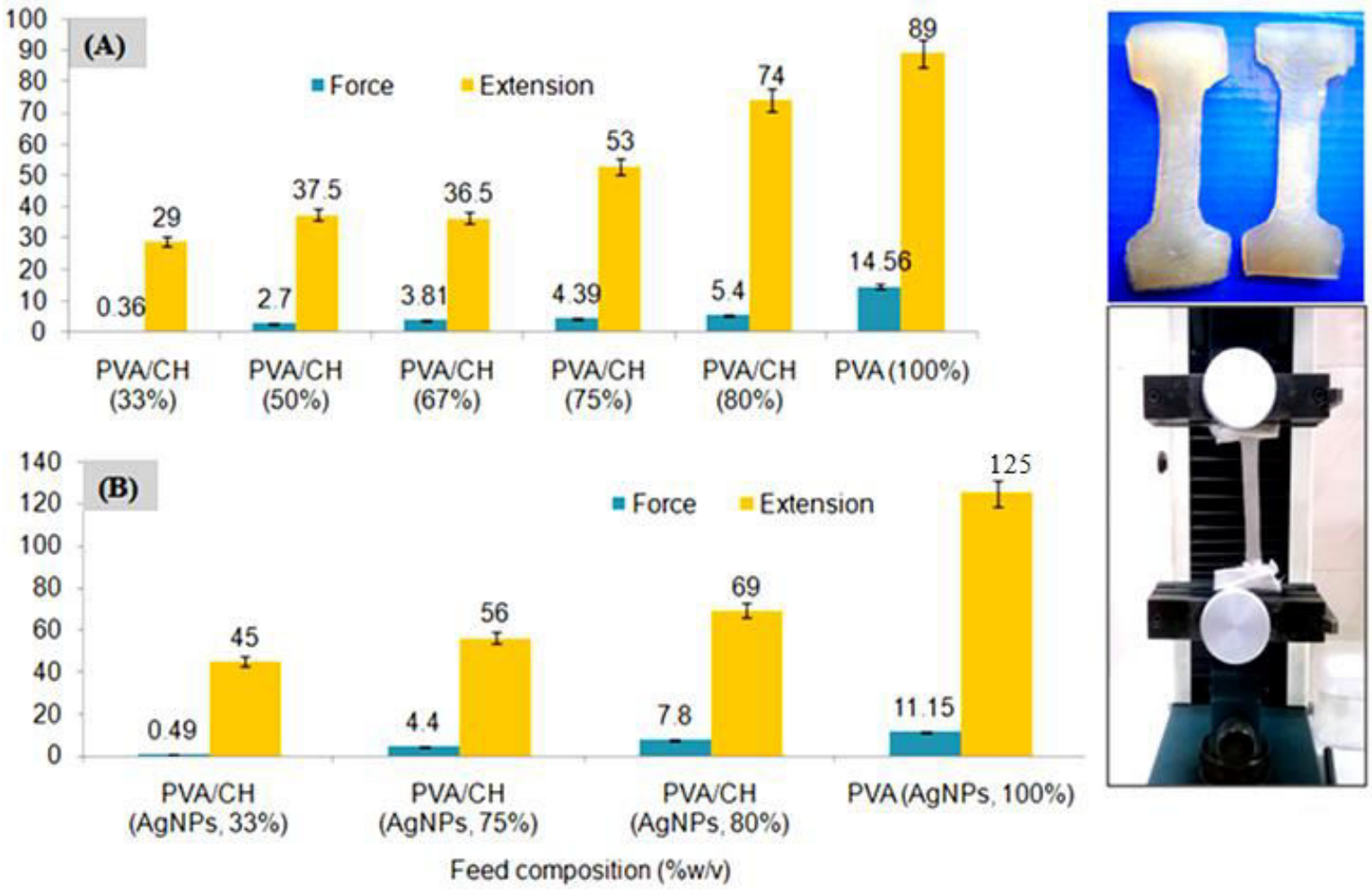

Figure 5.6 Typical demonstration of tensile strength i.e. force vs. extension values of (A) PVA/CH hydrogels without AgNPs, (B) PVA/CH/Ag hydrogels loaded with silver nanoparticles (Inset image showed, samples for tensile strength testing and tensile strength apparatus showing extension of PVA/CH hydrogels

the polymer and the silver nanoparticles. It can also be due to the fact that the AgNPs might act as a plasticizer to improve the flexibility of the composite films. During elongation, the movement and alignment of AgNPs within the polymeric network leave space for the rearrangement of the molecular chains in the composites [135]. Thus the hydrogel composites exhibited a comparatively higher elongation at break but lower tensile strength than the blank hydrogels i.e. without the AgNPs.

5.3.3.3 FT-IR spectral analysis

FTIR was used to observe peak shift caused due to the interaction between the two or more blended polymeric components such as hydrogen bonding or any other complex or formation of coordination bonds among the blended component. Hydrogen bond is formed between the proton donor and proton acceptor molecules. The intensity of hydrogen bonding depends on the acidity of hydrogen in the proton donor, alkalinity of proton acceptor and distance between the groups. The FTIR spectra show spectral characteristics features same as to that for individual polymers, but some bands shifts from their original positions. The FTIR spectra exhibit characteristic of stretching and bending vibrations of the prepared PVA/SA SHD films. FTIR absorption, bands positions and assignment of all the prepared samples are listed in figure and marked with arrows. Figure 5.7 (a)-(d) depicts the FTIR spectra of chitosan alone, PVA/CH hydrogels (without AgNPs), PVA alone and PVA/CH/Ag hydrogels respectively. In case of chitosan alone (figure 7A), the spectra demonstrated a peak at about 3300 –3430 cm^{-1}which can be assigned for the O–H stretching vibrations and the N–H extension vibrations of the polysaccharide moieties of chitosan. The signal appeared around 2890 $cm^{-1}$is corresponding to stretching vibration of the aliphatic C-H bonds, while peak noted at 1637 cm^{-1} is due to stretching vibrations of the amide C=O bonds. The FTIR spectra of PVA [Figure 5.7 (c)] depicts the characteristics broad spectrum peak at 3300 cm^{-1} (–OH stretching), 2918 cm^{-1} (symmetric $–CH_2–$) and at 1418 cm^{-1} and 1093 cm^{-1} for C–O groups.

For PVA/CH [Figure 5.7(b)] hydrogels characteristics peak of –OH and –NH are still present in the spectrum with higher intensity. For PVA/CH/Ag hydrogels [Figure 5.7(d)], the peak appeared in the chitosan spectrum at 3300 – 3430 cm^{-1} has showed a relative decrease of the transmittance indicating that the N-H vibration was affected due to the attachment of the NH_2 groups of chitosan with the Ag^+ ions during the electrochemical

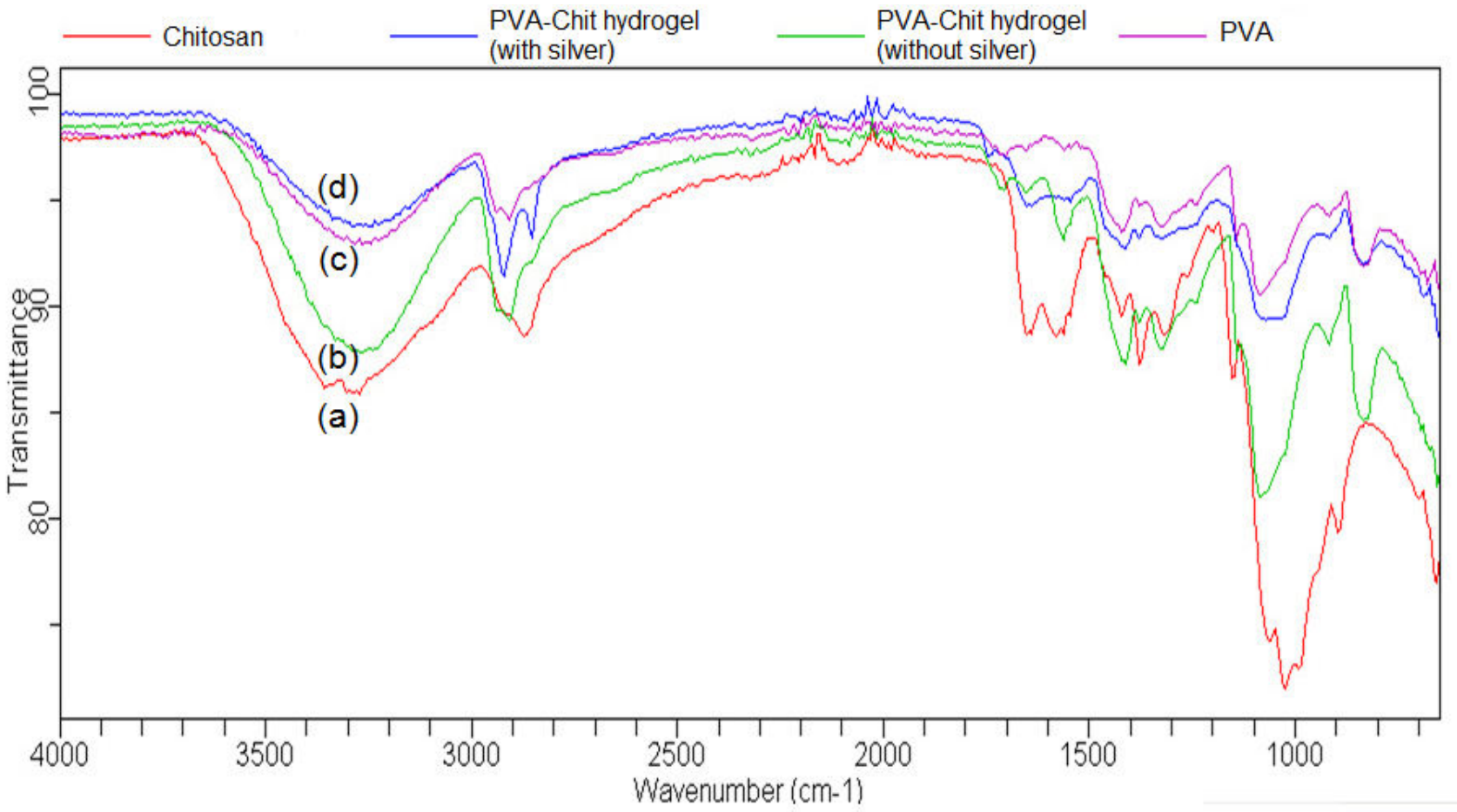

Figure 5.7 Demonstration of comparative ATR-FTIR spectra of (a) chitosan, (b) PVA/CH hydrogel, (c) PVA alone and (d) PVA/CH hydrogels (with AgNPs)

process [241]. Also a relative reduction in the intensity of the peak at 1637cm^{-1} has been noted due to deformation vibration of the amine group of chitosan. All other peaks of chitosan and PVA maintained their position in the corresponding PVA/CH and PVA/CH/Ag hydrogels with a little change in their peak intensity.

5.3.3.4 Thermo gravimetric analysis

The effect of silver nanoparticles on to the thermal stability of PVA/CH hydrogel was investigated by means of TG, DTA and DTG analysis. Thermo gravimetric analysis was performed with chitosan, PVA, PVA/CH and PVA/CH/Ag hydrogels followed by thermal degradation of hydrogels at a heating rate of 10 ºC/min (Figure 5.8 A, B, C and D). The TG and corresponding DTA curves of pure chitosan and PVA was recorded in nitrogen from 30 to 800 ºC as shown in figure 8A & B respectively followed by the first decomposition at a range of 30 to 250 ºC and accompanied by ~10 % and ~5 % weight loss. This stage can be assigned to the loss of residual water present in the samples. The second decomposition of chitosan and PVA alone started at 250 ºC and ending at 700 ºC, corresponds to around ~66 % and ~97 % of weight loss and was indicated by vaporization and burning of volatile part produced by the thermal decomposition of the polymeric chain [242].

DTG curve was used to identify the temperature at which maximum weight loss was observed. The T_{DTG} (i.e. the temperature at which maximum weight loss was observed by chitosan and PVA alone) was found to be 303 ºC (1.38 mg/min) and 293 ºC (1.45 mg/min) respectively, which may corresponds to loss of lattice water whereas, DTA curves showed the exothermic and endothermic weight loss. Chitosan loses up to −116 mJ/mg of heat through exothermic reaction while two peaks were observed for PVA alone i.e. at 223 ºC (5.99 uV) and 296 ºC (1.43 uV) which gain up to ~ 49 mJ/mg and 324 mJ/mg of heat through endothermic reaction respectively [242]. Hence, it is revealed that all polymeric structure must have initial decomposition at lower temperature due to presence of lattice water and it was also supported by exothermic as well as endothermic reaction. Similarly, blank PVA/CH hydrogels and PVA/CH/Ag hydrogels degrade in two steps and accomplished by ~96 % and ~ 94% weight loss (Figure 5.8 C & D). The DTG curve of blank and silver loaded hydrogels showed that its maximum decomposition rate with two temperature curves i.e. at 319ºC (1.06 mg/min) and 361 ºC (0.79 mg/min), respectively. The DTA curves for blank hydrogel (PVA/CH) and AgNPs loaded

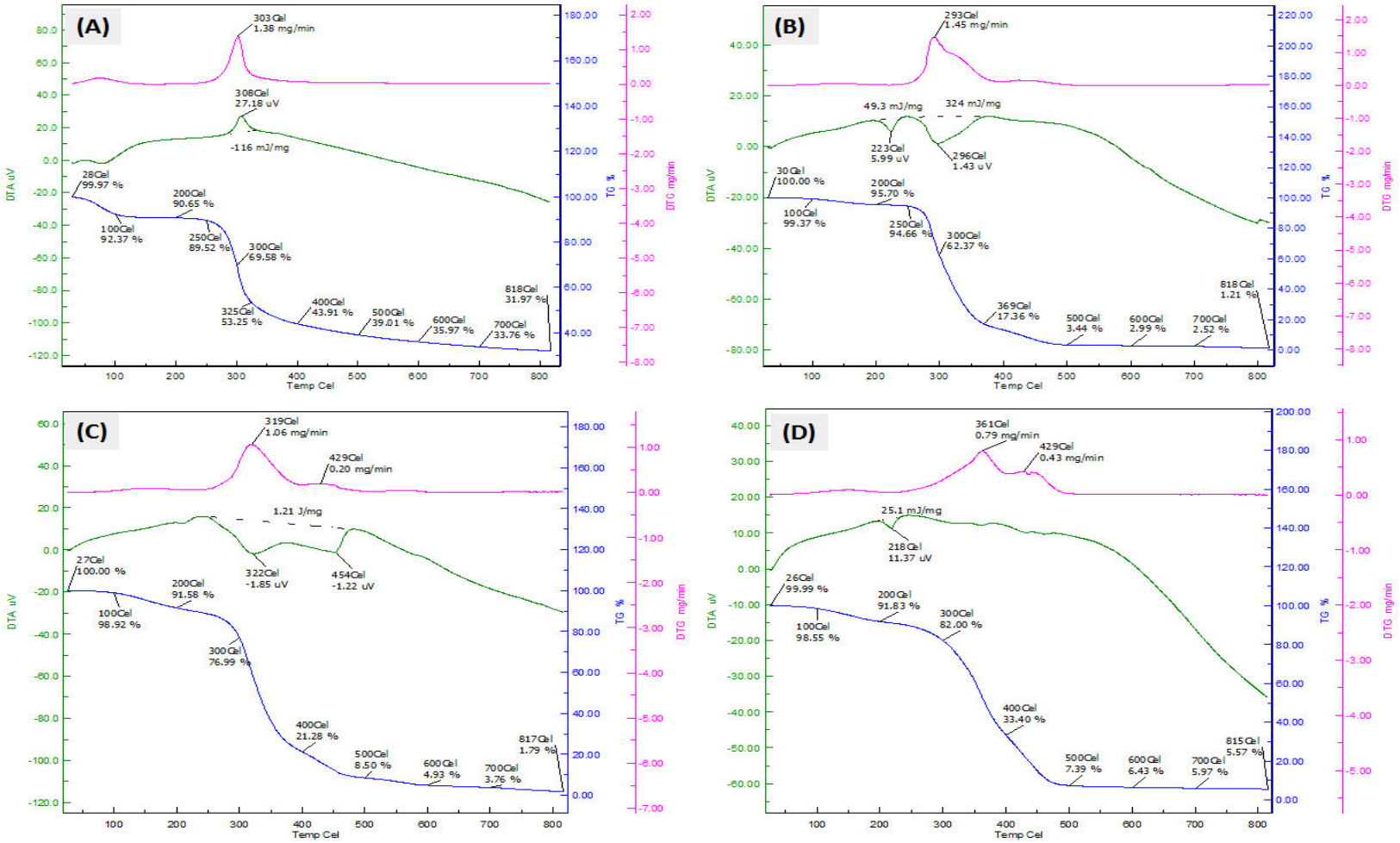

Figure 5.8 Thermo-gravimetric analysis studies showed polymeric interaction through thermal degradation behavior of PVA, CH, PVA/CH hydrogels and PVA/CH/Ag hydrogels containing AgNPs at a heating rate of 10 ℃/min

hydrogels (PVA/CH/Ag) showed that the thermal response features are consistent with the TGA analysis as reflected by the DTA peaks.

It can be seen from the DTA curves that the first two stages are endothermic for blank hydrogels (322 ºC) and (454ºC) as well as PVA/CH hydrogels with AgNPs (218 ºC) which gain up to 1.21J/mg and 25.1mJ/mg of heat (Figure 5.8 C & D). The endothermicity in the above peak indicates that energy is required to vaporize the absorbed water molecules from the hydrogel matrix.

5.3.4 Equilibrium swelling ratio (ESR)

From the water uptake behavior of the prepared hydrogels, it was found that the PVA/CH ratio and freeze thaw cycles are the key regulators for the swelling behavior, which further determines the morphology of the prepared hydrogels. Figure 5.9 depicts the effect of chitosan content on the ESR with respect to different pH media. ESR increased from 0.96 to 6.89 (7.1-fold, at pH 1.2) on increasing the content of CH (0% to 100%), while ESR increased from 2.9 to 5.21 (1.79-fold; pH 6.5) on increasing the PVA content (50% to 100%) in the PVA/CH hydrogels. In distilled water (DW), ESR increased from 2.5 to 9.3 (3.72-fold) with increasing CH content from 0 to 100% while opposite results were obtained on increasing or decreasing the PVA and CH content i.e. ESR decreased from 6.2 to 1.97 (3.1-fold) on decreasing the CH content from 100% to 50%, while on increasing the PVA content from 50 to 100% net ESR increased from 1.97 to 4.1 (2.08-folds). In addition to the above studies it was found that with increasing the ratio/content of chitosan in the hydrogel system, the ESR increases in all of the above pH media.

It is well known that swelling of hydrogels is strongly dependent on the functional groups attached to it. Since the prepared hydrogel blend contains chitosan as one of the major component and contains number on ionizable functional group such as (-NH2, OH) it swells in basic as well as in acidic media. Moreover, it is known that the effective pKa for chitosan is 6.5, the involving species are NH_3^+ and COOH (at pH 1-3), $NH_2$and COO^- (at pH 7-13) and $NH_3^+$and COO^-or $NH_2$and COOH (at pHs 4-7). Under acidic conditions, the swelling is mainly controlled by amino group (NH_2) on the C-2 carbon of chitosan component [272]. It is a weak base with intrinsic pKa of about 6.5, so gets protonated and the increased charge density on the polymer should enhance the osmotic pressure inside the hydrogel particles because of NH_3^+- NH_3^+electrostatic repulsion.

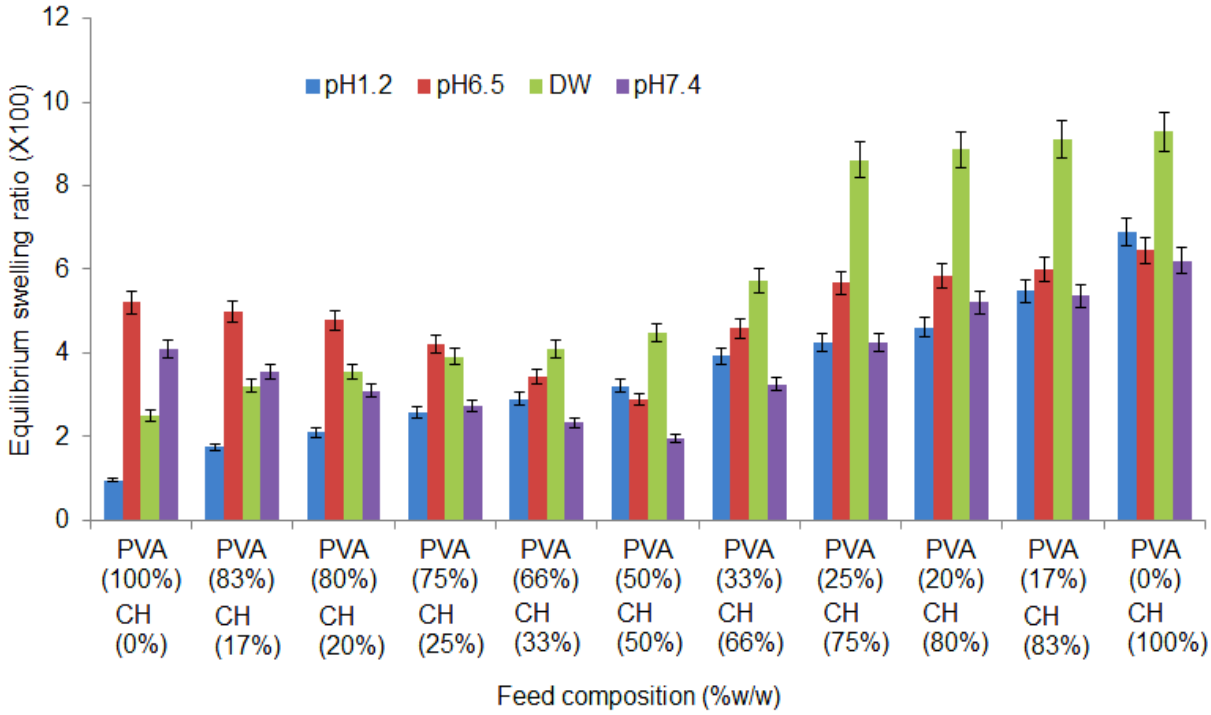

Figure 5.9 Demonstration of effect of PVA/CH ratio on the water uptake behavior (equilibrium swelling ratio; ESR) of PVA/CH hydrogel in distilled water (DW), pH 1.2, 6.5 and 7.4 (n=5; mean ± SD)

This osmotic pressure difference in the internal and external solution of the network is balanced by the swelling of hydrogels. However under a very acidic condition (pH 1-3), a screening effect of counter ions i.e. Cl^-, shields the charge of ammonium cations and prevent an efficient repulsion. But under pH 6.5 (or pH range 4 to 7) the majority of base and acidic groups are as $NH_3^+$and COO^- followed by ionic cross-linking of these groups or hydrogen bonding between amine and carboxylic group may lead to a kind of tighter cross-linking followed by lower swelling of hydrogel. At (pH >7), the carboxylic acid groups become ionized and the electrostatic repulsive forces between the charged sites (COO^-) causes increased swelling [272].

Whereas, PVA is an uncharged molecule, but -OH functional group of PVA might participate in hydrogen bonding, which lead to swelling of the hydrogel. The swelling behavior of the prepared hydrogel is greatly dependent on the number of freeze thaw cycles, increase number of cycle's results in formation of highly tighter network and it could be difficult to the surrounding liquid to diffuse into the tightly packed structure thus decreases the swelling capacity.

5.3.5 *In-vitro* degradation of PVA/CH hydrogels

Figure 5.10 (A & B) illustrates the weight loss profile of prepared PVA/CH hydrogels under *in-vitro* conditions (37 ± 0.2ºC, pH 6.8). It was observed that with increasing content of PVA in PVA/CH hydrogels from 0 to 50 % (and decreasing CH content from 100 to 50 %), percentage loss in weight decreased from 88.69 % to 74.23 % of its total weight within 3 days. Further increase in PVA content from 50 to 100 %, it decreased from 74.23 % to 47.6 %. It was observed that on increasing the content of chitosan in the PVA/CH hydrogel results in higher swelling and formation of loose network, which further increases the percentage degradation. The lower degradation of PVA with increased ratio of PVA in the hydrogels i.e. (PVA/CH) could be due to the formation of strong H-bonding among –OH groups of PVA chain, which further cause formation of tight network and less diffusion of external water medium inside the polymeric network.

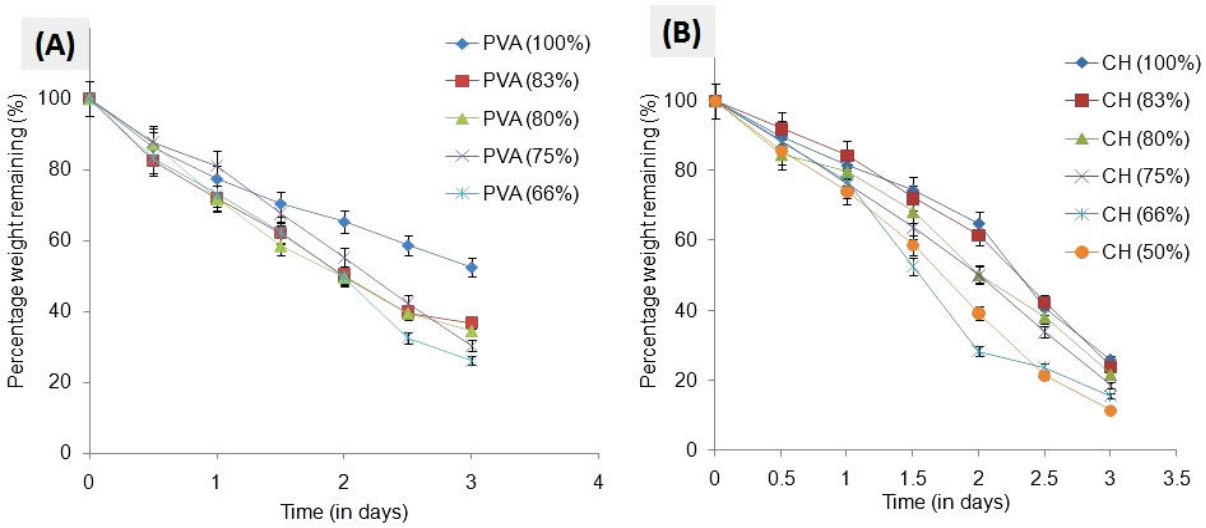

Figure 5.10 Effect of PVA and CH concentration on the weight loss profile of PVA/CH hydrogels (A) PVA/CH hydrogels (PVA concentration 50 to 100 %; 37 ± 0.2 ºC, pH 6.8), (B) PVA/CH hydrogels (CH concentration, 50 to 100%; 37 ± 0.2 ºC, pH 6.8), (mean ±SD; n=3)

5.3.6 Atomic absorption spectroscopy, drug loading and *In-vitro* drug release studies

Three randomly selected sites from PVA/CH/AgNPs hydrogel disc for content uniformity (Ag) were taken in order to determine the Ag content in PVA/CH/Ag hydrogel and AgNPs synthesized using *OS* extract (1 mg/ml) and sodium borohydride (1 mg/ml;

for comparison study). From AAS studies, 61.34 ± 0.12 mg/l, 75.05 ± 0.13 mg/l of silver was measured in samples (i.e. $AgNO_3$) synthesized by *OS* extract and sodium borohydride. While randomly selected sites of PVA/CH/Ag hydrogel discs contained average of 0.153 ± 0.009 mg/g of silver. The AAS study confirmed uniformity and considerable immobilization of silver in the PVA/CH hydrogels. The percentage loading of OS extract in PVA/CH hydrogels was found to be 84.8±1.11%. Higher loading could be due to increased solubilization of *OS* extract in the polymeric system. The results of AAS suggest that uniformity of silver ion concentration in the PVA/CH hydrogels could be due to the fact that silver ions interact more strongly and uniformly with PVA and CH chain leading to higher loading and uniformity of the AgNPs in the PVA/CH hydrogels having equal PVA and CH fraction.

Silver nanoparticles are generally non-reactive but in aqueous media releases silver ions which are responsible for intracellular accumulation of silver causing antimicrobial effects. Figure 5.11 (A) showed the release pattern of silver from the hydrogel disc as well as from AgNPs solution. The Hydrogels containing AgNPs and AgNPs solution releases ~84 % and 83.9% of Ag ions in 30 and 20 h respectively. Hydrogel containing OS extract and raw extract solution releases 84.3% and 82.5% of OS extract in 30 and 16 h respectively.

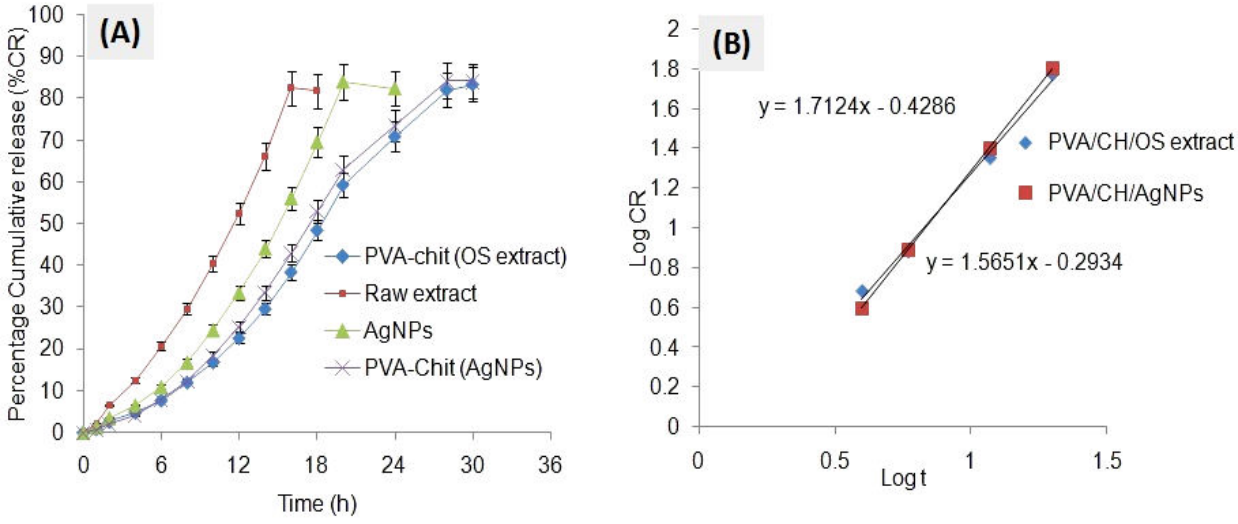

Figure 5.11 Demonstration of (A) release profile study of AgNPs and OS extract from AgNPs solution, PVA/CH/Ag, PVA/CH/OS hydrogels and OS extract solution, (B) drug release kinetics from PVA/CH hydrogels (mean ±SD; n=3)

The drug release kinetics was analyzed by plotting the log of cumulative release data versus log of time. According to Korsmeyer Peppas model, the values of PVA/CH/AgNPs and PVA/CH/OS extract hydrogels exponent 'n' is found to be >1 (Figure 5.11 B) which indicated a super case-II transport [251] i.e. AgNPs as well as OS extract was released due to degradation of hydrogels as well as through diffusion mechanism. The initial burst release behavior can be explained as the fast diffusion of the silver as well as OS extract molecules found on to the surface of PVA/CH hydrogels. Furthermore, higher release rate may be related to the higher swelling ratio of the PVA/CH hydrogels under saline and the weak H-bonding interaction between silver ions and polymeric network in the PBS. Moreover, the results of sustained release behavior (30 h) indicate that presence of nano-silver in the PVA/CH hydrogel network cause less swelling with respect to time. It could be due to the hydrophilicity and roughness of the hydrogel as well as chelation of some hydroxyl group with nano-silver of the network which further neutralizes the repulsions of the network causing sustained release of the silver as well as OS extract.

5.3.7 Biological evaluation of hydrogel film

5.3.7.1 *In-vitro* protein adsorption and blood compatibility study

As shown in Figure 5.12 (A) the adsorption of serum protein increases from 1 to 23 $\mu g/cm^2$ as the amount of chitosan increased from 0 to 75% (w/w). Interestingly, the PVA/CH hydrogels loaded with AgNPs showed a feasible adsorption of BSA as compared to that of hydrogels without AgNPs. The reason behind the less protein adsorption in the presence of AgNPs is not clear. Some factors such as chelation of hydroxyl group of the hydrogel network with AgNPs may be responsible for the less protein adsorption as compared to that of blank hydrogel. When blood contacts foreign materials plasma proteins are always adsorbed on to the surface of material and thus cause the adhesion of some platelets, white blood cells and red blood cells on to the plasma proteins layer. The aggregated platelets than release some materials like ATP and ADP, which further attracts more platelets to adhere on to the surface of protein which further results in formation of plugs. In the final stage of plugs formation, it induces formation of thrombin, thrombus or non-soluble fibrin like network [252].

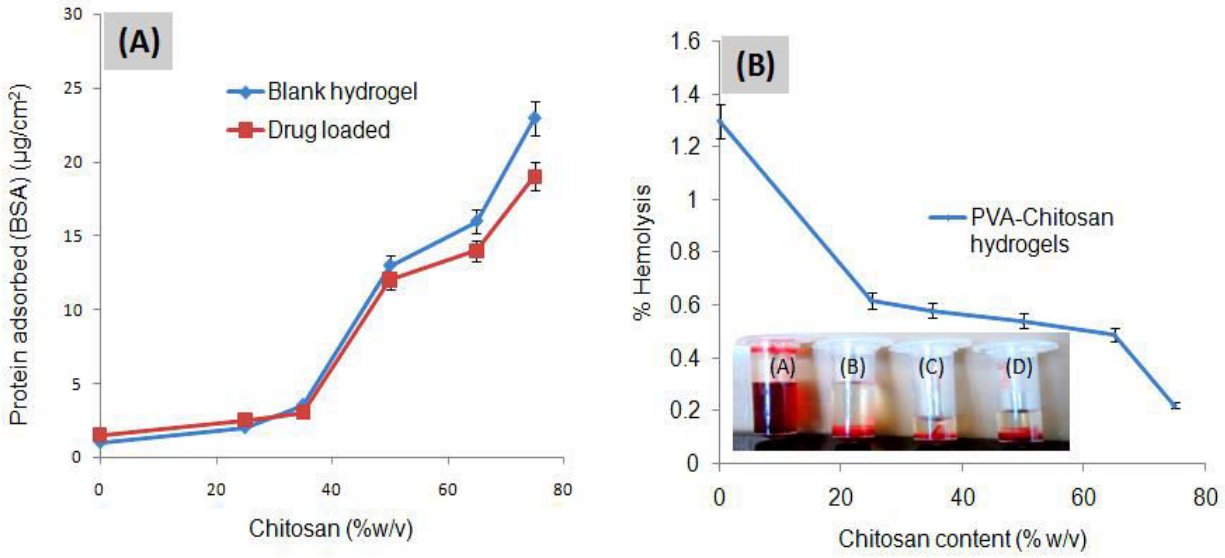

Figure 5.12 Graph showed (A) Effect of (CH concentration % w/v) PVA/CH hydrogels on protein adsorption, (B) Effect of (CH concentration %w/v) PVA/CH hydrogels on % hemolysis. Inset, images a, b, c and d shows % hemolysis caused by Triton X (+ve control), PBS (-ve control), blank hydrogels and AgNPs loaded hydrogels, respectively

The *in-vitro* percentage of hemolysis induced by hydrogels containing AgNPs in optimum concentration was found to be less than 5 % (critical safe hemolytic ratio for biomaterials according to American Society for Testing and Materials, 2000). It is clear from the depicted data that percentage hemolysis shown in Figure 5.12 (B) decreases from (1.3- 0.22 %) as we increase the concentration of chitosan in the hydrogel membranes, which shows good compatibility with the blood cells and can be further applied topically as wound dressings. This was due to the fact that both PVA and chitosan are highly biocompatible molecules and furthermore no chemical cross-linking was used.

5.3.7.2 *In-vitro* radical scavenging activity of extract released

The raw extract and extract released from the hydrogel inhibited 63.1% and 69.2 % of DPPH radicals in 14 and 28 h respectively (Figure 5.13). The purple color of DPPH was reduced to yellow colored diphenylpicryl hydrazine by antioxidant compounds. The phenolic compounds present in OS extract were mainly responsible for the antioxidant activity of the extract. Phenolic compounds fall into several categories; chief among these are the flavanoids which have potent antioxidant activity. Results of this study revealed that the plant extract contains phytochemicals constituents that are capable of denoting

hydrogen atom to the free radicals to scavenge the potential damage [273]. The *in-vitro* scavenging activity of formulations confirmed that sufficient polyphenolic compounds were released over a period of 28 h.

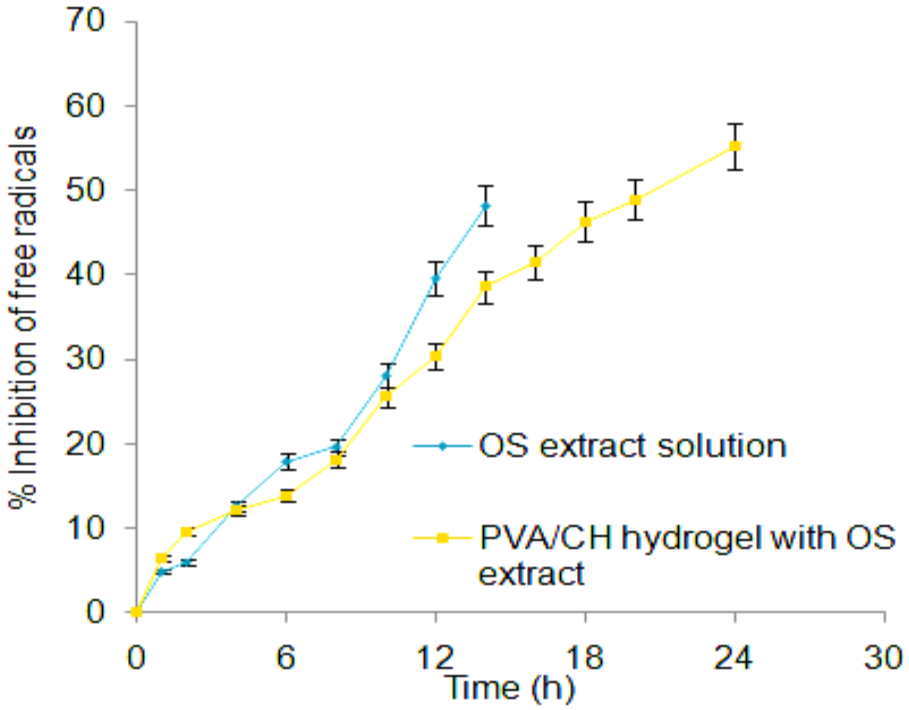

Figure 5.13 Figure showed free radical scavenging activity of OS extract solution and OS extract released from PVA/CH/OS hydrogels (mean ± SD; n=3)

5.3.8 *In-vitro* antimicrobial activity

The *in-vitro* antimicrobial properties of AgNPs and PVA/CH hydrogel films containing AgNPs were evaluated against gram negative *E. coli* and gram positive *S. aureus* bacteria by well diffusion technique. Figure 5.2 E, F, G and H and Table 5.1 exhibit the typical antimicrobial results by wells diffusion method measured by diameter of zone of inhibition under and around the tested samples. After 24 h of inoculation (37 ºC) our results demonstrates that Control (C) and plant extract (E) doesn't not show any zone of inhibition against *S. aureus* and *E. coli* (Figure 5.2 E & F), Whereas AgNPs and hydrogel disc showed a concentration dependent inhibitory effect against *S. aureus* and *E. coli.* It is also important to note that antimicrobial function of silver ion is believed to be due to as a contact active material or silver ion released. In the present study silver ion seems to inhibit the bacteria through contact active way as well as silver ion released. Figure 5.2 G & H showed the zone of inhibition of silver ions released from the hydrogel membranes

after 2, 6, 12 and 24 h respectively. It was found that the prepared AgNPs were found to be active against *S. aureus* as a clear zone of inhibition was recorded after predetermined time of intervals.

Table 5.1 Zone of inhibition of silver nanoparticles and PVA/CH/Ag hydrogels against *E. coli* and *S. aureus*

Zone of inhibition (mm) of AgNPs and PVA/CH/Ag hydrogels		
Samples	***E. coli***	***S. aureus***
Silver nanoparticles	5.2	8.1
PVA/CH/Ag hydrogels	6.3	9.3

The antimicrobial activity of silver loaded PVA/CH hydrogels could be attributed to the fact that silver nano-particles can interact with the sulfur and phosphorous containing proteins from cell which further attacking the respiratory chain with cell division leading to cell death [257]. It is also believed that silver molecules binds to thiol groups (-SH) in the enzyme and subsequently causes deactivation of the enzyme. The use of AgNPs has exhibited phenomenal antibacterial activity due to high surface area thereby, maintained its efficacy in a sustained manner for 24 h [210, 211].

5.4 CONCLUSION

In this objective, we demonstrated and utilized OS extract for the green synthesis of AgNPs loaded PVA/CH hydrogels using freeze thaw technique. The green synthesis for the reduction of silver nitrate solution is utilized for the synthesis of silver nanoparticles to lower the toxic effects associated with the chemical reduction such as sodium borohydride. Nanoparticles agglomeration was prevented through the use of high cross-linking and dense inter-polymeric network which further helps in the controlled release of Ag ions and OS extract. UV-vis, FTIR, SEM, TGA studies indicated that silver nanoparticles with a means diameter of 25 to 30 nm were successfully fabricated and homogeneously dispersed in the hydrogel network. FTIR, TGA and mechanical property confirmed that incorporation of AgNPs inside the hydrogel network enhance the stretching of the polymeric backbone chains, resulting in the higher tensile strength and

higher elongation of break. Moreover, the overall results possessed a highly interconnected porous structure, well distributed AgNPs, suitable tensile strength and biocompatibility, which would meet the basic criteria for the biomedical as well as controlled release of phytochemicals for biomedical applications such as wound dressings.

OVERALL SUMMARY AND FUTURE PROSPECTS

We have utilized different phytochemical extracts and "green approach" for the development of lipid based nanoemulsions and silver nanoparticles loaded nanocomposite hydrogels for controlled drug delivery. To fulfill this objective in the first process, nanoemulsion and SNEDDS were prepared using *Tinospora cordifolia* and *Berberis aristata* followed by their physiochemical characterization. While in the second process, *Ocimum sanctum* and *Ficus benghalensis* extracts were utilized for the green synthesis of silver nanoparticles. The prepared silver nanoparticles were further utilized for the development of PVA/CH and PVA/SA nanocomposite hydrogels. The above two processes is then characterized by means of their physiochemical characterization *i.e.* particle size, zeta potential, polydispersity index, Surface morphology using SEM, FTIR, TGA, thermodynamic stability, swelling, degradation behavior, tensile strength and their *in-vitro* drug release as well as *in-vitro* permeation studies. The overall study aimed for delivering and utilizing these herbal extracts for the synthesis of silver nanoparticles and their physicochemical characterization for better understanding of the factors involved in low oral and topical delivery, their toxicity and stability issues involved. The overall bottom up approach being utilized and their proposed outcomes are discussed to deal with our system. Future prospects and the practical applications of our approaches are also discussed briefly to provide new directions for the delivery of these herbal extracts for the treatment of various diseases like diabetes and diabetic ulcers in the coming research. The overall study is summarized below:

- *Tinospora cordifolia* and *Berberis aristata* loaded nanoemulsion and SNEDDS has been successfully explored for their controlled delivery and improved permeation, respectively.
- Solubility of extracts in various oils, surfactant and co-surfactant were carried out in order to screen the components to be used for the synthesis of nanoemulsion and SNEDDS. Drug solubility profile was determined by means of flask shaking method in various oil, surfactant and co-surfactant mixture, it was found that *Tinospora cordifolia* extract exhibit high solubility in a mixture of clove oil (Oil), span 80 (Surfactant) and ethanol (Co-surfactant) (i.e. 20.9 mg/ml) followed by clove oil alone (18.25 ± 0.0009 mg/ml) and neem oil (15.6 ± 0.0007 mg/ml). Whereas, *Berberis aristata* exhibit high solubility in a mixture of calendula oil, tween 80 and ethanol (i.e. 14.2 mg/ml).
- Pseudo-ternary phase diagram were constructed by means of titrating a series of mixture of oil, surfactant and co-surfactant with distilled water for the formation of

best nanoemulsion region. Nanoemulsions and SNEDDS were prepared by using ratio of components determined from the phase diagram. Vortex mixing and sonication process was applied in case of nanoemulsion to hasten as well as to obtain uniform particle size.

- The droplet size below 100 nm (~33.7 nm), higher zeta potential value (-31.2 mV) and high loading efficiency (83.8 %) were unique features of these nanoemulsions and SNEDDS.
- The *in-vitro* drug release profile study was performed using dialysis membrane method under proper sink conditions (pH 6.8; 37±0.5˚C; 50 rpm). *In-vitro* drug release profile study was performed to compare the release behavior of extracts from nanoemulsion as well as from raw extract solution (i.e. without nanoemulsion). The *in-vitro* release study demonstrates that nearly ~81 % and 74 % TC extract was released nanoemulsion and raw extract in 24 h and 10 h, respectively. While, ~96% and 80% of BA extract was release from SNEDDS and BA solution in 34 h and 12 h respectively, which is a critical step towards its improved delivery and bioavailability.
- Two sets of nanocomposite hydrogels based on PVA/CH and PVA/SA SHD were prepared by means of freeze thaw and cross-linking techniques. The green synthesis approach is utilized for the reduction of silver nitrate solution to form silver nanoparticles in order to lower the toxic effects associated with the chemical reduction such as sodium borohydride. The particle sizes of the prepared AgNPs were found to be in the range of 23.57- 30.1 nm with a pdi in the range of 0.66 to 0.84.
- Aerosolized nanocomposite hydrogels based on PVA and SA were introduced as a novel dressing to evaluate the potential of these aerosols based system in controlled drug delivery. On the other hand, it was concluded that the rate of cross-linking was not extensively affected by the concentration of AgNPs used but SHD films loaded with AgNPs retained their shape better, in terms of their mechanical property, flexibility and elasticity than films without AgNPs.
- The swelling behavior of both the nanocomposite hydrogels were found to pH dependent. It was concluded from the swelling behavior that swelling for both the nanocomposites hydrogels was highest in basic pH. On the other hand, the swelling behavior of PVA/SA sprayed hydrogel is greatly dependent on to the concentration and extent of cross-linker used (BA and $CaCl_2$). Excess cross-linking of PVA/SA SHD films results in formation of tighter interface and it could be difficult to the

surrounding liquid to diffuse into the tightly packed structure thus decreases the swelling capacity.

- ❖ The shifting and reduction in the peak intensity in the FTIR spectra for both the PVA/CH and PVA/SA hydrogels results in the formation of coordination bond between the electron rich groups indicates strong interaction among all the polymers and silver nanoparticles.
- ❖ From the degradation profile of PVA/CH as well as PVA/SA nanocomposite hydrogels it was concluded that increased PVA content provide strength to the nanocomposite hydrogels but reduces the degradation rate.
- ❖ The mechanical analysis of the synthesized PVA/CH nanocomposite hydrogels showed an increase in the tensile strength and elongation at break than that of blank hydrogels i.e. PVA/CH hydrogels without silver nanoparticles, clearly demonstrating a good mechanical behavior.
- ❖ It has been found that, when PVA alone (without incorporating AgNPs) was used for the measurement rheological properties; viscosity of PVA solution is less than that of PVA/Ag solution; which could be a useful parameter for the handling and delivery purpose of polymeric solutions.
- ❖ From the thermo-gravimetric analysis, it was observed that the introduction of silver nanoparticles in the PVA/CH and PVA/SA hydrogels network results in increased thermal stability.
- ❖ The surface morphology of PVA/CH and PVA/SA nanocomposite hydrogels showed a wrinkled and porous surface or structure with high uniformity which may further participated in sustained release of the silver nanoparticles as well as extract.
- ❖ It was noticed from the release profile study of PVA/SA SHD films that ~87±1.78 % and ~82±1.67 % of *FB* extract and silver ions were released from the SHD films respectively. Whereas, PVA/CH loaded with AgNPs and OS extract releases ~84 and 85% of AgNPs and OS extract in 30 h respectively.
- ❖ It was found from the *in-vitro* antimicrobial study that the silver ions released from PVA/CH and PVA/SA hydrogels showed a concentration dependent inhibitory effect against *S. aureus* and *E. coli.*
- ❖ The overall results and properties confirmed that these nanocomposite hydrogels can be a promising platform for the controlled delivery of these phytochemicals and silver nanoparticles.

FUTURE PROSPECTS

- Present study concluding that the characterization is carried out only *in-vitro*. There is a need to carry out the *in-vivo* studies for testing of these oil based nanoemulsions against diabetes and bioavailability measurement.
- Development of nanocomposite hydrogels with higher biocompatibility and testing against *in-vivo* wound healing activity is anticipated. Phytochemical delivery and the interaction with the living tissues seem to be major topic in the future research.

APPENDIX

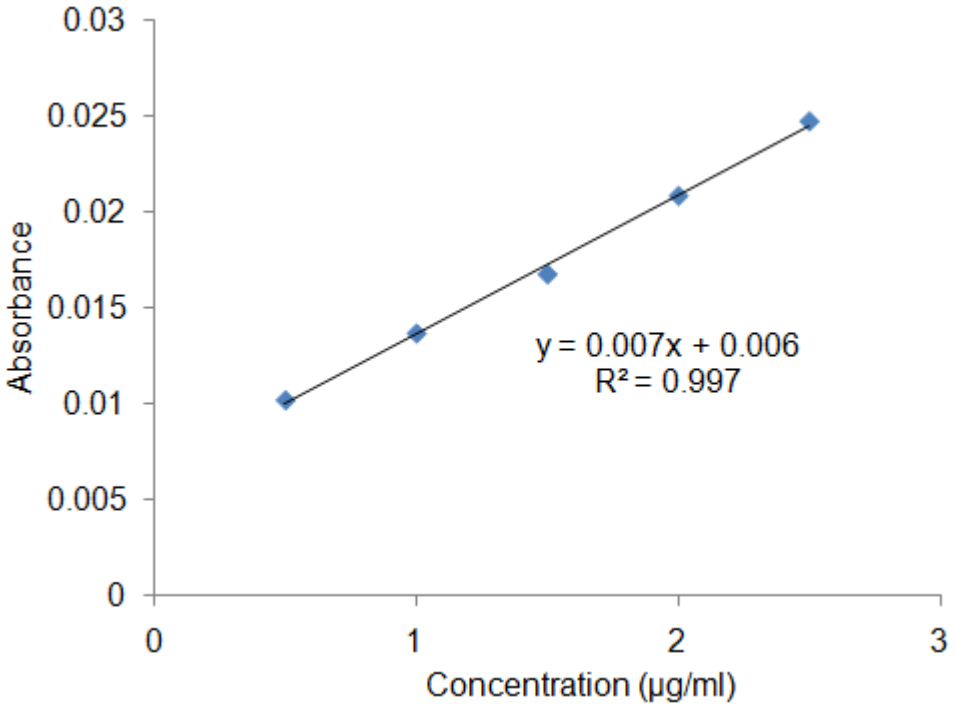

Figure 2A Standard calibration curve of standard Atropine

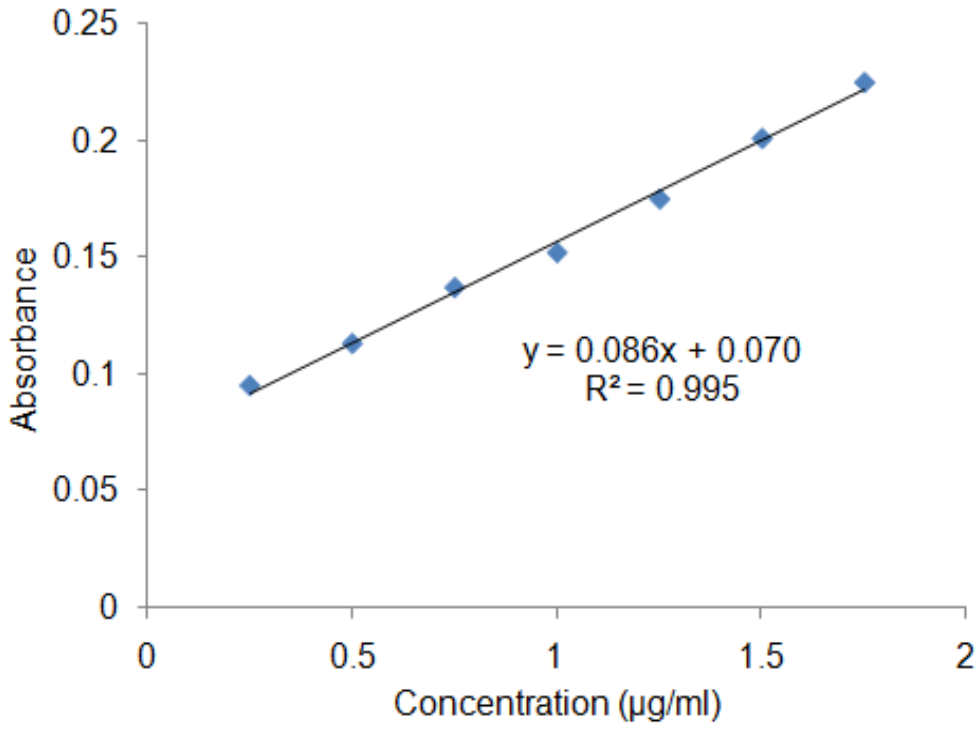

Figure 2B Standard calibration curve of standard Gallic acid

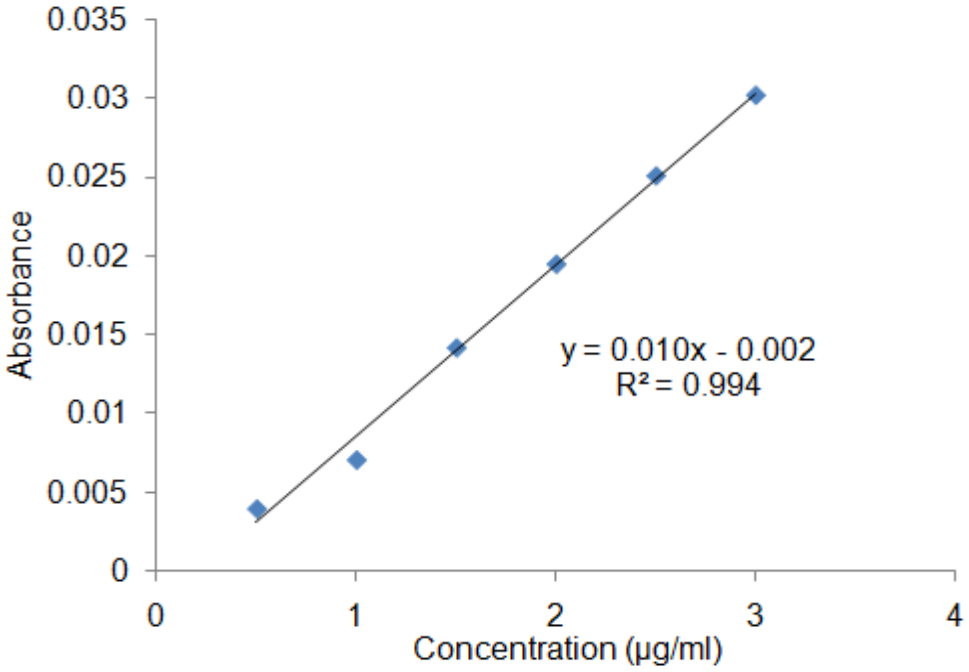

Figure 2C Standard calibration curve of standard Tannic acid

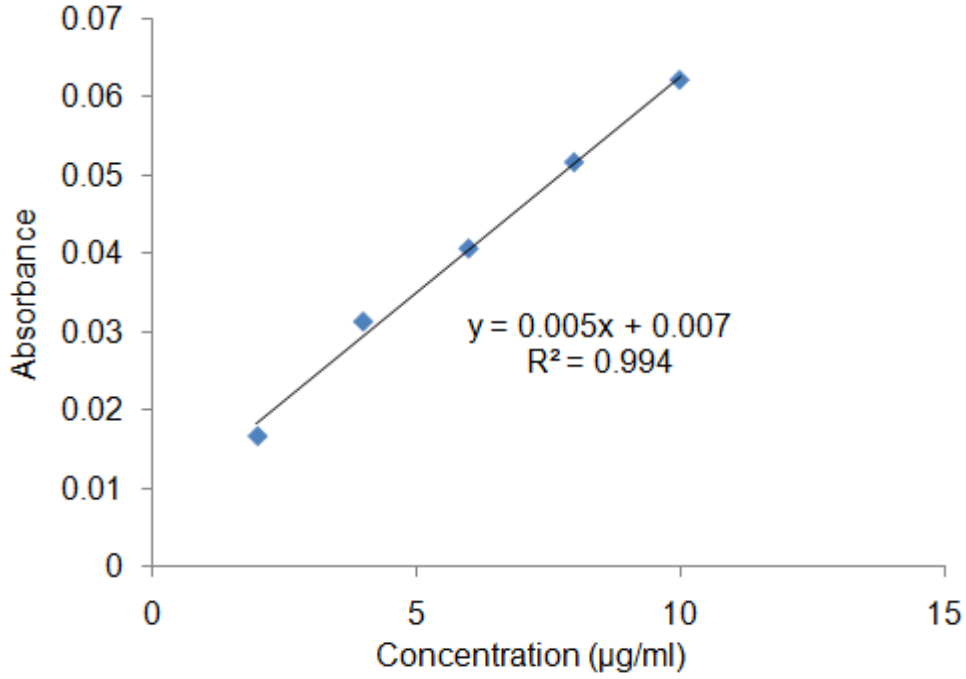

Figure 2D Standard calibration curve of standard Quercetin

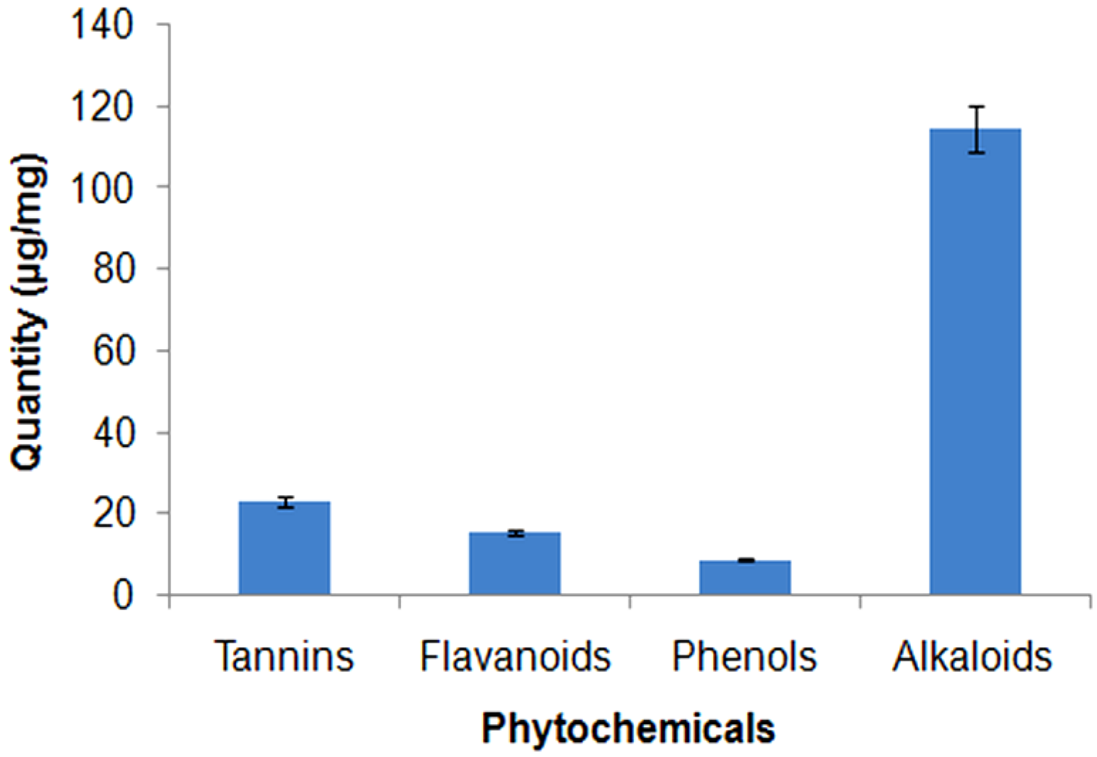

Figure 2E Quantitative phytochemical composition of *Berberis aristata*

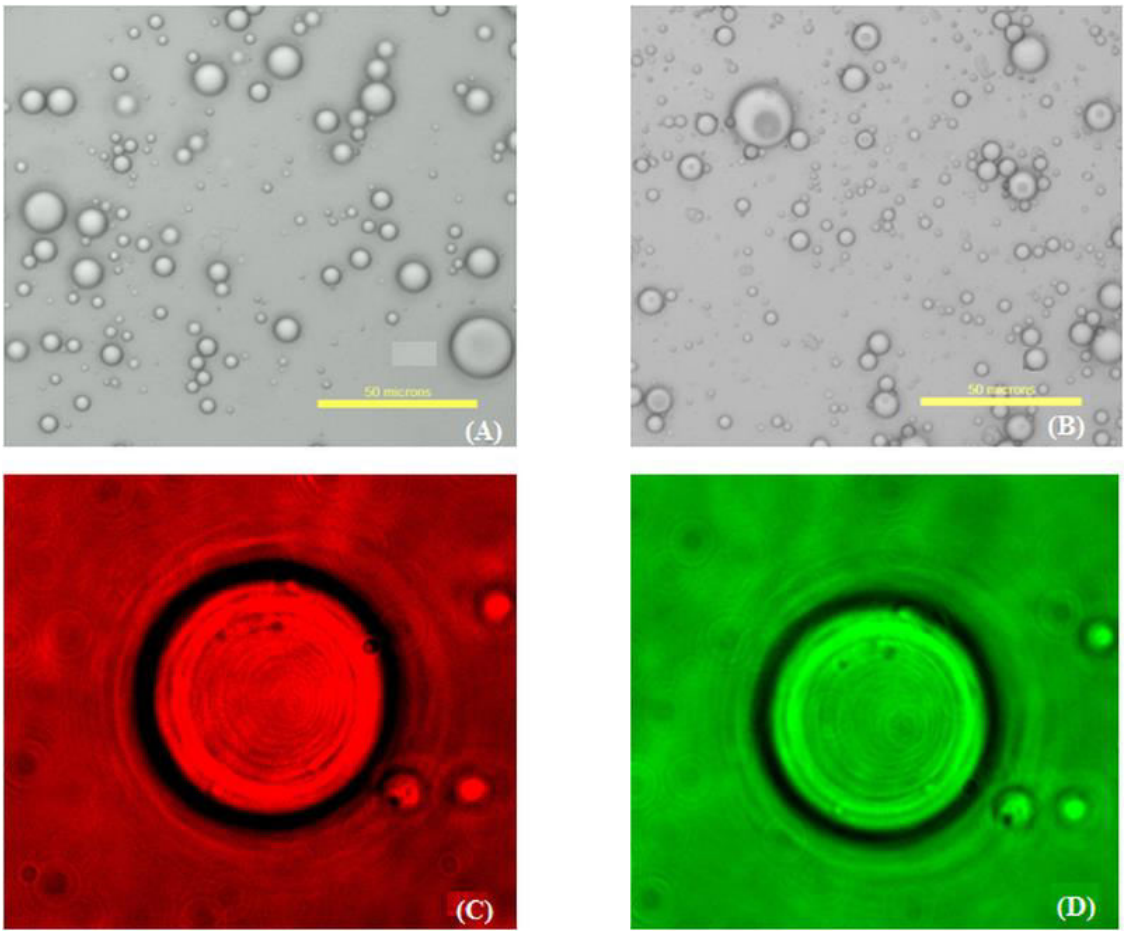

Figure 2F Phase contrast images showing particle shape of nanoformulations. (A) TWSNE, (B) PLSNE (Magnification 40 x); Fluorescent microscopic images (C) & (D) showed core-shell structure and drug distribution within the SNEDDS (Rhodamine B-Red and Calcein-Green)

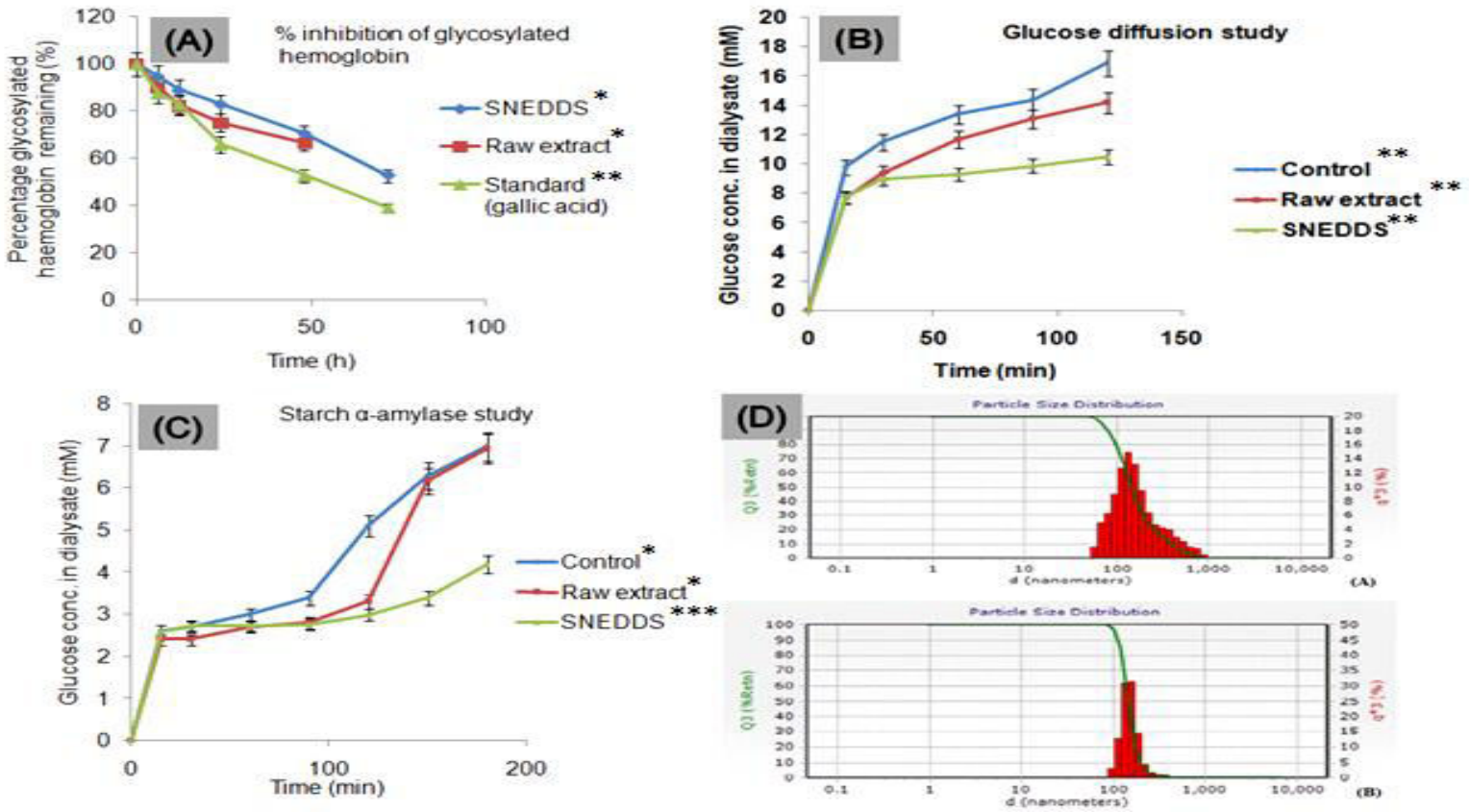

Figure 2G (A)Percentage inhibition of hemoglobin glycosylation (n=3; ±SD), (B) Effect of *B. aristata* extract on glucose diffusion across dialysis membrane (n=3; ±SD), (C) Effect of *B. aristata* extract on glucose diffusion in a starch-alpha amylase system (dual effect analysis) (n=3; ±SD) and (D) Particle size distribution for *B. aristata* loaded SNEDDS [using Tween 80 (A)], Particle size distribution for *B. aristata* loaded SNEDDS [using Pluronic F68 (B)]. The p values were obtained by one way ANOVA ($p \leq 0.05$). *Significant at $p<0.05$, ** significant at $p<0.01$, ***significant at $p<0.001$

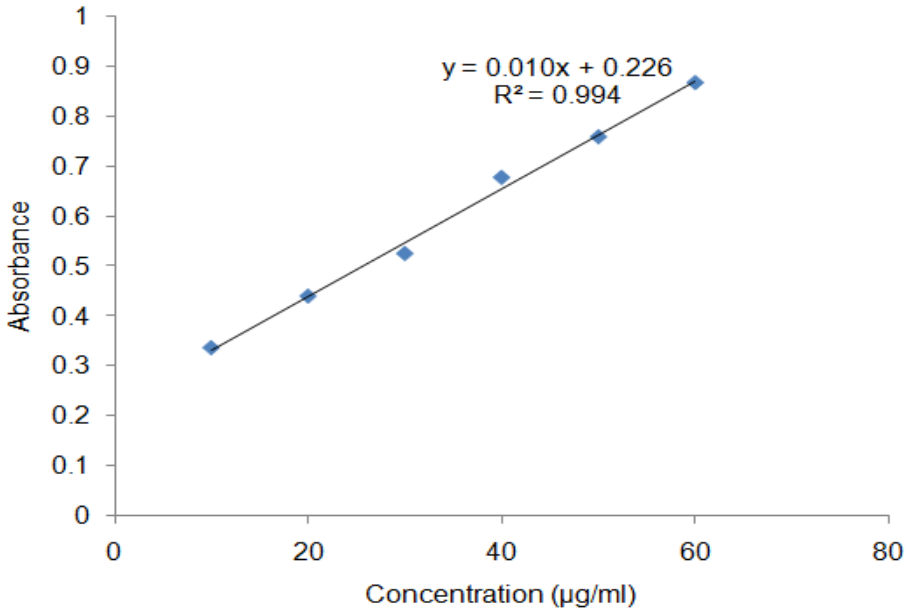

Figure 2H Standard calibration curve of *Ficus benghalensis* extract

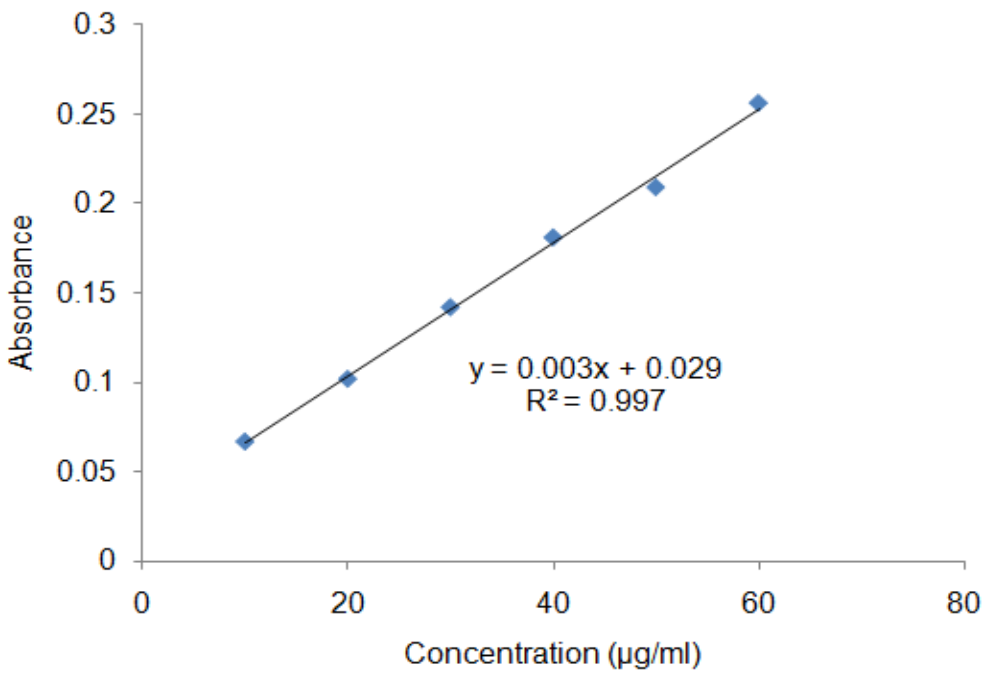

Figure 2I Standard calibration curve of standard silver

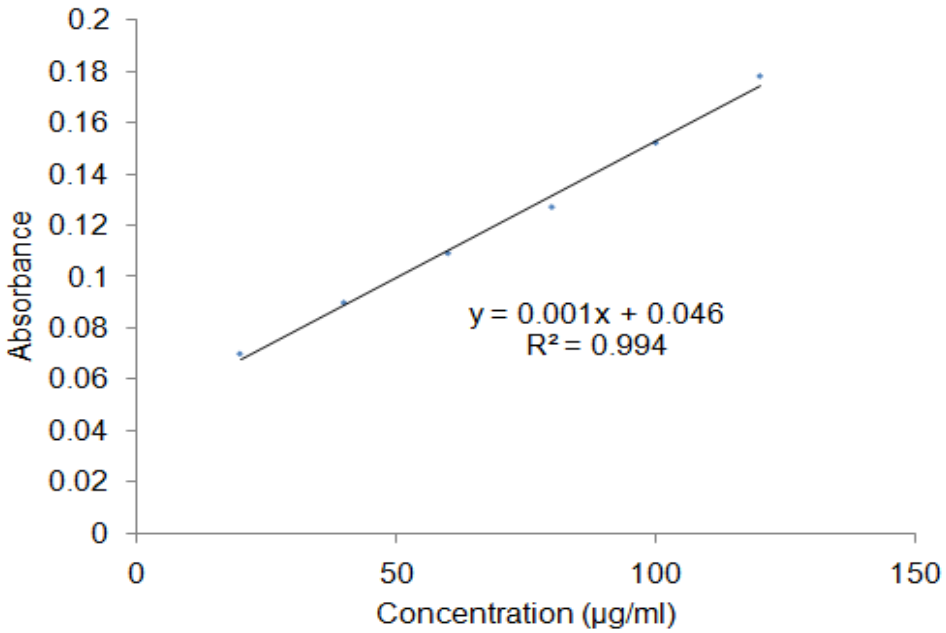

Figure 2J Standard curve of standard Bovine Serum Albumin (BSA)

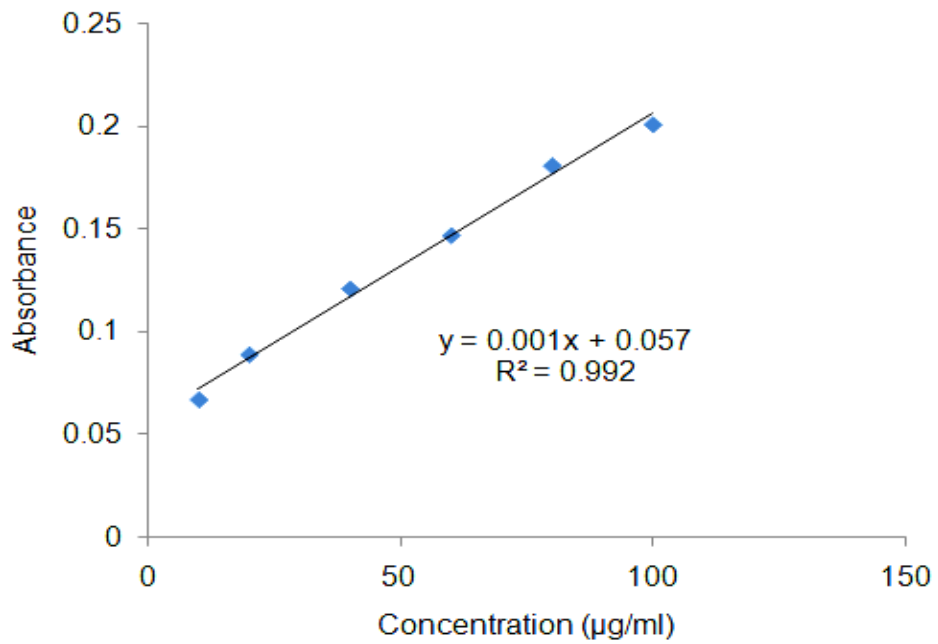

Figure 2K Standard curve of *Ocimum Sanctum* leaves extract

Figure 2L Tensile Test of PVA/CH hydrogels without silver nanoparticles (PVA; 33%)

Product	: Natural Polymer	**Load Range**	: 10 N
Batch	:	**Extension Range**	: 100 mm
Date	: 3/24/2015	**Test Speed**	: 20 mm/min
Operator	:	**Gauge Length**	: 25 mm
		Approach Speed	: 1.0 mm/min
		Preload	: 0.0 N

Specimen	Thick mm	Width mm	Tensile MPa	Max Force N	Elong at Max %	Stress at Break MPa
5	2.000	5.000	0.0362	0.3624	115.5	0.0291
		Mean	0.0362	0.3624	115.5	0.0291
		Std. Dev.	0	0	0	0
		Coe. Var.	0	0	0	0

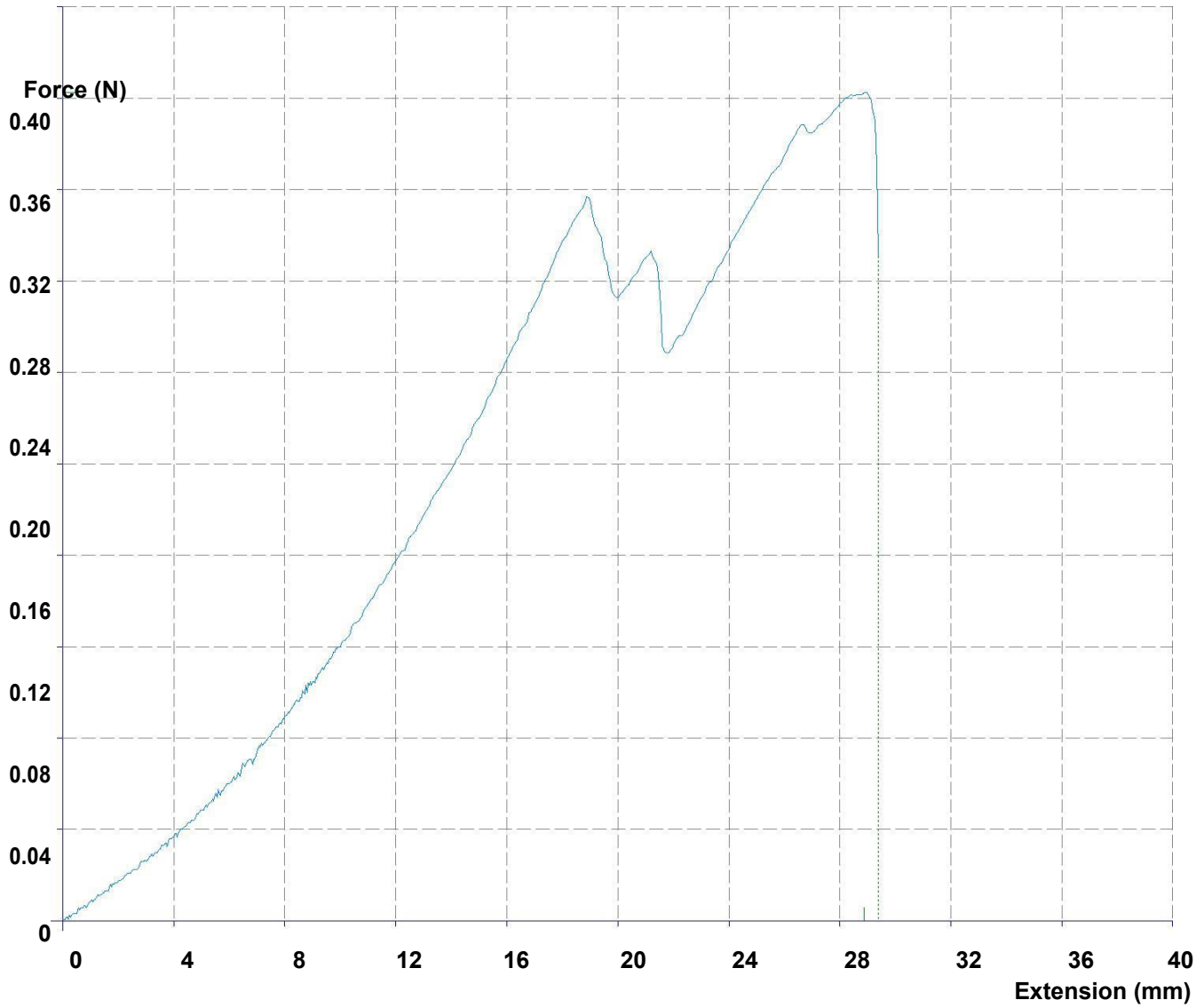

Figure 2M Tensile Test of PVA/CH hydrogels without silver nanoparticles (PVA; 50%)

Product	: Natural Polymer	**Load Range**	: 10 N
Batch	:	**Extension Range**	: 100 mm
Date	: 3/24/2015	**Test Speed**	: 20 mm/min
Operator	:	**Gauge Length**	: 25 mm
		Approach Speed	: 1.0 mm/min
		Preload	: 0.0 N

Specimen	Thick mm	Width mm	Tensile MPa	Max Force N	Elong at Max %	Stress at Break MPa
2	2.000	5.000	0.3992	3.992	147.0	0.3888
		Mean	0.3992	3.992	147.0	0.3888
		Std. Dev.	0	0	0	0
		Coe. Var.	0	0	0	0

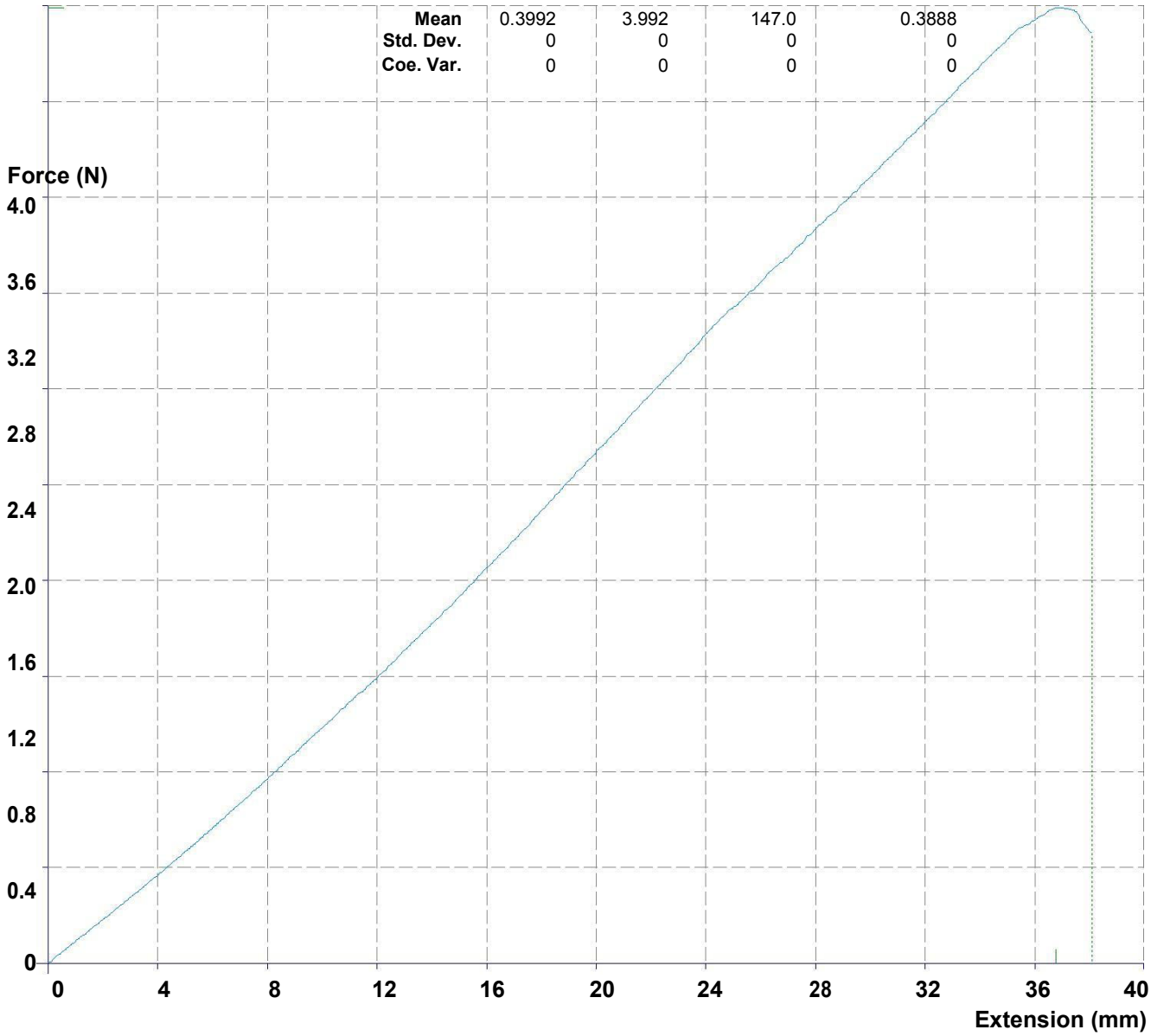

Figure 2N Tensile Test of PVA/CH hydrogels without silver nanoparticles (PVA; 67%)

Product	: Natural Polymer	**Load Range**	: 10 N
Batch	:	**Extension Range**	: 100 mm
Date	: 3/24/2015	**Test Speed**	: 20 mm/min
Operator	:	**Gauge Length**	: 25 mm
		Approach Speed	: 1.0 mm/min
		Preload	: 0.0 N

Specimen	Thick	Width	Tensile	Max Force	Elong at Max	Stress at Break
	mm	mm	MPa	N	%	MPa
1	2.000	5.000	0.3816	3.816	145.0	0.3816
Mean			0.3816	3.816	145.0	0.3816
Std. Dev.			0	0	0	0
Coe. Var.			0	0	0	0

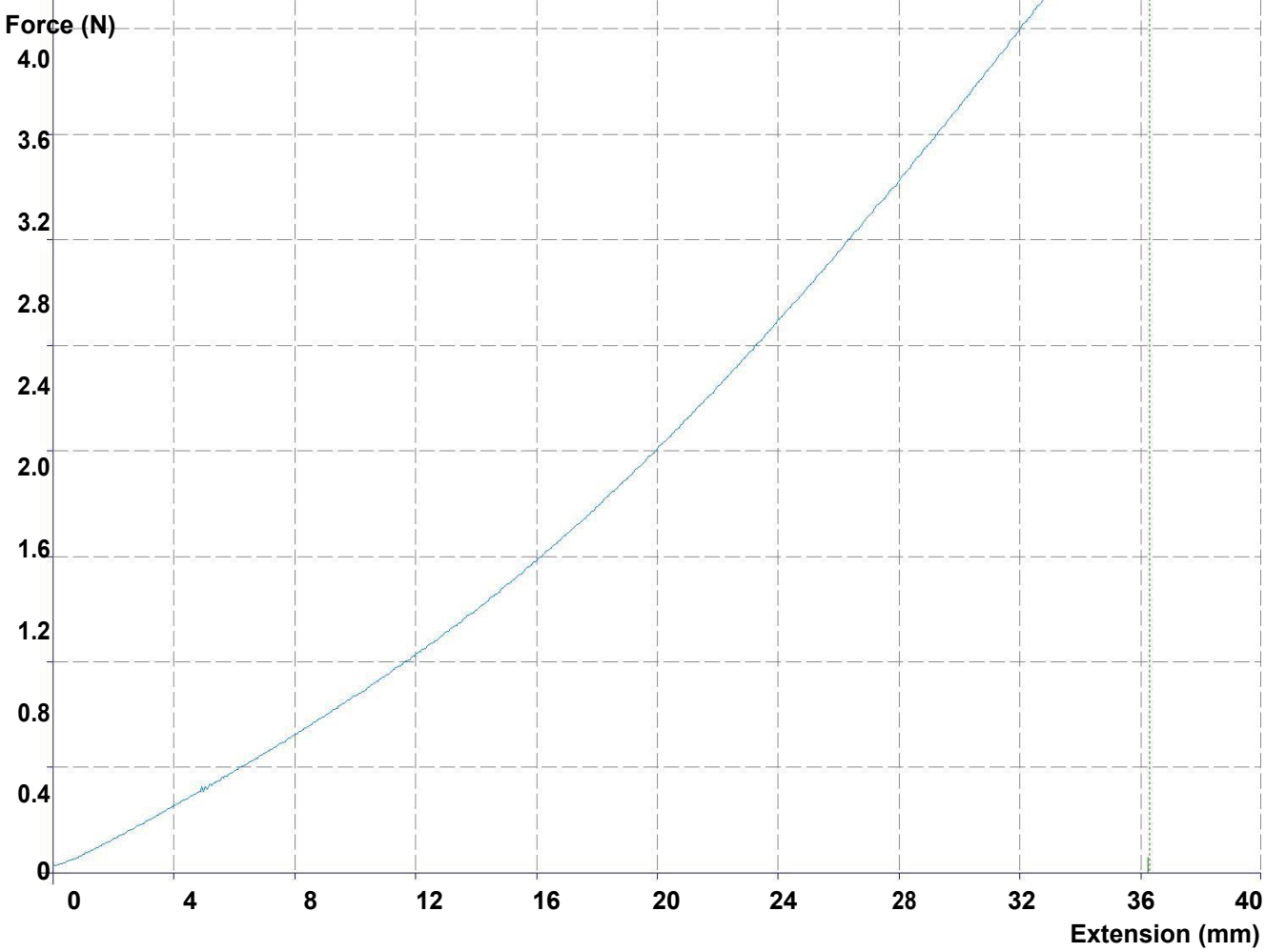

Figure 2O Tensile Test of PVA/CH hydrogels without silver nanoparticles (PVA; 75%)

Product	: Natural Polymer	**Load Range**	: 10 N
Batch	:	**Extension Range**	: 100 mm
Date	: 3/24/2015	**Test Speed**	: 20 mm/min
Operator	:	**Gauge Length**	: 25 mm
		Approach Speed	: 1.0 mm/min
		Preload	: 0.0 N

Specimen	Thick mm	Width mm	Tensile MPa	Max Force N	Elong at Max %	Stress at Break MPa
3	2.000	5.000	0.4390	4.390	210.0	0.4330
		Mean	0.4390	4.390	210.0	0.4330
		Std. Dev.	0	0	0	0
		Coe. Var.	0	0	0	0

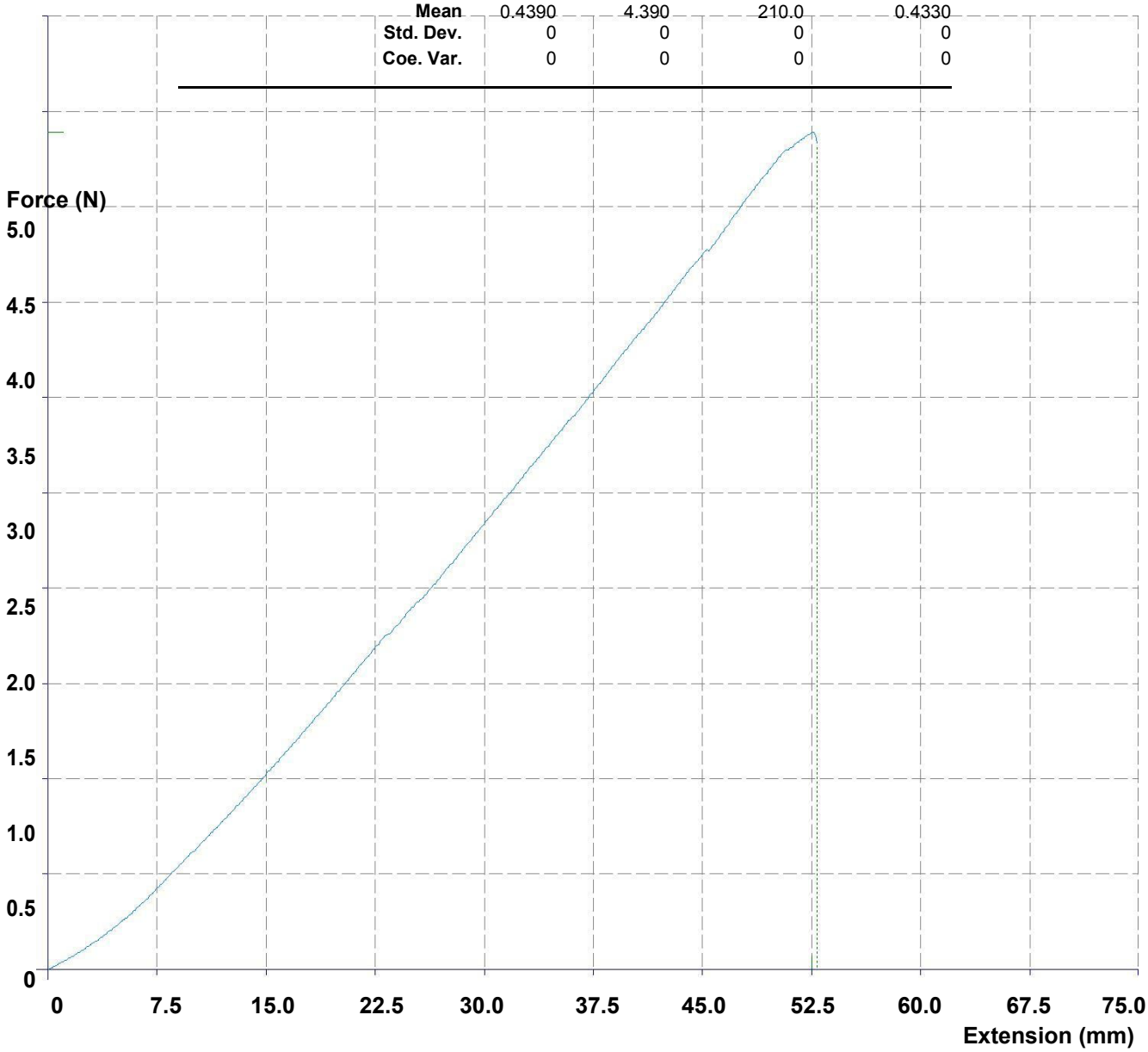

Figure 2P Tensile Test of PVA/CH hydrogels without silver nanoparticles (PVA; 80%)

Product	: Natural Polymer	**Load Range**	: 10 N
Batch	:	**Extension Range**	: 100 mm
Date	: 3/24/2015	**Test Speed**	: 20 mm/min
Operator	:	**Gauge Length**	: 25 mm
		Approach Speed	: 1.0 mm/min
		Preload	: 0.0 N

Specimen	Thick mm	Width mm	Tensile MPa	Max Force N	Elong at Max %	Stress at Break MPa
4	2.000	5.000	0.540	5.40	283.8	0.3893
		Mean	0.540	5.40	283.8	0.3893
		Std. Dev.	0	0	0	0
		Coe. Var.	0	0	0	0

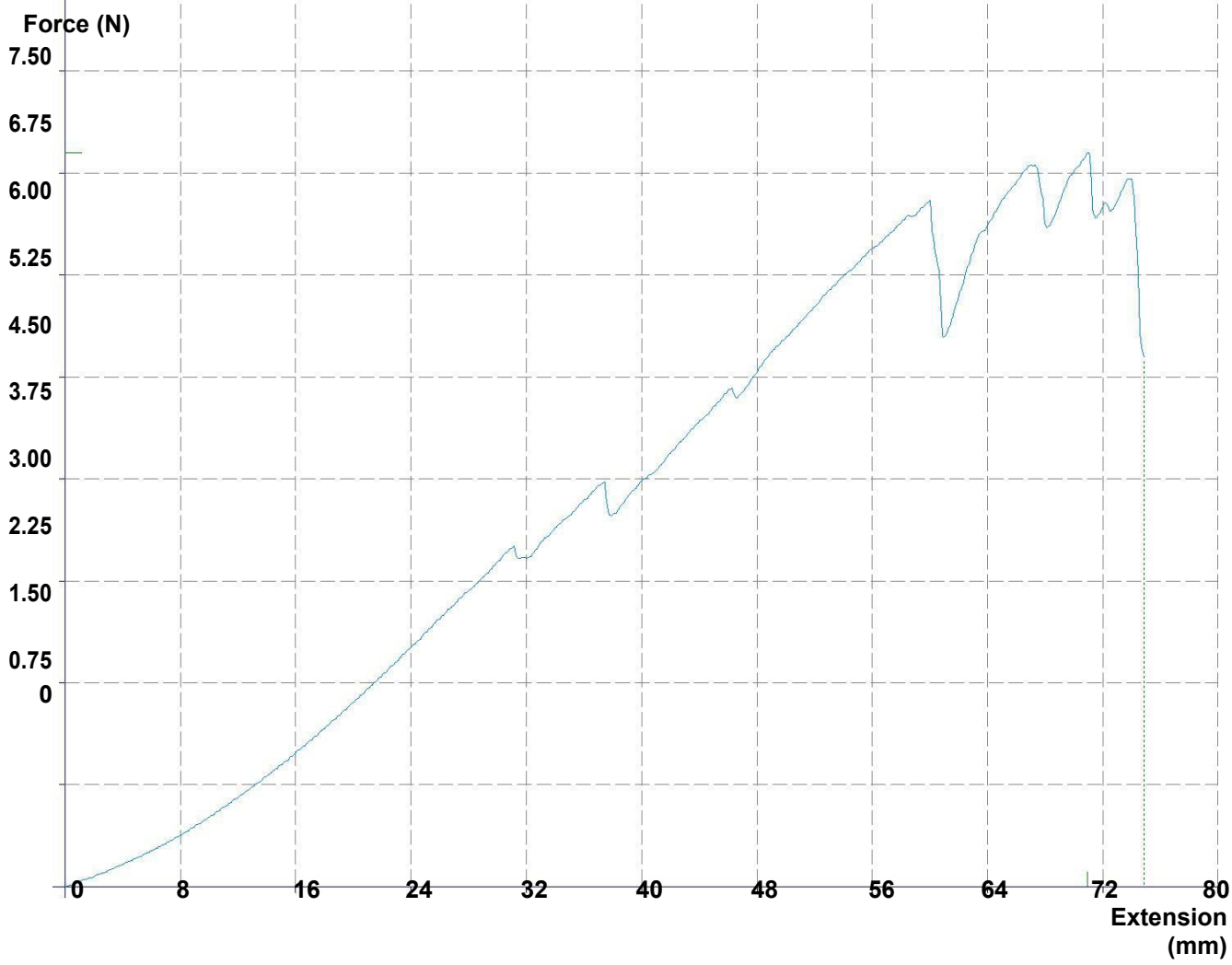

Figure 2Q Tensile Test of PVA/CH hydrogels without silver nanoparticles (PVA; 100%)

Product	: Natural Polymer	**Load Range**	: 10 N
Batch	:	**Extension Range**	: 100 mm
Date	: 3/24/2015	**Test Speed**	: 20 mm/min
Operator	:	**Gauge Length**	: 25 mm
		Approach Speed	: 1.0 mm/min
		Preload	: 0.0 N

Specimen	Thick mm	Width mm	Tensile MPa	Max Force N	Elong at Max %	Stress at Break MPa
A	2.000	5.000	1.457	14.56	329.2	1.194
		Mean	1.457	14.57	329.2	1.194
		Std. Dev.	0	0	0	0
		Coe. Var.	0	0	0	0

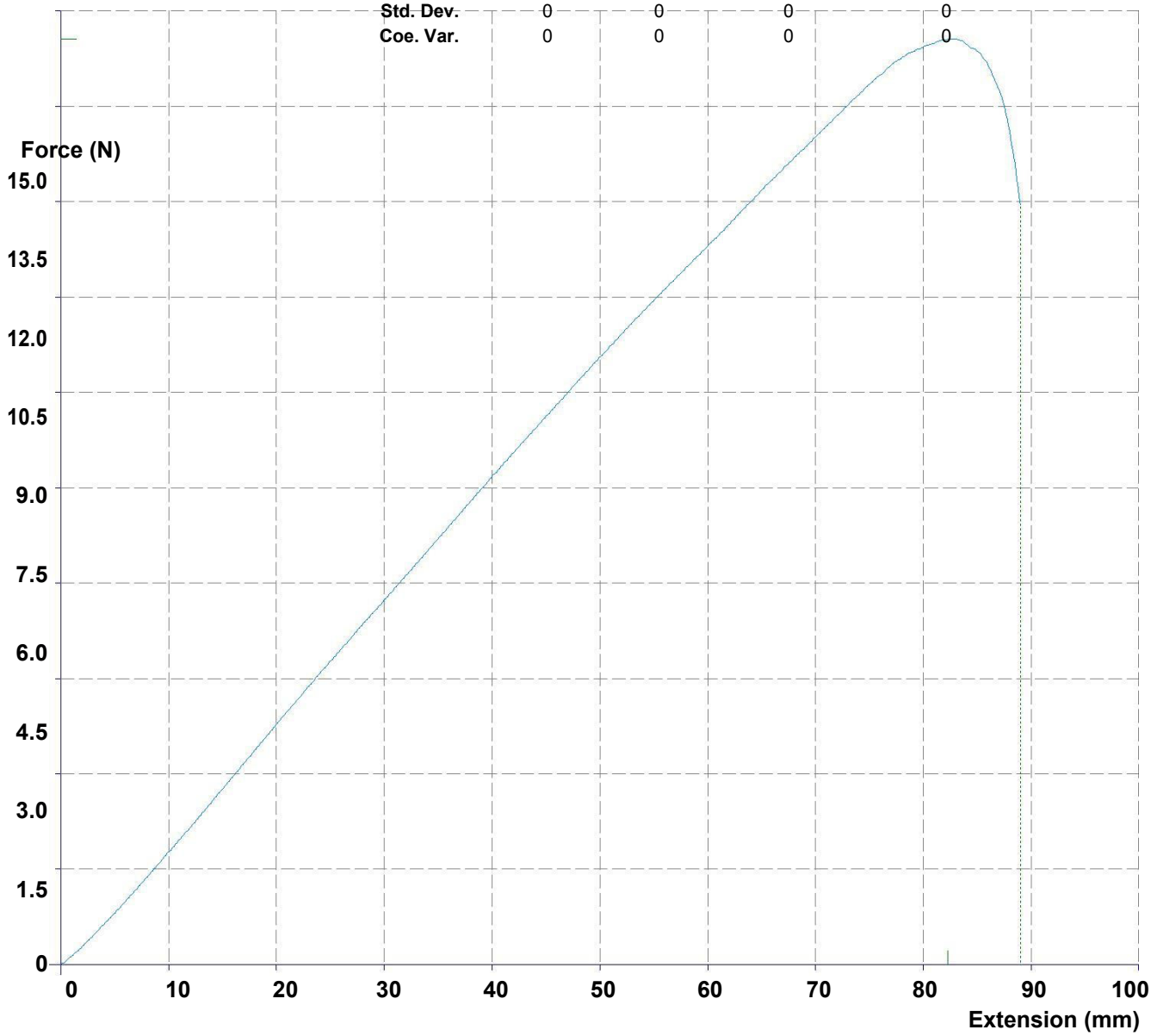

Figure 2R Tensile Test of PVA/CH/AgNPs hydrogels containing silver nanoparticles (PVA; 33%)

Product	: Natural Polymer	**Load Range**	: 10 N
Batch	:	**Extension Range**	: 100 mm
Date	: 3/24/2015	**Test Speed**	: 20 mm/min
Operator	:	**Gauge Length**	: 25 mm
		Approach Speed	: 1.0 mm/min
		Preload	: 0.0 N

Specimen	Thick mm	Width mm	Tensile MPa	Max Force N	Elong at Max %	Stress at Break MPa
5A	2.000	5.000	0.0496	0.4965	172.4	0.0006
		Mean	0.0497	0.4965	172.4	0.0006
		Std. Dev.	0	0	0	0
		Coe. Var.	0	0	0	0

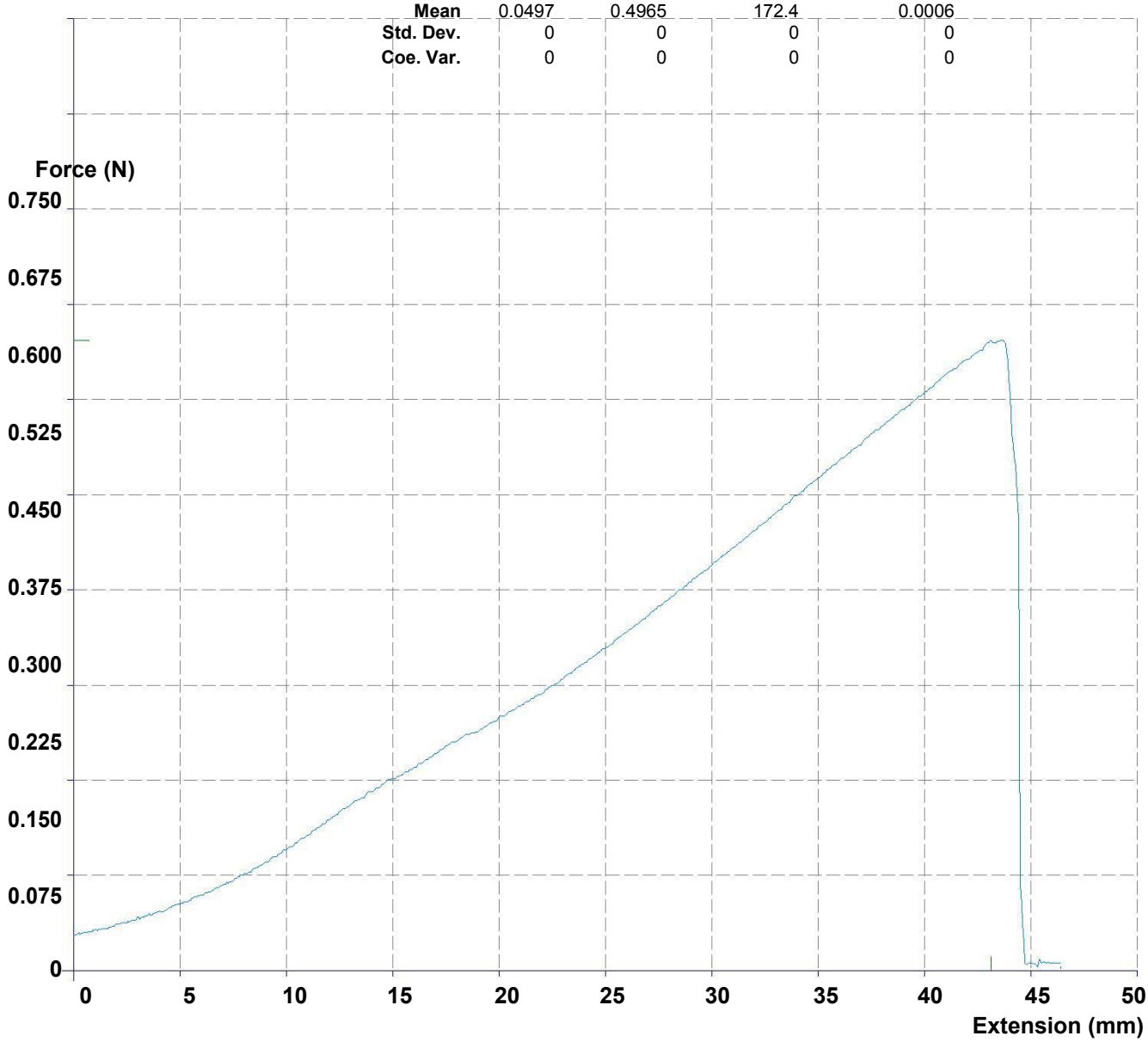

Figure 2S Tensile Test of PVA/CH/AgNPs hydrogels containing silver nanoparticles (PVA; 75%)

Product	: Natural Polymer	**Load Range**	: 10 N
Batch	:	**Extension Range**	: 100 mm
Date	: 3/24/2015	**Test Speed**	: 20 mm/min
Operator	:	**Gauge Length**	: 25 mm
		Approach Speed	: 1.0 mm/min
		Preload	: 0.0 N

Specimen	Thick mm	Width mm	Tensile MPa	Max Force N	Elong at Max %	Stress at Break MPa
3A	2.000	5.000	0.4455	4.455	218.1	0.4300
		Mean	0.4455	4.455	218.1	0.4300
		Std. Dev.	0	0	0	0
		Coe. Var.	0	0	0	0

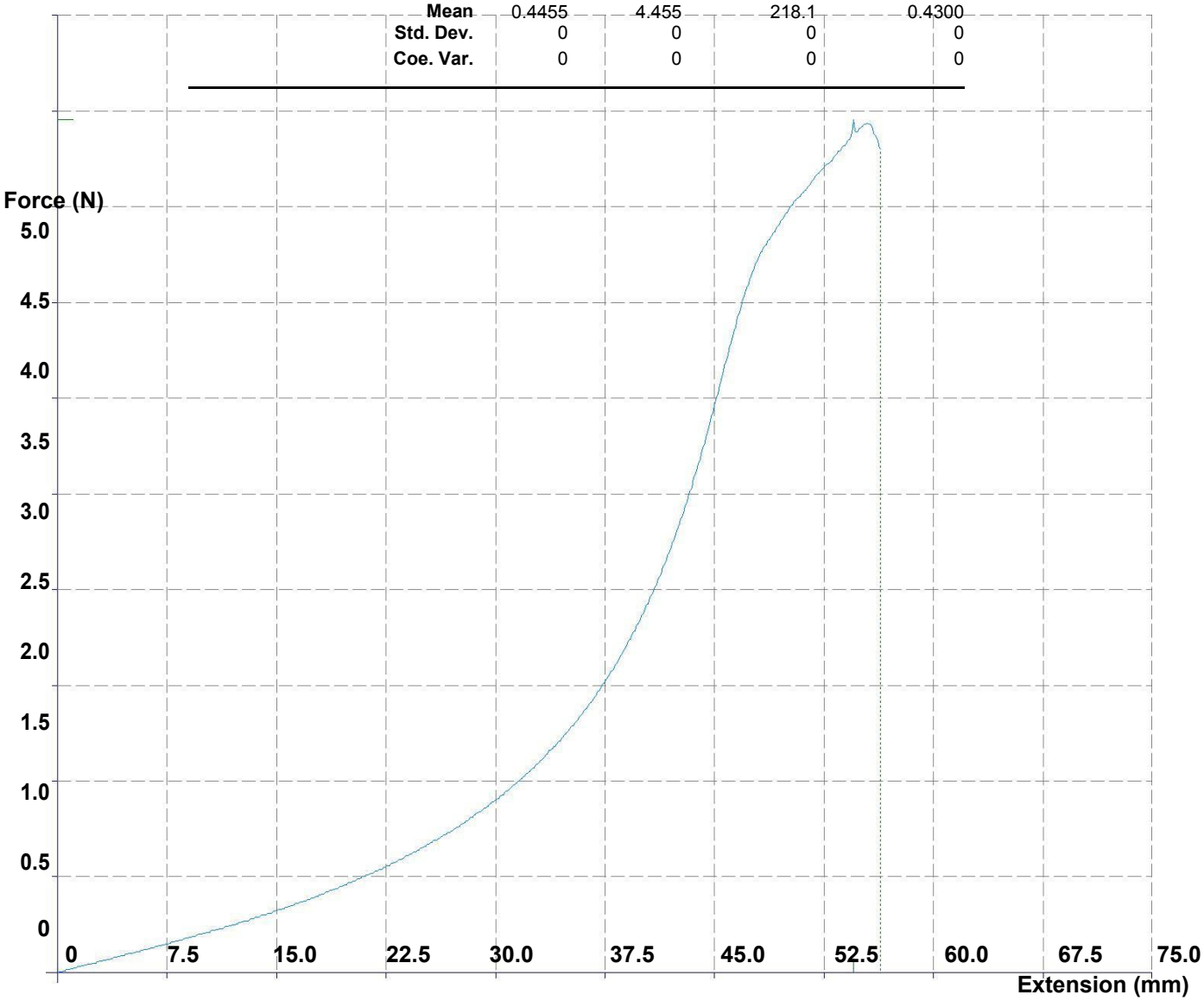

Figure 2T. Tensile Test of PVA/CH/AgNPs hydrogels containing silver nanoparticles (PVA; 80%)

Product	: ABC	**Load Range**	: 12 N
Batch	:	**Extension Range**	: 90 mm
Date	: 3/23/2015	**Test Speed**	: 20 mm/min
Operator	:	**Gauge Length**	: 25 mm
		Approach Speed	: 10 mm/min
		Preload	: 0.0 N

Specimen	Thick mm	Width mm	Tensile MPa	Max Force N	Elong at Max %	Stress at Break MPa
4A	2.000	5.000	0.775	7.75	279.3	0.774
		Mean	0.775	7.75	279.3	0.774
		Std. Dev.	0	0	0	0
		Coe. Var.	0	0	0	0

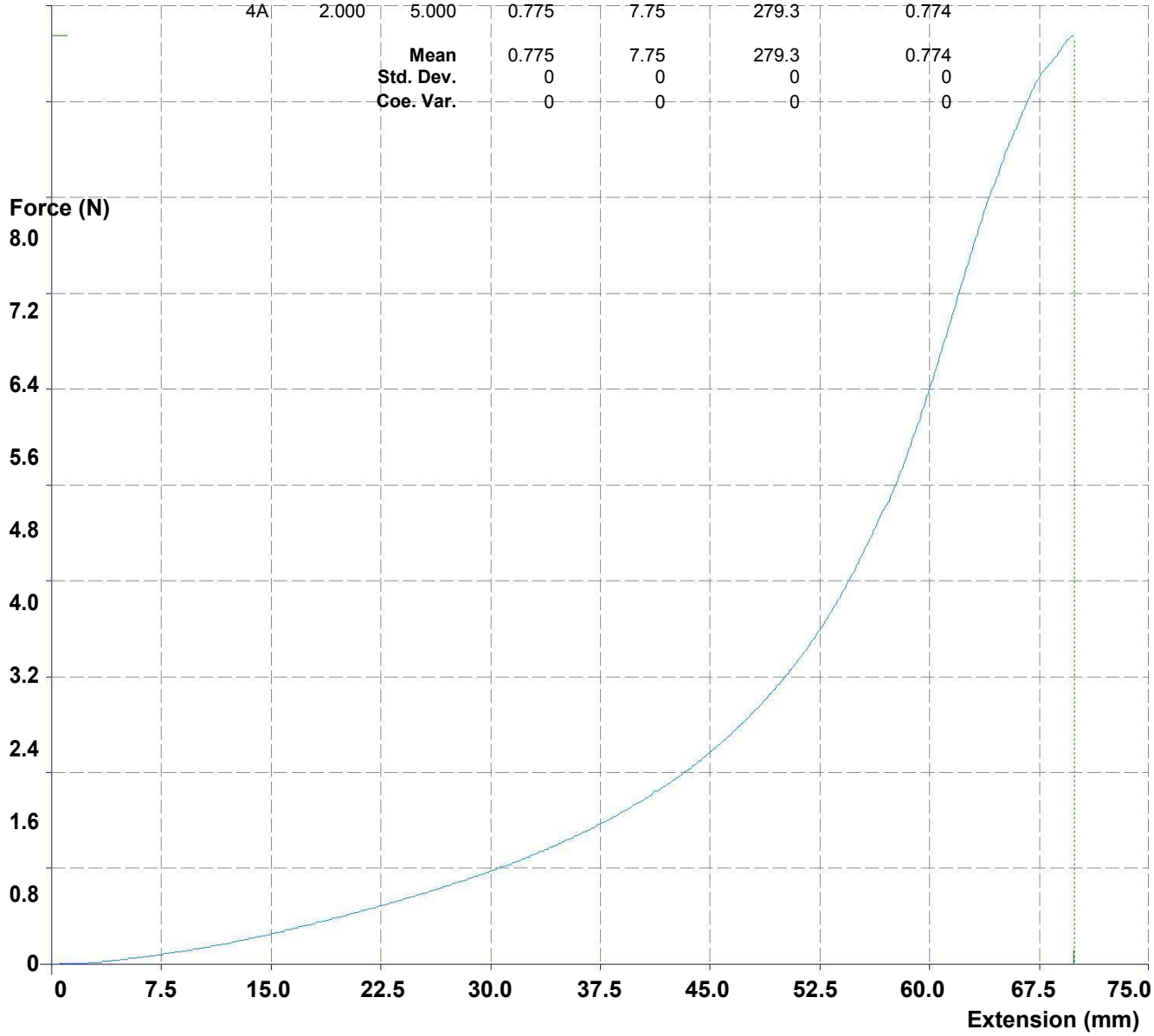

Figure 2U. Tensile Test of PVA/CH/AgNPs hydrogels containing silver nanoparticles (PVA; 100%)

Product	: Natural Polymer	**Stress Range**	: 10 MPa
Batch	: A	**Strain Range**	: 200 %
Date	: 6/11/2015	**Test Speed**	: 20 mm/min
Operator	:	**Gauge Length**	: 50 mm
		Approach Speed	: 50 mm/min
		Preload	: 0.0 N

Specimen	Thick mm	Width mm	Tensile MPa	Max Force N	Elong at Max %	Stress at Break MPa
A2	2.000	10.00	0.558	11.15	96.6	0.0063
		Mean	0.558	11.15	96.6	0.0063
		Std. Dev.	0	0	0	0
		Coe. Var.	0	0	0	0

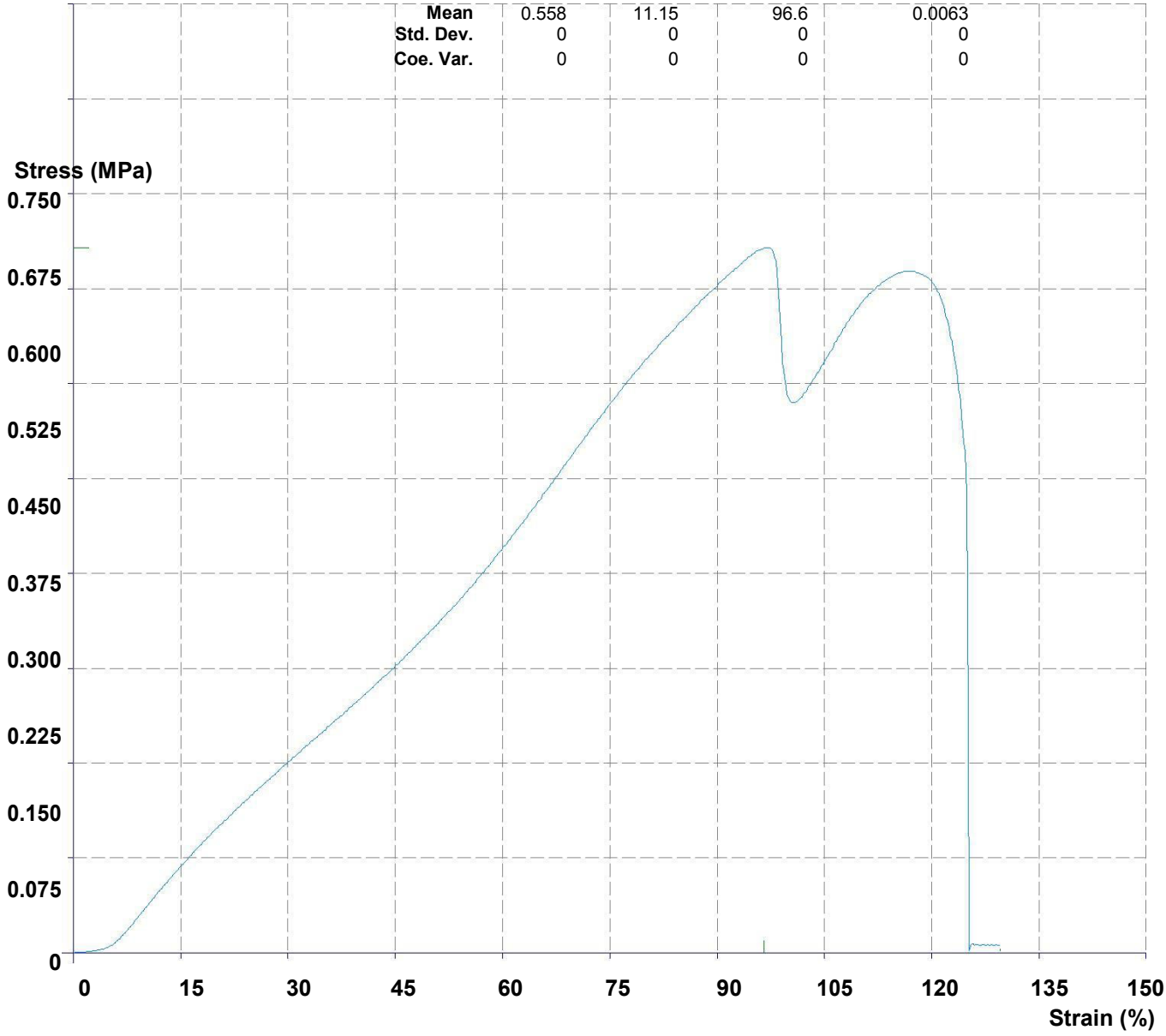

Table 2A Effect of extract on diffusion of glucose (n=3, ±SD)

Glucose in dialysate (mM)							
Time	15	30	60	90	120	150	200
Control	9.8±0.05	11.5±0.15	13.4±0.2	14.4±0.15	16.9±0.15	17.5±0.36	18.3±0.30
Raw extract	7.7±0.2	9.4±0.2	11.7±0.15	13.1±0.1	14.2±0.15	14.7±0.41	16±0.55
SNEDDS	7.76±0.11	8.97±0.05	9.3±0.15	9.9±0.15	10.5±0.15	11.16±0.20	12.03±0.37

Table 2B Effect of extract on diffusion of glucose across the dialysis membrane (n=3, ±SD)

Glucose concentration (mM/L)	**6 h**		**12 h**		**24 h**	
	100 mM	32 mM	100mM	32 mM	100 mM	32 mM
Control	18.3±0.45	11.8±0.45	23.53±0.59	14.85±0.41	23.99±0.28	16.26±0.30
Raw extract	10.23±0.15	5.36±0.15	23.1±0.69	14.97±0.15	23.33±0.20	15.9±0.05
SNEDDS	9.8±0.25	4.5±0.25	16.47±0.41	11.4±0.2	20.71±0.13	13.89±0.13

Table 2C Effect of extract on diffusion of glucose in a starch α-amylase system (n=3, ±SD)

	Glucose in dialysate (mM)						
Time	15	30	60	90	120	150	200
Control	2.6±0.2	2.7±0.15	3±0.15	3.4±0.1	5.1±0.45	6.29±0.25	6.98±0.06
Raw extract	2.4±0.05	2.4±0.1	2.7±0.15	2.8±0.11	3.3±0.1	6.1±0.20	6.9±0.15
SNEDDS	2.6±0.05	2.73±0.15	2.73±0.15	2.76±0.15	3±0.15	3.4±0.15	4.2±0.1

REFERENCES

[1] E. Roger, F. Lagarce, and J. P. Benoit, "Development and characterization of a novel lipid nanocapsule formulation of Sn38 for oral administration," *European Journal of Pharmaceutics and Biopharmaceutics,* 79, pp.181–188, 2011.

[2] P. Sunil, O. Maru, and M. Chan, "Novel lipid-based formulations enhancing the in-vitro dissolution and permeability characteristics of a poorly water-soluble model drug, piroxicam," *International Journal of Pharmaceutics*, 301, pp. 209–216, 2005.

[3] G. L. Amidon, H. Lennernas, V. P. Shah, and J. R. Crison, "A theoretical basis for a biopharmaceutic drug classification: the correlation in vitro drug product dissolution and in-vivo bioavailability," *Pharmaceutical Research,* 12, pp. 413–420, 1995.

[4] C. J. Porter, and W. N. Charman, "*In-vitro* assessment of oral lipid based formulations," *Advanced Drug Delivery Review,* 50, pp. 127–147, 2001

[5] B. J. Aungst, "Novel formulation strategies for improving oral bioavail-ability of drugs with poor membrane permeation or pre-systemic metabolism," *Journal of Pharmaceutical Sciences,* 82, pp. 979–987, 1993.

[6] C. W. Pouton, "Formulation of poorly water-soluble drugs for oral administration: physicochemical and physiological issues and the lipid formulation classification system," *European Journal of Pharmaceutical Sciences,* 29, pp. 278–287, 2006.

[7] V. Jannin, J. Musakhanian, and D. Marchaud, "Approaches for the development of solid and semi-solid lipid-based formulations," *Advanced Drug Delivery Reviews,* 60, pp. 734–746, 2008.

[8] C. W. Pouton, "Lipid formulations for oral administration of drugs: nonemulsifying, self-emulsifying and 'self-microemulsifying' drug delivery systems," *European Journal of Pharmaceutical Sciences,* 11, pp. S93–98, 2000.

[9] D. J. Hauss, S. E. Fogal, J. V. Ficorilli, C. A. Price, T. Roy, A. A. Jayaraj, and J. J. Keirns, "Lipid-based delivery systems for improving the bioavailability and lymphatic transport of a poorly water-soluble LTB4 inhibitor," *Journal of Pharmaceutical Sciences,* 87, pp. 1998; 87: 164–169.

[10] A. Dahan, and A. Hoffman, "Rationalizing the selection of oral lipid based drug delivery systems by an in-vitro dynamic lipolysis model for improved oral bioavailability of poorly water soluble drugs," *Journal of Controlled Release,* 129, pp. 1–10, 2008.

[11] L. Gibson, “Lipid-based excipients for oral drug delivery,” In: D. J. Hauss, Eds. “Oral lipid-based formulations: enhancing the bioavailability of poorly water soluble drugs,” New York: Informa Healthcare, 2007, pp. 33–61.

[12] H. Shrestha, R. Bala, and S. Arora, “Lipid-Based Drug Delivery Systems,” *Journal of Pharmaceutics*, 1-10, 2014.

[13] P. Shah, D. Bhalodia, and P. Shelat, “Nanoemulsion: A Pharmaceutical Review,” *Systematic Reviews in Pharmacy*, 1, pp. 24-32, 2010.

[14] S. Kotta, A. W. Khan, K. Pramod, S. H. Ansari, R. K. Sharma, and J. Ali, “Exploring oral nanoemulsions for bioavailability enhancement of poorly water-soluble drugs,” *Expert Opinion in Drug Delivery*, 9, pp. 585-598, 2012.

[15] R. P. Dixit, and M. S. Nagarsenker, “Self-nanoemulsifying granules of ezetimibe: design, optimization and evaluation,” *European Journal of Pharmaceutical Sciences*, 35, pp. 3183-3192, 2008.

[16] S. Shafiq, F. Shakeel, and S. Talegaonkar, “Development and bioavailability assessment of ramipril nanoemulsion formulation,” *European Journal of Pharmaceutics and Biopharmaceutics*, 66, pp. 2227-2243, 2007.

[17] A. G. Gaonkar, “Stable multiple emulsions comprising interfacial gelatinous layer, flavor-encapsulating multiple emulsions and low/no-fat food products comprising the same,” US Patent 5, 332, 595.

[18] P. Walstra, “Disperse system: basic considerations,” In: O. H. Fennema, editor. Food Chemistry. 3rd ed., New York: CRC Press, 1996**,** pp. 95-155.

[19] R. Chanamai, and D. J. McClements, “Impact of weighting agents and sucrose on gravitational separation of beverage emulsions,” *Journal of Agricultural and Food Chemistry,* 48, pp. 5561-5565, 2000.

[20] C. T. Tan, “Beverage flavor emulsion-A form of emulsion liquid membrane microencapsulation,” *Developments in Food Science,* 40, pp. 29-42, 1998.

[21] T. Schmidts, D. Dobler, C. Nissing, and F. Runkel, “Influence of hydrophilic surfactants on the properties of multiple W/O/W emulsions,” *Journal of Colloid and Interface Science,* 338, pp. 184-192, 2009.

[22] J. Su, J. Flanagan, and H. Singh, “Improving encapsulation efficiency and stability of water-in-oil-in-water emulsions using a modified gum Arabic (Acacia (sen) SUPER GUMTM),” *Food Hydrocolloids,* 22, pp. 112-120, 2008.

[23] F. Michaut, P. Perrin, and P. Hebraud, "Interface composition of multiple emulsions: rheology as a probe," *Langmuir,* 20, pp. 8576-8581, 2004.

[24] E. Dickinson, "Double emulsions stabilized by food biopolymers," *Food Biophysics*, 6, pp. 1-11, 2011.

[25] A. A. Date, and M. S. Nagarsenker, "Design and evaluation of self-nanoemulsifying drug delivery systems (SNEDDS) for cefpodoxime proxetil," *International journal of Pharmaceutics,* 329, pp. 166–172, 2007.

[26] C. Pouton, "Formulation of self-emulsifying drug delivery systems," *Advanced Drug Delivery Reviews,* 25, pp. 47-58, 1997.

[27] N. Anton, J. P. Benoit, and P. Saulnier, "Design and production of nanoparticles formulated from nano-emulsion templates – a review," *Journal of Controlled Release,* 128, pp. 185–199, 2008.

[28] K. Bouchemal, S. Briançon, E. Perrier, and H. Fessi, "Nanoemulsion formulation using spontaneous emulsification: solvent, oil and surfactant optimization," *International Journal of Pharmaceutics*, 280, pp. 241–251, 2004.

[29] N. Anton, and T. F. Vandamme, "The universality of low-energy nano-emulsification," *International Journal of Pharmaceutics,* 377, pp. 142–147, 2009.

[30] N. Sadurni, C. Solans, N. Azemar, and M. J. Garcia‐Celma, "Studies on the formation of O/W nano-emulsions, by low-energy emulsification methods, suitable for pharmaceutical applications," *European Journal of Pharmaceutical Sciences,* 26, pp. 438–445, 2005.

[31] C. W. Pouton, and C. J Porter, "Formulation of lipid-based delivery systems for oral administration: materials, methods and strategies," *Advanced Drug Delivery Reviews,* 60, pp. 625–637, 2008.

[32] C. J. Porter, A. M. Kaukonen, B. J. Boyd, G. A. Edwards, and W. N. Charman, "Susceptibility to lipase-mediated digestion reduces the oral bioavailability of danazol after administration as a medium-chain lipid-based microemulsion formulation," *Pharmaceutical Research,* 21, pp. 1405–1412, 2004.

[33] P. Lundin, M. Bojrup, H. Ljusberg-Wahren, B. Westro, and S. Lundin, "Enhancing effects of monohexanoin and two other medium-chain glyceride vehicles on intestinal absorption of desmopressin (dDAVP)," *Journal of Pharmacology and Experimental Therapeutics,* 282, pp. 585–590, 1997.

[34] A. A. Date, N. Desai, R. Dixit, and M. Nagarsenker, "Self-nanoemulsifying drug delivery systems:formulation insights, applications and advances," *Nanomedicine,* 5, pp. 1595–1616, 2010.

[35] E. B. Basalious, N. Shawky, and S. M. Badr-Eldin, "SNEDDS containing bioenhancers for improvement of dissolution and oral absorption of lacidipine. I: development and optimization," *International Journal of Pharmaceutics*, 391, pp. 203–211, 2010.

[36] R. J. Mountfield, S. Senepin, M. Schleimer, I. Walter, and B. Bittner, "Potential inhibitory effects of formulation ingredients on intestinal cytochrome P450," *International Journal of Pharmaceutics*, 211, pp. 89–92, 2000.

[37] E. D. Hugger, B. L. Novak, P. S. Burton, K. L Audus, and R. T. Borchardt, "A comparison of commonly used Polyethoxylated pharmaceutical excipients on their ability to inhibit p-glycoprotein activity *in-vitro*," *Journal of Pharmaceutical Sci*ences, 91, pp. 1991–2002, 2002.

[38] A. J. Tije, J. Verweij, W. J. Loos, and A. Sparreboom, "Pharmacological effects of formulation vehicles implications for cancer chemotherapy," *Clinical Pharmacokinetics,* 42, pp. 665–685, 2003.

[39] C. W. Pouton, "Properties and Uses of Common Formulation Lipids, Surfactants and Cosolvents, AAPS Workshop, March 2007.

[40] P. Constantinides, "Lipid microemulsions for improving drug dissolution and oral absorption: physical and biopharmaceutical aspects," *Pharmaceutical Research,* 12, pp. 1561-1572, 1995.

[41] S. Tenjarla, "Microemulsions: an overview and pharmaceutical applications," *Critical Reviews in Therapeutic Drug Carrier Systems,* 16, pp. 461-521, 1999.

[42] M. Fanun, "Colloids in Drug Delivery," CRC Press, 2010.

[43] R. N. Gursoy, and S. Benita, "Self-emulsifying drug delivery systems (SEDDS) for improved oral delivery of lipophilic drugs," *Biomedicine & Pharmacotherapy*, 58, pp. 173-182, 2004.

[44] R. G. Strickley, "Solubilizing excipients in oral and injectable formulations," *Pharmaceutical Research,* 21, pp. 201–230, 2004.

[45] A. A. Date, and M. S. Nagarsenker, "Parenteral microemulsions: an overview," *International Journal of Pharmaceutics,* 355, pp. 19–30, 2008.

[46] P. R. Nepal, H. K. Han, and H. K. Choi, "Preparation and *in vitro-in vivo* evaluation of Witepsol H35 based self-nanoemulsifying drug delivery systems

(SNEDDS) of coenzyme Q(10)," *European Journal of Pharmaceutical Sciences,* 39, pp. 224–232, 2010.

[47] F. S. Nielsen, E. Gibault, H. Ljusberg-Wahren, L. Arleth, J. S. Pedersen, and A. Mullertz, "Characterization of prototype selfnanoemulsifying formulations of lipophilic compounds," *Journal of Pharmaceutical Sci*ences, 96, pp. 876–892, 2007.

[48] J. M. Morais, O. Santos, T. Delicato, and P. Rocha‐Filho, "Characterization and evaluation of electrolyte influence on canola oil/water nano-emulsion," *Journal of Dispersion Sciences and Technology,* 27, pp. 1009–1014, 2006.

[49] H. Reiss, "Entropy induced dispersion of bulk liquids," *Journal of Colloid and Interface Science,* 53, pp. 61–70, 1975.

[50] T. Dabros, A. Yeung, J. Masliyah, and J. Czarnecki, "Emulsification through area contraction," *Journal of Colloids and Interface Science,* 210, pp. 222–224, 1999.

[51] M. J. Barea, M. J. Jekins, M. H. Gaber, et al. "Evaluation of Liposomes Coated with a pH Responsive Polymer," *International Journal of Pharmaceutics*, 402, pp. 89-94, 2010.

[52] H. S. Ruth, D. Attwood, G. Ktistis, and C. Taylor, "Phase Studies and Particle Size Analysis of Oil-in-Water Phos-pholipid Microemulsions," *International Journal of Pharmaceutics*, 116, pp. 253-261, 1995.

[53] S. Shafiq, S. Faiyaz, T. Sushma, F. J. Ahmad, R. K. Khar and M. Ali, "Development and Bioavailability Assess-ment of Ramipril Nanoemulsion Formulation," *European Journal of Pharmaceutics and Biopharmaceutics*, 66, pp. 227-243, 2007.

[54] B. B. Mishra, and V. K. Tiwari, "Natural products: an evolving role in future drug discovery," *European Journal of Medicinal Chemistry*, 46, pp. 4769–4807, 2011.

[55] S. Komal, B. Ranjan, C. Neelam, S. Birendra, and S. N. Kumar, "Berberis aristata: A Review," *International Journal of Research in Ayurveda and Pharmacy*, 2, pp. 383-388, 2011

[56] B. D. Rege, J. Kao, and J. Pollia, "Effects of nonionic surfactants on membrane transporters in Caco-2 cell monolayers," *European Journal of Pharmaceutical Sciences,* 16, pp. 237–246, 2002.

[57] E. D. Hugger, K. L. Audus, and R. T. Borchardt, "Effects of poly (ethylene glycol) on efflux transporter activity in Caco-2 cell monolayers," *Journal of Pharmaceutical Sciences,* 91, pp. 1980–1990, 2002.

[58] C. Brusewitz, A. Schendler, A. Funke, T. Wagner, and R. Lipp, "Novel poloxamer-based nanoemulsions to enhance the intestinal absorption of active compounds," *International Journal of Pharmaceutics*, 329, pp. 173–181, 2007.

[59] R. Subramanian, and K. M. Wasan, "Effect of lipid excipients on *in vitro* pancreatic lipase activity," *Drug Development and Industrial Pharmacy,* 29, pp. 885–890, 2003.

[60] S. Ren, M. J. Park, A. Kim, and B. J. Lee, "*In-vitro* metabolic stability of moisture-sensitive rabeprazole in human liver microsomes and its modulation by pharmaceutical excipients," *Archives of Pharmacal Res*earch, 31, pp. 406–413, 2008.

[61] G. Cornaire, J. Woodley, P. Hermann, A. Cloarec, C. Arellano, and G. Houin, "Impact of excipients on the absorption of P-glycoprotein substrates *in vitro* and *in vivo*," *International Journal of Pharmaceutics,* 278, pp. 119–131, 2004.

[62] K. M. R. Srivalli, and P. K. Lakshmi, "Overview of P-glycoprotein inhibitors: a rational outlook," *Brazilian Journal of Pharmaceutical sciences,* 48, pp. 353-368, 2012.

[63] E. V. Batrakova, and A. V. Kabanov, "Pluronic block co polymers: evolution of drug delivery concept from inert nanocarriers to biological response modifiers," *Journal of Controlled Release,* 130, pp. 98-106, 2008.

[64] J. A. Yanez, S. W. J. Wang, I. W. Knemeyer, M. A. Wirth, and K. B. Alton, "Intestinal lymphatic transport for drug delivery," *Advanced drug delivery reviews,* 63, pp. 923-942, 2011.

[65] N. L. Trevaskis, W. N. Charman, and C. J. Porter, "Lipid-based delivery system and intestinal lymphatic drug transport: a mechanistic update," *Advanced Drug Delivery Reviews,* 60, pp. 702-716, 2008.

[66] B. Bloom, I. L. Chaikoff, and Reinhardt, "Intestinal lymph as pathway for transport of absorbed fatty acids of different chain lengths," *American Journal of Physiology,* 166, pp. 451-455, 1951.

[67] J. Y. Kiyasu, B. Bloom, and I. L. Chaikoff, "The portal transport of absorbed fatty acids," *The Journal of Biological Chemistry,* 199, pp. 415-419, 1952.

[68] P. Tso, "Intestinal lipid absorption," in: L.R. Johnson, Ed., Physiology of the Gastrointestinal Tract, Raven Press, New York, 1994, pp. 1867-1907

[69] M. M. Hussain, "A proposed model for the assembly of chylomicrons," *Atherosclerosis*, 148, pp. 1-15, 2000.

[70] C. J. H. Porter, C. W. Pouton, J. F. Cuine, and W. N. Charman, "Enhancing intestinal drug solubilization using lipid based delivery systems," *Advanced drug delivery reviews,* 60, pp. 673-691, 2008.

[71] E. S. Mahdi, A. M. Noor, M. H. Sakeena, G. Z. Abdullah, M. F. Abdulkarim, and A. M. Sattar, "Formulation and in vitro release evaluation of newly synthesized palm kernel oil esters-based nanoemulsion delivery system for 30% ethanolic dried extract derived from local *Phyllanthusurinaria*for skin antiaging," *International Journal of Nanomedicine*, 6, pp. 2499–2512, 2011.

[72] F. J. O. Quintao, R. S. N. Tavares, S. A. Vieira-Filho, G. H. B. Souza, and O. D. H. Santos, "Hydroalcoholic extracts of *Velloziasquamata*: study of its nanoemulsions for pharmaceutical or cosmetic applications," *Brazilian Journal of Pharmacognosy,* 23, pp. 101-107, 2013.

[73] S. Jafari, Y. He, and B. Bhandari, "Nano-emulsion production by sonication and microfluidization- a comparison," *International Journal of Food Properties,* 9, pp. 475-485, 2006.

[74] M. V. Butnariu, and C. V. Giuchici, "The use of some nanoemulsions based on aqueous propolis and lycopene extract in the skin's protective mechanisms against UVA radiation," *Journal of Nanobiotechnology,* 3, pp. 1-9, 2011.

[75] R. Chaiittianan, and B. Sripanidkulchai, "Development of a nanoemulsion of Phyllanthus emblica L. branch extract," *Drug Development and Industrial Pharmacy,* 40, pp. 1597–1606, 2014.

[76] X. Y. Wang, Y. W. Wang, and R. Huang, "Enhancing stability and oral bioavailability of polyphenols using nanoemulsions," In: Micro/Nanoencapsulation of Active Food Ingredients. Q. R. Huang, P. Given and M. Qian, Eds. ACS Symposium Series 1007, Washington, DC, 2009.

[77] X. Wang, Y. Jiang, Y. Wang, M. Huang, C. T. Ho, and Q. Huang, "Enhancing anti-inflammation activity of curcumin through O/W nanoemulsions," *Food Chemistry,* 108, pp. 419-424, 2008.

[78] F. Donsi, Y. Wang, J. Li, and Q. Huang, "Preparation of curcumin sub-micrometer dispersions by high-pressure homogenization," *Journal of Agricultural and Food Chemistry,* 58, pp. 2848-2853, 2010.

[79] Q. Huang, H. Yu, and Q. Ru, "Bioavailability and delivery of nutraceuticals using nanotechnology," *Journal of Food Science,* 75, pp. R50-57, 2010.

[80] Y. Yuan, Y. Gao, J. Zhao, and L. Mao, "Characterization and stability evaluation of β-carotene nanoemulsions prepared by high pressure homogenization under various emulsifying conditions," *Food Research International,* 41, pp. 61-68, 2004.

[81] Y. Yuan, Y. Gao, L. Mao, and J. Zhao, "Optimization of conditions for the preparation of β-carotene nanoemulsions using response surface methodology," *Food Chemistry,* 107, pp. 1300-1306, 2008.

[82] L. Mao, D. Xu, J. Yang, F. Yuan, Y. Gao, and J. Zhao, "Effects of small and large molecule emulsifiers on the characteristics of β-carotene nanoemulsions prepared by high pressure homogenization," *Food Technology and Biotechnology,* 47, pp. 336-342, 2009.

[83] L. Mao, J. Yang, D. Xu, F Yuan, and Y. Gao, "Effects of homogenization models and emulsifiers on the physicochemical properties of β-carotene nanoemulsions," *Journal of Dispersion Science and Technology,* 31, pp. 986-993, 2010.

[84] W. Li, S. Yi, Z. Wang, S. Chen, S. Xin, J. Xie, and C. Zhao, "Self-nanoemulsifying drug delivery system of persimmon leaf extract: Optimization and bioavailability studies," *International Journal of Pharmaceutics,* 420, pp. 161-71, 2011.

[85] A. S. Saraf, "Applications of novel drug delivery system for herbal formulations," *Fitoterapia,* 81, pp. 680–689, 2010.

[86] O. Wichterle, and D. Lim, "Hydrophilic gels for biological use," *Nature,* 185, pp. 117–118, 1960.

[87] A.S. Hoffman, "Hydrogels for biomedical applications," *Advanced Drug Delivery Reviews,* 54, pp. 3–12, 2002

[88] N. A. Peppas, P. Bures, W. Leobandung, and H. Ichikawa, "Hydrogels in pharmaceutical formulations. *European Journal of Pharmaceutics and. Biopharmaceutics,* 50, pp. 27–46, 2000.

[89] R. Dagani, "Intelligent gels," *Chemical and Engineering News,* 75, pp. 26–37, 1997.

[90] J. A. Harvey, "Smart materials. In Encyclopedia of Chemical Technology, J. I. Kroschwitz and M. Howe-Grant, Eds. John Wiley & Sons, 1995, pp. 502–514.

[91] J .M. Guenet, "Thermoreversible gelation of polymers and biopolymers," Academic press, New York, 1992, pp. 89,

[92] M. L. Markey, and M. L. Bowman, M. Y. Y. V. Bergamini, "Chitin and chitosan," Elsevier Appl. Sci, M. L. Markey, M. L. Bowman, M. Y. Y. V. Bergamini, Eds. London 1989, pp. 713.

[93] M. M. Welz, and C. M. Ofner III, "Examination of self cross-linked gelatin as a hydrogel for controlled release," *Journal of Pharmaceutical Sciences,* 81, pp. 85-90, 1992.

[94] A. M. Lowman, and N. A. Peppas, "Hydrogels. In: Encyclopedia of controlled drug delivery," E. Mathiowitz, Eds. John wiley & sons, Inc, 1997, pp. 397.

[95] S. H. Gehrke, and P. I. Lee, "Hydrogels for drug delivery systems," In: specialized drug delivery systems, P. Tyle, Eds., Marcel Dekker, 1990, pp. 333.

[96] J. Chen, W. E. Blevins, H. Park, and K. Park, "Gastric retention properties of superporous hydrogel composites," *Journal of Controlled Release,* 64, pp. 39-51, 2000.

[97] K. Park, "Controlled drug delivery: challenges and strategies," Am. Chem. Soc., Washington, D.C. E. Park, Eds., pp. 629, 1997.

[98] M. N. V. R. Kumar, "A review on chitin and chitosan applications," *Reactive and Functional Polymer,* 46, pp. 1-27, 2000.

[99] N. Kumar, M. chaubal, A. J. Domb and M. N. V. R. Kumar, "Controlled release technology," In: Encyclopedia of polymer science and Technology, N. J. Hoboken, Eds., John Wiley & Sons, Inc., 5, 2003, pp. 697,.

[100] B. E. Ballard, "An overview of prolonged action drug dosage forms" in "Sustained and controlled release drug delivery systems" J. R. Robinson, Eds., Marcel Dekker Inc. New York, 1978.

[101] L. B. Peppas, "Polymers in Controlled Drug Delivery," Medical Plastics and Biomaterials Magazine, November 1997.

[102] K. V. R. Rao, and K. P Devi, "Swelling controlled-release systems: recent developments and applications. *International Journal of Pharmaceutics,* 48, pp. 1–13, 1988.

[103] J. A. Bouwstra and H. E. Junginger, "Hydrogels. In Encyclopaedia of Pharmaceutical Technology, J. Swarbrick and J. C. Boylan, Eds, Marcel Dekker, 1993, pp. 441–465.

[104] P. I. Lee, and C. J. Kim, "Probing the mechanisms of drug release from hydrogels," *Journal of Controlled Release,* 16, pp. 229–236, 1991.

[105] P. L. Ritger, and N. A. Peppas, "A simple equation for description of solute release I. Fickian and non-Fickian release from non-swellable devices in the form of slabs, spheres, cylinders or discs," *Journal of Controlled Release,* 5, pp. 23–26, 1987.

[106] N.A. Peppas, and N. M. Franson, "The swelling interface number as a criterion for prediction of diffusional solute release mechanisms in swellable polymers," *Journal of Polymer Science Part B; Polymer Physics,* 21, pp. 983–997, 1983.

[107] W. R. Good, "Diffusion of water soluble drugs from initially dry hydrogels," In Polymeric Delivery Systems, R. Kostelnik, Eds. Gordon and Breach, 1976, pp. 139–153,

[108] J. Kost, "Intelligent drug delivery systems," In Encyclopaedia of Controlled Drug Delivery, E. Mathiowitz, Eds. John Wiley& Sons, pp. 445–459, 1999.

[109] S. H. Gehrke, "Synthesis and properties of hydrogels used for drug delivery," In Transport Processes in Pharmaceutical Systems, G. L. Amidon et al., Eds. Marcel Dekker, pp. 473–546, 2000

[110] C. M. Klech, "Gels and jellies. In Encyclopedia of Pharmaceutical Technology, J. Swarbrick and J. C. Boylan, Eds. Marcel Dekker, pp. 415–439, 1990

[111] W. Zhao, X. Jin, Y. Cong, Y. Liu, and J. Fu, "Degradable natural polymer hydrogels for articular cartilage tissue engineering," *Journal of Chemical Technology and Biotechnology,* 88, pp. 327–39, 2013.

[112] L. Takashi, T. Hatsumi, M. Makoto, I. Takashi, G. Takehiko, and S. Shuji, "Synthesis of porous poly (N-isopropylacrylamide) gel beads by sedimentation polymerization and their morphology," *Journal of Applied Polymer Science,* 104, pp. 842-850, 2007.

[113] L. Yang, J. S. Chu, and J. A. Fix, "Colon-specific drug delivery: new approaches and in vitro/in vivo evaluation," *International Journal of Pharmaceutics,* 235, pp. 1–15, 2002.

[114] Z. Maolin, L. Jun, Y. Min, and H. Hongfei, "The swelling behaviour of radiation prepared semi-interpenetrating polymer networks composed of polyNIPAAm

and hydrophilic polymers," *Radiation Physics and Chemistry,* 58, pp. 397–400, 2000.

[115] F. Khoylou, and F. Naimian, "Radiation synthesis of superabsorbent polyethylene oxide/tragacanth hydrogel," *Radiation Physics and Chemistry,* 78, pp. 195-198, 2009.

[116] M. T. Razzak, D. Darwis, Zainuddin, and Sukirno, "Irradiation of polyvinyl alcohol and polyvinyl pyrrolidone blended hydrogel for wound dressing," *Radiation Physics and Chemistry,* 62, pp. 107-113, 2001.

[117] F. S. Palumbo, G. Pitarresi, D. Mandracchia, G. Tripodo, and G. Giammona, "New graft copolymers of hyaluronic acid and polylactic acid: Synthesis and characterization," *Carbohydrate Polymers,* 66, pp. 379-385, 2006.

[118] Y. Onuki, M. Nishikawa, M. Morishita, and K. Takayama, "Development of photocrosslinkedpolyacrylic acid hydrogel as an adhesive for dermatological patches: Involvement of formulation factors in physical properties and pharmacological effects," *International Journal of Pharmaceutics,* 349, pp. 47-52, 2008.

[119] A. Singh, M. Hosseini, and S. M. Hariprasad, "Polyethylene Glycol Hydrogel Polymer Sealant for Closure of SuturelessSclerotomies: A Histologic Study," *American Journal of Ophthalmology,* 150, pp. 346-351, 2010.

[120] W. E. Hennink, and C. F. V. Nostrum, "Novel crosslinking methods to design hydrogels," *Advanced Drug Delivery Reviews,* 54, pp. 13–36, 2002.

[121] R. Barbucci, G. Leone, and A. Vecchiullo, "Novel carboxymethylcellulose-based microporous hydrogels suitable for drug delivery. *Journal of Biomaterial Science Polymer Edition,* 15, pp. 607-619, 2004.

[122] H. M. Said, S. G. A. Alla, and A. W. M. El-Naggar, "Synthesis and characterization of novel gels based on carboxymethyl cellulose/acrylic acid prepared by electron beam irradiation," *Reactive and Functional Polymers,* 61, pp. 397–404, 2004.

[123] B. Fei, R. A. Wach, H. Mitomo, F. Yoshii, and T. Kume, "Hydrogel of biodegradable cellulose derivatives. I. Radiation-induced crosslinking of CMC," *Journal of Applied Polymer Science,* 78, pp. 278-283, 2000.

[124] T. Funami, M. Hiroe, S. Noda, I. Asai, S. Ikeda, and K. Nishimari, "Influence of molecular structure imaged with atomic force microscopy on the rheological

behavior of carrageenan aqueous systems in the presence or absence of cations," *Food Hydrocolloids,* 21, pp. 617-629, 2007.

[125] A. S. Hoffman, "Hydrogels for biomedical applications," *Advanced Drug Delivery Reviews,* 43, pp. 3–12, 2002.

[126] A. K. Bajpai, S. K. Shukla, S. Bhanu, and S. Kankane, "Responsive polymers in controlled drug delivery," *Progress in Polymer Science,* 33, pp. 1088-1118, 2008.

[127] Q. S. Zhao, Q. X. Ji, K. Xing, X. Y. Li, C. S. Liu, and X. G. Chen, "Preparation and characteristics of novel porous hydrogel films based on chitosan and glycerophosphate," *Carbohydrate Polymers,* 76, pp. 410-416, 2009.

[128] D. Magnin, J. Lefebvre, E. Chornet, and S. Dumitriu, "Physicochemical and structural characterization of a polyionic matrix of interest in biotechnology, in the pharmaceutical and biomedical fields. *Carbohydrate Polymers,* 55, pp. 437-453, 2004.

[129] M. Takigami, H. Amada, N. Nagasawa, T. Yagi, T. Kasahara, S. Takigami, and M. Tamada, "Preparation and properties of CMC gel," *Transactions of the Materials Research Society of Japan,* 32, pp. 713-716, 2007.

[130] P. Giannouli, and E. R. Morris, "Cryogelation of xanthan," *Food Hydrocolloids,* 17, pp. 495-501, 2003.

[131] L. S. Spinelli, A. S. Aquino, E. Lucas, A. R. d'Almeida, R. Leal, and A. L. Martins, "Adsorption of polymers used in drilling fluids on the inner surfaces of carbon steel pipes," *Polymer Engineering and Science,* 48, pp. 1885-1891, 2008.

[132] A. B. Lugao and S. M. Malmonge, "Use of radiation in the production of hydrogels," *Nuclear Instruments and Methods in Physics Research* B, 185, pp. 37-42, 2001.

[133] K. Shameli, M. B. Ahmad, E. J. Al-Mulla et al., "Green biosynthesis of silver nanoparticles using Callicarpa maingayi stem bark extraction," *Molecules*, 17, pp. 8506-85017, 2012.

[134] N. Duran, P. D. Marcato, R. D. Conti, et al., "Potential Use of Silver Nanoparticles on Pathogenic Bacteria, their Toxicity and Possible Mechanisms of Action," *Journal of Brazilian Chemical Society,* 21, pp. 949-959, 2010.

[135] N. Ngoc-Thang, and J. H. Liu, "A green method for in situ synthesis of poly(vinyl alcohol)/chitosan hydrogel thin films with entrapped silver

nanoparticles," *Journal of the Taiwan Institute of Chemical Engineers,* 45, pp. 2827-2833, 2014.

[136] S. Ravindra, Y. M. Mohan, N. N. Reddy, and K. M. Raju, "Fabrication of antibacterial cotton fibres loaded with silver nanoparticles via Green Approach," *Colloids and Surfaces A: Physicochemical and Engineering Aspects,* 367, pp. 31–40, 2010.

[137] M. M. Gulsonbi, K. B. Raj, and V. Jaisankar, "Green Synthesis of Silver Nano Particles using Plant Extracts in Semi- Hydrogel Networks of Poly(acrylamide) and Carbohydrates, Characterization and Biomedical Applications," *International Journal of Innovative Research in Science & Engineering*, pp. 2347-3207.

[138] S. Shaik, M. R. Kummara, S. Poluru，et al., "A Green Approach to Synthesize Silver Nanoparticles in Starch-co-Poly(acrylamide) Hydrogels by Tridax procumbens Leaf Extract and Their Antibacterial Activity," *International Journal of Carbohydrate Chemistry,* 2013, pp. 1-10, 2013.

[139] S. Garg, A. Chandra, A. Mazumder, and R. Mazumder, "Green synthesis of silver nanoparticles using *Arnebia nobilis* root extract and wound healing potential of its hydrogel," *Asian journal of pharmaceutics,* 8, pp. 95-101, 2014.

[140] M. A. Patel, P. K. Patel, and M. B. Patel, "Aqueous Extract of *Ficus bengalensis* Linn. Bark for Inflammatory Bowel Disease," *Journal of Young Pharmacist,* 2, pp. 130–136, 2010.

[141] S. K. Kothari, A. K. Bhattacharya, S. Ramesh, S. N. Garg and S. P. S. Khanuja, "Volatile Constituents in Oil from Different Plant Parts of Methyl Eugenol-Rich *Ocimum tenuiflorum* L.f. (syn. *O. sanctum* L.) Grown in South India," *Journal of Essential Oil Research,* 17, pp. 656–658, 2005.

[142] H. Ali, and S. Dixit, "Extraction optimization of Tinospora cordifolia and assessment of the anticancer activity of its alkaloid Palmatine," *The Science world Journal,* 2013, pp. 1-10, 2013.

[143] R. Tungpradit, S. Sinchaikul, S. Phutrakul, W. Wangkham, and S. T. Chen, "Anticancer compound screening and isolation: Coscinium fenestratum,

Tinospora crispa and Tinospora cordifolia," *Chiang Mai Journal of Science,* 37, pp. 476-488, 2013.

[144] J. D. Hauss, "Oral lipid-based formulations," *Advanced drug delivery Reviews,* 59, pp. 667-676, 2007.

[145] W. W. Zheng, L. Zhao, Y. M. Wei, Y. Ye, and S. H. Xiao, "Preparation and the in vitro evaluation of nanoemulsion system for the transdermal delivery of granisetron hydrochloride," *Chemical and Pharmaceutical Bulletin,* 58, pp. 1015-1019, 2010.

[146] S. Hongwu, L. Kaiyun, L. Wei, et. al., "Development and characterization of a novel nanoemulsion drug-delivery system for potential application in oral delivery of protein drugs," *International Journal of Nanomedicine*, 7, pp. 5529-5543, 2012.

[147] A. Jemal, F. Bary, M. M. Center, et. al., "Global cancer staticstics," *CA: A cancer Journal of Clinicians*, 61, pp. 69-90, 2011.

[148] R. Hanahann, and A. Weinberg, "The hallmarks of cancer cell," *Cell,* 100, pp. 57-70, 2000.

[149] M. A. Richardson, T. Sanders, J. L. Palmer, et. al., "Complementary/alternative medicine use in a comprehensive cancer center and the implications for oncology," *Journal of Clinical Oncology*, 18, pp. 2505-2514, 2000.

[150] M. Dhanasekaran, A. A. Baskar, S. Ignacimuthu, P. Agastian, "Chemopreventive potential of Epoxy clerodane diterpene from Tinospora cordifolia against diethylnitrosamine-induced hepatocellular carcinoma," *Investigational New Drugs*, 27, pp. 347-355, 2009.

[151] S. Yang, A. M. Evens, S. Prachand, et. al., "Mitochondrial-mediated apoptosis in lymphoma cells by the diterpenoid lactone andrographolide, the active component of andrographis paniculata," *Clinical Cancer Research*, 16, pp. 4755-4768, 2010.

[152] P. Kapur, B. M. Pereira, W. Wuttke, and H. Jarry, "Androgenic action of *Tinospora cordifolia* ethanolic extract in prostate cancer cell line LNCaP," Phytomedicine, 16, pp. 679-682, 2009.

[153] M. Sarala, V. Velu, C. Anandharamakrishnan, and R. P. Singh, "Spray drying of Tinospora cordifolia leaf and stem extract and evaluation of antioxidant activity," *Food Science and Technology*, 49, pp. 119–122, 2012.

[154] C. Bhandari, C. Vanaushadhi, 1st ed., vol. 3. Varanasi: Chaukhamba Sanskrit Sansthan, 2006.

[155] S. Deverux, and M. Q. F. Hatton, "Immediate side effect of large fraction radiotherapy," *Clinical Oncology*, 9, pp. 96-99, 1997.

[156] N. Singh, S. M. Singh, and P. Shrivastava, "Effect of Tinospora cordifolia on the antitumor activity of tumor associated macrophages-derived dendritic cells," *Immunopharmacology and Immunotoxicology*, 27, pp. 1-14, 2005.

[157] G. V. Srinivasan, K. P. Unnikrishnan, A. B. R. Shree, and I. Balachandran, "HPLC Estimation of berberine in Tinospora cordifolia and Tinospora sinensis," *Indian Journal of Pharmaceutical Sciences*, 70, pp. 96–99, 2008.

[158] V. Dewanto, X. Wu, and K. K. Adom, "Thermal Processing enhances the nutritional Value of Tomatoes by increasing total antioxidant activity," *Journal of Agriculture and Food Chemistry*, 42, pp. 3010-301, 2002.

[159] M. Ajanal, M. B. Gundkalle, and S. U. Nayak, "Estimation of total alkaloids in chitrakadivati by UV-Spectrophotometer," *Ancient Science of life,* 31, pp. 198-201, 2012.

[160] A. Azeem, M. Rizwan, and F. J. Ahmad, "Nanoemulsion Components Screening and Selection: a Technical Note," *AAPS Pharmaceutical Science Technology,* 10, pp. 69-76, 2009.

[161] Y. Wang, W. Wu, and L. Que, "Investigation on oil/Tween80/alcohol/water system pseudo-ternary phase diagrams and self-microemulsifying drug delivery system," *Journal of Chinese Pharmaceutical sciences,* 36, pp. 345–348, 2005.

[162] A. B. Mohd, K. Sanka, S. Bandi, P. V. Diwan, and N. Shastri, "Solid self-nanoemulsifying drug delivery system (S-NANOEMULSION) for oral delivery of glimepiride: development and antidiabetic activity in albino rabbits," *Drug delivery*, 22, pp. 499-508, 2015.

[163] A. J. Choi, C. J. Kim, Y. J. Cho, J. K. Hwang, and C. T. Kim, "Effects of Surfactants on the Formation and Stability of Capsaicin loaded Nanoemulsions," *Food Science and Biotechnology*, 18, pp. 1161-1172, 2009.

[164] Y. S. Elnaggar, M. A. Massik, and O. Y. Abdallah, "Self-nanoemulsifying drug delivery systems of tamoxifen citrate: design and optimization," *International Journal of Pharmaceutics*, 380, pp. 133-141, 2009.

[165] A. W. Khan, S. Kotta, S. H. Ansari, et al., "Self-nanoemulsifying drug delivery system (NANOEMULSION) of the poorly water-soluble grapefruit flavonoid

Naringenin: design, characterization, *in-vitro* and *in-vivo* evaluation," *Drug delivery,* 22, pp. 552-561, 2015.

[166] S. P. Jiang, S. N. He, Y. L. Li, et al., "Preparation and characteristics of lipid nanoemulsion formulations loaded with doxorubicin," *International Journal of Nanomedicine,* 8, pp. 3141-3150, 2013.

[167] H. Zhao, H. Lu, T. Gong, and Z. Zhang, "Nanoemulsion loaded with lycobetaine–oleic acid ionic complex: physicochemical characteristics, in vitro, in vivo evaluation, and antitumor activity," *International Journal of Nanomedicine*, 8, pp. 1959–1973, 2013.

[168] S. Ganta, A. Singh, Y. Rawal, et al., "Formulation development of a novel targeted theranostic nanoemulsion of docetaxel to overcome multidrug resistance in ovarian cancer," *Drug delivery*, 23, pp. 968-980, 2016.

[169] S. Bandyopadhyay, and O. P. Katare, "Optimized self nano-emulsifying systems of ezetimibe with enhanced bioavailability potential using long chain and medium chain triglycerides," *Colloids and Surface B: Biointerfaces,* 100, pp. 50– 61, 2012.

[170] S. Beg, P. S. Sandhu, R. S. Batra, et al., "QbD-based systematic development of novel optimized solid self-nanoemulsifying drug delivery systems (NANOEMULSION) of lovastatin with enhanced biopharmaceutical performance," *Drug delivery*, 22, pp. 765-784, 2015.

[171] O. Pradnya, B. Jitendra, K. Revan, "Evaluation of Antioxidant activity of traditional formulation Giloy satva and hydroalcoholic extract of the Curculigo orchioides gaertn," *Journal of Applied Pharmaceutical Science,* 2, pp. 209-213, 2012.

[172] S. C. Yang, and S. Benita, Enhanced absorption and drug targeting by positively charged submicron emulsions," *Drug Delivery Research*, 50, pp. 476–486, 2000.

[173] K. G. Marinova, R. G. Alargova, N. D. Denkov, et al., "Charging of oil–water interfaces due to spontaneous adsorption of hydroxyl ions," Langmuir, 12, pp. 2045–2051, 1996.

[174] T. R. Kommuru, B. Gurley, M. A. Khan, and I. K. Reddy, "Self emulsifying drug delivery systems (SEDDS) of coenzyme Q10: formulation development and bioavailability assessment," *International Journal of Pharmaceutics*, 212, pp. 233–246, 2001.

[175] M. Kreilgaard, E. J. Pedersen, and J. W. Jaroszewski, "NMR characterization and transdermal drug delivery potential of microemulsion systems," *Journal of Controlled Release*, 69, pp. 421–433, 2000.

[176] D. Attwood, "Microemulsions," In: J. Kreuter, Eds, "Colloidal Drug Delivery Systems," Marcel Dekker, New York, 1994, pp. 31-72.

[177] W. Warisnoicharoen, A. B. Lansley, and M. J. Lawrence, "Nonionic oil-in-water microemulsions: the effect of oil type on phase behaviour," *International Journal of Pharmaceutics*, 198, pp. 7-27, 2000.

[178] F. Chena, Y. Wanga, and F. Zhenga, "Studies on cloud point of agrochemical microemulsions," *Colloids and Surface A: Physicochemical and Engineering Aspects*, 175, pp. 257-262, 2000.

[179] D. Patel, and K. K. Sawant, "Oral bioavailability enhancement of acyclovir by self micro-emulsifying drug delivery system (SMEDDS)," *Drug Development and Industrial Pharmacy,* 33, pp. 1318-1326, 2007.

[180] F. S. Nielsen, K. B. Petersen, and A. Mullertz, "Bioavailability of probucol from lipid and surfactant based formulation in minipigs: influence of droplet size and dietary state," *European Journal of Pharmaceutical Sciences,* 69, pp. 553-62, 2008.

[181] D. Ghai, and V. R. Sinha, "Nanoemulsions as self-emulsified drug delivery carriers for enhanced permeability of the poorly water-soluble selective β_1-adrenoreceptor blocker Talinolol," *Nanomedicine: Nanotechnology, Biology and Medicine*, 8, pp. 618-626, 2012.

[182] T. Bansal, M. Jaggi, R. K. Khar, and S. Talegaonkar, "Emerging Significance of Flavonoids as P-Glycoprotein Inhibitors in Cancer Chemotherapy," *Journal of Pharmacy and Pharmaceutical Sciences*, 12, pp. 46-78, 2009.

[183] M. V. S Varma, Y. Ashokraj, C. S. Dey, et al., "P-glycoprotein inhibitors and their screening: a perspective from bioavailability enhancement," *Pharmacological Research*, 48, pp. 347-359, 2003.

[184] Y. L. LO, "Relationships between the hydrophilic–lipophilic balance values of pharmaceutical excipients and their multidrug resistance modulating effect in Caco-2 cells and rat intestines," *Journal of Controlled Release*, 90, pp. 37-48, 2003.

[185] A. Zhang, H. Sun, and X. Wang, "Potentiating Therapeutic Effects by Enhancing Synergism Based on Active Constituents from Traditional Medicine," *Phytotherapy Research,* 28, pp. 526–533, 2014.

[186] C. A. Lipinski, "Poor aqueous solubility – an industry wide problem in drug discovery," *American Pharmaceutical Review*, 5, pp. 82–85, 2002.

[187] J. Cui, B. Yu, Y. Zhao, et al., "Enhancement of oral absorption of curcumin by self-microemulsifying drug delivery systems," *International Journal of Pharmaceutics*, 371, pp. 148–155, 2009.

[188] D. Potdar, R.R. Hirwani, and S. Dhulap, "Phyto-chemical and pharmacological applications of Berberis aristata," *Fitoterpia,* 83, pp. 817–830, 2012.

[189] R. Steriti, "Berberine for diabetes mellitus type 2," *Natural Medicine Journal*, 2, pp. 5-6, 2010.

[190] W. J. Kong, H. Zhang, D. Q. Song, et al., "Berberine reduces insulin resistance through protein kinase C-dependent up-regulation of insulin receptor expression," *Metabolism*, 58, pp. 109-119, 2009.

[191] W. Hua, L. Ding, Y. Chen, B. Gong, J. He, and G. Xu, "Determination of berberine in human plasma by liquid chromatography-electrospray ionization-mass spectrometry," *Journal of Pharmaceutical and Biomedical Analysis,* 44, pp. 931–937, 2007.

[192] Y. T. Liu, H. P. Hao, H. G. Xie, et al., "Extensive Intestinal First-Pass Elimination and Predominant Hepatic Distribution of Berberine Explain Its Low Plasma Levels in Rats," *Drug Metabolism and Disposition,* 38, pp. 1779-1784, 2010.

[193] A. Maimoona1, I. Naeeml, and Z. Saddiqel, "Analysis of total flavonoids and phenolics in different fractions of bark and needle extracts of Pinusroxburghii and Pinus wallichiana," *Journal of Medicinal Plants Research*, 5, pp. 2724-2728, 2011.

[194] V. E. Tyler, "Phytomedicines in Western Europe: their potential impact on herbal medicine in the United States," *Herbalgram,* 30, pp. 24-30, 1994.

[195] H. Ahmad, I. Khan, and A. Wahid, "Antiglycation and antioxidation properties of Juglans regia and Calendula officinalis: possible role in reducing diabetic complications and slowing down ageing," *Journal of Traditional Chinese Medicine*, 32, pp. 411-414, 2012.

[196] A. S. Macedo, S. Quelhas, A. M. Silva, et al., "Nanoemulsions for delivery of flavonoids: formulation and in vitro release of rutin as model drug," *Pharmaceutical Development and Technology,* 19, pp. 677-680, 2014.

[197] S. Sharma, J. K. Sahni, J. Ali, and S. Baboota, "Effect of high-pressure homogenization on formulation of TPGS loaded nanoemulsion of rutin – pharmacodynamic and antioxidant studies," *Drug delivery,* 22, pp. 541-551, 2015.

[198] M. Van de Venter, S. Roux, L. C. Bungu, et al., "Antidiabetic screening and scoring of 11 plants traditionally used in South Africa," *Journal of Ethnopharmacology*, 119, pp. 81–86, 2008.

[199] R. A. Adisa, J. Oke, S. A. Olomu, and O. Olorunsogo, "Inhibition of human haemoglobin glycosylation by flavonoid containing leaf extract of Cnestis ferruginea," *Journal of the Cameroon Academy of Sciences,* 4, pp. 351-359, 2004.

[200] A. Srichamroen, and V. Chavasit, "In vitro retardation of glucose diffusion with gum extracted from malva nut seeds produced in Thailand," *Food Chemistry*, 127, pp. 455–460, 2011.

[201] S. Ou, K, Kwok, Y. Li, and L. Fu, "In vitro study of possible role of dietary fibre in lowering postprandial serum glucose," *Journal of Agricultural and Food Chemistry*, 127, pp. 1026–1029, 2001.

[202] V. K. Bajpai, J. I. Yoon, and S. C. Kang, "Antioxidant and antidermatophytic activities of essential oil and extracts of Metasequoia glyptostroboides Mikiex Hu," *Food and Chemical Toxicology*, 47, pp. 1355-1361, 2009.

[203] M. Y. Levy, and S. Benita, "Drug release from submicronized o/w emulsion: a new in vitro kinetic evaluation model," *International Journal of Pharmaceutics*, 66, pp. 29–37, 1990.

[204] S. Radhika, K. R. Senthil, and S. Sindhu, "Phytochemical investigation and evaluation of antihyperglycemic potential of Premna Corymbosa," *International Journal of Pharmacy and Pharmaceutical Sciences*, 5, pp. 352-356, 2013.

[205] R. P. Ferraris, S. Yasharpour, K. C. Lloyd, et al., "Luminal glucose concentration in the gut under normal conditions," *American Journal of Physiology*, 259, pp. G822–G837, 1990.

[206] S. Gropper, L. Smith and L. Groff, Advanced nutrition and human metabolism, 5th ed. Belmont, CA: Wadsworth, 2009.

[207] P. S. Murphy, and G. R. D Evans, "Advances in Wound Healing: A Review of Current Wound Healing Products," *Plastic Surgery International,* 2012, pp. 1-8, 2012.

[208] R. Cortivo, V. Vindigni, L. Lacobellis, et al., "Nanoscale particle Therapies for Wounds and Ulcers," *Nanomed*icine, 5, pp. 641-656, 2010.

[209] M. Jaiswal, A. Gupta, K. A. Dinda, and V. Koul, "An investigation study of gelatin release from semi-interpenetrating polymeric network hydrogel patch for excision wound healing on Wistar rat model," *Journal of Applied Polymer Science,* 132, 42120, 2015.

[210] P. S. K. Murthy, Y. M. Mohan, K. Varaprasada, et al., "First successful design of semi-IPN hydrogel-silver nanocomposites: a facile approach for antibacterial application," *Journal of Colloid and Interface Sciences,* 318, pp. 217–224, 2008.

[211] K. Varaprasad, K. Vimala, S. Ravindra, N. G. N. J. Reddy, et al., "Fabrication of silver nanocomposite films impregnated with curcumin for superior antibacterial applications.," *Journal of Material Science: Materials in Medicine,* 22, pp. 1863–1872, 2011.

[212] F. Yoshii, Y. Zhanshan, K. Isobe, K. Shiozaki, and K. Makunchi, "Electron beam crosslinked PEO and PEO/PVA hydrogels for wound dressing," *Radiation Physics and Chemistry*, 55, pp. 133–138, 1999.

[213] J. Wang, L. Lin, Q. Cheng, and L. Jiang, "A strong Bio-Inspired layered PNIPAM-clay nanocomposite hydrogel," *Angewandte Chemie,* 124, pp. 4754–4758, 2012.

[214] H. Kamata, Y. Akagi, Y. Kayasuga-Kariya et al., "Nonswellable hydrogel without Mechanical Hysteresis," *Science*, 343, pp. 873-875, 2014.

[215] Q. Cheng, L. Jiang, and Z. Tang, "Bioinspired Layered Materials with Superior Mechanical Performanc," *Accounts of Chemical Research,* 47, pp. 1256-1266, 2014.

[216] T. L. Sun, T. Kurokawa, S. Kuroda, et al., "Physical hydrogels composed of polyampholytes demonstrate high toughness and viscoelasticity," *Nature Materials,* 12, pp. 932-937, 2013.

[217] J. P. Gong, Y. Katsuyama, T. Kurokawa and Y. Osada, "Double-network hydrogels with extremely high mechanical strength," *Advanced Materials,* 15, pp. 1155-1158, 2003.

[218] B. Balakrishnan, M. Mohanty, P. R. Umashankar, and A. Jayakrishnan, "Evaluation of an in situ forming hydrogel wound dressing based on oxidized alginate and gelatin," *Biomaterials, 26*, pp. 6335–6342, 2005.

[219] Y. Dong, W. Hassan, R. Kennedy, et al., "Performance of an in situ formed bioactive hydrogel dressing from a PEG-based hyperbranched multifunctional copolymer," *Acta Biomaterialia*,10, pp. 2076-2085, 2014.

[220] Q. H. Tran, V. Q. Nguyen, and A. Le, "Silver nanoparticles: synthesis, properties, toxicology, applications and perspectives," *Advances in Natural Sciences: Nanoscience and Nanotechnology,* 4, pp. 033001, 2013.

[221] T. Gilchrist, and A. M. Martin, "Wound treatment with sorban-an alginate fibre dressing," *Biomater*ials, 4, pp. 317–320, 1983.

[222] J. Kasthuri, S. Veerapandian, and N. Rajendiran, "Biological synthesis of silver and gold nanoparticles using apiin as reducing agent," *Colloids and Surface B: Biointerfaces,* 68, pp. 55–60, 2009.

[223] S. D. Sarker, L. Nahar, and Y. Kumarasamy, "Microtitre plate-based antibacterial assay incorporating resazurin as an indicator of cell growth, and its application in the *in vitro* antibacterial screening of phytochemicals," *Methods*, 42, pp. 321-324, 2007.

[224] M. Jaiswal, A. K. Dinda, A. Gupta, and V. Koul, "Polycaprolactone diacrylate crosslinked biodegradable semi-interpenetrating networks of polyacrylamide and gelatin for controlled drug delivery," *Biomedical Materials,* 5, 065014, 2010.

[225] M. Jaiswal, F. Naz, A. K. Dinda, and V. Koul, "*In vitro* and *in vivo* efficacy of doxorubicin loaded biodegradable semi-interpenetrating hydrogel implants of poly (acrylic acid)/gelatin for post surgical tumor treatment," *Biomedical Materials,* 8, 045004, 2013.

[226] O. Suwantong, P. Opanasopit, U. Ruktanonchai, and P. Supaphol, "Electrospun Cellulose Acetate Fiber Mats Containing Curcumin and Release Characteristic of the Herbal Substance," *Polym*er, 48, pp. 7546–7557, 2007.

[227] M. C. Bonferoni, S. Rossi, F. Ferrari, and C. Caramella, "A modified Franz diffusion cell for simultaneous assessment of drug release and washability of mucoadhesive gels," *Pharmaceutical Development and Technology,* 4, pp. 45-53, 1999.

[228] A. Chhatri, A. K. Bajpai, S. S. Shandhu, et al., "Cryogenic fabrication of savlon loaded macroporous blends of alginate and polyvinyl alcohol (PVA). Swelling, deswelling and antibacterial behaviors," *Carbohydrate Polymers,* 83, pp. 876–882, 2011.

[229] D. K. Singh, and A. K. J. Ray, "Graft copolymerization of 2-hydroxyethyl methacrylate onto chitosan films and their blood compatibility," *journal of Applied Polymer Science,* 53, pp. 1115–1121, 1994.

[230] American Society for Testing and Materials: Standard Practices for Assessment of Haemolytic Properties of Materials, Philadelphia, ASTM F 756–00, 2000.

[231] A. M. Behrens, M. J. Sikorski, T. Li, et al., "Blood-aggregating hydrogel particles for use as a hemostatic agent," *Acta Biomaterialia*,10, pp. 701–708, 2014.

[232] W. C. Lin, D. J. Yu, and M. C. Yang, "Blood compatibility of novel poly(-glutamic acid)/polyvinyl alcohol Hydrogels," *Colloids and Surface B: Biointerfaces,* 47, pp. 43–49, 2006.

[233] M. Kokabi, M. Sirousazar, and Z. M. Hassan, "PVA–clay nanocomposite hydrogels for wound dressing," *European Polymer Journal,* 43, pp. 773-781, 2007.

[234] C. Perez, M. Pauli, P. Bezevque, et al., "An antibiotic assay by agar well diffusion method," *Acta Biologiae Medicine Experimentalis,* 15, pp. 113-115, 1990.

[235] R. Manian, N. Anusuya, P. Siddhuraju, and S. Manian, "The antioxidant activity and free radical scavenging potential of two different solvent extracts of Camellia sinensis (L.) O. Kuntz, Ficus bengalensis L. and Ficus racemosa L," *Food Chemistry*, 107, pp. 1000-1007, 2008.

[236] G. N. Xu, X. Qiao, X. Qiu, and J. Chen, "Preparation and characterization of stable monodisperse silver nanoparticles via photoreduction," *Colloids and Surface A: Physicochemical and Engineering Aspect,* 320, pp. 222–226, 2008.

[237] H. H. Lara, N. V. Ayala-Nunez, L. C. I. Turrent, et al., "Bactericidal effect of silver nanoparticles against multidrug-resistant bacteria," *World Journal of Microbiology and Biotechnology,* 26, pp. 615–621, 2010.

[238] S. Mandal, S. S. Kumar, B. Krishnamoorthy, and S. K. Basu, "Development and evaluation of calcium alginate beads prepared by sequential and simultaneous methods," *Brazilian Journal of Pharmaceutical Sciences,* 46, pp. 785-793, 2010.

[239] T. Miyazaki, Y. Takeda, S. Akane, et al., "Role of boric acid for poly (vinyl alcohol) film as a cross-linking agent: melting behaviors of the films with boric acid," *Polymer*, 51, pp. 5539–5549, 2010.

[240] J. O. Kim, J. K. Park, J. H. Kim, et al., "Development of polyvinyl alcohol–sodium alginate gel-matrix-based wound dressing system containing nitrofurazone," *International Journal of Pharmaceutics,* 359, pp. 79–86, 2008.

[241] R. M. Silverstein, G. C. Bassler and T. C. Morril, Spectroscopic identification of organic compounds, 5th ed. Wiley: Singapore.

[242] V. Georgieva, D. Zvezdova, and L. Vlaev, "Non-isothermal kinetics of thermal degradation of chitosan," *Chemistry Central Journal,* 6, 81, 2012

[243] H. Zhen, Y. Xiaoxu, P. Xi, et al., "Thermal Degradation Study of Sodium Alginate-Zeolite 4A Composites, Proceedings of the 17th IAPRI World Conference on Packaging China, pp. 406-409, October 2010.

[244] T. Çaykara, and S. J. Demirci, "Preparation and Characterization of Blend films of Poly(Vinyl Alcohol) and Sodium Alginate," *Journal of Macromolecular Science Part A: Pure and Applied Chemistry,* 43, pp. 1113-1121, 2006.

[245] K. L. Deng, H. B. Zhong, T. Tian, et al., "Drug release behavior of a pH/temperature sensitive calcium alginate/poly(N-acryloylglycine) bead with core-shelled structure," *Express Polymer Letter,* 4, pp. 773–780, 2010.

[246] P. R. S. Reddy, K. M. Rao, K. S. V. K. Rao, et al., "Synthesis of alginate based silver nanocomposite hydrogels for biomedical applications," *Macromolecular Research,* 22, pp. 832-842, 2014.

[247] S. K. Bajpai, and S. Sharma, "Investigation of swelling/degradation behaviour of alginate beads crosslinked with Ca^{2+} and Ba^{2+} ions," *Reactive and Functional Polymers,* 59, pp. 129–140, 2004.

[248] M. T. Islam, N. R. Guez-Hornedo, S. Ciotti, et al., "Rheological Characterization of Topical Carbomer Gels Neutralized to Different pH," *Pharmaceutical Research,* 21, pp. 1192-1199, 2004.

[249] M. H. Shukr, and G. F. Metwally, "Evaluation of Topical Gel Bases Formulated with Various Essential Oils for Antibacterial Activity against Methicillin-Resistant *Staphylococcus Aureus," Tropical Journal of Pharmaceutical Research,* 12, pp. 877-884, 2013.

[250] E. G. do-Nascimento, T. B. M. Sampaio, A. C. Medeiros, and E. P. De-Azevedo, "Evaluation of chitosan gel with 1% silver sulfadiazine as an

alternative for burn wound treatment in rats," *Acta Cirurgica Brasileira*, 24, pp. 460–465, 2009.

[251] P. Costa, and J. M. S. Lobo, "Modeling and comparison of dissolution profiles," *European Journal of Pharmaceutical Sciences,* 13, pp. 123–133, 2001.

[252] E. A. Kamoun, E. S. Kenawy, T. M. Tamer, et al., "Poly (vinyl alcohol)-alginate physically crosslinked hydrogel membranes for wound dressing applications: Characterization and bio-evaluation," *Arabian journal of chemistry,* 8, pp. 38-47, 2015.

[253] M. H. Huang, and M. C. Yang, "Swelling and biocompatibility of sodium alginate/poly(γ-glutamic acid) hydrogels," *Polymers for Advanced Technologies,* 21, pp. 561–567, 2010.

[254] M. A. Patel, P. K. Patel, and M. B. Patel, "Effects of ethanol extract of *Ficus bengalensis* (bark) on inflammatory bowel disease," Indian Journal of Pharmacology, 42, pp. 214–218, 2010.

[255] A. Sharma, M. Kumari, and M. V. J. Jagannadham, "Benghalensin, a Highly Stable Serine Protease from the Latex of Medicinal Plant Ficus benghalensis," *Journal of Agricultral and Food Chemistry,* 57, pp. 11120–11126, 2009.

[256] C. A. Rice-Evans, N. Miller, and G. Paganga, "Antioxidant properties of phenolic compounds," *Trends in Plant science,* 2, pp. 152-159, 1997.

[257] M. Rai, A. Yadav, and A. Gade, "Silver nanoparticles as a new generation of antimicrobials," *Biotechnology Advances,* 27, pp. 76–83, 2009.

[258] U. Klueh, V. Wagner, S. Kelly, A. Johnson, and J. D. Bryers, "Efficacy of silver-coated fabric to prevent bacterial colonization and subsequent device-based biofilm formation," *Journal of Biomedical Materials Research Part B: Applied Biomaterials,* 53, pp. 621-631, 2000.

[259] I. Chopra, "The increasing use of silver-based products as antimicrobial agents: a useful development or a cause for concern?," *The Journal of Antimicrobial Chemotherapy,* 59, pp. 587-590, 2007.

[260] P. Dibrov, J. Dzioba, K. K. Gosink, and C. C. Hase, "Chemiosmotic mechanism of antimicrobial activity of Ag(+) in Vibrio cholera," Antimicrobial Agents and Chemotherapy, 46: pp. 2668–2670, 2002.

[261] V. Thomas, M. Namdeo, Y. M. Mohan, et al., "Review on polymer, hydrogel and microgel metal nanocomposites: a facile nanotechnological approach,"

Journal of Macromolecular Science, Part A: Pure and Applied Chemistry, 45, pp. 107, 2008.

[262] J. Huang, Q. Li, D. Sun, et al., "Biosynthesis of silver and gold nanoparticles by novel sundried *Cinnamomum camphora* leaf," *Nanotechnology,* 18, pp. 105104–105115, 2007.

[263] A. R. V. Nestor, V. S. Mendieta, M. A. C. Lopez, et al., "Solvent less synthesis and optical properties of Au and Ag nanoparticles using *Camiellia sinensis* extract," *Materials Letters,* 62, pp. 3103–3105, 2008.

[264] L. L. Balassa, and J. F. Prudden, "Application of chitin and chitosan in wound healing acceleration, in Chitin, chitosan and related enzymes, Academic Press, San Diego, pp. 296–305, 1984.

[265] X. Chen, and H. J. Schluesener, "Nanosilver: a nanoproduct in medical application," *Toxicology Letters,* 176, pp. 1-12, 2008.

[266] Y. M. Mohan, K. Lee, T. Premkumar, and K. E. Geckeler, "Hydrogel networks as nanoreactors: A novel approach to silver nanoparticles for antibacterial applications," Polymer, 48, pp. 158-164, 2007.

[267] P. Logeswari, S. Silambarasan, and J. Abraham, "Synthesis of silver nanoparticles using plants extract and analysis of their antimicrobial property," *Journal of Saudi Chemical Society*, 19, pp. 311-317, 2015.

[268] N. A. Peppas, and S. R. Stauffer, "Reinforced uncrosslinkedpoly(- vinyl alcohol) gels produced by cyclic freezing–thawing processes: a short review," *Journal of Controlled Release,* 16, pp. 305–310, 1991.

[269] B. B. Mandal, S. Kapoor, and S. C. Kundu, "Silk fibroin/polyacrylamide semi-interpenetrating network hydrogels for controlled drug release," *Biomaterials,* 30, pp. 2826–36, 2009.

[270] M. Changez, V. Koul, B. Krishna, A. K. Dinda, and V. Choudhary, "Studies on biodegradation and release of gentamicin sulphate from interpenetrating network hydrogels based on poly(acrylic acid) and gelatin: *in vitro* and *in* vivo," *Biomaterials,* 25, pp. 139–46, 2004

[271] M. L. Oyen, "Mechanical characterization of hydrogel materials," *International Materials Reviews,* 59: pp. 44-59, 2014.

[272] M. Sadeghi, and M. Yarahmadi, "Synthesis and characterization of superabsorbent hydrogel based on chitosan-g-poly (acrylic acid-coacrylonitrile)," *African Journal of Biotechnology*, 10, pp. 12265-12275, 2011.

[273] P. X. Nunes, S. F. Silva, R. J. Guedes, and S. Almeida, “Biological oxidations and antioxidant activity of natural products, Phytochemicals as nutraceuticals - Global Approaches to Their Role in Nutrition and Health,” V. Rao, Eds. 2012.

PUBLICATIONS AND PRESENTATIONS

PAPERS IN INTERNATIONAL REFEREED JOURNALS:

Kumar A, Jaiswal M, (2016) Design and *in-vitro* investigation of nanocomposite hydrogel based *in-situ* spray dressing for chronic wounds and synthesis of silver nanoparticles using green chemistry. Journal of Applied Polymer Science, 133, 43260.

Kumar A, Sanjay, Jaiswal M, (2012) Enhanced Intestinal Permeability of Tinospora cordifolia Extract through Nanoemulsion Formulation: *In-Vitro* and *Ex-Vivo* Studies. Journal of Nanopharmaceutics and Drug Delivery, 2, 1-10.

Kumar A, Jaiswal M, (2014) Nanotechnological Approach to Improve Oral Antidiabetic Efficacy of Phytochemicals Extracted from Tinospora Cordifolia: *In-Vivo* and *Ex-Vivo* Studies. Indo Global Journal of Pharmaceutical Sciences, 4, 210.

Jaiswal M, **Kumar A,** Sharma S, (2016) Development, characterization and application of carbopol 934 based nanogel for intranasal delivery of *Centella asiatica* extract: *In-vitro* and *ex-vivo* permeation study. Journal of Pharmaceutical Investigation, 46, 79-89.

Kumar A, Jaiswal M (2016) Enhanced antidiabetic activity of Berberis aristata through formulation of SNEDDS: *in-vitro* and *ex-vivo* studies. Journal of Nanopharmaceutics and drug delivery (**Accepted**).

Kumar A, Jaiswal M, (2016) A green synthesis of silver nanoparticles from *Ocimum sanctum* leaves extract loaded in PVA/chitosan hydrogels: synthesis, characterization and antimicrobial activity for wound healing applications. (**Communicated**)

PRESENTATIONS IN NATIONAL AND INTERNATIONAL CONFERENCES:

Kumar A "Gastro-retentive drug delivery system for Indinavir sulfate: An approach for sustained release with Zero-Order Kinetics" International conference on Pharmaceutical sciences organized by Division of Pharmaceutical sciences, Shri Guru Ram Rai Institute of Technology, February 14^{th}-15^{th} 2014.

Sajay, **Kumar A**, Jaiswal M "Formulation and *in-vitro* evaluation of *Holarrhena anti-dysentrica* loaded hydrogels prepared by free radical polymerization method" International conference on Pharmaceutical sciences organized by Division of Pharmaceutical sciences, Shri Guru Ram Rai Institute of Technology, February 14^{th}-15^{th} 2014.